© 2011 Lanhua Hu

OXIDATIVE TREATMENT OF EMERGING MICROPOLLUTANTS AND VIRAL PATHOGENS BY POTASSIUM PERMANGANATE AND FERRATE: KINETICS AND MECHANISMS

BY

LANHUA HU

DISSERTATION

Submitted in partial fulfillment of the requirements
for the degree of Doctor of Philosophy in Environmental Engineering in Civil Engineering
in the Graduate College of the
University of Illinois at Urbana-Champaign, 2011

Urbana, Illinois

Doctoral Committee:

Associate Professor Timothy J. Strathmann, Chair and Director of Research
Professor Benito J. Mariñas
Professor Charles J. Werth
Assistant Professor Michael C. Dodd, University of Washington

ABSTRACT

Providing clean drinking water is a primary challenge of this century. The ubiquitous occurrence of pharmaceutically active compounds (PhACs), including antibiotics, anticonvulsants, painkillers, estrogenic hormones, lipid regulators, beta-blockers, antihistamines, X-ray contrast media, etc., in drinking water sources has been reported in recent years. The presence of these contaminants, although at low concentrations, raises public concerns about potential adverse effects on aquatic ecology and human health. Another emerging concern in drinking water safety is the formation of toxic disinfection by-products (DBPs) when treating water with conventional disinfectants (i.e., free chlorine), and thus alternative disinfectants and disinfection processes are sought to control DBPs formation while still providing a sufficient barrier to pathogens. Chemical oxidation processes involving permanganate [MnO_4^-, Mn(VII)] and ferrate [FeO_4^{2-}, Fe(VI)] salts are promising technologies for treatment of many PhACs. Permanganate is already widely used in water treatment facilities (e.g., for treatment of taste and odor compounds, soluble iron(II) and manganese(II)), while ferrate is an emerging water treatment oxidant that also has potential for use as an alternative disinfectant. This study investigates the oxidative transformation of PhACs using permanganate and ferrate and the use of ferrate for inactivation of a surrogate viral pathogen, MS2 bacteriophage.

Survey tests show that permanganate and ferrate are both selective oxidants that target compounds with specific electron-rich moieties, including olefin, phenol, amine, cyclopropyl, thioether, and alkyne groups. Detailed kinetics studies were undertaken to characterize Mn(VII) oxidation of five representative PhACs that exhibit moderate to high reactivity (carbamazepine, CBZ; ciprofloxacin, CPR; lincomycin, LCM; trimethoprim, TMP; and 17α-ethinylestradiol, EE2), Fe(VI) oxidation of one representative PhAC (CBZ), and Fe(VI) inactivation of MS2 phage (Fe(VI) reactions with other PhACs were not conducted because recent literature reports addressed the topic). The Mn(VII) and Fe(VI) reactions examined with PhAC and MS2 phage were found to follow generalized second-order rate laws, first-order in oxidant concentration and first-order in target contaminant concentration. The temperature dependence of reaction rate constants was found to follow the Arrhenius equation. Changing of solution pH had varying effects on reaction rates, attributed to change in electron density on the target reactive groups

upon protonation/deprotonation. The effects of pH on reaction rates were quantitatively described by kinetic models considering parallel reactions between different individual contaminant species and individual oxidant species. For Mn(VII) reactions, removal of PhACs in drinking water utility source waters was generally well predicted by kinetic models that include temperature, KMnO$_4$ dosage, pH, and source water oxidant demand as input parameters.

A large number of reaction products from Mn(VII) oxidation of CBZ, CPR, LCM, TMP, and EE2 and Fe(VI) oxidation of CBZ were identified by liquid chromatography-tandem mass spectrometry (LC-MS/MS). Structures of reaction products were proposed based on MS spectral data along with information collected from proton nuclear magnetic resonance (^{1}H-NMR), chromatographic retention time, and reported literature on Mn(VII) reactions with specific organic functional groups. Mn(VII) and Fe(VI) rapidly oxidize CBZ by electrophilic attack at the olefinic group on the central heterocyclic ring. Mn(VII) oxidation of CPR was found to occur primary on the tertiary aromatic amine group on the piperazine ring, with minor reactions on the aliphatic amine and the cyclopropyl group. LCM was oxidized by Mn(VII) through the aliphatic amine group on the pyrrolidine ring and thioether group attached to the pyranose ring. TMP oxidation by Mn(VII) was proposed to occur at the C=C bonds on the pyrimidine ring and the bridging methylene group. EE2 oxidation by Mn(VII) resulted in several types of products, including dehydrogenated EE2, hydroxylated EE2, phenolic ring cleavage products, and products with structural modifications on the ethynyl group.

Although little mineralization of PhAC solutions was observed after Mn(VII) treatment, results from bioassay tests of three antibiotics show that the antibacterial activity was effectively removed upon reaction with Mn(VII), demonstrating that incomplete oxidation of PhACs during Mn(VII) treatment will likely be sufficient to eliminate the pharmaceutical activity of impacted source waters.

Overall, results show that reactions with Mn(VII) likely contribute to the fate of many PhACs in water treatment plants that currently use Mn(VII), and the kinetic model developed in this study can be used to predict the extent of PhAC removal by Mn(VII) treatment. For water contaminated with highly Mn(VII)-reactive PhACs (e.g., carbamazepine, estradiol), specific application of Mn(VII) may be warranted. Results suggest Fe(VI) may be a useful disinfecting agent, but more work is needed to characterize its activity and mode of inactivating with other pathogens of concern.

To Zifeng and Sophia

ACKNOWLEDGMENTS

This dissertation would not have been possible without the help and support of many people. My deepest gratitude is to my advisor, Prof. Timothy J. Strathmann. I have been incredibly fortunate to have such an excellent advisor, who always trusts, supports, and encourages me. I am truly deeply indebted to him for all his patience, guidance, and advice through my ups and downs. I would like to specially thank him for his time and efforts on reading and revising all my manuscripts. I would also like to express my gratitude to my committee members, Prof. Benito J. Mariñas, Prof. Charles J. Werth, and Prof. Michael C. Dodd. Prof. Mariñas has been a great mentor to me and had provided me with invaluable research and career advice. I am thankful to Prof. Werth and Prof. Dodd for their constructive suggestions and input to this work.

Prof. Vernon Snoeyink is thanked for his help in improving my spoken English through the CASE program and also his academic and career advice. Thanks to our lab manager, Shaoying Qi, for all his help on instrument training and chemical ordering.

I would like to thank all my past and current colleagues in the Strathmann group for all the discussions in group meetings and the times spent together in the lab and office, especially Tias Paul, Dongwook Kim, Jinyong Liu, Heather Martin, Mathew Sugihara, Genevieve Nano, Adam Bussan, and Linsay Knitt. Tias has been a wonderful colleague, office mate, lab mate, and more importantly, friend. Thank you for all the discussions on research, culture, life, babies, etc. Jinyong is appreciated for his help on my experiments and for discussions on research. I would also like to thank all my friends on the fourth floor of Newmark for the good times we spent together in classes, labs, picnics and conferences. Numerous friends outside the department are appreciated for their friendship and support.

I would not have made it here without the love and support of my family. I thank my parents for their love and for giving me the full freedom to choose my life path. I thank my dear husband, Zifeng Lu, for his unconditional love and support throughout these difficult years. Zifeng also helped tremendously in the formatting of this dissertation. I am lucky to have my precious daughter Sophia along my side in the last year of my graduate studies. She brings sunshine and laughter to the gloomy days of endless writing. My parents-in-law are also greatly appreciated for their help on caring for Sophia.

TABLE OF CONTENTS

CHAPTER 1
INTRODUCTION

1.1 Motivation

Worldwide occurrence of pharmaceutically active compounds (PhACs) in drinking water sources (e.g., surface waters and groundwater) has been well documented in recent years [1-11]. A series of national reconnaissances conducted by the U.S. Geological Survey found many organic wastewater contaminants in streams, groundwater and finished drinking water throughout the U.S. [1, 12-14]. Detected compounds include antibiotics, anticonvulsants, painkillers, cytostatic drugs, estrogenic hormones, lipid regulators, beta-blockers, antihistamines, X-ray contrast media, and emerging classes of nitrogenous disinfection byproducts. Pharmaceuticals end up in aquatic environments as a result of incomplete metabolism in humans and animals, improper disposal of unused medication, and ineffective removal in municipal sewage treatment plants (STPs) [15]. **Table 1.1** summarizes the results of some recent surveys of the occurrence of selected pharmaceutical compounds in U.S. surface water, groundwater, and finished drinking water.

Although concentrations of PhACs detected in drinking water sources are typically at levels of ng/L to μg/L [12, 16, 17] as shown in **Table 1.1**, there remains serious public concerns about potential accumulative health effects of long-term exposure to even low levels of these biologically active compounds, especially considering unknown interactive effects of complex pharmaceutical mixtures (e.g., synergistic or antagonistic toxicity). In one recent study, it was reported that the growth of human embryonic cells was inhibited by a mixture of 13 therapeutic drugs at environmental levels [18]. The presence of PhACs in surface waters is also of concern because of their potential toxicity to aquatic organisms. Richards and co-workers reported adverse effects of pharmaceutical mixtures on aquatic microcosms [19]. There also remains considerable ongoing debate about the potential for development of increased antibiotic resistance in pathogenic microorganisms due to continuous exposure to sub-therapeutic concentrations of antibiotic compounds discharged to the environment [20-22]. One study reported an increase of the selection rates of an antibiotic resistance gene upon exposure to 20 μg/L of oxytetracycline [23]. The presence of trace antibiotics in groundwater is newly reported to affect the nitrate levels in the water by altering the composition of the nitrate-reducing microcosms and inhibiting their

nitrate reduction capabilities [24]. Furthermore, endocrine disrupting chemicals (e.g., synthetic steroid hormones) often exhibit non-monotonic dose-response relationships wherein ultra-low concentrations (i.e. ng/L) can elicit biological effects [25].

Waterborne viral pathogens have been found in drinking water sources for decades [26-28], and disinfection processes using free chlorine as the primary disinfectant have been applied in drinking water facilities for over a century [29]. In 2006, the U.S. Environmental Protection Agency (USEPA) released the Long Term 2 Enhanced Surface Water Treatment Rule (LT2ESWTR) and Stage 2 Disinfectants and DBPs Rule (Stage 2 DBPR) in response to the control of *Cryptosporidium parvum* oocysts and disinfection by-products (DBPs) formation [30]. As a result, many U.S. drinking water utilities have begun to switch the primary disinfectant from free chlorine to other alternative processes, most often UV disinfection or treatment with combined chlorine. This practice raises emerging concerns related to viral pathogens, especially enteric viruses, because viruses are much more resistant to inactivation by UV light and combined chlorine than to free chlorine [29, 30].

Because of issues described above, there is growing interest in the water treatment community in the fate and degradation of emerging chemical micropollutants and viral pathogens in both natural aquatic environments and during conventional treatment processes, and the development of new technologies to more effectively protect drinking water quality from these threats. These are the issues that motivate the work described in this thesis.

1.2 *Pharmaceutical Reactions with Drinking Water Oxidants*

Many PhACs contain electron-rich functional groups that are susceptible to oxidation during drinking water treatment, including phenol, amine, olefin, and thioether groups. Previous studies have investigated the oxidative treatment of PhACs by common drinking water oxidants and disinfectants, including ozone, free and combined chlorine, and chlorine dioxide [31-34]. The homogeneous aqueous oxidation of PhACs can typically be modeled with second-order rate laws:

$$\frac{d[\text{PhAC}]}{dt} = -k_2[\text{PhAC}][\text{Oxidant}] \qquad (1.1)$$

where k_2 is the apparent second-order rate constant ($M^{-1} s^{-1}$), which can vary widely with solution conditions. **Table 1.2** summarizes the results of several recent studies on the reactivity of three drinking water oxidants with commonly detected PhACs. Overall, ozone reacts the fastest with most PhACs, exhibiting k_2 values ranging from <1 $M^{-1} s^{-1}$ to 7×10^9 $M^{-1} s^{-1}$ at pH 7 [31, 35-41].

Chlorine dioxide and free chlorine exhibit lower reactivity with the PhACs examined [32-34, 42-48]. Studies also report high reactivity of PhACs with hydroxyl radicals generated through advanced oxidation processes, including ozonation, with k_2 values approaching diffusion-controlled limitations (10^9-10^{10} M^{-1} s^{-1} at 25 °C) [31, 49]. Although extremely reactive, their poor selectivity might result in ineffective treatment, particularly in organic-rich matrices and waters with high alkalinity that act to scavenge hydroxyl radicals.

Various effects were observed on the pharmaceutical activity of PhAC solutions after treatment with water oxidants. Lee and coworkers [50] demonstrated that reactions between several oxidants and the steroidal hormone 17α-ethinylestradiol eliminate the estrogenic activity of solutions and attributed the reductions in activity to formation of initial reaction products that elicit substantially reduced estrogenic responses in the *in vitro* bioassays. Dodd and coworkers [51] found that reactions of O_3 and ·OH with most classes of antibiotics lead to stoichiometric deactivation, indicating that reaction products exhibit significantly reduced potencies. In contrast, reports show that chlorination can sometimes produce byproducts that are more toxic than the parent compounds [52]. Also, O_3 and ·OH reactions with the β-lactams penicillin G and cephalexin was reported to yield some products that retain significant antibacterial potency, identified as the stereoisomeric (*R*)-sulfoxides of the parent antibiotics [53].
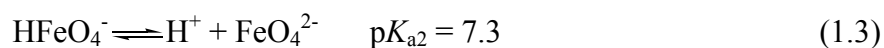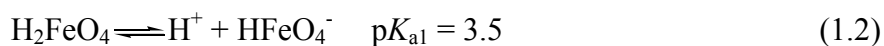
1.3 Permanganate and Ferrate Chemistry

Chemical oxidation processes involving salts of permanganate [MnO_4^-; Mn(VII)] and ferrate [FeO_4^{2-}; Fe(VI)] ions may be promising technologies for treatment of many PhACs and pathogens due to their unique chemical and physical properties. Potassium permanganate ($KMnO_4$) is already widely used in water treatment processes to control taste and odor, remove color, control biological growth, and remove dissolved iron and manganese [29]. It has also been used extensively for in-situ chemical oxidation (ISCO) processes in subsurface remediation applications [54, 55]. When compared to other common drinking water oxidants, Mn(VII) is still a relatively strong oxidant with a standard reduction potential (E^0) of 1.68 V (versus a standard hydrogen electrode) under acidic conditions, higher than that of dissolved oxygen (1.23 V), chlorine dioxide (0.95 V), and hypochlorite (1.48 V) as shown in **Table 1.3** [56]. Mn(VII) has been reported to oxidize a wide range of persistent organic chemicals, including phenols, chlorinated ethenes, and polycyclic aromatic hydrocarbons, etc. [54] Mn(VII) can be used as an alternative chemical to pre-chlorination

and has been reported to greatly reduce formation of halogenated disinfection byproducts (DBPs) during drinking water treatment by oxidizing chlorine DBP precursors [57].

Potassium ferrate (K_2FeO_4) is also gaining increasing attention as an environmentally friendly oxidant for use in water treatment. While naturally occurring iron is usually present in the +2 (ferrous) and +3 (ferric) oxidation states, iron in ferrate exists at the +6 oxidation state (there are also less stable Fe(V) and Fe(IV) ferrate redox states), which gives rise to its strong oxidation potential. Fe(VI) has an even higher E^0 (2.20 V) than ozone (2.08 V) under acidic conditions [56], and Fe(VI) exhibits elevated reactivity with a wide range of organic and inorganic compounds [58]. Permanganate and ferrate also share a number of properties that make them advantageous alternative oxidants for water and wastewater treatment applications. Both oxidants produce innocuous reduction products (e.g., $MnO_{2(s)}$ and $Fe(OH)_{3(s)}$), which can function as efficient coagulants and adsorbents for removing other contaminants from water (e.g., DBP precursors) [58, 59]; $MnO_{2(s)}$ has also been shown to act as an oxidant for PhACs [60-64].

Whereas Mn(VII) exists predominantly as the deprotonated MnO_4^- species throughout the pH range of natural waters (pK_a for $HMnO_4$ = -2.25 [65]), Fe(VI) has a more complex acid-base chemistry that needs to be considered when assessing aqueous redox reactions. The fully protonated acid form of ferrate (H_2FeO_4) is a much weaker acid than $HMnO_4$ as shown in Equation (1.2) and (1.3), and this results in variable Fe(VI) speciation throughout the pH range of natural waters (**Figure 1.1**) [58].

$$H_2FeO_4 \rightleftharpoons H^+ + HFeO_4^- \quad pK_{a1} = 3.5 \qquad (1.2)$$

$$HFeO_4^- \rightleftharpoons H^+ + FeO_4^{2-} \quad pK_{a2} = 7.3 \qquad (1.3)$$

As a result, Fe(VI) redox reactions are often reported to be highly dependent on solution pH [58]. In addition, Fe(VI) auto-decomposes in water according to the stoichiometry shown in Equation (1.4) [58].

$$4\ FeO_4^{2-} + 10\ H_2O \rightarrow 4\ Fe(OH)_{3(s)} + 3O_2\uparrow + 8\ OH^- \qquad (1.4)$$
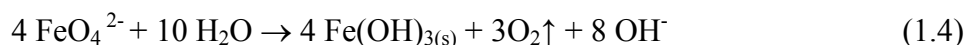
Rates of auto-decomposition increase dramatically with decreasing pH, and Fe(VI) does not persist for long at pH ≤ 7. Whereas Fe(VI) auto-decomposition complicates practical applications of Fe(VI) treatment processes, it also eliminates concerns about overdosing of Fe(VI) during treatment applications since the resulting decomposition product, $Fe(OH)_{3(s)}$, is harmless and will be removed by downstream sedimentation and filtration processes.

1.4 Research Objectives and Thesis Outline

Although Mn(VII) and Fe(VI) are potential drinking water oxidants, little is currently known about their effectiveness for PhAC and/or viral treatment, and the work described in this thesis aims to fill this knowledge gap in the field of water treatment chemistry. The primary objectives of this research were to: (a) characterize the kinetics and mechanisms of reactions between representative PhACs and Mn(VII)/Fe(VI); (b) assess the potential use of these reactions to remove problematic PhACs and associated pharmaceutical activity during drinking water treatment operations; and (c) examine the inactivation kinetics of bacteriophage MS2, a surrogate viral pathogen, by treatment with Fe(VI).

Initially, a large group of PhACs were tested for their reactivity with Mn(VII) and Fe(VI). **Figure 1.2** and **Figure 1.3** summarizes the survey results for Mn(VII) and Fe(VI) oxidation, respectively. For Mn(VII), ten compounds out of eighteen PhACs tested showed moderate to high reactivity with Mn(VII), with >50% degradation being observed within 1 h. Six PhACs (acetaminophen, bisphenol A, carbamazepine, chlortetracycline, 17α-ethinylestradiol, and triclosan) showed very high reactivity, with complete degradation occurring in less than 10 min, whereas four compounds (ciprofloxacin, diclofenac, lincomycin, and trimethoprim) exhibited moderate reactivity with Mn(VII). For Fe(VI), eight out of twelve tested PhACs (acetaminophen, atenolol, carbamazepine, diclofenac, ciprofloxacin, 17α-ethinylestradiol, sulfamethoxazole and triclosan) showed moderate to high reactivity with Fe(VI). Surprisingly, Fe(VI) did not show a major enhanced reactivity with PhACs when compared to Mn(VII) despite of its higher oxidation potential. Therefore, detailed kinetics and mechanisms studies in this research were more focused on PhAC reactions with Mn(VII) because Mn(VII) is already commonly used in water treatment and is more stable and readily available to utilities than Fe(VI) and recent studies have already reported on Fe(VI) reactions with several of the surveyed PhACs [66-68].

Chapter 2 focuses on the oxidation kinetics and mechanism of an anticonvulsant drug, carbamazepine (CBZ), by Mn(VII) and Fe(VI). Chapter 3 discusses the kinetics of Mn(VII) oxidation of three common antibiotics: ciprofloxacin (CPR), lincomycin (LCM), and trimethoprim (TMP). Chapter 4 details the identification of reaction products and pathways for the three antibiotics, along with results from experiments assessing the effects of Mn(VII) treatment on the antibacterial potency of solutions. Chapter 5 presents the kinetics and products of Mn(VII) reactions with the synthetic hormone, 17α-ethinylestradiol (EE2). Chapter 6

describes the inactivation kinetics of a non-pathogenic surrogate for enteric viruses, MS2 phage, by Fe(VI). Chapter 7 summarizes key findings from the thesis research, describes implications of the study to water and wastewater treatment, and outlines future research needs.

1.5 References Cited

[1]   Kolpin D. W., Furlong E. T., Meyer M. T., Thurman E. M., Zaugg S. D., Barber L. B. and Buxton H. T. Pharmaceuticals, hormones, and other organic wastewater contaminants in U.S. streams, 1999-2000: A national reconnaissance. *Environmental Science & Technology*, **2002**, 36: 1202-1211.

[2]   Daughton C. G. and Ternes T. A. Pharmaceuticals and personal care products in the environment: Agents of subtle change. *Environmental Health Perspectives*, **1999**, 107: 907-938.

[3]   Heberer T. Occurrence, fate, and removal of pharmaceutical residues in the aquatic environment: A review of recent research data. *Toxicology Letters*, **2002**, 131: 5-17.

[4]   Ternes T. A. Occurrence of drugs in German sewage treatment plants and rivers. *Water Research*, **1998**, 32: 3245-3260.

[5]   Vieno N. M., Harkki H., Tuhkanen T. and Kronberg L. Occurrence of pharmaceuticals in river water and their elimination a pilot-scale drinking water treatment plant. *Environmental Science & Technology*, **2007**, 41: 5077-5084.

[6]   Monteiro S. C. and Boxall A. B. A. Occurrence and fate of human pharmaceuticals in the environment. *Reviews of Environmental Contamination and Toxicology, Vol 202*, **2010**, 202: 53-154.

[7]   Mompelat S., Le Bot B. and Thomas O. Occurrence and fate of pharmaceutical products and by-products, from resource to drinking water. *Environment International*, **2009**, 35: 803-814.

[8]   Snyder S. A. Occurrence, treatment, and toxicological relevance of EDCs and pharmaceuticals in water. *Ozone: Science and Engineering*, **2008**, 30: 65-69.

[9]   Snyder S. A. and Benotti M. J. Endocrine disruptors and pharmaceuticals: Implications for water sustainability. *Water Science and Technology*, **2010**, 61: 145-154.

[10]   Singh S. P., Azua A., Chaudhary A., Khan S., Willett K. L. and Gardinali P. R. Occurrence and distribution of steroids, hormones and selected pharmaceuticals in South Florida

coastal environments. *Ecotoxicology*, **2010**, 19: 338-350.

[11]   Conn K. E., Lowe K. S., Drewes J. E., Hoppe-Jones C. and Tucholke M. B. Occurrence of pharmaceuticals and consumer product chemicals in raw wastewater and septic tank effluent from single-family homes. *Environmental Engineering Science*, **2010**, 27: 347-356.

[12]   Focazio M. J., Kolpin D. W., Barnes K. K., Furlong E. T., Meyer M. T., Zaugg S. D., Barber L. B. and Thurman M. E. A national reconnaissance for pharmaceuticals and other organic wastewater contaminants in the United States - II) Untreated drinking water sources. *Science of the Total Environment*, **2008**, 402: 201-216.

[13]   Barnes K. K., Kolpin D. W., Furlong E. T., Zaugg S. D., Meyer M. T. and Barber L. B. A national reconnaissance of pharmaceuticals and other organic wastewater contaminants in the United States - I) Groundwater. *Science of the Total Environment*, **2008**, 402: 192-200.

[14]   Stackelberg P. E., Furlong E. T., Meyer M. T., Zaugg S. D., Henderson A. K. and Reissman D. B. Persistence of pharmaceutical compounds and other organic wastewater contaminants in a conventional drinking-water-treatment plant. *Science of the Total Environment*, **2004**, 329: 99-113.

[15]   Heberer T. Tracking persistent pharmaceutical residues from municipal sewage to drinking water. *Journal of Hydrology*, **2002**, 266: 175-189.

[16]   Snyder S. A., Westerhoff P., Yoon Y. and Sedlak D. L. Pharmaceuticals, personal care products, and endocrine disruptors in water: Implications for the water industry. *Environmental Engineering Science*, **2003**, 20: 449-469.

[17]   Rahman M. F., Yanful E. K. and Jasim S. Y. Endocrine disrupting compounds (EDCs) and pharmaceuticals and personal care products (PPCPs) in the aquatic environment: Implications for the drinking water industry and global environmental health. *Journal of Water and Health*, **2009**, 7: 224-243.

[18]   Pomati F., Castiglioni S., Zuccato E., Fanelli R., Vigett D., Rossetti C. and Calamari D. Effects of a complex mixture of therapeutic drugs at environmental levels on human embryonic cells. *Environmental Science & Technology*, **2006**, 40: 2442-2447.

[19]   Richards S., Wilson C., Johnson D., Castle D., Lam M., Mabury S., Sibley P. and Solomon K. Effects of pharmaceutical mixtures in aquatic microcosms. *Environmental Toxicology and Chemistry*, **2004**, 23: 1035-1042.

[20] Goni-Urriza M., Capdepuy M., Arpin C., Raymond N., Caumette P. and Quentin C. Impact of an urban effluent on antibiotic resistance of riverine *Enterobacteriaceae* and *Aeromonas* spp. *Applied and Environmental Microbiology*, **2000**, 66: 125-132.

[21] Iwane T., Urase T. and Yamamoto K. Possible impact of treated wastewater discharge on incidence of antibiotic resistant bacteria in river water. *Water Science and Technology*, **2001**, 43: 91-99.

[22] Schwartz T., Kohnen W., Jansen B. and Obst U. Detection of antibiotic-resistant bacteria and their resistance genes in wastewater, surface water, and drinking water biofilms. *FEMS Microbiology Ecology*, **2003**, 43: 325-335.

[23] Knapp C. W., Engemann C. A., Hanson M. L., Keen P. L., Hall K. J. and Graham D. W. Indirect evidence of transposon-mediated selection of antibiotic resistance genes in aquatic systems at low-level oxytetracycline exposures. *Environmental Science & Technology*, **2008**, 42: 5348-5353.

[24] Underwood J. C., Harvey R. W., Metge D. W., Repert D. A., Baumgartner L. K., Smith R. L., Roane T. M. and Barber L. B. Effects of the antimicrobial sulfamethoxazole on groundwater bacterial enrichment. *Environmental Science & Technology*, **2011**, Article ASAP.

[25] Welshons W. V., Thayer K. A., Judy B. M., Taylor J. A., Curran E. M. and vom Saal F. S. Large effects from small exposures. I. Mechanisms for endocrine-disrupting chemicals with estrogenic activity. *Environmental Health Perspectives*, **2003**, 111.

[26] Chang S. L. Waterborne viral infections and their prevention. *Bulletin of the World Health Organization*, **1968**, 38: 401-414.

[27] Dowd S. E., Gerba C. P. and Pepper I. L. Confirmation of the human-pathogenic microsporidia *enterocytozoon bieneusi*, *encephalitozoon intestinalis*, and *vittaforma corneae* in Water. *Applied and Environmental Microbiology*, **1998**, 64: 3332-3335.

[28] Grabow W. O. K. and Albert B. Chapter 1 Overview of health-related water virology. *Perspectives in Medical Virology*: Elsevier **2007**:1-25.

[29] MWH. *Water Treatment: Principles and Design*, 2nd ed. Hoboken: Wiley, **2005**.

[30] Page M. A., Shisler J. L. and Marinas B. J. Kinetics of adenovirus type 2 inactivation with free chlorine. *Water Research*, **2009**, 43: 2916-2926.

[31] Huber M. M., Canonica S., Park G. Y. and von Gunten U. Oxidation of pharmaceuticals

during ozonation and advanced oxidation processes. *Environmental Science & Technology*, **2003**, 37: 1016-1024.

[32] Pinkston K. E. and Sedlak D. L. Transformation of aromatic ether- and amine-containing pharmaceuticals during chlorine disinfection. *Environmental Science & Technology*, **2004**, 38: 4019-4025.

[33] Huber M. M., Korhonen S., Ternes T. A. and von Gunten U. Oxidation of pharmaceuticals during water treatment with chlorine dioxide. *Water Research*, **2005**, 39: 3607-3617.

[34] Dodd M. C., Shah A. D., von Gunten U. and Huang C.-H. Interactions of fluoroquinolone antibacterial agents with aqueous chlorine: Reaction kinetics, mechanisms, and transformation pathways. *Environmental Science & Technology*, **2005**, 39: 7065-7076.

[35] Andreozzi R., Caprio V., Marotta R. and Vogna D. Paracetamol oxidation from aqueous solutions by means of ozonation and H_2O_2/UV system. *Water Research*, **2003**, 37: 993-1004.

[36] Benner J., Salhi E., Ternes T. and von Gunten U. Ozonation of reverse osmosis concentrate: Kinetics and efficiency of beta blocker oxidation. *Water Research*, **2008**, 42: 3003-3012.

[37] Deborde M., Rabouan S., Duguet J. P. and Legube B. Kinetics of aqueous ozone-induced oxidation of some endocrine disruptors. *Environmental Science & Technology*, **2005**, 39: 6086-6092.

[38] Dodd M. C., Buffle M. O. and von Gunten U. Oxidation of antibacterial molecules by aqueous ozone: Moiety-specific reaction kinetics and application to ozone-based wastewater treatment. *Environmental Science & Technology*, **2006**, 40: 1969-1977.

[39] Qiang Z., Adams C. and Surampalli R. Determination of ozonation rate constants for lincomycin and spectinomycin. *Ozone: Science and Engineering*, **2004**, 26: 525-537.

[40] Rosal R., Rodriguez A., Perdigon-Melon J. A., Petre A., Garcia-Calvo E., Gomez M. J., Aguera A. and Fernandez-Alba A. R. Degradation of caffeine and identification of the transformation products generated by ozonation. *Chemosphere*, **2009**, 74: 825-831.

[41] Suarez S., Dodd M. C., Omil F. and von Gunten U. Kinetics of triclosan oxidation by aqueous ozone and consequent loss of antibacterial activity: Relevance to municipal wastewater ozonation. *Water Research*, **2007**, 41: 2481-2490.

[42] Chamberlain E. and Adams C. Oxidation of sulfonamides, macrolides, and carbadox with free chlorine and monochloramine. *Water Research*, **2006**, 40: 2517-2526.

[43] Deborde M., Rabouan S., Gallard H. and Legube B. Aqueous chlorination kinetics of some endocrine disruptors. *Environmental Science & Technology*, **2004**, 38: 5577-5583.

[44] Dodd M. C. and Huang C. H. Transformation of the antibacterial agent sulfamethoxazole in reactions with chlorine: Kinetics, mechanisms, and pathways. *Environmental Science & Technology*, **2004**, 38: 5607-5615.

[45] Dodd M. C. and Huang C. H. Aqueous chlorination of the antibacterial agent trimethoprim: Reaction kinetics and pathways. *Water Research*, **2007**, 41: 647-655.

[46] Gallard H., Leclercq A. and Croue J. P. Chlorination of bisphenol A: kinetics and by-products formation. *Chemosphere*, **2004**, 56: 465-473.

[47] Gould J. P. and Richards J. T. The kinetics and products of the chlorination of caffeine in aqueous solution. *Water Research*, **1984**, 18: 1001-1009.

[48] Rule K. L., Ebbett V. R. and Vikesland P. J. Formation of chloroform and chlorinated organics by free-chlorine-mediated oxidation of triclosan. *Environmental Science & Technology*, **2005**, 39: 3176-3185.

[49] Yuan F., Hu C., Hu X. X., Qu J. H. and Yang M. Degradation of selected pharmaceuticals in aqueous solution with UV and UV/H$_2$O$_2$. *Water Research*, **2009**, 43: 1766-1774.

[50] Lee Y., Escher B. I. and von Gunten U. Efficient removal of estrogenic activity during oxidative treatment of waters containing steroid estrogens. *Environmental Science & Technology*, **2008**, 42: 6333-6339.

[51] Dodd M. C., Kohler H. P. E. and von Gunten U. Oxidation of antibacterial compounds by ozone and hydroxyl radical: Elimination of biological activity during aqueous ozonation processes. *Environmental Science & Technology*, **2009**, 43: 2498-2504.

[52] Hu J. Y., Aizawa T. and Ookubo S. Products of aqueous chlorination of bisphenol A and their estrogenic activity. *Environmental Science & Technology*, **2002**, 36: 1980-1987.

[53] Dodd M. C., Rentsch D., Singer H. P., Kohler H. P. E. and von Gunten U. Transformation of β-lactam antibacterial agents during aqueous ozonation: Reaction pathways and quantitative bioassay of biologically-active oxidation products. *Environmental Science & Technology*, **2010**, 44: 5940-5948.

[54] Waldemer R. H. and Tratnyek P. G. Kinetics of contaminant degradation by permanganate. *Environmental Science & Technology*, **2006**, 40: 1055-1061.

[55] Yan Y. E. and Schwartz F. W. Kinetics and mechanisms for TCE oxidation by

permanganate. *Environmental Science & Technology*, **2000**, 34: 2535-2541.

[56]　Sharma V. K. Use of iron(VI) and iron(V) in water and wastewater treatment. *Water Science and Technology*, **2004**, 49: 69-74.

[57]　Singer P. C., Borchardt J. H. and Colthurst J. M. The effects of permanganate pretreatment on trihalomethane formation in drinking water. *Journal American Water Works Association*, **1980**, 72: 573-578.

[58]　Sharma V. K. Potassium ferrate(VI): An environmentally friendly oxidant. *Advances in Environmental Research*, **2002**, 6: 143-156.

[59]　Jiang J. Q. and Lloyd B. Progress in the development and use of ferrate(VI) salt as an oxidant and coagulant for water and wastewater treatment. *Water Research*, **2002**, 36: 1397-1408.

[60]　Lin K., Liu W. and Gan J. Oxidative removal of bisphenol A by manganese dioxide: Efficacy, products, and pathways. *Environmental Science & Technology*, **2009**, 43: 3860-3864.

[61]　Zhang H. C. and Huang C. H. Oxidative transformation of fluoroquinolone antibacterial agents and structurally related amines by manganese oxide. *Environmental Science & Technology*, **2005**, 39: 4474-4483.

[62]　Xu L., Xu C., Zhao M. R., Qiu Y. P. and Sheng G. D. Oxidative removal of aqueous steroid estrogens by manganese oxides. *Water Research*, **2008**, 42: 5038-5044.

[63]　Zhang H. and Huang C.-H. Reactivity and transformation of antibacterial N-oxides in the presence of manganese oxide. *Environmental Science & Technology*, **2005**, 39: 593-601.

[64]　Zhang H., Chen W.-R. and Huang C.-H. Kinetic modeling of oxidation of antibacterial agents by manganese oxide. *Environmental Science & Technology*, **2008**, 42: 5548-5554.

[65]　Wiberg E., Wiberg N. and Holleman A. F. *Inorganic Chemistry*, 1st ed. San Diego: Academic Press, **2001**.

[66]　Sharma V. K., Mishra S. K. and Nesnas N. Oxidation of sulfonamide antimicrobials by ferrate(VI) [$Fe^{VI}O_4^{2-}$]. *Environmental Science & Technology*, **2006**, 40: 7222-7227.

[67]　Sharma V. K., Li X. Z., Graham N. and Doong R. A. Ferrate(VI) oxidation of endocrine disruptors and antimicrobials in water. *J Water Supply: Res Technol - AQUA*, **2008**, 57: 419-426.

[68]　Sharma V. K. Oxidative transformations of environmental pharmaceuticals by Cl_2, ClO_2,

O$_3$, and Fe(VI): Kinetics assessment. *Chemosphere*, **2008**, 73: 1379-1386.

[69]   Benotti M. J., Trenholm R. A., Vanderford B. J., Holady J. C., Stanford B. D. and Snyder S. A. Pharmaceuticals and endocrine disrupting compounds in U.S. drinking water. *Environmental Science & Technology*, **2009**, 43: 597-603.

[70]   Loraine G. A. and Pettigrove M. E. Seasonal variations in concentrations of pharmaceuticals and personal care products in drinking water and reclaimed wastewater in Southern California. *Environmental Science & Technology*, **2006**, 40: 687-695.

[71]   Qiang Z. and Adams C. Potentiometric determination of acid dissociation constants (pK_a) for human and veterinary antibiotics. *Water Research*, **2004**, 38: 2874-2890.

1.6 Figures and Tables
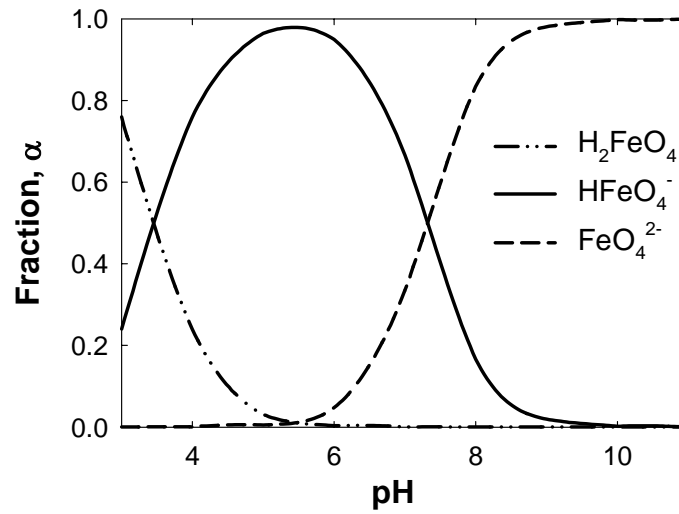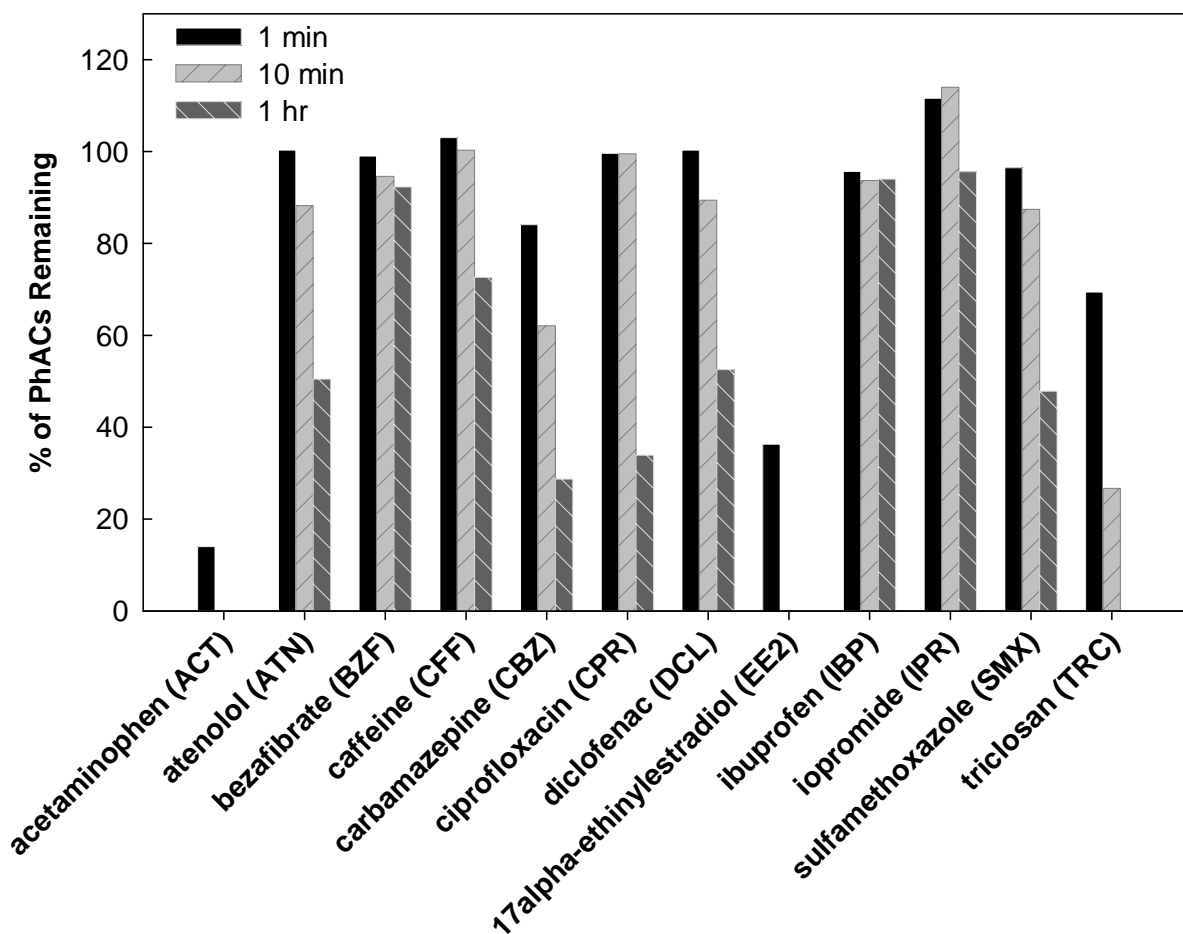

Figure 1.1 Change of ferrate speciation with pH.
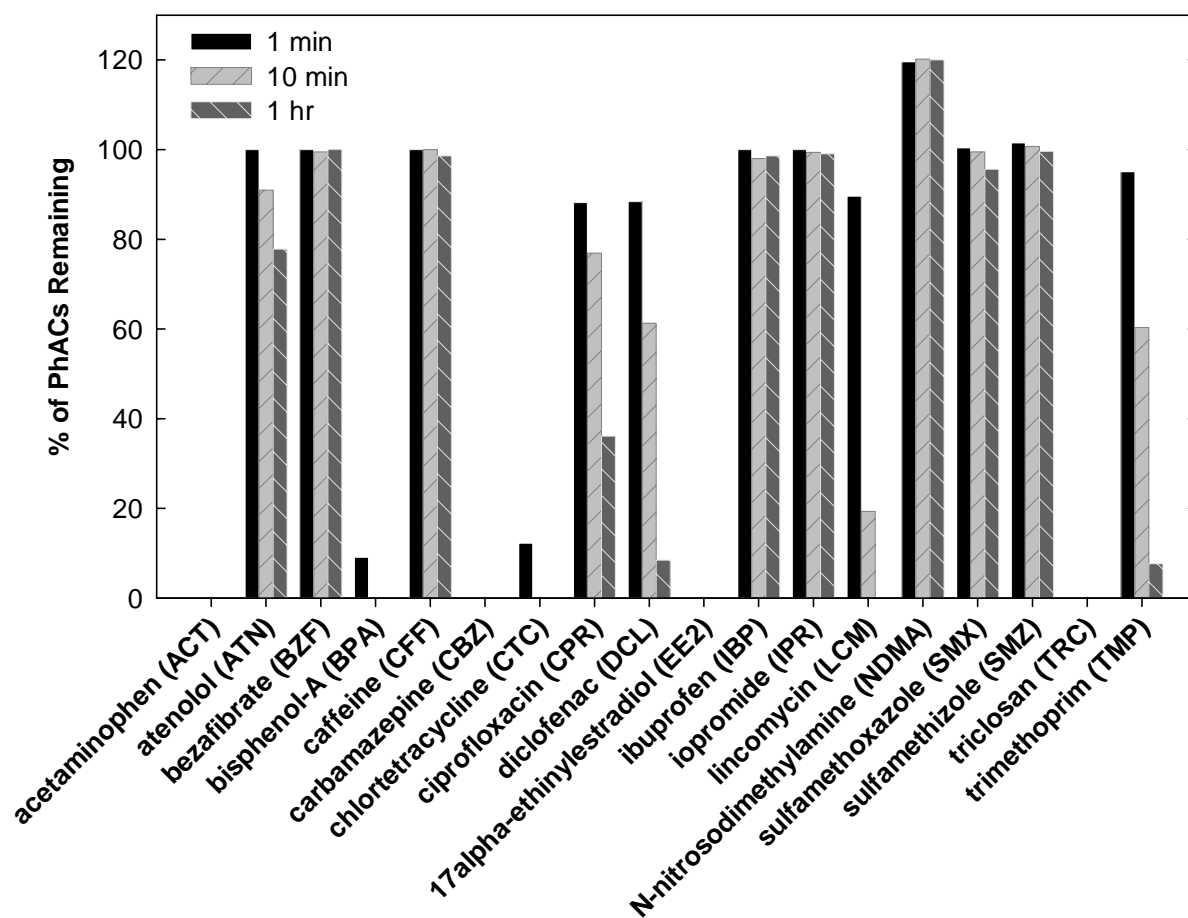
Figure 1.2 Survey results of PhAC reactivity with Mn(VII). Individual bars represent the percent of each PhAC remaining after treatment with Mn(VII) for 1 min, 10 min and 1 h. Reaction conditions: $[Mn(VII)]_0 = 500 \ \mu M$, $[PhAC]_0 = 10 \ \mu M$, 25 ^{o}C, pH 8.0 (10 mM bicarbonate buffer).

Figure 1.3 Survey results of PhAC reactivity with Fe(VI). Individual bars represent the percent of each PhAC remaining in solution after treatment with Fe(VI) for 1 min, 10 min and 1 h. Reaction conditions: $[Fe(VI)]_0 = 100\ \mu M$, $[PhAC]_0 = 10\ \mu M$, $25\ ^oC$, pH = 9.0 (50 mM phosphate + 5 mM borate buffer).

Table 1.1 Occurrence of PhACs surveyed in this study in U.S. streams, groundwater and finished drinking water

Target PhACs (abbreviation)	Surface water[a]			Groundwater[b]		Finished drinking Water[c]
	max. (μg/L)	med. (μg/L)	Detection frequency	max. (μg/L)	Detection frequency	max. (μg/L)
acetaminophen (ACT)	10	0.11	23.8%	0.38	6.4%	
atenolol (ATN)						0.018[69]
bisphenol A (BPA)	12	0.14	41.2%	2.55	29.8%	0.42
caffeine (CFF)	6	0.081	61.9%	0.13	12.8%	0.12
carbamazepine (CBZ)	0.19 [12]		21.6%			0.26
chlortetracycline (CTC)	0.69	0.42	2.4%			
ciprofloxacin (CPR)	0.03	0.02	2.6%			
17α-ethinylestradiol (EE2)	0.83	0.073	15.7%			
ibuprofen (IBP)	1	0.2	9.5%	3.11	2.15%	0.93 [70]
lincomycin (LCM)	0.73	0.06	19.2%	0.32	5.4%	
sulfamethizole (SMZ)	0.13	0.13	1%			
sulfamethoxazole (SMX)	1.9	0.15	19%	1.11	23.4%	0.003 [70]
triclosan (TRC)	2.3	0.14	57.6%			0.73 [69]
trimethoprim (TMP)	0.71	0.15	12.5%			

[a] Data from Kolpin et al. [1] unless otherwise noted. The number of samples analyzed is from 84 to 104 for different PhACs.
[b] Data from Barnes et al. [13] The number of samples analyzed is from 37 to 47 for different PhACs.
[c] Data from Stackelberg et al. [14] unless otherwise noted.

Table 1.2 Reactivity of selected PhACs with common drinking water oxidants[a]

Target PhACs	Ozone O_3 k_2 (M^{-1} s^{-1})	Free chlorine HOCl/OCl$^-$ k_2 (M^{-1} s^{-1})	Chlorine dioxide ClO_2 k_2 (M^{-1} s^{-1})
acetaminophen	3.1×10^6 [35]	1.1×10^2 [43]	
atenolol	2×10^3 [36]	1.3×10^{-2} [32]	
bezafibrate	5.9×10^2 [31]		<0.01 [33]
bisphenol A	1×10^6 [37]	20 [46]	
caffeine	0.7 [40]	1.6×10^2 [47]	
carbamazepine	3×10^5 [31]		<0.015 [33]
ciprofloxacin	1.9×10^4 [38]	7.6×10^5 [34]	
diclofenac	1×10^6 [31]		1×10^4 [33]
17α-ethinylestradiol	7×10^9 [31]	1.1×10^2 [43]	10^5 [33]
ibuprofen	9.6 [31]	negligible [32]	<0.01 [33]
iopromide	<1 [31]		<0.01 [33]
lincomycin	6.6×10^5 [71]		
sulfamethizole		5.6×10^2 [42]	
sulfamethoxazole	2.5×10^6 [31]	1.8×10^3 [44]	1×10^3 [33]
triclosan	3.8×10^7 [41]	4.7×10^2 [48]	
trimethoprim	2.7×10^5 [38]	56 [45]	

[a] k_2: values presented are apparent second-order rate constants at pH 7 and ambient temperature (20-25 ºC). Reaction between free chlorine and caffeine was determined to be second-order with respect to [HOCl] and first order with respect to [caffeine], and the unit of rate constant is M^{-2} s^{-1}.

Table 1.3 Standard reduction potential of Mn(VII) and Fe(VI) compared to other oxidants[a]

Oxidant	Reaction	E^0 (V)
permanganate, Mn(VII)	$MnO_4^- + 4H^+ + 3e^- \rightleftharpoons MnO_{2(s)} + 2H_2O$	1.68
	$MnO_4^- + 2H_2O + 3e^- \rightleftharpoons MnO_{2(s)} + 4OH^-$	0.59
ferrate, Fe(VI)	$FeO_4^{2-} + 8H^+ + 3e^- \rightleftharpoons Fe^{3+} + 4H_2O$	2.20
	$FeO_4^{2-} + 4H_2O + 3e^- \rightleftharpoons Fe(OH)_{3(s)} + 5OH^-$	0.70
ozone	$O_3 + 2H^+ + 2e^- \rightleftharpoons O_2 + H_2O$	2.08
	$O_3 + 2H_2O + 2e^- \rightleftharpoons O_2 + 2OH^-$	1.24
hypochlorite	$HOCl + H^+ + 2e^- \rightleftharpoons Cl^- + H_2O$	1.48
	$OCl^- + H_2O + 2e^- \rightleftharpoons Cl^- + 2OH^-$	0.84
hydrogen peroxide	$H_2O_2 + 2H^+ + 2e^- \rightleftharpoons 2H_2O$	1.78
	$H_2O_2 + 2e^- \rightleftharpoons 2OH^-$	0.88
chlorine dioxide	$ClO_2 + e^- \rightleftharpoons ClO_2^-$	0.95
dissolved oxygen	$O_2 + 4H^+ + 4e^- \rightleftharpoons 2H_2O$	1.23
	$O_2 + 2H_2O + 2e^- \rightleftharpoons 4OH^-$	0.40

[a] Adapted from Sharma (2004)

CHAPTER 2

OXIDATION OF CARBAMAZEPINE BY POTASSIUM PERMANGANATE AND FERRATE: REACTION KINETICS AND MECHANISM[1]

2.1 Abstract

Experimental studies were conducted to examine the oxidation of carbamazepine, an anticonvulsant drug widely detected in surface waters and sewage treatment effluent, by potassium salts of permanganate [$KMnO_4$; Mn(VII)] and ferrate [K_2FeO_4; Fe(VI)]. Results show that both Mn(VII) and Fe(VI) rapidly oxidize carbamazepine by electrophilic attack at an olefinic group in the central heterocyclic ring, leading to ring-opening and a series of organic oxidation products. Reaction kinetics follow a generalized second-order rate law, with apparent rate constants at pH 7.0 and 25 °C of $3.0(\pm0.3)\times10^2$ M^{-1} s^{-1} for Mn(VII) and $70(\pm3)$ M^{-1} s^{-1} for Fe(VI). Mn(VII) reaction rates exhibit no pH dependence, whereas Fe(VI) reaction rates increase dramatically with decreasing pH, due to changing acid-base speciation of Fe(VI). Further studies with Mn(VII) show that most common non-target water constituents, including natural organic matter, have no significant effect on rates of carbamazepine oxidation; reduced metals and (bi)sulfide exert a stoichiometric Mn(VII) demand that can be incorporated into the kinetic model. The removal of carbamazepine in two utility source waters treated with $KMnO_4$ agrees closely with predictions from the kinetic model that was parameterized using experiments conducted in deionized water at much higher reagent concentrations.

2.2 Introduction

Recent studies report widespread occurrence of pharmaceutical compounds in aquatic environments [1-3]. Although most pharmaceuticals are detected at trace levels (ng/L−μg/L), concerns about the effects of long-term exposure on public health and aquatic ecology remain, especially considering unknown synergistic effects of pharmaceutical mixtures [4, 5]. Pomati and co-workers recently reported that growth of human embryonic cells was inhibited by a mixture of

---

pharmaceuticals present in water at environmentally relevant concentrations [5], and others report adverse effects of pharmaceutical mixtures on aquatic microcosms [6]. As a result, there are growing public concerns about the treatment and fate of pharmaceuticals.

Chemical oxidation processes involving permanganate [MnO_4^-; Mn(VII)] and ferrate [FeO_4^{2-}; Fe(VI)] salts are promising technologies for treatment of some pharmaceuticals. Both oxidants exhibit large reduction potentials (E^0_{KMnO4} = +1.68 V, E^0_{K2FeO4} = +2.20 V at acidic conditions) [7], but are considered selective oxidizing agents because their kinetic reactivity with different classes of organic chemicals spans several orders of magnitude [7, 8]. Mn(VII) is already widely used by utilities for control of dissolved manganese, taste/odor/color, and biological growth [9]. Mn(VII) has also been reported to oxidize a wide range of persistent organic contaminants [8]. Fe(VI) is attracting growing attention for several water treatment applications because of the reagent's selective oxidizing properties [7, 10-14]. The instability of Fe(VI) salts has limited their use in field treatment applications, but recent efforts are focused on developing technologies for on-site Fe(VI) generation [15]. Mn(VII) and Fe(VI) are also attractive oxidizing agents because they are nonhalogenating and generate insoluble and environmentally benign reduction products (e.g.,$MnO_{2(s)}$ and $Fe(OH)_{3(s)}$) that can be readily removed through sedimentation/filtration. Furthermore, the $MnO_{2(s)}$ and $Fe(OH)_{3(s)}$ products can act as coagulants and adsorbents to promote physical removal of pharmaceuticals and other constituents of concern (e.g., disinfection byproduct precursors) [7, 11].

Carbamazepine (CBZ) is a widely prescribed anticonvulsant and mood-stabilizing drug that has been detected frequently in treated wastewater effluent and drinking water sources at concentrations up to 6.3 μg/L [2, 4, 16-18]. High effluent concentrations of CBZ result from low removal efficiencies during conventional wastewater treatment; some studies report removal efficiencies for CBZ of only ~7% [2, 16]. It has also been suggested that the CBZ-glucuronide conjugate, a common human metabolite, can also be dissociated back to the parent drug during biological treatment processes [17].
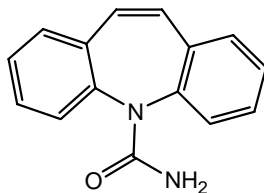
carbamazepine (CBZ)

Earlier contributions have examined oxidative treatment of CBZ with chlorine and chlorine dioxide (both are ineffective) [19], ozone [20], and advanced oxidation processes [21], but information on treatment with Mn(VII) and Fe(VI) is lacking. This contribution describes for the first time the oxidation of CBZ by potassium permanganate and ferrate salts, with a focus on characterizing the pathways and kinetic parameters for CBZ-Mn(VII) and CBZ-Fe(VI) reactions. Because Mn(VII) is widely used by utilities, additional experiments were also conducted with the oxidant to assess the effects of important non-target water constituents (e.g., natural organic matter, dissolved ions), and to compare kinetic model predictions with measurements of CBZ removal during treatment of utility source waters.

2.3 Materials and Methods

2.3.1 Reagents

All solutions were prepared in reagent-grade deionized water (18 MΩ·cm; Barnstead Nanopure system). Unless otherwise indicated, all chemicals were of high purity and were used as received from Sigma-Aldrich-Fluka. Suwannee River natural organic matter (NOM) from a reverse osmosis isolate was obtained from the International Humic Substances Society. Deuterated methanol was obtained from Cambridge Isotope Laboratories. K_2FeO_4 was prepared according to Delaude et al. [22], yielding a material with an iron content that was 98% Fe(VI). Fe(VI) stock solutions were prepared in a 5 mM phosphate/1 mM borate buffer (pH ~9.1) mixture that is reported to stabilize Fe(VI) and slow autodecomposition [23]; stock solutions were used within 30 min of preparation to minimize artifacts from Fe(VI) autodecomposition.

2.3.2 Identification of Reaction Products

To identify reaction products, a series of phosphate-buffered CBZ solutions (100 μM CBZ; pH 7.0) were treated with varying doses of Mn(VII) or Fe(VI) (50−300 μM) for >2 h (tests demonstrated that reactions come to completion within this time). The resulting solutions were then filtered (0.2 μm PTFE) to remove Mn(IV) or Fe(III) (hydr)oxide products, and filtrates were analyzed by liquid chromatography-tandem mass spectrometry (LC-MS/MS) with positive-mode electrospray ionization (ESI[+]). The major final product of CBZ-Mn(VII) reactions was further characterized by proton nuclear magnetic resonance (^{1}H NMR) spectroscopy after concentrating

from a 1 L reaction using a solid phase extraction procedure described below for utility water experiments. Details of analytical procedures are provided in the Section 2.5.

2.3.3 Kinetic Experiments

Batch kinetic experiments were conducted in 0.1 L water-jacketed glass beakers connected to a constant-temperature water bath. Reactions were initiated by spiking excess Mn(VII) or Fe(VI) into pre-equilibrated solutions containing 5 μM CBZ, 25 mM phosphate buffer, and non-target water constituents of interest. Aliquots were then periodically collected and quenched with hydroxylamine (quenching with thiosulfate yielded the same results) before analyzing with high-performance liquid chromatography with photodiode array detection (HPLC-PDA). For kinetic experiments examining the influence of reduced non-target water constituents (Fe^{2+}, Mn^{2+}, HS^-), MOPS buffer was used in place of phosphate because tests showed that metal coordination by phosphate affected reaction rates. It should be noted that MOPS reacts with Mn(VII), but the reaction occurs much more slowly than the CBZ reaction being monitored.

A procedure similar to that described by Lee and coworkers [23] was used to monitor CBZ-Fe(VI) reactions to account for Fe(VI) autodecomposition during individual batch experiments. Fe(VI) concentration was monitored simultaneously with CBZ concentrations by colorimetric analysis [24], and the Fe(VI) exposure ($\int_0^t [Fe(VI)] \cdot dt$) corresponding to each CBZ measurement was calculated (procedure details provided with the results).

2.3.4 Experiments in Utility Source Waters

Experiments were conducted to test the accuracy of the CBZ-Mn(VII) kinetic model in two utility source waters at conditions more relevant to water treatment operations (1−4 mg/L $KMnO_4$, 10 μg/L CBZ). The 10 μg/L initial CBZ concentration was chosen to be closer to ambient concentrations (ng/L to μg/L), but high enough to permit analysis with HPLC-PDA. $KMnO_4$ was dosed into a series of 0.5 L CBZ-amended utility source water samples and allowed to react under constant mixing for a desired time period (1−30 min) before quenching with hydroxylamine. Samples were then filtered (0.45 μm glass fiber) to remove suspended solids and concentrated by solid phase extraction (SPE) with a method adapted from Ternes et al. [25]. Solutions were passed through Oasis HLB SPE cartridges (Waters, 500 mg, LP) at a flow rate of 10 mL/min using a Visiprep vacuum manifold (Sigma-Aldrich). SPE cartridges were sequentially preconditioned

with 3×2 mL hexane, 3×2 mL methanol, 1 mL water, 2 mL of 1 g/L tetramethylammonium hydroxide, and then 5×2 mL water. After extraction, SPE cartridges were dried under a gentle stream of air for one hour. CBZ concentrates were then eluted with 4×1 mL methanol and evaporated to dryness before reconstituting in 1 mL of a 20 mM phosphate buffer (pH 6.0) for analysis. Sulfamethoxazole, which tests showed to be unreactive with Mn(VII), was used as a surrogate standard to account for varying extraction efficiency.

2.4 Results and Discussion

2.4.1 Reaction Products

Experiments demonstrate that CBZ is rapidly oxidized in water by both Mn(VII) and Fe(VI), and reactions yield a number of products detected by LC-MS/MS (**Table 2.1**). For CBZ-Mn(VII) reactions, 12 products were detected, whereas only six were detected for CBZ-Fe(VI) reactions. Most of the analytes have greater molecular weights than CBZ, and are suggestive of oxygen insertion into the structure. In addition, four of the products are shared by Mn(VII) and Fe(VI) reactions, suggesting similar reaction mechanisms. The fact that CBZ oxidation by Fe(VI) yields fewer products might be attributed to higher reactivity of Fe(VI) with some of the products formed initially (e.g., alcohols [7]), which prevents buildup and detection of these analytes in solution. Structures are proposed for each intermediate/product based upon the molecular ion masses and MS/MS fragmentation patterns (MS/MS fragmentation patterns provided in **Table 2.1**; proposed fragmentation pathways provided in **Table 2.2**; mass spectra provided in **Table A.1.** in Appendix A). Comparison of the structures indicates transformation of the olefinic double bond in the central heterocyclic ring to alcohol, aldehyde, ketone, and carboxyl groups, whereas the two outside aromatic rings remain intact. The formation of different products under different Mn(VII) and Fe(VI) dosing is shown in **Table 2.3**.

For four products (II, III, VII, IX) where the proposed structures would result from cyclization reactions [26, 27], e.g.,

(2.1)
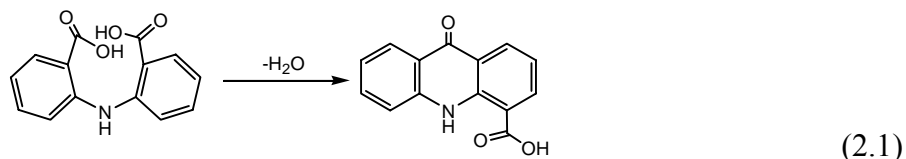
alternative structures consistent with fragmentation patterns can and have been proposed

elsewhere [20, 28]. To confirm the validity of the proposed cyclization products, ^{1}H NMR spectroscopy was used to analyze the structure of III, one of the major final stable products of the CBZ-Mn(VII) reaction. Spectra obtained for the isolated reaction product (**Figure 2.1**) agree closely with spectra collected for an authentic standard of 4-carboxy-9-acridanone, which corresponds to the proposed structure for III.

2.4.2   Proposed CBZ Oxidation Pathways

Reaction pathways for CBZ oxidation by Mn(VII) and Fe(VI) are proposed in **Figure 2.2** and **Figure 2.3** (identified structures indicated with Roman numerals). The proposed pathways for reactions with both oxidants are similar in that reactions are initiated by electrophilic attack at the olefinic double bond on the central heterocyclic ring by Mn(VII) or Fe(VI). There are two possible initiation steps: (a) formation of a cyclic ester through a 3+2 electrocyclic addition of the oxidant to the olefinic bond; or (b) formation of a four-centered organometallic complex from a 2+2 addition to the olefinic bond. Both mechanisms have been reported for alkene oxidation by Mn(VII) [29, 30]. Although, to our knowledge, there are no previous reports addressing the mechanisms of alkene oxidation by Fe(VI), reactions with alcohols have been proposed to be initiated by a 2+2 addition of an Fe=O bond to the α−C−H group [31]. Electron transfer from CBZ to the oxidant then leads to decomposition and hydrolysis to a range of products, including alcohols, aldehydes, and other compounds derived from oxidation of the olefinic carbon atoms. Reaction steps labeled with dashed arrows involve intramolecular cyclization via electrophilic aromatic substitution as illustrated in Equation (2.1) [26, 27]. Intramolecular cyclization of VI to III was previously reported [26, 27]. Several steps also involve hydrolysis of the urea group (−NHCONH$_2$) on the central heterocyclic ring, which is enhanced following oxidation of the olefin group to more electron-withdrawing carbonyl moieties. Acid hydrolysis of phenylurea, having a similar structure with CBZ, has been reported previously [32]. According to the reaction schemes, Mn(VII) and Fe(VI) mediate incomplete oxidation of CBZ to organic byproducts rather than mineralization to inorganic products. This was confirmed by observing no significant decreases in dissolved organic carbon in Mn(VII)- and Fe(VI)-treated CBZ solutions (**Figure 2.4**). The lone nitrogen atom in CBZ also remains intact in all the products identified, indicating no nitrogen mineralization either. Thus, further studies will be needed to assess the effects of CBZ oxidation on pharmaceutical potency and/or toxicity since the parent compound is not mineralized.

2.4.3 Kinetic Parameters for CBZ-Mn(VII) Reactions

Results from experiments designed to measure kinetic parameters of CBZ-Mn(VII) reactions are summarized in **Figure 2.5**. Batch experimental results (e.g., see **Figure 2.5A**) show that CBZ is rapidly oxidized by Mn(VII). For example, ~90 % of CBZ is oxidized by 75 μM Mn(VII) in <2 min. **Figure 2.5A** also shows that CBZ oxidation follows a pseudo-first-order rate law when Mn(VII) concentration is in excess. Measured pseudo-first-order rate constants (k_{obs}, s^{-1}) for all batch experiments are summarized **Table 2.4**. **Figure 2.5B−D** show the effects of Mn(VII) concentration, pH, and temperature on reaction kinetics.

Results in **Figure 2.5B** show that k_{obs} varies linearly with Mn(VII) concentration, demonstrating a first-order dependence on Mn(VII) concentration. Thus, CBZ-Mn(VII) reaction kinetics follow a generalized second order rate law,

$$-\frac{d[CBZ]}{dt} = k_{obs}[CBZ] = k_2[Mn(VII)][CBZ] \qquad (2.2)$$

where k_2 represents the apparent second-order rate constant, which is determined to be equal to $3.0(\pm0.3)\times10^2$ M^{-1} s^{-1} at pH 7.0 and 25 °C (uncertainties ± 1σ). Compared with other water treatment oxidants, Mn(VII) is fairly effective in treating CBZ. Huber and co-workers [19] reported that ClO$_2$ ($k_2 < 0.015$ M^{-1} s^{-1} at pH 7, 20 °C) and Cl$_2$ ($k_2 < 1.5$ M^{-1} s^{-1}; estimated from a reported half-life minimum) both react very slowly with CBZ. At the other end of the spectrum, O$_3$ ($k_2 \approx 3\times10^5$ M^{-1} s^{-1}) and ·OH ($k_2 = 8.8\times10^9$ M^{-1} s^{-1}) oxidize CBZ much more rapidly than Mn(VII) [33]. However, the higher reactivity of these oxidants is balanced by their shorter lifetimes in natural waters; half-lives for O$_3$ and ·OH in water with typical amounts of dissolved organic matter are estimated to be a few minutes and a few microseconds, respectively [34].

Figure 2.5C shows that varying pH has no significant effect on CBZ-Mn(VII) reaction kinetics. The lack of pH dependence is not surprising because neither Mn(VII) nor CBZ possess pK_a values near the pH range examined. This result also demonstrates that minor species of either reactant (e.g., HMnO$_4$, $pK_a = -2.25$ [35]) are not significant contributors to the observed reaction rates.

The temperature dependence shown in Figure 2.5D follows Arrhenius behavior, exhibiting a linear relationship between measured rate constants and the reciprocal of absolute temperature (T):

$$\ln k_2 = \frac{-E_a}{R} \cdot \frac{1}{T} + \ln A \qquad (2.3)$$

where E_a is the apparent activation energy, R is the universal gas constant, and A is the Arrhenius pre-exponential constant. Fitting Equation (2.3) to experimental data yields $E_a = 22(\pm 2)$ kJ/mol. The fit-derived value of E_a falls at the lower end of the range expected for reactions under chemical control, and indicates a rather small temperature dependence [36]. The enthalpic (ΔH^{++}) and entropic (ΔS^{++}) contributions to the activation energy were determined to be 19(± 1) kJ/mol and -140(± 5) J/K/mol, respectively, by fitting the temperature-dependent kinetic data with the Eyring equation [37]:

$$\ln \frac{k_2}{T} = \frac{-\Delta H^{++}}{R} \cdot \frac{1}{T} + \ln \frac{k_B}{h} + \frac{\Delta S^{++}}{R} \qquad (2.4)$$

where k_B is Boltzmann's constant, h is Planck's constant. Activation parameters for the Mn(VII) reaction with trichloroethene (TCE), a compound containing an olefin group as the reaction site, similar to CBZ, were reported to be $E_a = 41.46$ kJ/mol, $\Delta H^{++} = 39$ kJ/mol, and $\Delta S^{++} = -115$ J/K/mol (note: value of ΔS^{++} has been corrected from original reference to correct a calculation error) [30]. The E_a and ΔH^{++} values (variables are directly related) for the CBZ-Mn(VII) reaction are much lower than those reported for the TCE-Mn(VII) reaction, indicating a smaller energy difference between the transition state and the reactants for the former. The large difference in E_a and ΔH^{++} values is also consistent with the large difference in rate constants measured for the two compounds that are believed to react by similar mechanisms (3.0×10^2 M^{-1} s^{-1} for CBZ vs 6.7×10^{-1} M^{-1} s^{-1} for TCE). ΔS^{++} provides information about the level of order in the transition state complex, so the similarity in values for CBZ and TCE reactions is consistent with formation of similar activated complexes with Mn(VII) in the transition state.

2.4.4   Kinetic Parameters for CBZ-Fe(VI) Reactions

In general, CBZ reacts more slowly with Fe(VI) than with an equivalent concentration of Mn(VII). **Figure 2.6A** shows the degradation of both CBZ and Fe(VI) during a typical batch reaction. Although initially present in significant stoichiometric excess, Fe(VI) autodecomposes rapidly at circumneutral pH and cannot be assumed to remain constant during reactions with CBZ [7]. Therefore, a pseudo-first-order rate law is not appropriate for modeling CBZ degradation, and so a different procedure was used to obtain kinetic parameters for CBZ-Fe(VI) reactions. A

second-order rate law Equation (2.5) is assumed for individual batch reactions, as reported previously for Fe(VI) reactions with phenolic hormones [23]:

$$-\frac{d[CBZ]}{dt} = k_2[Fe(VI)][CBZ]$$ (2.5)

An approach described by Lee and co-workers is then used to determine values of k_2 [23]. First, Equation (2.5) is rearranged and d[CBZ]/[CBZ] is integrated to yield the following expression:

$$\ln(\frac{[CBZ]_t}{[CBZ]_0}) = -k_2\int_0^t[Fe(VI)]dt$$ (2.6)

The term $\int_0^t[Fe(VI)]\cdot dt$ is defined as "Fe(VI) exposure", similar to "$C\cdot t$" values commonly used to model disinfection processes where decay of the disinfectant is accounted for during pathogen inactivation studies [23]. Since the variation of Fe(VI) concentration over time is measured, the Fe(VI) exposure corresponding to each measurement of CBZ concentration can be calculated by numerical integration using a trapezoidal method as illustrated in the shadowed area of **Figure 2.6A**. Then, according to Equation (2.6), a plot of $\ln([CBZ]_t/[CBZ]_0)$ versus the corresponding Fe(VI) exposure data should yield a linear correlation with a slope representing k_2 for the batch reaction (**Figure 2.6A** inset). Measured k_2 values for all batch experiments are summarized in **Table 2.5**. The batch reaction shown in **Figure 2.6A** yields $k_2 = 70$ ($\pm$3) M^{-1} s^{-1}. This is roughly 25% of the k_2 value for the CBZ-Mn(VII) reaction at the same pH and temperature. The slower kinetics for CBZ-Fe(VI) reactions are somewhat unexpected but are likely due to the elevated reactivity of Mn(VII) with olefin groups [8, 30]. In general, Fe(VI) is considered a stronger oxidant than Mn(VII) and more reactive with organic compounds at room temperature and circumneutral pH. For example, Fe(VI) oxidizes substituted phenols 2−10 times faster than Mn(VII) at pH7 [8, 23].

Unlike Mn(VII), Fe(VI) reactivity is, in general, highly pH dependent due to the metal's varying acid-base speciation (**Figure 2.6B**) [7]. H_2FeO_4 is a diprotic acid with pK_{a1} of 3.5 and pK_{a2} of 7.3 [7]. The effect of pH on measured k_2 values for CBZ-Fe(VI) reactions is shown in **Figure 2.6C**. Rate constants increase nearly 300-fold when pH decreases from 11 to 6. Since CBZ does not possess a relevant pK_a, the pH dependency can be quantitatively modeled by assuming that individual Fe(VI) species react with CBZ via parallel reactions with independent second-order rate constants:

$$CBZ + H_2FeO_4 \xrightarrow{k_{\alpha1}} Products$$ (2.7)

$$\text{CBZ} + \text{HFeO}_4^- \xrightarrow{\ k_{\alpha2}\ } \text{Products} \tag{2.8}$$

$$\text{CBZ} + \text{FeO}_4^{2-} \xrightarrow{\ k_{\alpha3}\ } \text{Products} \tag{2.9}$$

If equilibrium between Fe(VI) species is maintained (i.e., acid-base reactions are much faster than redox reactions), measured k_2 values are equal to the weighted sum contributions of individual pathways:

$$k_2 = k_{\alpha1}\alpha_1 + k_{\alpha2}\alpha_2 + k_{\alpha3}\alpha_3 \tag{2.10}$$

The Fe(VI) speciation fractions α_1, α_2, and α_3 can be calculated as a function of pH, and the variation of k_2 can be fit with Equation (2.10) to obtain estimates of the individual second-order rate constants. The solid line in **Figure 2.6C** represents the best fit results, where $k_{\alpha2} = 1.4(\pm0.5)\times10^2\ \text{M}^{-1}\,\text{s}^{-1}$, and $k_{\alpha3} = 3.8(\pm1.9) \times 10^{-1}\ \text{M}^{-1}\,\text{s}^{-1}$ (the first term in Equation (2.10) was found to be insignificant, presumably because α_1 is so small over the pH range examined; reactions at pH < 6 cannot be monitored because Fe(VI) rapidly autodecomposes). Dashed lines in **Figure 2.6C** represent the predicted contributions of the individual reaction pathways to the net reactivity of Fe(VI) with CBZ. The fitting result indicates that HFeO_4^- is much more reactive than FeO_4^{2-}, in agreement with a number of previous reports of Fe(VI) reactivity [14, 23, 38]. The protonation of FeO_4^{2-} reduces the electron-donating capacity of the coordinated oxygen ligands, thereby making the metal center more electron deficient and a stronger oxidant [38].

2.4.5   Effect of Non-target Water Constituents on CBZ-Mn(VII) Reactions

Because of its greater reactivity with CBZ and current widespread use by utilities, Mn(VII) reactivity with CBZ was examined further to evaluate the influence of important non-target water constituents and to test the accuracy of a kinetic model for predicting CBZ removal in utility source waters. Batch kinetic studies indicate that high concentrations of most water constituents, including 10 mM Ca^{2+}, Mg^{2+}, HCO_3^-, NH_4^+, and NO_3^-, 20 mg/L $\text{FeOOH}_{(s)}$ and $\text{SiO}_{2(s)}$, and 10−20 mg/L of NOM, have no significant effect on CBZ-Mn(VII) reaction rates (**Table 2.4**). The results are also consistent with the observation of very little or no demand for Mn(VII) of these substances over 60 min measured in separate tests. Although the tested NOM source (Suwannee River) shows no apparent effect, a wider diversity of NOM sources will need to be evaluated to conclude whether or not NOM influences rates of CBZ reactions with Mn(VII) during water treatment.

In contrast to the substances described above, the presence of three reduced species (RS) with known Mn(VII) reactivity, Fe^{2+}, Mn^{2+}, and HS^-, decreases the apparent rate of CBZ oxidation

substantially. **Figure 2.7** show that values of k_{obs} decrease linearly with increasing concentrations of the RS. Furthermore, no differences in k_{obs} measurements are noted when the RS are added simultaneously with CBZ compared to when the RS are added 1 min before adding CBZ. This indicates that Mn(VII) reacts much faster with these substances than with CBZ, and that their net effect on rates of CBZ oxidation can be quantified by assuming an effective concentration of Mn(VII) in the kinetic model, where

$$[Mn(VII)]_{eff} = [Mn(VII)]_{dosed} - [Mn(VII)]_{demand} \tag{2.11}$$

and [Mn(VII)]demand can be estimated using the net stoichiometry of Mn(VII) reacting with individual RS. At pH 7, experiments show that the apparent net stoichiometric demands for Mn(VII) with RS are $\approx 1/3[Fe^{2+}]$, $\approx 2/3[Mn^{2+}]$, and $\approx 2.7/3[HS^-]$. Additional details on the determination of stoichiometric demands are described in the Section 2.5.

2.4.6 Predictive Model for Water Treatment of CBZ

Based on the kinetic parameters obtained for CBZ-Mn(VII) reactions in laboratory solutions, in both the presence and absence of non-target water constituents, the following predictive model was developed to describe CBZ oxidation in natural water:

$$[CBZ] = [CBZ]_0 \exp\left\{ -k_{2,298K} \exp\left[\frac{-E_a}{R}\left(\frac{1}{T} - \frac{1}{298} \right) \right] [Mn(VII)]_{eff}\, t \right\} \tag{2.12}$$

where $k_{2\,(298K)} = 3.0\times10^2$ M^{-1} s^{-1}, $E_a = 22$ kJ/mol, and [Mn(VII)]$_{eff}$ is determined according to Equation (2.11). However, [Mn(VII)]$_{eff} \approx$ [Mn(VII)]$_{dosed}$ for surface water sources where RS are typically present at only very low concentrations. Equation (2.12) assumes that [Mn(VII)]$_{eff}$ is in large excess of CBZ, which is typical of utilities where permanganate is used. The model can be used to estimate CBZ removal in existing water treatment utilities or Mn(VII) dosing required to meet a specific treatment objective.

The accuracy of Equation (2.12) was tested for treatment of two drinking water utility source waters amended with 10 μg/L CBZ. The two utilities use surface water reservoirs as sources with similar water quality characteristics (**Table 2.6**). Results presented in **Figure 2.8** show generally good agreements between model predictions and measurements of CBZ removal during treatment with 1−4 mg/L KMnO$_4$. Both measurements and model prediction show >95% CBZ treatment is achieved within 30 min when the source waters are treated with 2 mg/L KMnO$_4$ (**Figure 2.8A**).The degree of CBZ treatment achieved for a reaction time of 10 min increases with

increasing KMnO$_4$ dose (**Figure 2.8B**), and model predictions fall within one standard deviation of the measured values. Thus, these results indicate that Equation (2.12), which was developed from "clean system" laboratory experiments using high reagent concentrations, can be used to estimate CBZ removal during permanganate treatment processes at water utilities.

2.5 Supporting Information

2.5.1 Details of Analytical Procedures

CBZ concentrations during kinetic studies were determined by high-performance liquid chromatography-photodiode array (HPLC-PDA) detection (Shimadzu AVP system). A Novapak C18 column (3.9×150 mm, 4 μm particle size) was used as the stationary phase, and a mobile phase with 25% acetonitrile/75% aqueous buffer (10 mM hydroxylamine, pH 6) was used with an isocratic flow rate of 1 mL/min. Dissolved organic carbon (DOC) measurements of Mn(VII)- and Fe(VI)-treated CBZ solutions was carried out using a Phoenix 8000 TOC analyzer (Tekmar-Dohrmann, Cincinnati, OH).

Mn(VII) and Fe(VI) concentrations were determined spectrophotometrically using a double-beam spectrophotometer (Shimadzu UV-2401PC). The concentration of Mn(VII) stock solutions was verified by direct absorbance measurement at λ = 525 nm (ε = 2460 M^{-1} cm^{-1}) [8]. Fe(VI) concentration was determined colorimetrically by measuring the absorbance of Fe(VI)-oxidized 2,2'-azino-bis(3-ethylbenzothiazoline-6-sulfonate) (ABTS) at λ = 415 nm (ε = 34000 M^{-1} cm^{-1}), according to a procedure described by Lee et al. [24].

Reaction products were identified by liquid chromatography-tandem mass spectrometry (LC-MS/MS) analysis performed on a Thermo Finnigan LCQ DecaXP system outfitted with a Thermo Surveyor HPLC. Separation was accomplished using an Agilent C-18 column (Zorbax, Eclipse XDB-C18, 2.1×150 mm, 3.5 μm particle size). A gradient method with a flow rate of 0.2 mL/min was used with two mobile phases (A: 95% H$_2$O/5% acetonitrile/0.1% formic acid; B: 5% water/95% acetonitrile/0.1% formic acid). Phase A was maintained at 100% for the first 3 min, then the percentage of phase B was linearly increased to 25% during the next 12 min, then to 50% during the following 40 min. MS analyses were conducted in positive mode electrospray ionization (ESI$^+$) over a mass-to-charge (m/z) range from 50–800, and a quadruple ion trap MS was used to separate ions with varying m/z values. Further fragmentation of selected ions was

achieved through collision-induced dissociation (CID), with an oscillating radiofrequency alternating current voltage of 31 V. No quantification of individual products was completed at this time because reference standards are not available for most of the identified compounds.

A proton nuclear magnetic resonance (^{1}H-NMR) spectrum for the major final product of CBZ-Mn(VII) reactions (product III in **Table 2.1**) was acquired with a Varian Unity 400 MHz instrument, in a 5 mm Nalorac QUAD probe, after dissolving in deuterated methanol. Chemical shifts (δ) are reported in ppm and referenced to residual protonated methanol at $\delta = 3.34$ ppm. General parameters for the one-pulse experiments at ambient temperature were a 4300 Hz spectral width, 64 scans, a 90° pulse width, and 18K data points. Data processing was performed with NUTS software (Acorn NMR) with line broadening of no more than 0.3 Hz and zero filling to 32K points. The spectrum of the final product was compared against the spectrum of a reference standard of 4-carboxy-9-acridaone.

Water quality characteristics for source waters obtained from surface reservoirs used by two central Illinois drinking water utilities were determined using standard methods of analysis. Source water pH was measured using an Orion 3-star plus benchtop pH meter following a 3 point calibration (pH 4, 7, and 10). Alkalinity was determined by titrating source water samples to pH 4.5 using a standardized 0.01 N nitric acid solution. The permanganate demand of the source waters was determined after adjusting solutions to pH 7 and dosing with 4 mg/L of $KMnO_4$, then measuring the residual Mn(VII) concentrations spectrophotometrically as a function of exposure time. Total dissolved solids (TDS) was determined gravimetrically after evaporating 1 L of filtered water (0.7 μm, Millipore glass fiber, 90 mm diameter) and drying the resulting residue at 105 ºC for >1 h and cooling in a desiccator. Total suspended solids (TSS) was determined by weighing the filters after drying overnight at 103-105 ºC and cooling in a desiccator. Total organic carbon (TOC) analysis was conducted using a Phoenix 8000 TOC analyzer (Tekmar-Dohrmann, Cincinnati, OH). Standardized potassium biphthalate solutions (Aqua solutions, Deer Park, TX) were used to prepare reference TOC standards. Ammonium concentrations were determined using the colorimetric nesslerization method (HACH Method 8038). Briefly, samples were derivatized using Nessler reagents and absorbance was measured at $\lambda = 254$ nm. Concentrations of inorganic anions (nitrate, chloride, and sulfate) were determined by ion chromatography using a Dionex ICS-2000 system equipped with a conductivity detector. An IonPac AS18 anion-exchange column (4×250 mm with 7.5 μm particle size) was used with a mobile phase containing 36 mM KOH

operated at a flow rate of 1.0 mL/min.

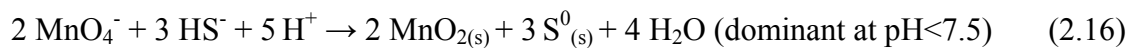## 2.5.2 Effects of Reduced Species on Reaction Kinetics

The presence in solution of reduced inorganic species, Fe^{2+}, Mn^{2+}, and HS^-, decreases the apparent rate of CBZ oxidation substantially. **Figure 2.7** shows that measured values of k_{obs} for CBZ reacting with a 75 µM dose of Mn(VII) decrease linearly with increasing concentrations of each reduced species (RS). Tests also show no differences in k_{obs} when the RS are added to the Mn(VII) solution either simultaneously with CBZ or 1 minute prior to introducing CBZ, indicating that the RS react much faster than CBZ. As a result, the net effect of RS on rates of CBZ oxidation can be quantified by assuming an effective concentration, rather than dosed concentration, of Mn(VII) when making kinetic model predictions, where:

$$[Mn(VII)]_{eff} = [Mn(VII)]_{dosed} - [Mn(VII)]_{demand} \qquad (2.13)$$

$[Mn(VII)]_{demand}$ can be estimated for waters for which concentrations of individual RS are known using the net stoichiometric demand ratios for individual RS reacting with Mn(VII) at the conditions under consideration. The net stoichiometric demand ratios can be calculated by comparing the second-order rate constant for CBZ-Mn(VII) reactions ($300\ M^{-1}\ s^{-1}$) with the slopes obtained from the plots of k_{obs} versus concentration of individual RS (**Figure 2.7**). The ratio between these two numbers is indicative of the stoichiometric coefficient between Mn(VII) and the RS because the first-order rate constant for CBZ-Mn(VII) reactions is linearly dependent on Mn(VII) concentration remaining after reaction with RS and thus is negatively related to Mn(VII) concentration consumed by RS. Using this approach, the estimated net stoichiometric demand ratios for Mn(VII) reacting with Fe^{2+} is ($94/300 \approx 1/3$) and for Mn(VII) reacting with Mn^{2+} is ($175/300 \approx 2/3$) from data in **Figure 2.7**, consistent with the following reaction stoichiometries:

$$2\ MnO_4^- + 3\ Mn^{2+} + 2\ H_2O \rightarrow 5\ MnO_{2(s)} + 4\ H^+ \qquad (2.14)$$

$$MnO_4^- + 3\ Fe^{2+} + 7\ H_2O \rightarrow MnO_{2(s)} + 3\ Fe(OH)_{3(s)} + 5\ H^+ \qquad (2.15)$$
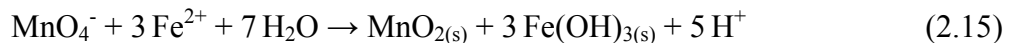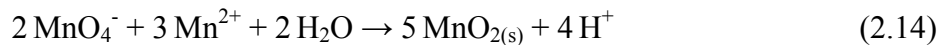
The effect of HS^- is more complex since the stoichiometric ratio between HS^- and Mn(VII) is known to vary from 2:3 to 8:3 depending on solution conditions (e.g., pH, exposure to oxygen). A combination of the following reactions can occur [39]:

$$2\ MnO_4^- + 3\ HS^- + 5\ H^+ \rightarrow 2\ MnO_{2(s)} + 3\ S^0_{(s)} + 4\ H_2O \text{ (dominant at pH<7.5)} \qquad (2.16)$$

$$8\ MnO_4^- + 3\ HS^- \rightarrow 8\ MnO_{2(s)} + 3\ SO_4^{2-} + 5\ OH^- \text{ (dominant at pH>7.5)} \qquad (2.17)$$
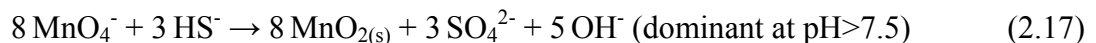
The observed slope in **Figure 2.7** for HS^- indicates a net stoichiometric demand ratio of 2.7/3

(267/300) for Mn(VII) reacting with HS⁻, indicating the occurrence of both Equation (2.16) and (2.17), but a likely predominance of Equation (2.16) under conditions examined (pH 7.0), in agreement with expectations from the reported pH criteria.

2.6 References Cited

[1]   Kolpin D. W., Furlong E. T., Meyer M. T., Thurman E. M., Zaugg S. D., Barber L. B. and Buxton H. T. Pharmaceuticals, hormones, and other organic wastewater contaminants in US streams, 1999-2000: A national reconnaissance. *Environmental Science & Technology*, **2002**, 36: 1202-1211.

[2]   Ternes T. A. Occurrence of drugs in German sewage treatment plants and rivers. *Water Research*, **1998**, 32: 3245-3260.

[3]   Tixier C., Singer H. P., Oellers S. and Muller S. R. Occurrence and fate of carbamazepine, clofibric acid, diclofenac, ibuprofen, ketoprofen, and naproxen in surface waters. *Environmental Science & Technology*, **2003**, 37: 1061-1068.

[4]   Daughton C. G. and Ternes T. A. Pharmaceuticals and personal care products in the environment: Agents of subtle change? *Environmental Health Perspectives*, **1999**, 107: 907-938.

[5]   Pomati F., Castiglioni S., Zuccato E., Fanelli R., Vigetti D., Rossetti C. and Calamari D. Effects of a complex mixture of therapeutic drugs at environmental levels on human embryonic cells. *Environmental Science & Technology*, **2006**, 40: 2442-2447.

[6]   Richards S., Wilson C., Johnson D., Castle D., Lam M., Mabury S., Sibley P. and Solomon K. Effects of pharmaceutical mixtures in aquatic microcosms. *Environmental Toxicology and Chemistry*, **2004**, 23: 1035-1042.

[7]   Sharma V. K. Potassium ferrate(VI): an environmentally friendly oxidant. *Advances in Environmental Research*, **2002**, 6: 143-156.

[8]   Waldemer R. H. and Tratnyek P. G. Kinetics of contaminant degradation by permanganate. *Environmental Science & Technology*, **2006**, 40: 1055-1061.

[9]   *MWH Water Treatment: Principles and Design*, 2nd ed. Hoboken: Wiley, **2005**.

[10]   Jiang J. Q. Research progress in the use of ferrate(VI) for the environmental remediation. *Journal of Hazardous Materials*, **2007**, 146: 617-623.

[11]   Jiang J. Q. and Lloyd B. Progress in the development and use of ferrate(VI) salt as an

oxidant and coagulant for water and wastewater treatment. *Water Research*, **2002**, 36: 1397-1408.

[12] Sharma V. K. Disinfection performance of Fe(VI) in water and wastewater: A review. *Water Science and Technology*, **2007**, 55: 225-232.

[13] Sharma V. K., Li X. Z., Graham N. and Doong R. A. Ferrate(VI) oxidation of endocrine disruptors and antimicrobials in water. *Journal of Water Supply Research and Technology-Aqua*, **2008**, 57: 419-426.

[14] Sharma V. K., Mishra S. K. and Nesnas N. Oxidation of sulfonamide antimicrobials by ferrate(VI) [$Fe^{VI}O_4^{2-}$]. *Environmental Science & Technology*, **2006**, 40: 7222-7227.

[15] Licht S. and Yu X. W. Electrochemical alkaline Fe(VI) water purification and remediation. *Environmental Science & Technology*, **2005**, 39: 8071-8076.

[16] Heberer T. Tracking persistent pharmaceutical residues from municipal sewage to drinking water. *Journal of Hydrology*, **2002**, 266: 175-189.

[17] Ikehata K., Naghashkar N. J. and Ei-Din M. G. Degradation of aqueous pharmaceuticals by ozonation and advanced oxidation processes: A review. *Ozone: Science & Engineering*, **2006**, 28: 353-414.

[18] Ternes T. A. Analytical methods for the determination of pharmaceuticals in aqueous environmental samples. *Trac-Trends in Analytical Chemistry*, **2001**, 20: 419-434.

[19] Huber M. M., Korhonen S., Ternes T. A. and von Gunten U. Oxidation of pharmaceuticals during water treatment with chlorine dioxide. *Water Research*, **2005**, 39: 3607-3617.

[20] McDowell D. C., Huber M. M., Wagner M., von Gunten U. and Ternes T. A. Ozonation of carbamazepine in drinking water: Identification and kinetic study of major oxidation products. *Environmental Science & Technology*, **2005**, 39: 8014-8022.

[21] Vogna D., Marotta R., Andreozzi R., Napolitano A. and d'Ischia M. Kinetic and chemical assessment of the UV/H_2O_2 treatment of antiepileptic drug carbamazepine. *Chemosphere*, **2004**, 54: 497-505.

[22] Delaude L. and Laszlo P. A novel oxidizing reagent based on potassium ferrate(VI). *Journal of Organic Chemistry*, **1996**, 61: 6360-6370.

[23] Lee Y., Yoon J. and von Gunten U. Kinetics of the oxidation of phenols and phenolic endocrine disruptors during water treatment with ferrate (Fe(VI)). *Environmental Science & Technology*, **2005**, 39: 8978-8984.

[24] Lee Y., Yoon J. and von Gunten U. Spectrophotometric determination of ferrate (Fe(VI)) in water by ABTS. *Water Research*, **2005**, 39: 1946-1953.

[25] Ternes T. A., Hirsch R., Mueller J. and Haberer K. Methods for the determination of neutral drugs as well as betablockers and β_2-sympathomimetics in aqueous matrices using GC/MS and LC/MS/MS. *Fresenius Journal of Analytical Chemistry*, **1998**, 362: 329-340.

[26] Atwell G. J., Cain B. F., Baguley B. C., Finlay G. J. and Denny W. A. Potential antitumor agents .43. Synthesis and biological-activity of dibasic 9-aminoacridine-4-carboxamides, a new class of antitumor agent. *Journal of Medicinal Chemistry*, **1984**, 27: 1481-1485.

[27] Dzierzbicka K. and Kolodziejczyk A. M. Synthesis and antitumor activity of conjugates of muramyldipeptide or normuramyldipeptide with hydroxyacridine/acridone derivatives. *Journal of Medicinal Chemistry*, **2003**, 46: 183-189.

[28] Chiron S., Minero C. and Vione D. Photodegradation processes of the antiepileptic drug carbamazepine, relevant to estuarine waters. *Environmental Science & Technology*, **2006**, 40: 5977-5983.

[29] Strassner T. and Busold M. A density functional theory study on the mechanism of the permanganate oxidation of substituted alkenes. *Journal of Organic Chemistry*, **2001**, 66: 672-676.

[30] Yan Y. E. and Schwartz F. W. Kinetics and mechanisms for TCE oxidation by permanganate. *Environmental Science & Technology*, **2000**, 34: 2535-2541.

[31] Lee D. G. and Gai H. F. Kinetics and mechanism of the oxidation of alcohols by ferrate ion. *Canadian Journal of Chemistry-Revue Canadienne De Chimie*, **1993**, 71: 1394-1400.

[32] Oconnor J. and Barnett J. W. Acid-hydrolysis of phenylurea, 4-fluorophenylurea, and 3-methylphenylurea. *Journal of the Chemical Society-Perkin Transactions 2*, **1973**: 1457-1461.

[33] Huber M. M., Canonica S., Park G. Y. and von Gunten U. Oxidation of pharmaceuticals during ozonation and advanced oxidation processes. *Environmental Science & Technology*, **2003**, 37: 1016-1024.

[34] Westerhoff P., Aiken G., Amy G. and Debroux J. Relationships between the structure of natural organic matter and its reactivity towards molecular ozone and hydroxyl radicals. *Water Research*, **1999**, 33: 2265-2276.

[35] Wiberg E., Wiberg N. and Holleman A. F. *Inorganic chemistry*, 1st ed. New York:

Academic Press, **2001**.

[36]   Levine I. N. *Physical Chemistry*: McGraw-Hill, **1978**.

[37]   Eyring H. The activated complex in chemical reactions. *Journal of Chemical Physics*, **1935**, 3: 107-115.

[38]   Sharma V. K., Smith J. O. and Millero F. J. Ferrate(VI) oxidation of hydrogen sulfide. *Environmental Science & Technology*, **1997**, 31: 2486-2491.

[39]   Walton J., Labine P. and Reidies A. In: Eckenfelder W W, Bowers A R and Roth J A, eds. *Chemical Oxidation: Technologies for the Nineties*: CRC Press **1997**:214.

2.7 Figures and Tables
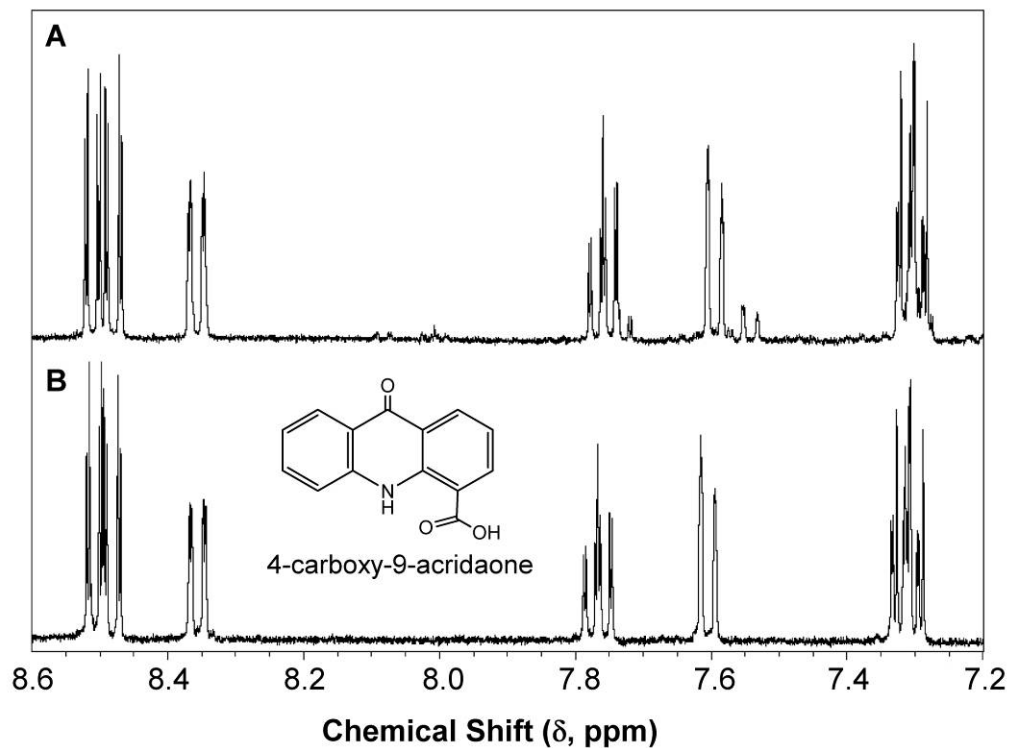
Figure 2.1. Aromatic region of 1H-NMR spectra of (A) isolated final product from CBZ-Mn(VII) reaction, and (B) 4-carboxy-9-acridanone reference standard. The spectra agree closely, with the exception of a few additional small peaks in the sample isolated from the reaction mixture, which are presumed to be due to impurities in the solid phase extract.
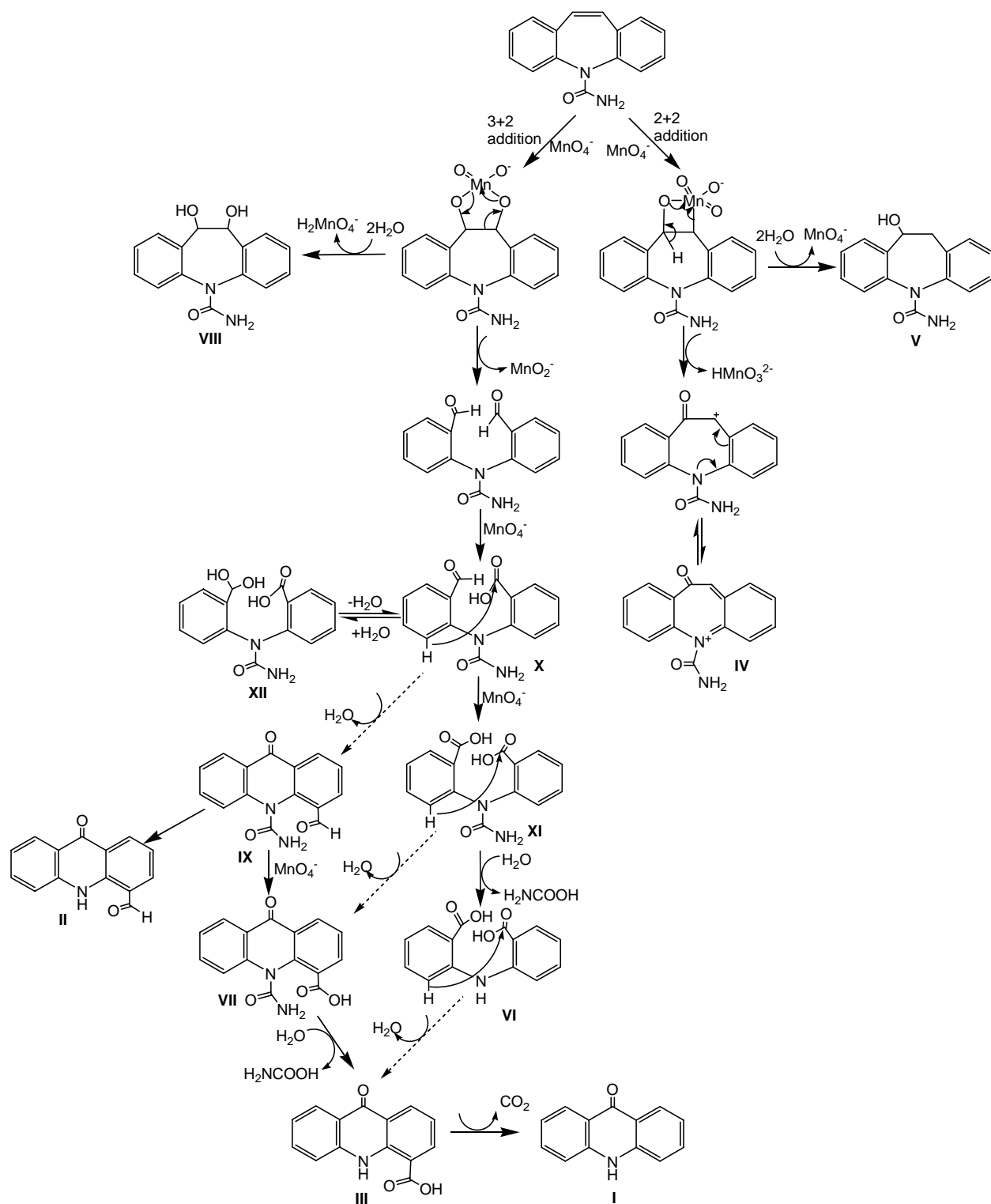
Figure 2.2. Reaction pathways for CBZ oxidation by Mn(VII).
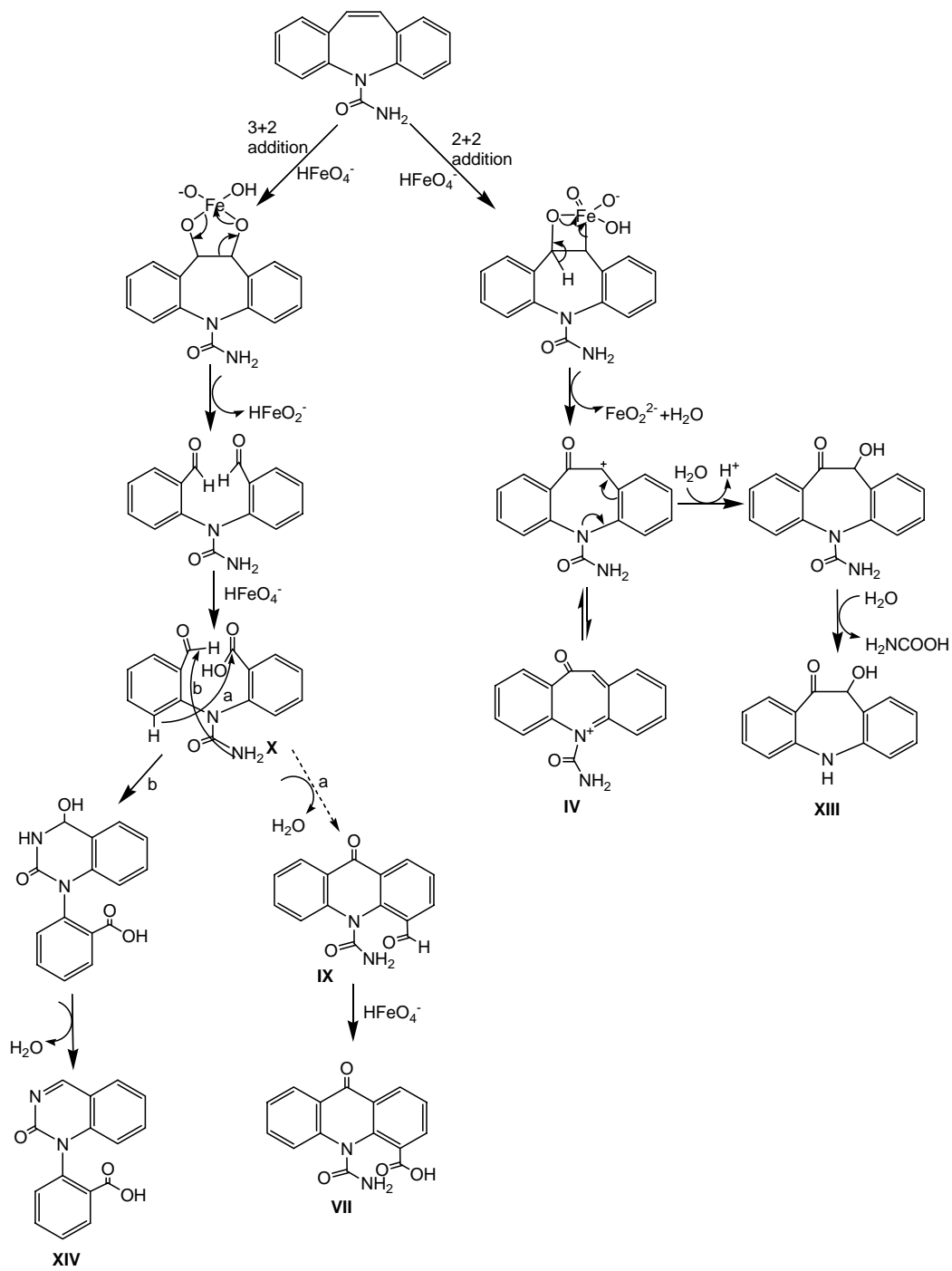
Figure 2.3. Reaction pathways for CBZ oxidation by Fe(VI).
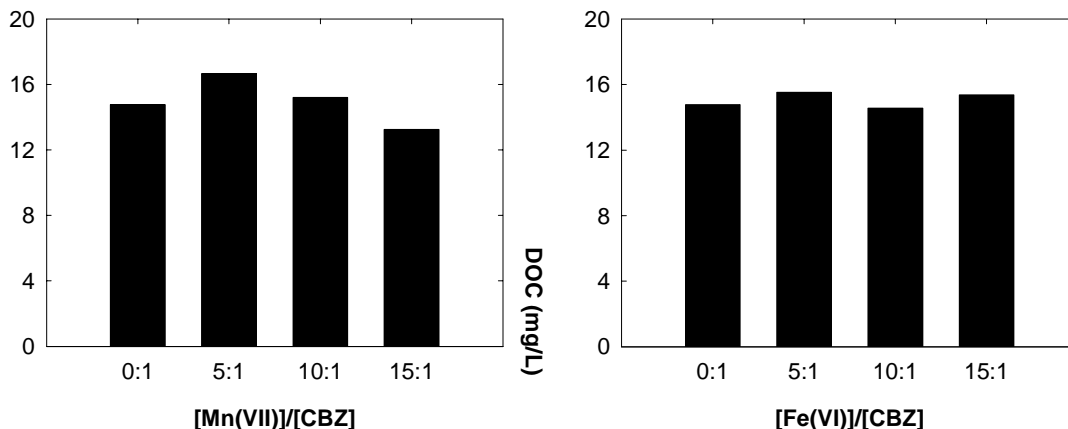
Figure 2.4. Dissolved organic carbon remaining in CBZ solutions following treatment with Mn(VII) and Fe(VI). Reaction condition: $[CBZ]_0 = 80$ μM, varying [Mn(VII)] and [Fe(VI)], pH 7.0 (25 mM phosphate buffer), 25 °C. Reactions were allowed to run for >10 h to reach completion before filtering (0.2 μm PTFE) and analyzing.
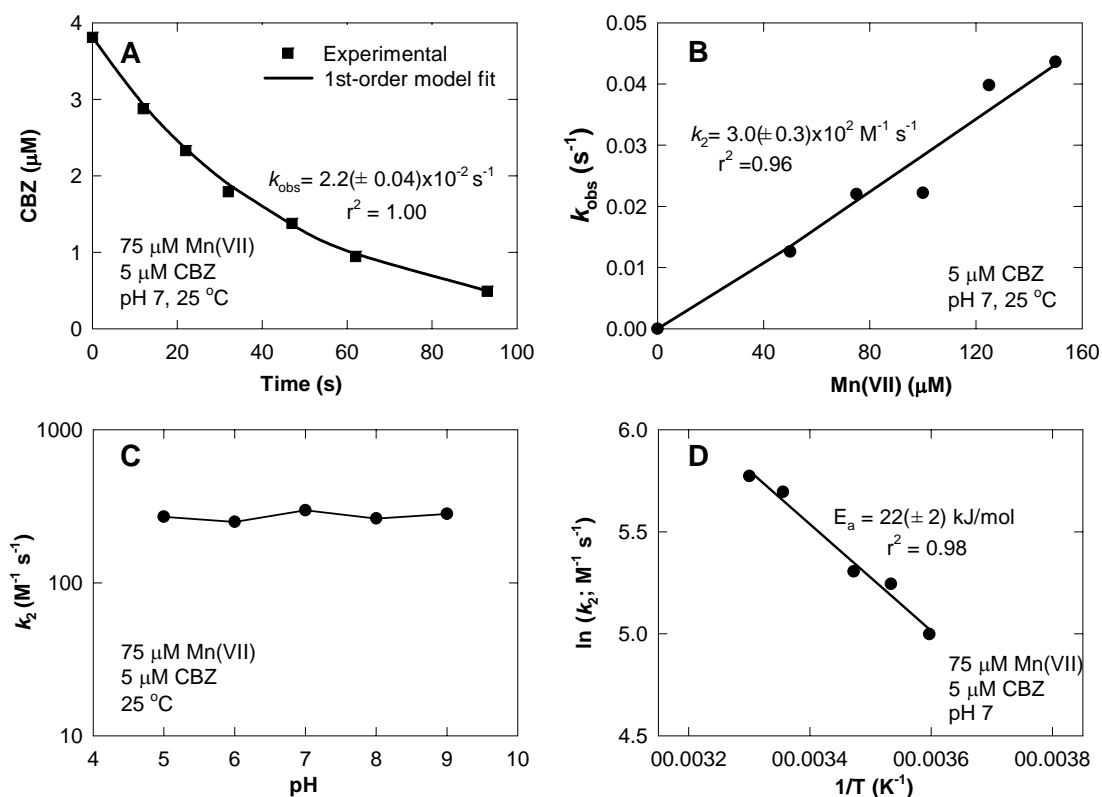
Figure 2.5. Kinetics of CBZ oxidation by Mn(VII). (A) Results from a typical batch reaction, (B) effect of Mn(VII) concentration, (C) effect of pH, and (D) effect of temperature.
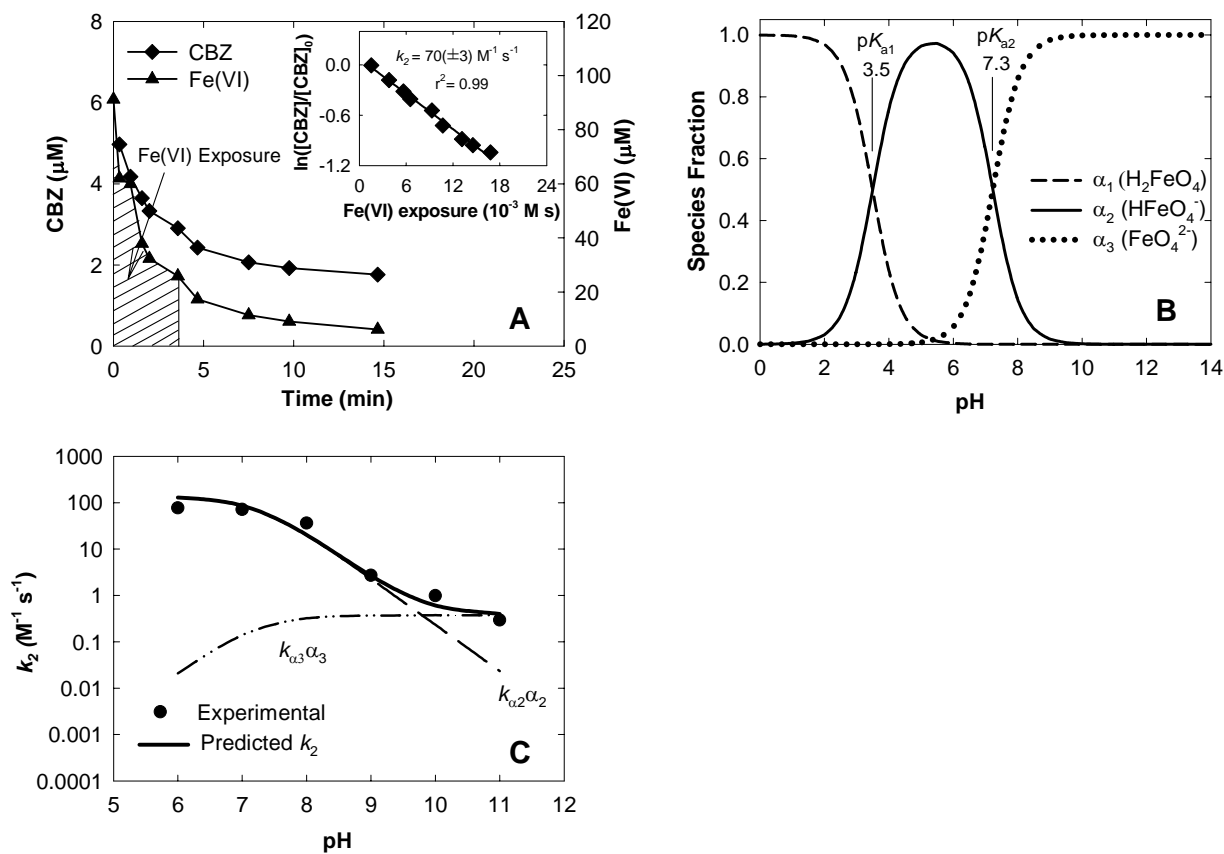
Figure 2.6. Kinetics of CBZ-Fe(VI) reactions. (A) CBZ and Fe(VI) degradation in a batch reaction ([CBZ]$_0$ = 5 μM, [Fe(VI)]$_0$ = 100 μM, pH 7, 25 mM phosphate buffer, 25 °C). Inset shows fit of batch kinetic data from panel A using Equation (2.6), (B) calculated Fe(VI) speciation versus pH, (C) effect of pH on rate constants for CBZ-Fe(VI) reactions and associated model fit (pH 6−11, [CBZ]$_0$ = 5 μM, [Fe(VI)]$_0$ = 100 μM, 25 mM phosphate buffer (+5 mM borate buffer for pH 9−11 at 25 °C). The solid line in panel C depicts the model fit results, and dashed lines show predicted contributions of reactions with HFeO$_4^-$ and FeO$_4^{2-}$ to the overall k_2 values measured at different pH conditions.
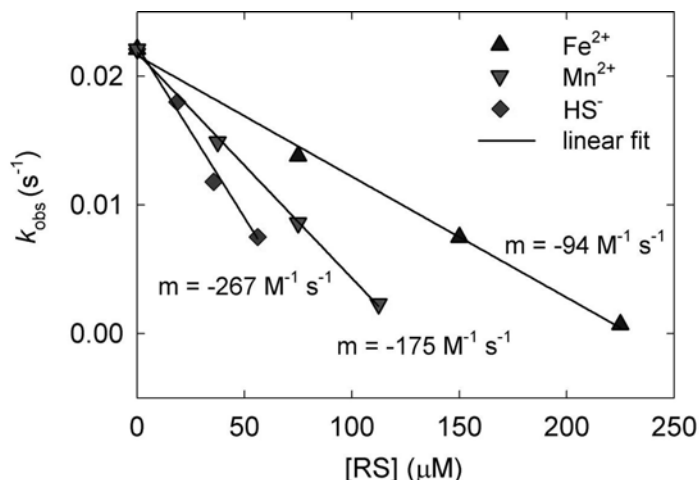
**Figure 2.7. Effect of reduced species (RS) on the rate of CBZ oxidation by Mn(VII).
Reaction Conditions: $[CBZ]_0 = 5$ μM, $[Mn(VII)]_{dosed} = 75$ μM, pH 7.0 (1 mM MOPS buffer),
25 °C.**
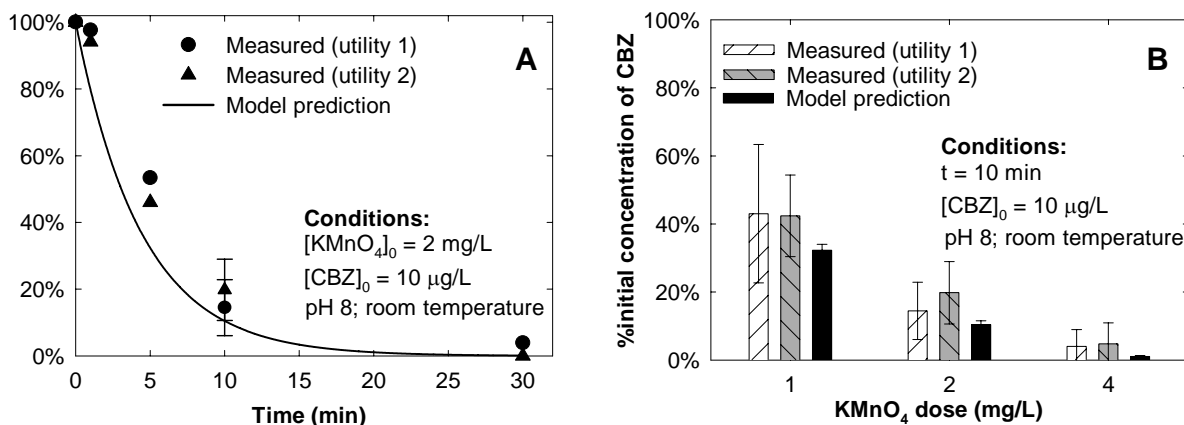
**Figure 2.8. Comparison of kinetic model predictions and measured removal of CBZ during
treatment of utility source waters with KMnO$_4$: (A) Removal of CBZ as a function of time
in source waters treated with 2 mg/L KMnO$_4$; (B) Removal of CBZ after 10 min in source
waters dosed with different concentrations of KMnO$_4$. CBZ concentrations reported
relative to Mn(VII)-free control samples, where negligible CBZ degradation is observed.
Uncertainties indicated by 1 SD provided when replicate samples measured.**

Table 2.1. Reaction products detected by LC-MS/MS during CBZ-Mn(VII) and CBZ-Fe(VI) reactions
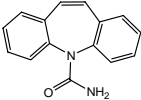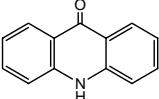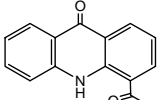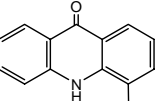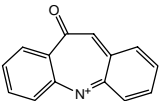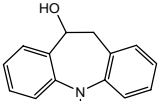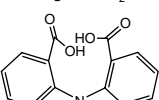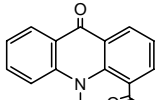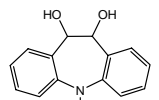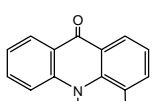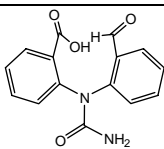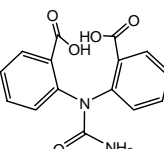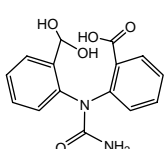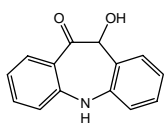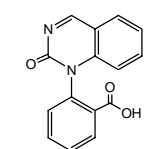
Product ID	ESI(+) MS m/z [a]	ESI (+) MS^2 m/z	Proposed Structure	Product of Mn(VII)[b]	Product of Fe(VI)[b]
CBZ	237	237, 220, 194[c]			
I	196	n.d.[d]		√	
II	224	196[c]		√	
III[e]	240	240, 222[c]		√	
IV	251	251[c], 223, 208, 180		√	√
V	255	237[c], 219, 195, 167		√	
VI	258	240[c], 222, 196		√	
VII	267	250, 239, 224[c], 196		√	√
VIII	271	253[c], 210		√	
IX	283	265[c], 240, 222, 196		√	√

Table 2.1. (cont.)

Product ID	ESI(+) MS m/z [a]	ESI (+) MS^2 m/z	Proposed Structure	Product of Mn(VII)[b]	Product of Fe(VI)[b]
X	285	267[c], 239, 224, 196		√	√
XI	301	283, 258[c], 240		√	
XII	303	285[c], 267		√	
XIII	226	208[c], 198, 180			√
XIV	267	249[c], 221			√

[a] m/z values shown are for protonated molecular ions (M+H)$^+$.

[b] Table 2.3 lists the [Mn(VII)]/[CBZ] and [Fe(VI)]/[CBZ] ratios where individual products were detected.

[c] indicates the most abundant fragment ion.

[d] no MS/MS spectrum for this compound is obtained because this is a minor product and is not selected by the instrument to proceed to further fragmentation.

[e] proposed structure confirmed by ^{1}H-NMR.

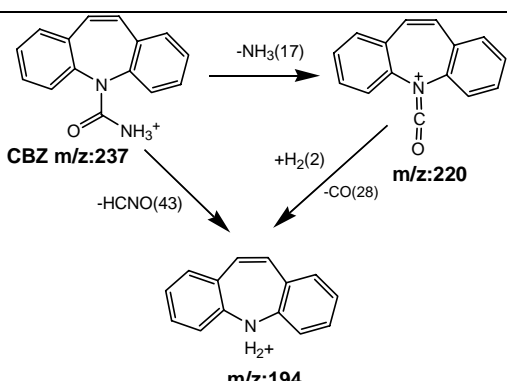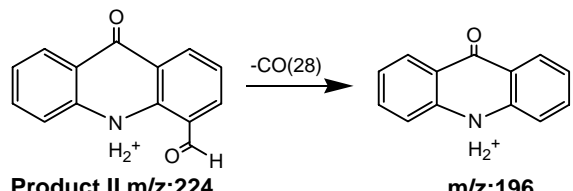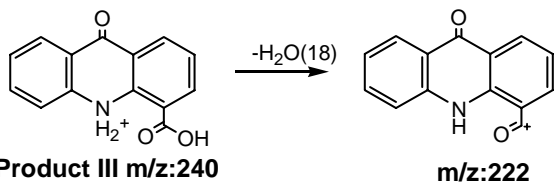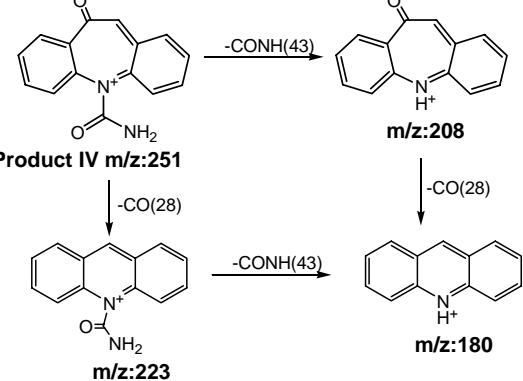**Table 2.2. ESI(+) MS/MS spectra and structural interpretation of reaction products**

Product	Fragmentation Pathways
CBZ	
II	
III	
IV	
V	

Table 2.2. (cont.)

Product	Fragmentation Pathways

VI

Product VI m/z:258 → -H₂O(18) → m/z:240

$-H_2O(18)$, $-CO(28)$, $-CO_2(44)$, $-H_2O(28)$

m/z:222, m/z:196

VII

Product VII m/z:267

$-CONH(43)$, m/z:224, $-NH_3(17)$, m/z:250

$-CO(28)$, m/z:196, $-CO(28)$, m/z:239, $-CONH(43)$

VIII

Product VIII m/z:271 → $-H_2O(18)$ → m/z:253 → $-CONH(43)$ → m/z:210

IX

Product IX m/z:283 → $-H_2O(18)$ → m/z:265

$-CONH$, $-CONH(43)$, $-CO_2(44)$, $-H_2O(18)$

m/z:196, m/z:240, m/z:222

Table 2.2. (cont.)
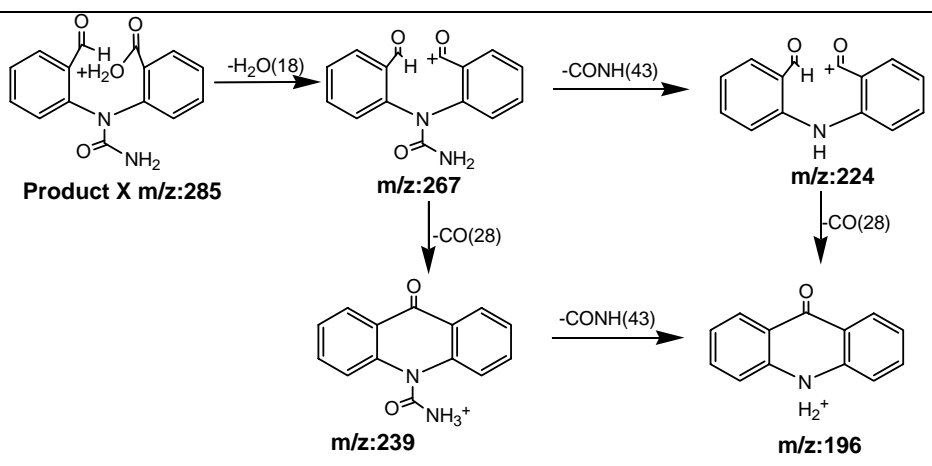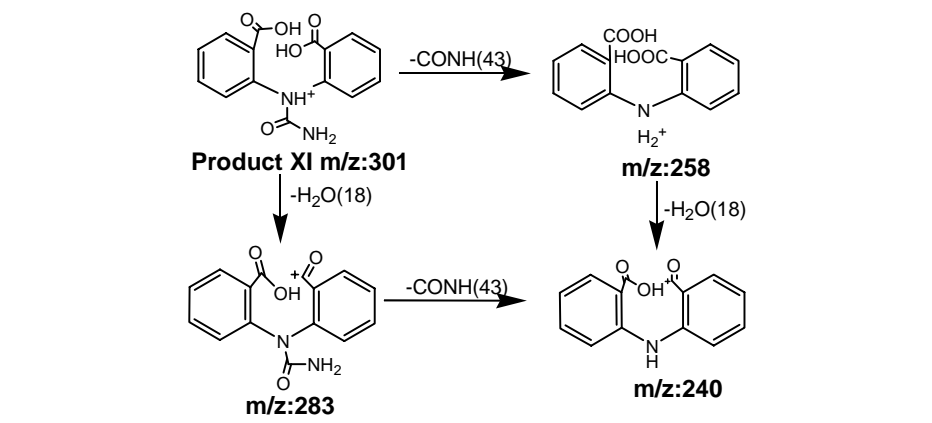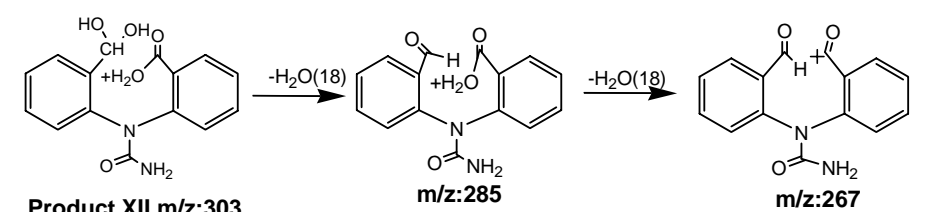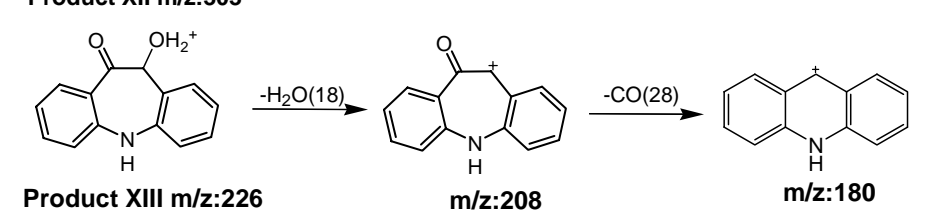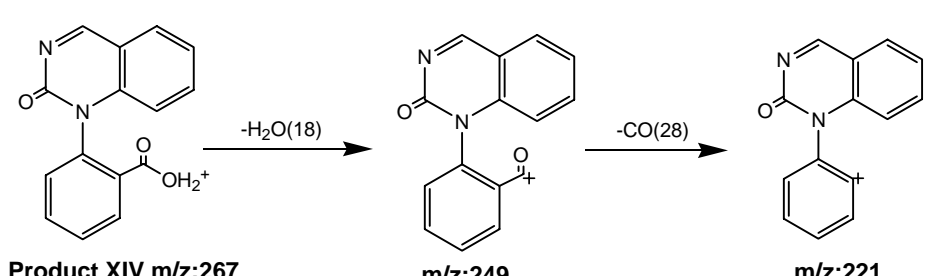
Product	Fragmentation Pathways

X

Product X m/z:285 → -H₂O(18) → m/z:267 → -CONH(43) → m/z:224

m/z:267 → -CO(28) → m/z:239

m/z:224 → -CO(28) → m/z:196

m/z:239 → -CONH(43) → m/z:196

XI

Product XI m/z:301 → -CONH(43) → m/z:258

Product XI m/z:301 → -H₂O(18) → m/z:283

m/z:258 → -H₂O(18) → m/z:240

m/z:283 → -CONH(43) → m/z:240

XII

Product XII m/z:303 → -H₂O(18) → m/z:285 → -H₂O(18) → m/z:267

XIII

Product XIII m/z:226 → -H₂O(18) → m/z:208 → -CO(28) → m/z:180

XIV

Product XIV m/z:267 → -H₂O(18) → m/z:249 → -CO(28) → m/z:221

47

Table 2.3. Formation of CBZ products under different Mn(VII) and Fe(VI) dosing

Product ID	[Mn(VII)]/[CBZ]				[Fe(VI)]/[CBZ]			
	0.5:1	1:1	2:1	3:1	0.5:1	1:1	2:1	3:1
I				√				
II			√	√				
III			√	√				
IV	√	√	√		√	√	√	√
V		√	√					
VI			√	√				
VII	√	√	√			√	√	√
VIII	√	√	√	√				
IX			√	√			√	√
X	√	√						√
XI			√	√				
XII	√	√						
XIII					√	√	√	
XIV						√	√	√

Table 2.4. Measured pseudo-first-order rate constants for CBZ oxidation by Mn(VII)

pH	T (°C)	$[Mn(VII)]_0$ (μM)	$[CBZ]_0$ (μM)	Non-Target Water Constituents	[Buffer] (mM)	k_{obs}[a] (10^{-2} s^{-1})
5	25	75	3.9	N/A	25[b]	2.0(±0.1)
6	25	75	3.9	N/A	25[b]	1.9(±0.2)
7	25	75	3.8	N/A	25[b]	2.2(±0.04)
8	25	75	4.4	N/A	25[b]	2.0(±0.1)
9	25	75	3.9	N/A	25[b]	2.1(±0.04)
7	5	75	3.6	N/A	25[b]	1.2(±0.03)
7	10	75	3.6	N/A	25[b]	1.5(±0.04)
7	15	75	3.8	N/A	25[b]	1.6(±0.04)
7	30	75	3.8	N/A	25[b]	2.6(±0.08)
7	25	50	4.0	N/A	25[b]	1.3(±0.02)
7	25	75	4.1	N/A	25[b]	2.2(±0.1)
7	25	100	4.1	N/A	25[b]	2.2(±0.1)
7	25	125	4.1	N/A	25[b]	4.0(±0.1)
7	25	150	4.1	N/A	25[b]	4.4(±0.1)
7	25	75	4.4	10 mg/L NOM	25[b]	2.2(±0.1)
5	25	75	5.2	20 mg/LNOM	25[b]	2.1(±0.1)
6	25	75	5.1	20 mg/L NOM	25[b]	2.4(±0.1)
7	25	75	5.2	20 mg/L NOM	25[b]	2.1(±0.1)
7	25	75	4.0	10 mM $MgCl_2$	25[b]	2.0(±0.1)
7	25	75	3.9	10 mM $CaCl_2$	25[b]	2.2(±0.03)
7	25	75	3.9	10 mM NH_4Cl	25[b]	1.8(±0.04)
7	25	75	3.9	10 mM $NaHCO_3$	25[b]	1.9(±0.03)
7	25	75	3.8	10 mM $NaNO_3$	25[b]	2.1(±0.04)
7	25	75	5.3	20 mg/L FeOOH	25[b]	2.5(±0.1)
7	25	75	5.1	20 mg/L SiO_2	25[b]	2.1(±0.04)
7	25	75	5.2	75 μM Fe^{2+}	1[c]	1.4(±0.01)
7	25	75	4.9	150 μM Fe^{2+}	1[c]	0.75(±0.01)
7	25	75	5.1	225 μM Fe^{2+}	1[c]	0.071(±0.008)
7	25	75	4.9	37.5 μM Mn^{2+}	1[c]	1.5(±0.01)
7	25	75	4.9	75 μM Mn^{2+}	1[c]	0.86(±0.01)
7	25	75	6.1	112.5 μM Mn^{2+}	1[c]	0.23(±0.01)
7	25	75	5.2	18.75 μM HS^-	1[c]	1.8(±0.03)
7	25	75	5.2	37.5 μM HS^-	1[c]	1.2(±0.04)
7	25	75	5.1	75 μM HS^-	1[c]	0.76(±0.01)

[a] Uncertainties represent 1 σ derived from linear regression.
[b] Phosphate buffer.
[c] MOPS buffer

Table 2.5. Measured second order rate constants for CBZ-Fe(VI) batch reactions

pH[a]	T (°C)	[Fe(VI)]$_0$ (µM)	[CBZ]$_0$ (µM)	k_2 (M^{-1} s^{-1})[b]
6	25	68[c]	5	76(±4)
7	25	91	5	70(±3)
8	25	94	5	36(±4)
9	25	108	5	2.7(±0.1)
10	25	102	5	0.97(±0.02)
11	25	93	5	0.29(±0.02)

[a] 25 mM phosphate buffer (+5 mM borate buffer for pH 9−11).
[b] Uncertainties represent 1 σ derived from linear regression.
[c] The lower Fe(VI) initial concentration at pH 6 is due to the faster Fe(VI) self-decomposition during pre-mixing.

Table 2.6. Composition of central Illinois drinking water utility source waters

	Utility 1	Utility 2
Source	reservoir	reservoir
pH	8.02	7.99
Alkalinity (mg L^{-1} as CaCO$_3$)	106	136
60 min KMnO$_4$ demand (mg L^{-1})	0.7	0.6
TDS (mg L^{-1})	225	245
TSS (mg L^{-1})	7	6
TOC (mg L^{-1})	4	4
Ammonia (mg L^{-1} as N)	non-detectable	non-detectable
Nitrate (mg L^{-1} as N)	3	10
Chloride (mg L^{-1})	52	29
Sulfate (mg L^{-1} as S)	67	75

CHAPTER 3

OXIDATION KINETICS OF ANTIBIOTICS DURING WATER TREATMENT WITH POTASSIUM PERMANGANATE[1]

3.1 Abstract

The ubiquitous occurrence of antibiotics in aquatic environments raises concerns about potential adverse effects on aquatic ecology and human health, including the promotion of increased antibiotic resistance. This study examined the oxidation of three widely detected antibiotics (ciprofloxacin, lincomycin, and trimethoprim) by potassium permanganate [$KMnO_4$; Mn(VII)]. Reaction kinetics were described by second-order rate laws, with apparent second-order rate constants (k_2) at pH 7 and 25 °C in the order of 0.61($\pm$0.02) M^{-1} s^{-1} (ciprofloxacin) < 1.6($\pm$0.1) M^{-1} s^{-1} (trimethoprim) < 3.6($\pm$0.1) M^{-1} s^{-1} (lincomycin). Arrhenius temperature dependence was observed with apparent activation energies (E_a) ranging from 49 kJ mol^{-1} (trimethoprim) to 68 kJ mol^{-1} (lincomycin). Rates of lincomycin and trimethoprim oxidation exhibited marked pH dependences, whereas pH had only a small effect on rates of ciprofloxacin oxidation. The effects of pH were quantitatively described by considering parallel reactions between $KMnO_4$ and individual acid-base species of the target antibiotics. Predictions from a kinetic model that included temperature, $KMnO_4$ dosage, pH, and source water oxidant demand as input parameters agreed reasonably well with measurements of trimethoprim and lincomycin oxidation in six drinking water utility sources. Although Mn(VII) reactivity with the antibiotics was lower than that reported for ozone and free chlorine, its high selectivity and stability suggests a promising oxidant for treating sensitive micropollutants in organic-rich matrices (e.g., wastewater).

3.2 Introduction

Antibiotics are therapeutic agents used to treat bacterial infections in humans and animals, and they are also widely used as livestock growth promoters [1]. Many commonly prescribed antibiotics are now ubiquitous in aquatic environments, especially those that receive effluent from wastewater treatment facilities [2-8]. Fluoroquinolones, lincosamides, trimethoprim, and

---

sulfonamides have been among the most frequently detected antibiotics [5, 6, 9]. For example, a national survey detected ciprofloxacin, lincomycin, trimethoprim, and sulfamethoxazole in 2.6, 19.2, 12.5, and 12.5%, respectively, of streams sampled throughout the U.S. [5]. Despite the low concentrations at which these chemicals have been detected (ng/L−µg/L), serious concerns exist about the adverse effects of antibiotics on aquatic ecology and human health, especially when considering potential synergistic effects of mixtures of antibiotics and other pharmaceutically active compounds. Pomati and co-workers [10] reported that growth of human embryonic cells was inhibited by a mixture of 13 pharmaceuticals (including four antibiotics) at environmental concentrations. Other researchers have also reported that long-term exposure to low levels of antibiotics promoted increased antibiotic resistance among microbial populations in effluent-impacted environments [11-14]. As a result, there has been growing interest in the environmental fate and drinking water treatment of antibiotics and related micropollutants.

Current water and wastewater treatment practices were not specifically designed to treat antibiotic micropollutants. Antibiotics have been detected in effluents from wastewater treatment facilities [8, 15, 16], and one recent study reported detection of a large number of pharmaceuticals in drinking water sources as well as finished drinking water [2]. Therefore, better understanding of the fate of antibiotics during individual water and wastewater treatment processes is needed to optimize operations to treat micropollutants of concern and eliminate the pharmaceutical activity of treated waters. Permanganate [MnO_4^-; Mn(VII)], widely used by water utilities (e.g., for treatment of taste and odor compounds, soluble iron(II) and manganese(II) [17]), is a promising technology for oxidative treatment of antibiotics and related micropollutants. Mn(VII) is a strong oxidant that reacts selectively with organic chemicals that contain electron-rich moieties, including phenolic, olefin, amino, thiol, ether, aldehyde, and ketone groups [18-20]. In addition, unlike chlorine-based oxidants, reactions with Mn(VII) do not produce halogenated byproducts, and the insoluble reduction product, $MnO_{2(s)}$, can enhance coagulation processes [17]. However, to date little information is available on Mn(VII) reactions with important classes of antibiotics. This study examined for the first time aqueous reactions between Mn(VII) and three commonly detected antibiotics (**Table 3.1**: ciprofloxacin, CPR; lincomycin, LCM; and trimethoprim, TMP) under natural water conditions. Detailed kinetics experiments were conducted to characterize reactions, including examining the effects of Mn(VII) concentration, temperature, and pH. The effects of pH were quantitatively interpreted by considering changes in acid-base speciation of the

52

target antibiotics. Results from experiments conducted in well-characterized laboratory solutions were used to develop a predictive kinetic model for antibiotic treatment in drinking water sources of variable composition, and the model was validated using tests conducted in source waters obtained from six drinking water utilities.

3.3 Materials and Methods

3.3.1 Reagents and Materials

All chemicals were of high purity and were used as received from Sigma-Aldrich-Fluka (St. Louis, MO). Solutions were prepared in reagent-grade deionized water (>17.8 MΩ·cm). Glassware was washed by soaking in a 1 M HCl for >24 h and repeatedly rinsing with deionized water.

3.3.2 Reaction Kinetics

Batch experiments were conducted to characterize the oxidation kinetics of CPR, LCM, and TMP using procedures similar to those previously reported [21]. Typically, batch reactions were conducted in 100 mL water-jacketed beakers connected to a circulating water bath for temperature control. Reactions were initiated by spiking excess concentration of Mn(VII) into pre-equilibrated and pH-adjusted solutions containing 10−20 μM target antibiotic and 25 mM phosphate buffer. Although a recent study reported that phosphate buffer enhanced Mn(VII) oxidation of triclosan [22], tests showed no enhancement of phosphate buffer on Mn(VII)-antibiotic reaction rates (a slight inhibition was observed for CPR, attributed to the prevention of autocatalytic reactions when $MnO_{2(s)}$ was formed). After initiating reactions, aliquots were periodically collected and quenched with excess hydroxylamine, which rapidly reduced residual Mn(VII) and $MnO_{2(s)}$ to Mn^{2+}. Residual antibiotic concentrations in the collected aliquots were then measured by high performance liquid chromatography with photodiode array detection (HPLC-PDA) to track the reaction progress.

3.3.3 Utility Source Water Experiments

LCM and TMP were also examined as representative antibiotics in a larger study on Mn(VII) reactivity with pharmaceutically active compounds in surface waters obtained from six drinking water utilities. For these experiments, a much lower initial antibiotic concentration (10

µg/L) was used to better mimic environmental levels (ng/L−µg/L), while still being high enough to permit accurate measurement by HPLC-PDA following solid phase extraction (SPE). In these experiments, reactions were initiated by spiking varying amounts of Mn(VII) into a series of 500 mL unfiltered source water samples maintained at room temperature (measured for each reaction) and amended with the target antibiotics. After the desired reaction time, excess hydroxylamine was added to each reactor to quench any further reaction. Water samples were then filtered (0.45 µm glass fiber) and concentrated using SPE before analyzing with HPLC-PDA.

3.3.4   Analytical

Antibiotic concentrations were determined using high performance liquid chromatography equipped with UV-Vis photodiode array detection (HPLC-PDA; Shimadzu AVP System; Columbia, MD). The stationary phase was a Novapak C-18 column (3.9×150 mm, 4 µm particle size; Waters Corporation, Milford, MA) and the mobile phase (1 mL/min) was an isocratic mixture of acetonitrile and an aqueous buffer. For CPR, the aqueous buffer was 2.5 mM sodium-1-heptanesulfonate adjusted to pH 2.2. For LCM and TMP, the buffer was 10 mM hydroxylamine adjusted to pH 6. The percentages (v/v) of acetonitrile used for CPR, LCM, and TMP were 15%, 12%, and 15%, respectively.

Prior to HPLC-PDA analysis, residual antibiotics present in solutions from experiments conducted in utility source waters were pre-concentrated using a solid phase extraction (SPE) method adapted from Hao et. al [23]. SPE cartridges (Oasis HLB, 500 mg, LP; Waters) were preconditioned sequentially with 5 mL methanol and 5 mL deionized water followed by washing with 5 mL of 5% methanol in water. 10 µg/L sulfamethoxazole (SMX) was added as a non-reactive internal standard to quenched reactor samples to account for varying extraction efficiency, and a Visiprep vacuum manifold (Sigma-Aldrich, St. Louis, MO) was then used to introduce the 500 mL samples at 10 mL/min. After extraction, SPE cartridges were dried under a gentle stream of air for 1 h before eluting with 5 mL methanol. The eluates were then evaporated to dryness and reconstituted in 1 mL deionized water before analyzing with HPLC-PDA. SPE recoveries for LCM, TMP and SMX were 49.3±10.4%, 70.6±12.7%, and 61.7±9.5%, respectively. Quantification was accomplished by calibration against external reference standards after correcting for SPE recoveries using the internal standard.

Utility source water characteristics were determined using procedures described previously [21]. To independently quantify the matrix oxidant demand during utility source water experiments, Mn(VII) decay in each source water was determined spectrophotometrically ($\lambda = 525$ nm) in 5 cm-optical-path cuvettes using a double-beam spectrophotometer (Shimadzu UV-2401PC). Solutions were filtered (0.2 µm PTFE) prior to analysis to eliminate spectral interference from MnO_2 precipitates.

3.4 Results and Discussion

3.4.1 Reaction Kinetics

Initial tests showed that three antibiotics (CPR, LCM, and TMP) exhibited marked reactivity with Mn(VII), whereas two other commonly detected sulfonamide antibiotics (sulfamethoxazole and sulfamethizole) were unreactive with Mn(VII) on time scales relevant to water treatment processes (≤ 1 h). The kinetics of CPR, LCM, and TMP oxidation in batch reactions followed a pseudo-first order rate law when the Mn(VII) concentration was in large excess of the initial antibiotic concentration (**Figure 3.1**), indicating that reactions were first-order with respect to antibiotic concentration. Pseudo-first-order rate constants (k_{obs}, s^{-1}) determined for all batch reactions are listed in **Table 3.2**. **Figure 3.2A** shows that measured k_{obs} values increased linearly with increasing Mn(VII) concentration, demonstrating that reactions were also first-order with respect to Mn(VII) concentration. Thus, reaction kinetics for the target antibiotics followed a generalized second-order rate law:

$$\frac{d[ATB]_{tot}}{dt} = -k_2[Mn(VII)]_{tot}[ATB]_{tot} \qquad (3.1)$$

where $[Mn(VII)]_{tot}$ and $[ATB]_{tot}$ represent the total Mn(VII) and antibiotic concentrations, respectively, and k_2 is the apparent second order rate constant (k_2, M^{-1} s^{-1}). At pH 7 and 25 °C, k_2 values for the reactions were 0.61 ± 0.02 M^{-1} s^{-1} (CPR), 3.6 ± 0.1 M^{-1} s^{-1} (LCM), and 1.6 ± 0.1 M^{-1} s^{-1} (TMP) (uncertainties = 1 σ) (**Figure 3.2A**). Waldemer and coworkers [19] reported the reaction rate constants between Mn(VII) and a wide range of organic compounds at circumneutral pH and room temperature conditions, including chlorinated alkanes and alkenes, aromatic hydrocarbons, ethers, nitro explosives, and substituted phenols, with k_2 values that ranged from 7×10^{-6} to 2×10^2 M^{-1} s^{-1}. In comparison with this range of reactivities, the three antibiotics were within the more reactive end of the spectrum, only being less reactive than compounds that possess highly

55

Mn(VII)-reactive olefin and phenolic functional groups [24, 25]. At similar conditions, we found that the anticonvulsant drug carbamazepine, which contains an olefin group, was more reactive with Mn(VII) (k_2 = 3.0×10^2 M^{-1} s^{-1} [21]) than the antibiotics examined here.

Previous studies showed antibiotic oxidation by several drinking water oxidants, including ozone and free chlorine [26-29]. Oxidation rate constants for the three antibiotics with Mn(VII) were lower than those reported for reactions with ozone (1.9×10^4 M^{-1} s^{-1} for CPR, 6.6×10^5 M^{-1} s^{-1} for LCM, and 2.7×10^5 M^{-1} s^{-1} for TMP) and free chlorine (7.6×10^5 M^{-1} s^{-1} for CPR and 56 M^{-1} s^{-1} for TMP) under comparable conditions. The relative reactivity of the three oxidants with these antibiotics qualitatively followed the trend in calculated standard reduction potentials at pH 7 ($E_{H,7}$): Mn(VII) (1.13 V vs NHE) < free chlorine (1.27 V) < ozone (1.67 V). Although Mn(VII) was less reactive with the antibiotics than free chlorine and ozone, its high selectivity may result in greater stability in organic-rich aquatic matrices (e.g., wastewater), and a larger fraction of the applied Mn(VII) dosage may be available to react with the target antibiotics in these systems. However, further research is needed to directly compare the treatment effectiveness of equivalent dosages of different oxidants in diverse aquatic matrices.

The proposed Mn(VII)-reactive functional groups in the structures of the three antibiotics are summarized in **Table 3.1** (dashed circles). The piperazine ring in the CPR structure contains secondary aliphatic and tertiary aromatic amine groups that are potential sites of Mn(VII) reaction. These groups have previously been identified as sites of fluoroquinolone oxidation by ozone, chlorine, and MnO$_2$ [26, 28, 30]. Mn(VII) reaction at the piperazine ring was supported by the very low reactivity observed with flumequine, a structurally related fluoroquinolone that lacks the piperazine ring moiety (**Figure 3.3**).

LCM contains a tertiary aliphatic amine on the pyrrolidine ring and a thioether group on the pyranose ring that are potential target sites for Mn(VII) oxidation. These groups have been proposed as sites for ozone reaction [26], and the reactivity of Mn(VII) with aliphatic amines and thioether compounds has been documented [31-33].

Dodd and co-workers [26, 27] postulated that ozone and chlorine react with TMP either through the trimethoxybenzene or pyrimidine rings. Kinetics experiments using substructural analogues of these moieties (3,4,5-trimethoxytoluene and 1,4-diaminopyrimidine) showed that Mn(VII) was much more reactive with 1,4-diaminopyrimidine (**Figure 3.4**), indicating that this was the likely site for TMP oxidation. Mn(VII) oxidation of the 5,6 double bond in pyrimidine

rings (structural ring positions indicated in) within nucleic acids has been well documented [34]. In addition, Freeman et al. [35] reported a rate constant for Mn(VII) reaction with the pyrimidine compound uracil ($k_2 = 1.9$ M^{-1} s^{-1} at pH 7 and 25 °C) similar to the value measured for TMP in this study, and the 5,6 double bond was proposed as the reaction site. However, additional measurements of reaction products are necessary to unambiguously determine the sites of Mn(VII) reactions with the three target antibiotics (see Chapter 4).

Rate constants for Mn(VII) reactions with the antibiotics exhibited temperature dependence consistent with the Arrhenius equation (**Figure 3.2B**), with apparent activation energies (E_a) of 54 ± 3 kJ/mol for CPR, 68 ± 4 kJ/mol for LCM, and 49 ± 5 kJ/mol for TMP. This corresponded to a doubling of reaction rates for every 9, 8, and 10 °C increase, respectively, in temperature. A previous study on Mn(VII) oxidation of CPR in highly alkaline solution reported much weaker temperature dependence [36], suggesting that a different reaction mechanism operates under natural water conditions.

Figure 3.5 shows that solution pH had varying effects on Mn(VII) reactions with the target antibiotics. Mn(VII) reactions with CPR exhibited a relatively weak pH dependence, where k_2 only varied from 0.6 to 1.0 M^{-1} s^{-1} from pH 5 to 9 (**Figure 3.5A**). Although the effect of pH was relatively small, replicate experiments confirmed that the difference was significant at the 95% confidence level. The weak pH dependence was somewhat surprising because the acid-base speciation of CPR changed over this pH range, and CPR reactions with ozone and free chlorine were strongly pH dependent [26, 28], with the proposed secondary aliphatic amine target moiety being two orders-of-magnitude more reactive when deprotonated. The small pH dependence observed suggested that Mn(VII) was mainly targeting the tertiary aromatic amine (N1 site; structural positions indicated in **Table 3.1**) on the piperazine ring instead of the aliphatic amine (N4), similar to the mechanism proposed for fluoroquinolone reactions with MnO$_2$ [30]. Whereas the N4 amine undergoes deprotonation over the pH range examined, speciation of the N1 nitrogen remains unchanged. This conclusion was further supported by the fact that modification of the N4 site had very little effect on Mn(VII) reactivity (ciprofloxacin versus enrofloxacin in **Figure 3.3**). The small change in k_2 observed with changing pH may have been due to limited contributions of the N4 amine to overall CPR reactivity or to the effects of N4 protonation/deprotonation on electron density at the N1 amine site.

LCM reactivity increased significantly with increasing pH, with two orders-of-magnitude

increase in k_2 when pH increased from 5 to 9 (**Figure 3.5B**). Ozone reaction with LCM showed a similar pH dependence [26], consistent with the dominant reactive site being the tertiary amine group on the pyrrolidine ring, which underwent a change in acid-base speciation over the pH range examined. Deprotonation increases electron density on the amine nitrogen, increasing reactivity with oxidants.

TMP exhibited an opposite pH dependence trend to that observed for LCM, where k_2 decreased by more than one order-of-magnitude when pH increased from 5 to 9 (**Figure 3.5C**). The pH dependence also contrasted with the trend reported for TMP reactions with free chlorine [27] and ozone [26]. Although the proposed Mn(VII)-reactive site (5,6 olefinic double bond) did not change acid-base speciation, the neighboring N1 site (**Table 3.1**) was protonated at pH < pK_{a2}, which in turn could have affected reactivity with Mn(VII). Olefins react with Mn(VII) by formation of a 3 + 2 cyclic diester intermediate [21, 25, 37, 38]. The olefin carbon atoms act as electrophiles during diester formation, so the presence of electron-withdrawing groups on neighboring atoms increases reaction rates by enhancing electrophilicity of the reacting carbon atoms [37, 38]. Thus, Mn(VII) reactivity with TMP increased with decreasing pH because protonation of the N1 atom increased the electron withdrawing character of this group adjacent to the reaction site.

3.4.2   Correlating Kinetics with Antibiotic Speciation

The effects of pH on reaction kinetics were quantitatively related to changes in acid-base speciation of the target antibiotics. Although permanganate exhibits acid-base chemistry, the pK_a of $HMnO_4$ is very low (-2.25 [39]), and the conjugate base, MnO_4^-, was the dominant species over the pH range examined. The three target antibiotics have various acid-base groups with characteristic pK_a values [26, 29, 40] that were used to calculate the distribution of species present at different pH conditions. The pH dependency of reaction rates then resulted from individual antibiotic species reacting with MnO_4^- via parallel reactions that could be described by independent second-order rate constants:

$$MnO_4^- + ATB_i \rightarrow Products, k_{2i}; i = 1,2,3\ldots \qquad (3.2)$$
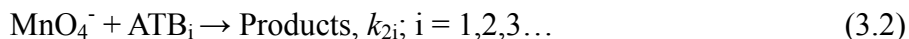
where ATB_i represents individual species of the target antibiotic and i refers to the species protonation level (e.g., 1 = fully protonated, 2 = first conjugate base, etc.). For example, LCM_1 represents the monoprotonated lincomycin species, whereas LCM_2 is the neutral molecule. Thus,

58

k_{21} is the species-specific second-order rate constant for deprotonated MnO_4^- reaction with the monoprotonated LCM_1. If equilibrium between antibiotic species was maintained during redox reactions with Mn(VII) [41], the effect of pH on the apparent oxidation rate constant could be quantitatively described by Equation (3.3):

$$-\frac{d[ATB]_{tot}}{dt} = k_2[Mn(VII)]_{tot}[ATB]_{tot} = \sum_i k_{2i}\alpha_i[Mn(VII)]_{tot}[ATB]_{tot} \qquad (3.3)$$

and it follows that

$$k_2 = \sum_i k_{2i}\alpha_i \qquad (3.4)$$

where α_i represents the fraction of antibiotic species i, which can be calculated as a function of pH using the reported pK_a values. **Figure 3.5** shows the results of least-squares fitting of the kinetic data for each antibiotic with Equation (3.4) and the predicted contribution of individual species to the overall rate constants (i.e., $k_{2i}\alpha_i$). The model fits agreed closely with experimental data and the fit-derived species-specific rate constants are summarized in **Table 3.1**. For CPR, the small difference between k_{ij} values was attributed to the fact that Mn(VII) was reacting predominantly with the aromatic N1 site which did not change speciation. Deprotonation of the neighboring N4 can have a small effect on electron density at the reactive N1 site through inductive effects, possibly explaining the small difference between k_{22} and k_{23}. For LCM, k_{22} was nearly two orders-of-magnitude greater than k_{21}, attributed to increased electron density of the deprotonated amine group on the pyrrolidine ring. For TMP, k_{22} was much larger than k_{23}, which was attributed to enhanced Mn(VII) reactivity with the 5,6-double bond when the neighboring heterocyclic nitrogen atom was in the more electron-withdrawing protonated state [37, 38].

The correlation observed between Mn(VII) reaction rates and acid-base speciation of the antibiotics contrasted with recent reports of Mn(VII) reactivity with phenolic micropollutants [22, 42]. The reason for the difference was unclear, but may be due to the effects of ligands and autocatalytic mechanisms that complicate modeling of Mn(VII) reactions with phenolic moieties [42].

3.4.3 Mn(VII) Treatment of Antibiotics in Utility Source Waters

The oxidative treatment of LCM and TMP by Mn(VII) was also analyzed in six utility source waters, whose properties are summarized in **Table 3.3** and **Table 3.4**. **Figure 3.6A** and **B** summarizes the measured removal of LCM and TMP in utility source waters with three different

doses of $KMnO_4$ (2, 6, and 18 mg/L). Results showed a general trend of increasing antibiotic removal with increasing $KMnO_4$ doses. For LCM, an average of 60% removal was observed for a 6 mg/L $KMnO_4$ dose and 30 min reaction time, whereas only about 20% of TMP was oxidized by the same $KMnO_4$ dosage and a longer reaction time (120 min). In comparison, the anticonvulsant drug carbamazepine, which contains a Mn(VII)-reactive olefin group, was removed to a much greater degree in some of the same source waters [21], with 80% removal being observed after treatment with 2 mg/L $KMnO_4$ for 10 min. **Figure 3.6A** and **B** also shows that the extent of LCM and TMP removal varied among the six source waters, which was attributed to differences in key water quality characteristics, including pH and the matrix $KMnO_4$ demand (**Table 3.3** and **Table 3.4**). The strong influence of pH is shown in **Figure 3.5**. $KMnO_4$ demand of the source water matrix reduces the effective Mn(VII) concentration available to react with target antibiotics.

It should be noted that the $KMnO_4$ dosages used here were greater than those typically used in drinking water treatment facilities (e.g., for Mn removal, taste-and-odor control, etc.), and little removal of the tested antibiotics would be expected at most facilities currently using $KMnO_4$. To specifically target antibiotic removal, higher $KMnO_4$ dosages and/or longer reactor residence times will be needed. Use of $KMnO_4$ to specifically target antibiotic removal might be more applicable in wastewater treatment facilities with longer retention times, higher organic loadings to consume residual $KMnO_4$, and built-in solids removal capabilities to handle the associated residual solids. Further research is needed to measure antibiotic removal at actual wastewater and drinking water treatment facilities during the application of $KMnO_4$.

3.4.4 Predictive Kinetic Model for Water Treatment

Antibiotic oxidation by Mn(VII) during water treatment can be predicted using Equation (3.5) along with kinetic parameters described for individual target antibiotics in previous sections:

$$[\text{ATB}] = [\text{ATB}]_0 \exp\left\{ -\underbrace{(\sum_i k_{2i}\alpha_i)}_{1} \times \underbrace{\exp\left[\frac{-E_a}{R}\left(\frac{1}{T} - \frac{1}{298}\right)\right]}_{2} \times \underbrace{(Ct_{Mn(VII)})}_{3} \right\} \qquad (3.5)$$

where $[\text{ATB}]_0$ and $[\text{ATB}]$ are the antibiotic concentration initially present before treatment and the concentration remaining after Mn(VII) treatment, respectively. Term 1 calculates the apparent second-order rate constants at 25 °C and the pH of interest by accounting for the effects of antibiotic acid-base speciation on reactivity with Mn(VII) (**Table 3.1**). Term 2 corrects the

apparent rate constant to the temperature of interest using E_a values determined above (**Figure 3.2B**). R and T represent the universal gas constant and absolute temperature, respectively. In term 3, $Ct_{Mn(VII)}$ is the integrated Mn(VII) exposure during treatment ($\int_0^t$ [Mn(VII)·dt), which accounts for the applied Mn(VII) dosage, treatment time, and oxidant demand of the source water matrix; this is equivalent to the widely used Ct concept for modeling disinfection processes. **Figure 3.7** illustrates how $Ct_{Mn(VII)}$ is determined by measuring Mn(VII) decay as a function of time in the matrix of interest. The $Ct_{Mn(VII)}$ corresponding to each source water was determined by measuring Mn(VII) consumption in the absence of antibiotics in separate experiments (**Table 3.4**).

Equation (3.5) can be used to either estimate the expected antibiotic removal percentage for an existing Mn(VII) dose and reaction time used at a treatment facility or to determine the Mn(VII) dose and/or reaction time required to achieve a desired treatment goal. The accuracy of Equation (3.5) was tested by comparing model predictions with the measurements in the utility source waters. Results of the comparison are summarized in **Figure 3.6C** and **D**. It can be seen that the majority of model predictions agreed with measurements at the 95% confidence level. While most model predictions agreed closely with measured values in the six utility source waters, all model predictions for TMP and LCM agreed within a factor of 2.8 and 3.2, respectively, of measured values. The close agreement between measurements and model predictions was especially notable given that experiments in the utility source waters were conducted at conditions that differ significantly from those used to parametrize Equation (3.5) (e.g., much lower initial antibiotic and Mn(VII) concentrations, poorly characterized source waters, suspended solids present). Reactions of both antibiotics with Mn(VII) were highly pH dependent, so discrepancies may have been due, in part, to errors in pH measurements. Underpredictions of the model may also resulted from autocatalytic processes involving the $MnO_{2(s)}$ product [43, 44] and the effects of unknown ligands (e.g., NOM) that were present in the sourcewaters [42], factors that were not considered in the model, but which might have accelerated oxidation of the antibiotics. Although Equation (3.5) could be modified to include autocatalytic processes and ligand effects, it will be difficult to predict these processes a priori in natural water matrices of varying composition. Instead, we recommend that Equation (3.5) be used to provide a conservative baseline prediction of antibiotic treatment, and then consider that any autocatalytic processes and ligand effects may act to provide an additional level of treatment (i.e., a safety factor) above model predictions. Since reactions with Mn(VII) under water treatment conditions are not expected to mineralize the

antibiotics [21], additional studies are needed to identify the products of these reactions and assess the effects of treatment on the antibiotic activity of solutions.

3.5 References Cited

[1]   Walsh C. *Antibiotics: Actions, origins, resistance*. Washington, DC: ASM Press, **2003**.

[2]   Benotti M. J., Trenholm R. A., Vanderford B. J., Holady J. C., Stanford B. D. and Snyder S. A. Pharmaceuticals and endocrine disrupting compounds in US drinking water. *Environmental Science & Technology*, **2009**, 43: 597-603.

[3]   Heberer T. Occurrence, fate, and removal of pharmaceutical residues in the aquatic environment: a review of recent research data. *Toxicology Letters*, **2002**, 131: 5-17.

[4]   Hirsch R., Ternes T., Haberer K. and Kratz K. L. Occurrence of antibiotics in the aquatic environment. *Science of the Total Environment*, **1999**, 225: 109-118.

[5]   Kolpin D. W., Furlong E. T., Meyer M. T., Thurman E. M., Zaugg S. D., Barber L. B. and Buxton H. T. Pharmaceuticals, hormones, and other organic wastewater contaminants in US streams, 1999-2000: A national reconnaissance. *Environmental Science & Technology*, **2002**, 36: 1202-1211.

[6]   Lindberg R. H., Wennberg P., Johansson M. I., Tysklind M. and Andersson B. A. V. Screening of human antibiotic substances and determination of weekly mass flows in five sewage treatment plants in Sweden. *Environmental Science & Technology*, **2005**, 39: 3421-3429.

[7]   Miao X. S., Bishay F., Chen M. and Metcalfe C. D. Occurrence of antimicrobials in the final effluents of wastewater treatment plants in Canada. *Environmental Science & Technology*, **2004**, 38: 3533-3541.

[8]   Ternes T. A. Occurrence of drugs in German sewage treatment plants and rivers. *Water Research*, **1998**, 32: 3245-3260.

[9]   Ye Z. Q., Weinberg H. S. and Meyer M. T. Trace analysis of trimethoprim and sulfonamide, macrolide, quinolone, and tetracycline antibiotics in chlorinated drinking water using liquid chromatography electrospray tandem mass spectrometry. *Analytical Chemistry*, **2007**, 79: 1135-1144.

[10]   Pomati F., Castiglioni S., Zuccato E., Fanelli R., Vigetti D., Rossetti C. and Calamari D. Effects of a complex mixture of therapeutic drugs at environmental levels on human

embryonic cells. *Environmental Science & Technology*, **2006**, 40: 2442-2447.

[11]   Baquero F. Low-level antibacterial resistance: A gateway to clinical resistance. *Drug Resistance Updates*, **2001**, 4: 93-105.

[12]   Gilliver M. A., Bennett M., Begon M., Hazel S. M. and Hart C. A. Enterobacteria: Antibiotic resistance found in wild rodents. *Nature*, **1999**, 401: 233-234.

[13]   Goni-Urriza M., Capdepuy M., Arpin C., Raymond N., Caumette P. and Quentin C. Impact of an urban effluent on antibiotic resistance of riverine *Enterobacteriaceae* and *Aeromonas* spp. *Applied and Environmental Microbiology*, **2000**, 66: 125-132.

[14]   Iwane T., Urase T. and Yamamoto K. Possible impact of treated wastewater discharge on incidence of antibiotic resistant bacteria in river water. *Water Science and Technology*, **2001**, 43: 91-99.

[15]   Spongberg A. L. and Witter J. D. Pharmaceutical compounds in the wastewater process stream in Northwest Ohio. *Science of the Total Environment*, **2008**, 397: 148-157.

[16]   Watkinson A. J., Murby E. J. and Costanzo S. D. Removal of antibiotics in conventional and advanced wastewater treatment: Implications for environmental discharge and wastewater recycling. *Water Research*, **2007**, 41: 4164-4176.

[17]   *MWH Water Treatment: Principles and Design*, 2nd ed. Hoboken: Wiley, **2005**.

[18]   Ladbury J. W. and Cullis C. F. Kinetics and mechanism of oxidation by permanganate. *Chemical Reviews*, **1958**, 58: 403-438.

[19]   Waldemer R. H. and Tratnyek P. G. Kinetics of contaminant degradation by permanganate. *Environmental Science & Technology*, **2006**, 40: 1055-1061.

[20]   Walton J., Labine P. and Reidies A. In: Eckenfelder W W, Bowers A R and Roth J A, eds. *Chemical Oxidation: Technologies for the Nineties*: CRC Press **1992**:205-230.

[21]   Hu L., Martin H. M., Arcs-Bulted O., Sugihara M. N., Keatlng K. A. and Strathmann T. J. Oxidation of carbamazepine by Mn(VII) and Fe(VI): Reaction kinetics and mechanism. *Environmental Science & Technology*, **2009**, 43: 509-515.

[22]   Jiang J., Pang S. Y. and Ma J. Oxidation of triclosan by permanganate (Mn(VII)): Importance of ligands and in situ formed manganese oxides. *Environmental Science & Technology*, **2009**, 43: 8326-8331.

[23]   Hao C. Y., Lissemore L., Nguyen B., Kleywegt S., Yang P. and Solomon K. Determination of pharmaceuticals in environmental waters by liquid chromatography/electrospray

ionization/tandem mass spectrometry. *Analytical and Bioanalytical Chemistry*, **2006**, 384: 505-513.

[24] Lee D. G. and Sebastian C. F. The oxidation of phenol and chlorophenols by alkaline permanganate. *Canadian Journal of Chemistry*, **1981**, 59: 2776-2779.

[25] Yan Y. E. and Schwartz F. W. Kinetics and mechanisms for TCE oxidation by permanganate. *Environmental Science & Technology*, **2000**, 34: 2535-2541.

[26] Dodd M. C., Buffle M. O. and Von Gunten U. Oxidation of antibacterial molecules by aqueous ozone: Moiety-specific reaction kinetics and application to ozone-based wastewater treatment. *Environmental Science & Technology*, **2006**, 40: 1969-1977.

[27] Dodd M. C. and Huang C. H. Aqueous chlorination of the antibacterial agent trimethoprim: Reaction kinetics and pathways. *Water Research*, **2007**, 41: 647-655.

[28] Dodd M. C., Shah A. D., von Gunten U. and Huang C. H. Interactions of fluoroquinolone antibacterial agents with aqueous chlorine: Reaction kinetics, mechanisms, and transformation pathways. *Environmental Science & Technology*, **2005**, 39: 7065-7076.

[29] Qiang Z. M. and Adams C. Potentiometric determination of acid dissociation constants (pK_a) for human and veterinary antibiotics. *Water Research*, **2004**, 38: 2874-2890.

[30] Zhang H. C. and Huang C. H. Oxidative transformation of fluoroquinolone antibacterial agents and structurally related amines by manganese oxide. *Environmental Science & Technology*, **2005**, 39: 4474-4483.

[31] Mazeikiene R. and Malinauskas A. The autocatalytic oxidation of aniline by persulfate and permanganate as a means for the deposition of a thin polyaniline film. *Journal of Chemical Research-S*, **1999**: 622-623.

[32] Rawalay S. S. and Shechter H. Oxidation of primary secondary and tertiary amines with neutral permanganate. A simple method for degrading amines to aldehydes and ketones. *Journal of Organic Chemistry*, **1967**, 32: 3129-3131.

[33] Walton J., Labine P. and Reidies A. In: Eckenfelder W W, Bowers A R and Roth J A, eds. *Chemical Oxidation: Technologies for the Nineties*: CRC Press **1997**:214.

[34] Hayatsu H. The 5,6-double bond of pyrimidine nucleosides, a fragile site in nucleic acids. *Journal of Biochemistry*, **1996**, 119: 391-395.

[35] Freeman F., Fuselier C. O., Armstead C. R., Dalton C. E., Davidson P. A., Karchesfski E. M., Krochman D. E., Johnson M. N. and Jones N. K. Permanganate ion oxidations .13.

Soluble manganese(IV) species in the oxidation of 2,4(1*H*,3*H*)-pyrimidinediones (uracils). *Journal of the American Chemical Society*, **1981**, 103: 1154-1159.

[36]   Thabaj K. A., Kulkarni S. D., Chimatadar S. A. and Nandibewoor S. T. Oxidative transformation of ciprofloxacin by alkaline permanganate - A kinetic and mechanistic study. *Polyhedron*, **2007**, 26: 4877-4885.

[37]   Henbest H. B., Jackson W. R. and Robb B. C. G. Electronic effects in reactions of olefins with permanganate ion and with osmium tetroxide. *Journal of the Chemical Society (B)*, **1966**: 803-807.

[38]   Nelson D. J. and Henley R. L. Relative rates of permanganate oxidation of functionalized alkenes and the correlation with the ionization potentials of those alkenes. *Tetrahedron Letters*, **1995**, 36: 6375-6378.

[39]   Wiberg E., Wiberg N. and Holleman A. F. *Inorganic chemistry*, 1st ed. New York: Academic Press, **2001**.

[40]   Barron D., Jimenez-Lozano E., Irles A. and Barbosa J. Influence of pH and pK_a values on electrophoretic behaviour of quinolones in aqueous and hydro-organic media. *Journal of Chromatography A*, **2000**, 871: 381-389.

[41]   Cohen B., Huppert D. and Agmon N. Diffusion-limited acid-base nonexponential dynamics. *Journal of Physical Chemistry A*, **2001**, 105: 7165-7173.

[42]   Jiang J., Pang S. Y. and Ma J. Role of ligands in permanganate oxidation of organics. *Environmental Science & Technology*, **2010**, 44: 4270-4275.

[43]   Crimi M. L. and Siegrist R. L. Impact of reaction conditions on MnO_2 genesis during permanganate oxidation. *Journal of Environmental Engineering*, **2004**, 130: 562-572.

[44]   Insausti M. J., Mata-Perez F. and Alvarez-Macho M. P. Kinetic study of the oxidation of glycine by permanganate ions in acid medium. *Collection of Czechoslovak Chemical Communications*, **1996**, 61: 232-241.

[45]   Barron D., Jimenez-Lozano E., Irles A. and Barbosa J. Influence of pH and pK_a values on electrophoretic behaviour of quinolones in aqueous and hydro-organic media. *Journal of Chromatography*, **2000**, 871: 381-389.

[46]   Qiang Z. and Adams C. Potentiometric determination of acid dissociation constants (pK_a) for human and veterinary antibiotics. *Water Research*, **2004**, 38: 2874-2890.
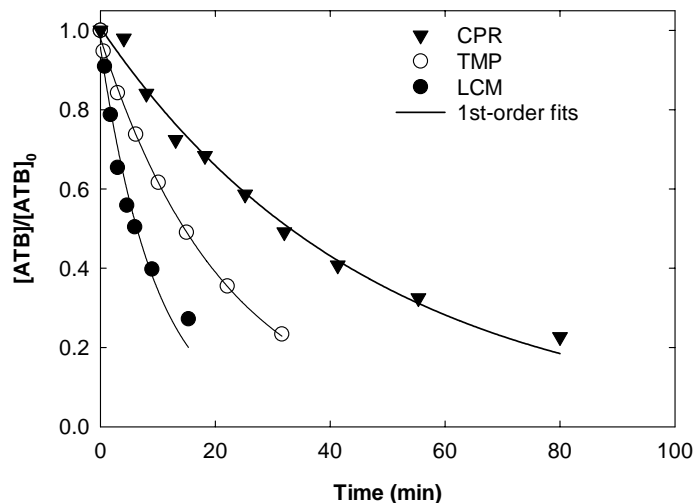
3.6 Figures and Tables

Figure 3.1. Oxidation of antibiotics by Mn(VII) during batch reactions and pseudo-first-order model fits. Experimental conditions: $[CPR]_0 = 10$ µM, $[LCM]_0 = 20$ µM, $[TMP]_0 = 10$ µM, $[Mn(VII)]_0 = 500$ µM, 25 ºC, pH 7, 25 mM phosphate buffer.
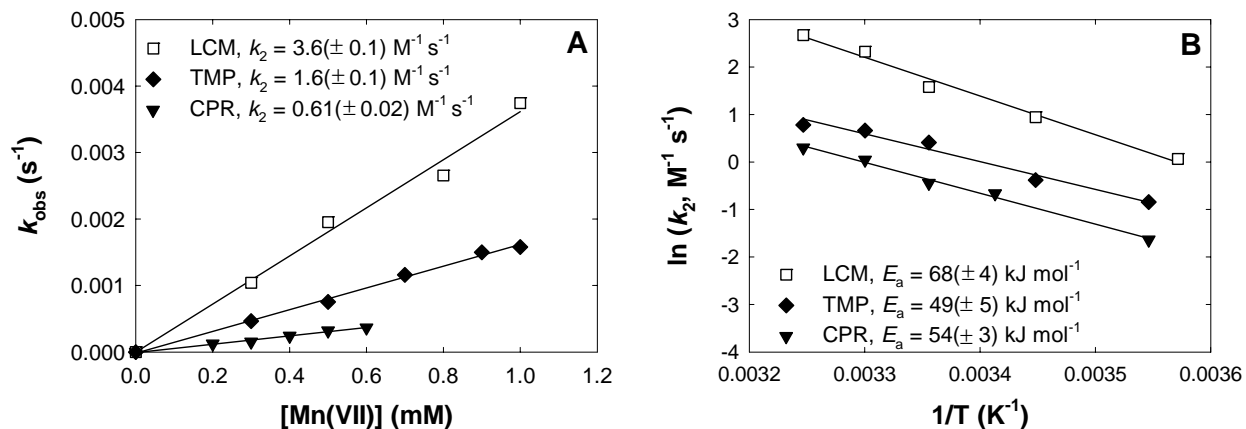

Figure 3.2. Effect of (A) Mn (VII) concentration and (B) temperature on measured rate constants for oxidation of antibiotics. Reaction conditions. $[CPR]_0 = 10$ µM, $[LCM]_0 = 20$ µM, $[TMP]_0 = 10$ µM, 25 mM phosphate buffer, pH 7, 25 °C for (A); $[CPR]_0 = 10$ µM, $[LCM]_0 = 20$ µM, $[TMP]_0 = 10$ µM, $[Mn(VII)]_0 = 500$ µM, 25 mM phosphate, pH 7 for (B). Lines represent linear regressions of measured data. Uncertainties represent 1 σ.
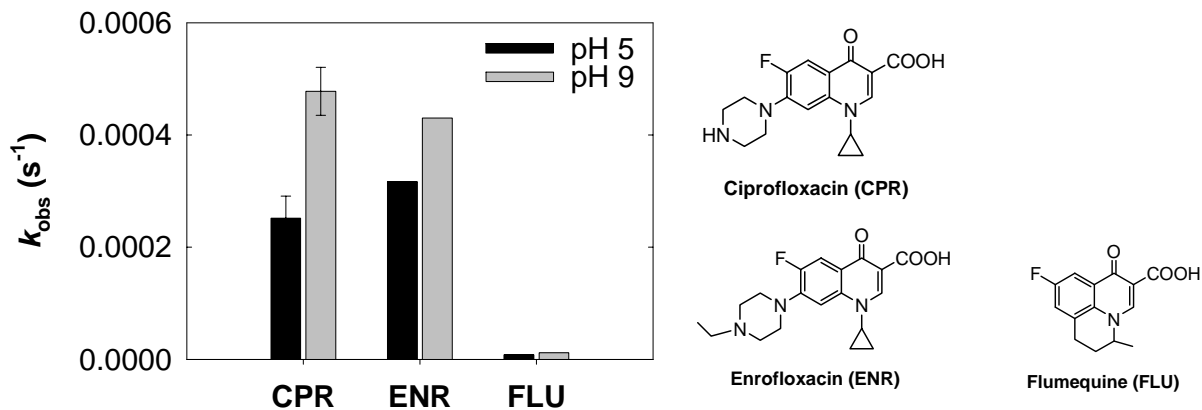
Figure 3.3. Reactivity of ciprofloxacin and structurally related fluoroquinolones with Mn(VII) at pH 5 and pH 9. Conditions: [fluoroquinolone]$_0$ = 10 μM, [Mn(VII)]$_0$ = 500 μM, 25 mM phosphate buffer, 25 °C.
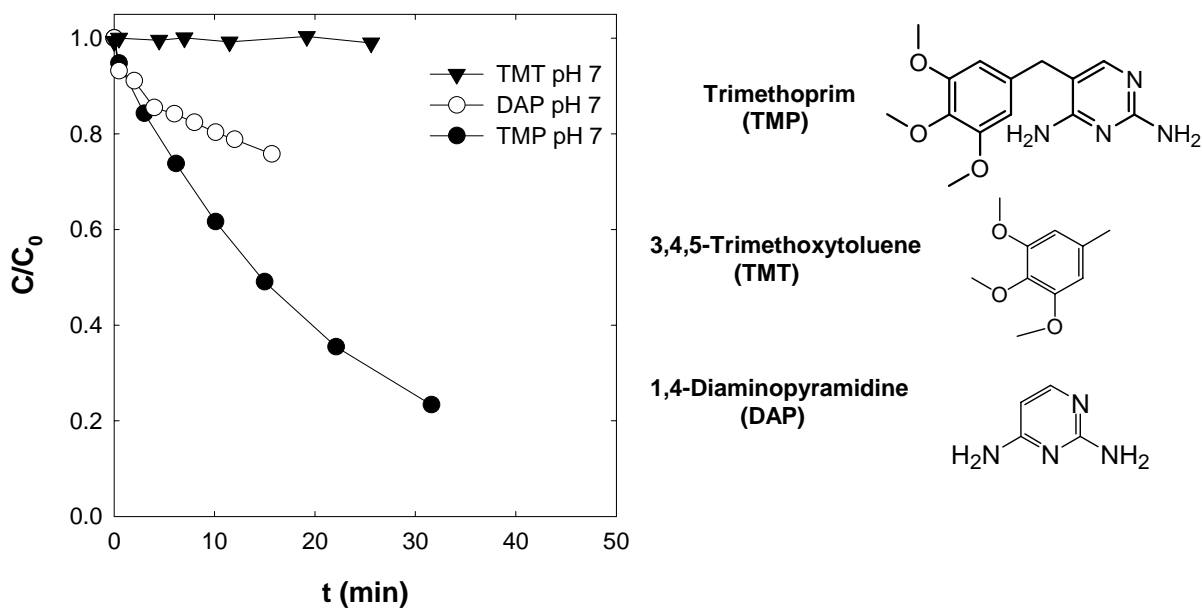
Figure 3.4. Mn(VII) oxidation of trimethoprim (TMP) in comparison to two analogues that represent sub-structural moieties within the TMP structure. Experimental conditions: C$_0$ = 10 μM, [Mn(VII)]$_0$ = 500 μM, 25 °C, pH 7, 25 mM phosphate buffer.
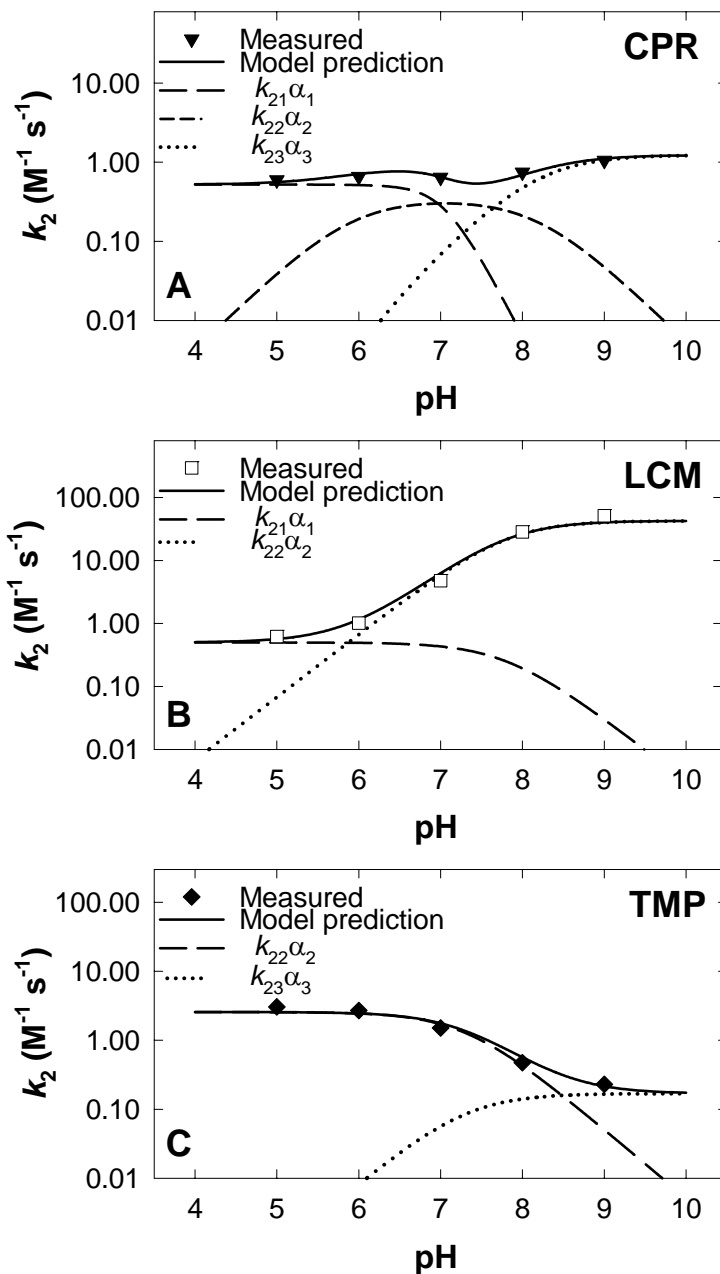
Figure 3.5. Effect of pH on measured and model-predicted rate constants for Mn(VII) reactions with (A) ciprofloxacin, (B) lincomycin, and (C) trimethoprim. Reaction conditions: $[CPR]_0 = 10\ \mu M$, $[LCM]_0 = 20\ \mu M$, $[TMP]_0 = 10\ \mu M$, $[Mn(VII)]_0 = 500\ \mu M$, 25 mM phosphate, 25 °C. Symbols represent measurements and lines indicate overall model predictions with Equation (3.4) (solid) and contributions of individual antibiotic species to the apparent rate constants (dashed, dotted). Fit-derived kinetic parameters for each antibiotic are listed in Table 3.1.
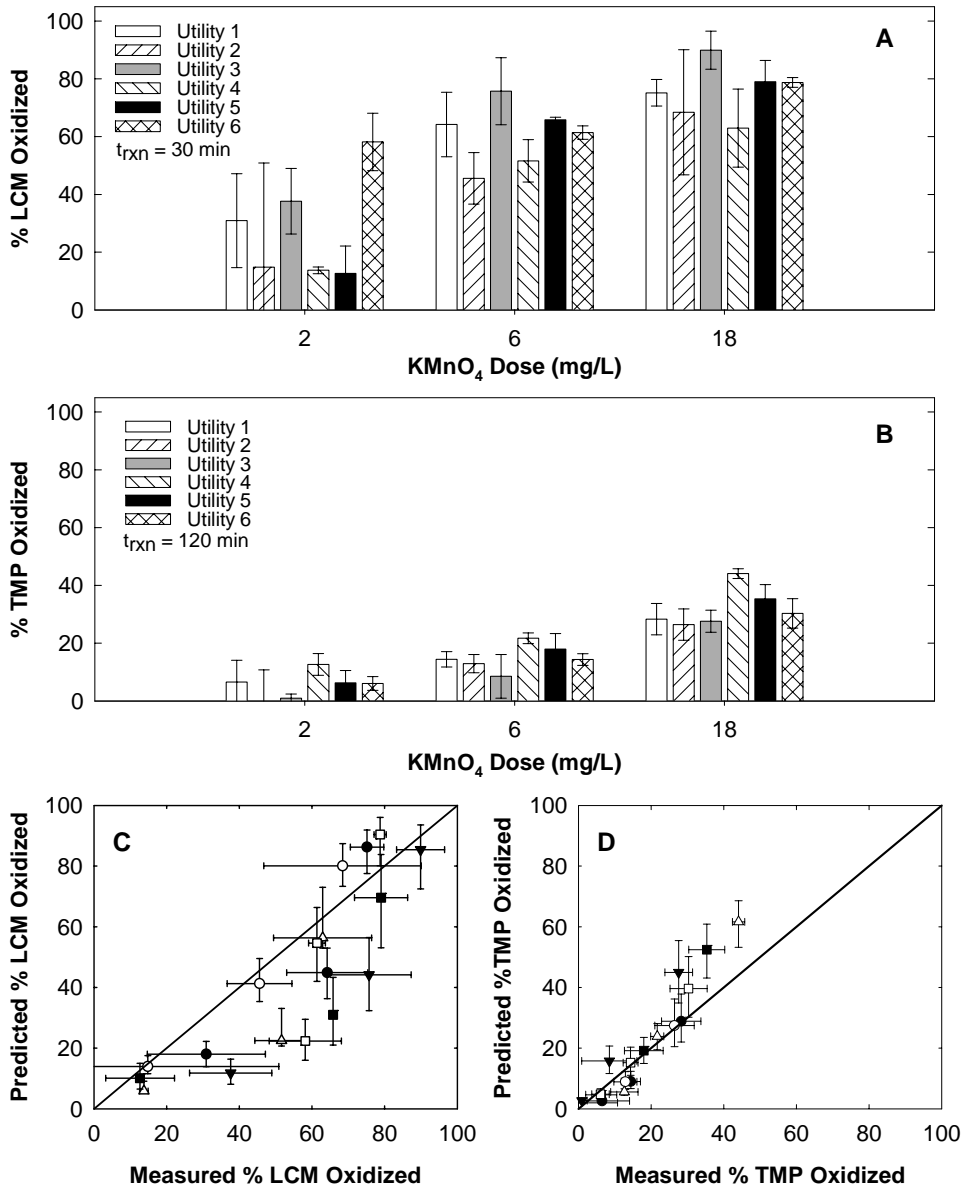
Figure 3.6. Measured oxidation of (A) LCM and (B) TMP during Mn(VII) treatment in six utility source waters at varying applied KMnO$_4$ dosages. Comparison of measurements and model predictions with Equation (3.5) for (C) LCM and (D) TMP. Conditions: $[ATB]_0 = 10$ μg/L, pH unadjusted (see Table 3.3), room temperature, $t_{rxn} = 30$ min (LCM) and 120 min (TMP). Uncertainties for measured values are triplicate-averaged 95% confidence levels, and uncertainties for predicted values are obtained by assuming ± 0.2 pH and ± 1 °C uncertainties. Different symbols in panels C and D refer to experiments conducted in different source waters.
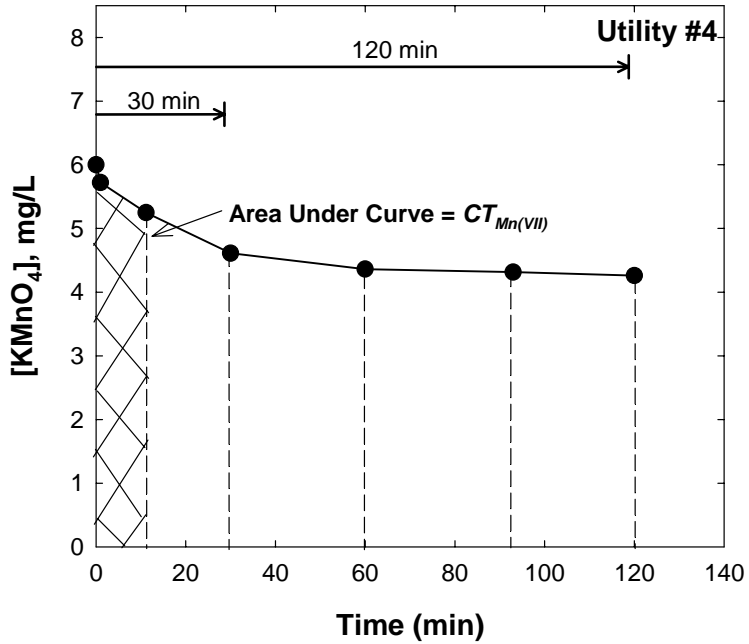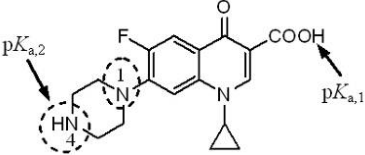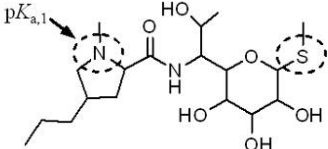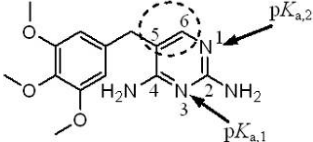
Figure 3.7. Representative degradation of KMnO₄ in utility source water and illustration of Mn(VII) exposure ($Ct_{Mn(VII)}$) calculations. [KMnO₄]₀ = 6 mg/L, unfiltered source water.

Table 3.1. Summary of pK_a values and species-specific rate constants for Mn(VII)-antibiotic reactions

Antibiotic	Structure[a]	p$K_{a,1}$	p$K_{a,2}$	k_{21}[b] (M^{-1} s^{-1})	k_{22}[b] (M^{-1} s^{-1})	k_{23}[b] (M^{-1} s^{-1})
CPR		5.9[45]	8.2[45]	0.52(±0.05)	0.34(±0.08)	1.2(±0.1)
LCM		7.8[46]	---	0.5(±0.1)	43(±6)	---
TMP		3.2[26]	7.1[26]	---	2.6(±0.3)	0.17(±0.05)

[a] Structures shown for neutral species. Arrows showing sites of protonation for antibiotics and numbers indicate order of deprotonation. Proposed reactive groups are highlighted with dashed circles. Numbers on TMP structure indicate pyrimidine ring positions referred to in the discussion.
[b] Rate constants at 25 °C. Uncertainties represent 1 σ from model fitting.

Table 3.2. Measured pseudo-first-order rate constants for antibiotic oxidation by Mn(VII)

	pH	T (°C)	$[Mn(VII)]_0$ (μM)	$[ATB]_0$ (μM)	[Phosphate] (mM)	k_{obs}[a] (10^{-3} s^{-1})
CPR	7	25	200	10	25	0.12(±0.01)
	7	25	300	10	25	0.15(±0.01)
	7	25	400	10	25	0.24(±0.01)
	7	25	500	10	25	0.32(±0.01)
	7	25	600	10	25	0.37(±0.01)
	5	25	500	10	25	0.30(±0.01)
	5	25	500	10	25	0.22(±0.01)
	5	25	500	10	25	0.24(±0.01)
	6	25	500	10	25	0.31(±0.01)
	7	25	500	10	25	0.35(±0.01)
	7	25	500	10	25	0.26(±0.01)
	8	25	500	10	25	0.39(±0.01)
	9	25	500	10	25	0.58(±0.02)
	9	25	500	10	25	0.44(±0.02)
	9	25	500	10	25	0.47(±0.02)
	7	9	500	10	25	0.097(±0.006)
	7	20	500	10	25	0.26(±0.01)
	7	30	500	10	25	0.52(±0.01)
	7	35	500	10	25	0.68(±0.02)
	7	25	500	10	5	0.37(±0.02)
	5	25	500	10	25	0.32(±0.01)
ENR	5	25	500	10	25	0.32(±0.01)
	9	25	500	10	25	0.43(±0.01)
FLU	5	25	500	10	25	0.008(±0.01)
	9	25	500	10	25	0.01(±0.002)

Table 3.2. (cont.)

	pH	T (°C)	[Mn(VII)]$_0$ (μM)	[ATB]$_0$ (μM)	[Phosphate] (mM)	k_{obs}[a] (10^{-3} s^{-1})
LCM	7	25	300	20	25	1.0(±0.1)
	7	25	500	20	25	2.0(±0.1)
	7	25	800	20	25	2.7(±0.1)
	7	25	1000	20	25	3.7(±0.2)
	5	25	500	20	25	0.31(±0.02)
	6	25	500	20	25	0.55(±0.05)
	7	25	500	20	25	2.3(±0.1)
	8	25	500	20	25	13(±1)
	9	25	500	20	25	24(±1)
	7	7	500	20	25	0.53(±0.01)
	7	17	500	20	25	1.3(±0.1)
	7	30	500	20	25	5.1(±0.1)
	7	35	500	20	25	7.2(±0.2)
TMP	7	25	300	10	25	0.46(±0.01)
	7	25	500	10	25	0.75(±0.01)
	7	25	700	10	25	1.16(±0.02)
	7	25	900	10	25	1.50(±0.01)
	7	25	1000	10	25	1.58(±0.01)
	5	25	500	10	25	1.52(±0.01)
	6	25	500	10	25	1.35(±0.01)
	7	25	500	10	25	0.70(±0.01)
	8	25	500	10	25	0.24(±0.01)
	9	25	500	10	25	0.12(±0.01)
	5	25	500	10	25	1.55(±0.01)
	6	25	500	10	25	1.21(±0.01)
	7	9	500	10	25	0.19(±0.01)
	7	17	500	10	25	0.34(±0.02)
	7	30	500	10	25	0.97(±0.01)
	7	35	500	10	25	1.11(±0.05)
TMT	7	25	500	10	25	0.002(±0.001)
DAP	7	25	500	10	25	0.26(±0.03)

[a] Uncertainties represent 1 σ derived from linear regression.

Table 3.3. Utility source water characteristics

Utility	1	2	3	4	5	6
Source Water Type	Reservoir	Reservoir	River	River	River	Reservoir
pH	8.34	8.05	8.01	7.13	7.44	7.83
Ammonia (mg/L as N)	0.3	0.3	0.7	0.4	0.6	0.2
Alkalinity (mg/L as CaCO$_3$)	198	144	166	92	70	100
TOC (mg/L)	4	4.3	N/D[a]	N/D[a]	1.3	N/D[a]
TSS (mg/L)	29	5.3	17	1.2	20	< 1
TDS (mg/L)	533	174	663	556	177	617
Chloride (mg/L)	18.5	36	28.3	295	17.2	88.1
Nitrate (mg/L)	21.3	12	12.8	14.2	6.2	8.0
Sulfate (mg/L)	19.4	13	90.5	24.6	46.3	238

[a] Below detection limit.

Table 3.4. Permanganate decay in utility source waters

Utility 1	t (min)	1	10	30	60	91	120
	[KMnO$_4$] (mg/L)	5.3	4.8	4.7	4.1	3.9	3.8
Utility 2	t (min)	1	22	44	60	90	120
	[KMnO$_4$] (mg/L)	5.6	4.8	4.2	3.9	3.7	3.5
Utility 3	t (min)	1	12	30	63	91	120
	[KMnO$_4$] (mg/L)	5.6	5.1	4.6	4.6	4.2	4.1
Utility 4	t (min)	1	11	27	61	93	120
	[KMnO$_4$] (mg/L)	5.7	5.2	4.7	4.3	4.3	4.3
Utility 5	t (min)	1.3	15.5	31	60	90.5	120
	[KMnO$_4$] (mg/L)	6	5.3	4.9	4.6	4.3	3.9
Utility 6[a]	t (min)	1	14	29	59	89	120
	[KMnO$_4$] (mg/L)	6.2	5.8	5.7	5.6	5.6	5.4

[a] Source water samples for Utility 6 collected following application of chlorine at intake pumps, which reduced KMnO$_4$ demand.

CHAPTER 4

OXIDATION OF ANTIBIOTICS DURING WATER TREATMENT WITH POTASSIUM PERMANGANATE: REACTION PATHWAYS AND DEACTIVATION[1]

4.1 Abstract

Recent work demonstrates that three widely administered antibiotics (ciprofloxacin, lincomycin, and trimethoprim) are oxidized by potassium permanganate [$KMnO_4$; Mn(VII)] under conditions relevant to water treatment operations. However, tests show that little to no mineralization occurs during reactions with Mn(VII), so studies were undertaken to characterize the reaction products and pathways and to assess the effects of Mn(VII)-mediated transformations on the antibacterial activity of solutions. Several oxidation products were identified for each antibiotic by liquid chromatography-tandem mass spectrometry (LC-MS/MS). For ciprofloxacin, twelve products were identified, consistent with oxidation of the tertiary aromatic and secondary aliphatic amine groups on the piperazine ring and the cyclopropyl group. For lincomycin, seven products were identified that indicate structural changes to the pyrrolidine ring and thioether group. For trimethoprim, seven products were identified, consistent with Mn(VII) reaction at C=C double bonds on the pyrimidine ring and the bridging methylene group. Oxidation pathways are proposed based on the identified products. Bacterial growth inhibition bioassays (*E. coli* DH5α) show that the mixture of products resulting from Mn(VII) reactions with the antibiotics collectively retain negligible antibacterial potency in comparison to the parent antibiotics. These results suggest that permanganate can be an effective reagent for eliminating the pharmaceutical activity of selected micropollutants during drinking water treatment.

4.2 Introduction

The ubiquitous occurrence of antibiotics in aquatic environments [1-4] has raised numerous concerns, including possible adverse effects on aquatic ecology [5, 6] and human health [7], but the

---

[1] A modified version of Chapter 4 was published in *Environmental Science & Technology*, **2011**, 45, 3635-3642. (L. Hu lead author with co-authors A. M. Stemig, K. H. Wammer, and T. J. Strathmann).

greatest concern is the potential for increased antibiotic resistance among microbial populations continuously exposed to low levels of antibiotics [8, 9]. A growing body of research indicates that conventional water and wastewater treatment practices are inadequate for removing some antibiotic micropollutants and their associated antibacterial activity [10-12]. Thus, extensive efforts are underway to characterize the fate of antibiotics during water treatment processes [10, 13, 14] and to develop new treatment processes to more effectively treat contaminated water sources [15-18].

Past studies report on oxidative treatment of antibiotics, including reactions with chlorine [19-22], chlorine dioxide [16, 18], ozone [23-25], ferrate [26], and UV-TiO$_2$ photocatalysis [27-30]. However, there is limited knowledge on the treatment of antibiotics with permanganate, [MnO$_4^-$; Mn(VII)], an oxidizing agent commonly used to oxidatively precipitate and promote adsorption of reduced metals (Mn, As, and Fe), control biofouling, and address taste and odor problems [31]. Mn(VII) oxidizes a wide range of organic pollutants [32-34], and a recent contribution [35] by the authors shows that three widely administered antibiotics (ciprofloxacin, lincomycin, and trimethoprim) are oxidized by Mn(VII) under conditions relevant to water treatment operations. Reaction kinetics can be described by considering parallel reactions between MnO$_4^-$ and different acid-base species of the target antibiotics, and treatment efficiency in utility source waters can be predicted by considering the pH and temperature dependence of reaction kinetics plus the matrix oxidant demand [35].

Mn(VII) is a selective oxidant that targets electron-rich functional groups [32, 36], and Mn(VII) reactions with organic compounds typically generate a series of incomplete oxidation products and yield little mineralization [33]. Thus, characterizing the reaction products and elucidating the controlling reaction mechanisms is important for identifying the Mn(VII)-reactive moieties in the target contaminants and predicting Mn(VII) reactivity with related compounds that possess the same functional groups. In addition, identifying the structures of reaction products generated from pharmaceutically active compounds can be useful for assessing whether or not Mn(VII) reactions transform structural features critical to the pharmaceutical modes of action [15, 37, 38]. Analysis of reaction products can be coupled with bioassays to link chemical treatment endpoints with biological effects [38-40]. Lee and coworkers [38] demonstrated that reactions between several oxidants and the steroidal hormone 17α-ethinylestradiol eliminate the estrogenic activity of solutions and attributed the reductions in estrogenicity to formation of initial reaction products that elicit substantially reduced estrogenic responses in the in vitro bioassays. Dodd and

coworkers [15] found that reactions of O_3 and $\cdot OH$ with most classes of antibiotics lead to stoichiometric deactivation (i.e., one mole-equivalent of potency is eliminated for each mole of parent antibiotic degraded), indicating that reaction products exhibit significantly reduced potencies. In contrast, O_3 and $\cdot OH$ reactions with the β-lactams penicillin G and cephalexin yield some products that retain significant antibacterial potency, identified as the stereoisomeric (R)-sulfoxides of the parent antibiotics [41].

This contribution examines the products, pathways, and deactivation of three antibiotics (ciprofloxacin, lincomycin, and trimethoprim) during reactions with Mn(VII); this follows a previous report describing the kinetics of these reactions [35]. For each antibiotic, several reaction products are identified based on information collected with liquid chromatography-tandem mass spectrometry (LC-MS/MS). This information is then used to elucidate the pathways for reactions with Mn(VII). Finally, bacterial growth inhibition bioassays are employed to quantify the effects of Mn(VII) treatment on the antibacterial potency of solutions. The target antibiotics are among the most frequently detected in wastewater effluents [10-12]. Ciprofloxacin (CPR) is a fluoroquinolone antibiotic that is active against both gram-positive and gram-negative bacteria. CPR acts by inhibiting microbial DNA replication and repair by targeting two enzymes, DNA topoisomerase II (DNA gyrase) and DNA topoisomerase IV [42]. Lincomycin (LCM) is a lincosamide antibiotic that acts by blocking protein synthesis when binding to the 23S rRNA portion of the 50S subunit of bacterial ribosomes and causing premature dissociation of the peptidyl-tRNA from the ribosome [43]. Trimethoprim (TMP) is a dihydrofolate reductase (DHFR) inhibitor that prevents DNA replication by competing with dihydrofolate for binding to DHFR [37].

4.3 Materials and Methods

4.3.1 Reagents and Analytical

Unless otherwise indicated, all chemicals were of high purity and were used as received from Sigma-Aldrich-Fluka. Tryptone, yeast extract, and agar were purchased from Becton, Dickenson, and Company (Sparks, MD). Iso-Sensitest bacterial growth medium was purchased from Oxoid (Basingstoke, Hampshire, England). Details of analytical methods for measuring parent antibiotic concentrations, mass spectra of reaction products, dissolved organic carbon (DOC), and optical density of bacterial incubations are provided in Section 4.5.1.1.

4.3.2 Reaction Products

To identify reaction products resulting from Mn(VII) reactions with each target antibiotic, a series of 20 mL ammonium acetate-buffered (pH 7) antibiotic solutions were treated with varying doses of Mn(VII). Ammonium acetate was used instead of phosphate buffer, used in earlier kinetics experiments [35], to aid ionization and eliminate the matrix effect of phosphate in the mass spectrometer. Elevated initial antibiotic concentrations (160 μM for CPR, 400 μM for LCM, and 200 μM for TMP) and Mn(VII) concentrations (100−800 μM) were also used to facilitate detection. Sufficient time was allowed for oxidation reactions to reach completion. Tests demonstrated negligible adsorption of the parent antibiotics to $MnO_{2(s)}$, the reduction product of Mn(VII). Samples were then filtered before analyzing by liquid chromatography-electrospray ionization-tandem mass spectrometry (LC-ESI-MS/MS; details provided in Section 4.5.1.1). A similar series of Mn(VII)-reacted antibiotic samples were also prepared and analyzed for residual DOC.

4.3.3 Antibacterial Activity Bioassays

Quantitative bioassays were adapted from procedures described previously [39] to compare the bacterial growth inhibition potential of solutions containing the parent antibiotics with Mn(VII)-reacted solutions. For each target antibiotic, a series of solutions (pH 7) were dosed with varying concentrations of Mn(VII) and allowed sufficient time for reactions to reach completion. Growth of *Escherichia coli* reference strain DH5α was then measured in untreated and Mn(VII)-treated antibiotic solutions and compared against antibiotic-free blanks to quantify the relative potency of solutions. Bacterial growth after 6 hours was quantified by measuring the change in optical density at $\lambda = 600$ nm (ΔOD_{600}). Details of the sample preparation and bioassay procedures are provided in Section 4.5.1.2.

4.4 Results and Discussion

An earlier contribution by the authors established that CPR, LCM, and TMP are readily degraded upon reaction with Mn(VII) [35]. Although oxidation of the antibiotics is presumed, DOC measurements after treatment with different dosages of Mn(VII) show that little or no mineralization of the organic compounds occurs during the reactions (**Figure 4.1**). Instead, reactions lead to incomplete oxidation, and LC-MS/MS analysis reveals a variety of organic

products for each antibiotic (**Table 4.1−Table 4.3** and detailed discussion on procedures for product identification provided in Section 4.5.2). The following sections summarize the products identified and the proposed Mn(VII) reaction pathways for CPR, LCM and TMP.

4.4.1   Mn(VII)-Ciprofloxacin Reactions

Twelve products from Mn(VII)-CPR reactions were identified and their proposed structures are shown in **Table 4.1** (products numbered sequentially based on molecular weight). The proposed structures are consistent with the expected importance of two principal Mn(VII) reaction sites, the tertiary aromatic amine and the secondary aliphatic amine groups on the piperazine ring substituent [35]. In addition, there are two products (III and VI) reflecting structural changes to the cyclopropyl group. However, the core fluoroquinolone structure remains intact in all the products identified, which is consistent with kinetics data for flumequine (a structurally related fluoroquinolone lacking the piperazine ring and cyclopropyl group substituents) showing little reactivity with Mn(VII) [35]. Structural changes to the piperazine ring include dealkylation (I and IV) and formation of alcohols (XI and XII) and amides (II, V, VII, VIII, IX, and X). Oxidation of the cyclopropyl group leads to ring cleavage and formation of acetyl (III) and allyl aldehyde (VI) moieties. Several of the observed products (I, II, IV, V, VII, and X) have also been reported for CPR reactions with other oxidants, including O_3 (I and IV) [25], ClO_2 (I, IV, and X) [18], HOCl (I and IV) [22], $MnO_{2(s)}$ (I, IV, V, and X) [44], alkaline permanganate (pH>12) (I and IV) [45], photolysis (I, IV, and VII) [46] and photocatalysis (I, II, IV, and X) [47].

CPR reaction with Mn(VII) is proposed to proceed by several pathways illustrated in **Figure 4.2**, based upon both the identified products and literature reports of Mn(VII) reactions with amines and olefin groups. Structures identified by LC-MS/MS are indicated by Roman numerals and unidentified intermediates are indicated by italicized letters. The proposed reaction mechanisms are consistent with conclusions drawn from kinetics experiments that the tertiary aromatic amine in the piperazine ring is the primary reactive site [35]. According to Rawalay et al. [48], tertiary amines are oxidized by neutral permanganate to enamines ($RCH=CRNR_2$) and/or to Schiff bases ($RCH=NR$). Both enamines and Schiff bases can then undergo further hydrolysis to form aldehydes and degraded amines, which are subject to further oxidation. C-C bonds in cyclopropyl groups have been reported to possess partial characteristics of highly Mn(VII)-reactive olefin bonds [33, 49], including π character and sp^2 hybridization, and thus are

expected to be susceptible to Mn(VII) oxidation [50].

The initiation step of Mn(VII)-CPR reactions is proposed to be the oxidative formation of an enamine (intermediate A: *Int. A*) from the aromatic amine group, as reported by Rawalay and coworkers [48]. The enamine intermediate can then be transformed by multiple parallel reactions to produce a series of products through either hydrolysis or further Mn(VII) oxidation of the newly formed C=C double bonds [33, 49]. The partially dealkylated product IV is formed when *Int. A* undergoes two consecutive hydrolysis steps. The ring-opened amide product X is produced by oxidation of the enamine C=C double bond in *Int. A*. The enamine can also be hydrolyzed to mono-hydroxylated intermediates (*Int. B* and *Int. C*), further oxidation of which yields the carbonyl products VIII and VII, respectively. Hydrolysis of *Int. B* yields a ring-opened geminal diol intermediate (structure not shown), which quickly converts to *Int. E*. Hydrolysis of the aromatic amide group in X forms product V. Similar to the initiation step with CPR, the amine groups in *Ints. B, C,* and *E* and product V can be oxidized to their respective enamines (*Ints. D, F, G,* and *H*), and subsequent oxidation of the associated olefin groups yield XIIa/XI, XIIb, *Int. I*, and II, respectively. Product IX is formed by further oxidation of the hydroxyl group in XI to a ketone group. The cyclopropyl group in *Int. I* is oxidized to yield aldehyde (III) and carboxylic acid (VI) products; the same products can also be obtained through cyclopropyl group oxidation followed by Mn(VII) reaction at the piperazine ring. Hydrolysis of *Int. H* produces I with the piperazine ring fully dealkylated. Collectively, the identified reaction products indicate that Mn(VII) reactions alter the piperazine and cyclopropyl substituents, but leave the core fluoroquinolone group intact, so it is unclear how oxidation by Mn(VII) will affect the antibacterial activity of CPR solutions.

4.4.2   Mn(VII)-Lincomycin Reactions

Seven products were detected for Mn(VII)-LCM reactions, and their proposed structures are summarized in **Table 4.2**. Reactions with Mn(VII) transform the aliphatic amine group on the pyrrolidine ring and the methyl thioether (-SCH$_3$) moiety, which are the same reactive sites proposed for O$_3$ [51]. Oxidation of the pyrrolidine ring amine group leads to dealkylation (I) and formation of iminiums (IIa and IIb), alcohols (Va and Vb), amides (IV and VII), and cyclic ester (III) products. Oxidation of the thioether group yields the corresponding sulfone (R$_1$R$_2$SO$_2$, VI and VII) products. Pospisil and coworkers [52] reported the formation of sulfone product VI upon oxidation of LCM with H$_2$O$_2$ and biotransformation of LCM using cell free extracts of two

Streptomyces bacteria.

It is interesting to note that the pyranose ring remains intact in the LCM-Mn(VII) oxidation products, in contrast to a recent study which reports cleavage of the ring in clindamycin (a structurally related lincosamide of LCM) by $MnO_{2(s)}$ [17]. The difference in observations may be due to different mechanisms by which the Mn-based oxidants react with organic compounds or to the fact that the pyranose ring might be destabilized by surface complex formation on $MnO_{2(s)}$ prior to oxidation. Alternatively, the LC-MS/MS procedure used in this study may have poor sensitivity for detecting any ring-cleavage products of LCM that might have formed during reactions with Mn(VII).

Figure 4.3 shows the proposed pathways for LCM oxidation by Mn(VII). Mn(VII) reaction with the pyrrolidine ring amine group is initiated by formation of iminiums (*Int. A*, products IIa and IIb). Hydrolysis of the iminiums, *Int. A*, products IIa and IIb, yields demethylation product I, hydroxylated products Va and Vb, respectively. Va is then oxidized by Mn(VII) to form the amide product IV. Hydrolysis of I yields a ring-cleavage intermediate *B*, which is further oxidized to form an imine intermediate *C*. Oxidation of *Int. C* yields *Int. D*, with a carboxylic acid and a hydroxyl groups formed at each end of the opened pyrrolidine ring. Intramolecular esterification of *Int. D* then yields a stable five-member cyclic ester III. Sulfone products, VI and VII, form as a result of direct oxidation of the thioether group on LCM and IV [53], respectively. Although sulfoxide products of LCM were not observed here, they are likely intermediate precursors for oxidation of thioether to sulfone products [54]. Like CPR, LCM-Mn(VII) reactions yield products with structures similar to the parent compound, so the effects on antibacterial activity are also unclear.

4.4.3   Mn(VII)-Trimethoprim Reactions

For TMP-Mn(VII) reactions, seven products were detected by LC-MS/MS (**Table 4.3**). The products show that Mn(VII) reacts with the pyrimidine ring and the methylene group that bridges to the trimethoxybenzene ring. Reaction at the pyrimidine group is consistent with results of kinetics studies conducted with analogues of the two ring systems in the TMP structure [35], where Mn(VII) oxidation of 1,4-diaminopyrimidine is much faster than oxidation of 3,4,5-trimethoxytoluene. Oxidation of the C=C double bonds (C4=C5, or C5=C6) on the pyrimidine ring yields alcohol, aldehyde, ketone and carboxylic acid products (I, II, V, VI and VII),

consistent with previous reports of olefin group oxidation [33, 49]. Mn(VII) reaction with the bridging methylene group produces a hydroxylated TMP (IV) and a ketone (III). This bridging methylene group is also reported as the active site for TMP photolysis [55].

Figure 4.4 shows the proposed mechanisms for Mn(VII)-TMP reactions. Reaction is initiated by 3+2 cyclic addition of Mn(VII) to the C4=C5 or C5=C6 double bond on the pyrimidine ring. Freeman and co-workers [56] report a similar mechanism for Mn(VII) oxidation of uracil (2,4-dihydroxylpyrimidine), which is structurally similar to the 2,4-diaminopyrimidine moiety in TMP. This mechanism is also consistent with well documented Mn(VII) reactions with olefin groups [33, 49], indicating that the C=C bonds in the diaminopyrimidine ring have olefinic characteristics. Oxidation of the C=C double bonds yields hydroxyl, aldehyde, ketone, and carboxylic acid products. For example, oxidation at the C5=C6 bond first produces dihydroxylated TMP (VII), with further oxidation cleaving the pyrimidine ring and yielding Vb. Vb then undergoes hydrolysis to yield II. Oxidation on the C4=C5 bond yields Va, and further hydrolysis of the amide group in Va yields the carboxylic products VI or I. Alternatively, reactions can be initiated by a hydride abstraction from the bridging methylene group to form a carbocation intermediate, which yields IV upon hydroxylation. Further oxidation of IV yields a ketone product III. Mn(VII) reaction at the bridging methylene group is attributed to activation by the two attached rings. Hydride abstraction by Mn(VII) is documented [57] and carbocation intermediates of pyrimidines have been previously reported [58].

For TMP, the integrity of the pyrimidine ring is reported to be essential for antibacterial activity [37]. Thus, since several of the observed products include modifications to the pyrimidine ring, including ring opening, at least partial deactivation of TMP can be anticipated during Mn(VII) treatment.

4.4.4   Antibacterial Activity

A variety of organic products are identified for Mn(VII)-antibiotic reactions, but the potency of these reaction products relative to the parent antibiotics remains unclear. Quantitative bioassays were conducted to address the effects of Mn(VII) treatment on the potency of antibiotic solutions. Figure 4.5 shows the measured antibacterial concentration-growth inhibition curves for untreated and Mn(VII)-treated antibiotic solutions. Bacterial growth in untreated samples is plotted as a function of antibiotic concentration over a serial dilution series, whereas growth in

Mn(VII)-treated samples is plotted as a function of the residual undegraded antibiotic concentration measured following treatment with different Mn(VII) dosages. Growth of *E. coli* strain DH5α in solutions exposed to antibiotics and reaction products is indicated by ΔOD_{600}, the change in optical density of the solution at 600 nm after a 6-h incubation. Large ΔOD_{600} values correspond to strong growth and minimal growth inhibition from analytes in solution. Comparing the measured growth of *E. coli* DH5α in the presence of untreated antibiotics (closed triangles) versus in the presence of Mn(VII)-treated antibiotics (open triangles), few differences can be found in terms of bacterial growth inhibition, indicating that antibacterial potency in Mn(VII)-treated samples can be attributed mostly to the residual parent compound remaining after Mn(VII) treatment. If products had exhibited significant potency, ΔOD_{600} curve would have shifted to the left and downward. Change of bacterial growth inhibition with antibiotic concentration can be quantified by fitting measured data with a Boltzmann curve [39],

$$y = A_2 + \frac{(A_1 - A_2)}{1 + e^{(x - x_0)/dx}} \tag{4.1}$$

where x is the log of antibiotic concentration, y is the 6-h ΔOD_{600}, A_1 is the value of y corresponding to no growth inhibition, A_2 is the value of y corresponding to maximum growth inhibition, dx is the slope, and x_0 is the midpoint of the curve, corresponding to the log of the median effective antibiotic concentration (EC50). Model fits for both untreated and Mn(VII)-treated antibiotic solutions are shown in **Figure 4.5**. Fit-derived log(EC50) values for Mn(VII)-treated and untreated solutions are not significantly different at the 95% confidence level, confirming that bacterial growth inhibition in the Mn(VII)-reacted samples can be attributed mainly to the residual parent compound concentration remaining after Mn(VII) treatment, and the Mn(VII) reaction product mixture collectively contributes negligible antibacterial activity to the samples in comparison to the parent antibiotic. This does not preclude some minor oxidation products from possessing similar or even greater activities than their parent antibiotics, but their concentrations are too low to detect their effects in the bioassay. These findings are notable because they demonstrate that incomplete oxidation of antibiotics during Mn(VII) water treatment processes will likely be sufficient to eliminate the antibacterial activity of impacted source waters.

Reductions in antibiotic potency upon Mn(VII) treatment can be interpreted in light of the identified reaction products. For CPR, although the core fluoroquinolone structure remains intact following reaction with Mn(VII), oxidation of the piperazine and cyclopropyl substituents can also

be expected to reduce potency [40, 59]. Quinolones having small or linear substituents at the C-7 position (see **Figure 4.2**) have been reported to exhibit lower potency than analogues substituted with heterocyclic rings containing peripheral basic nitrogens like CPR [59]. In addition, cyclopropyl group substitution at the N-1 position is reported to be optimal for fluoroquinolone antibacterial activity [59]. Thus, oxidation of the piperazine and cyclopropyl rings forms a series of products that are expected to exhibit reduced potency.

None of the functional groups in LCM believed to be responsible for binding to 23S rRNA of bacteria (carbonyl and ring-bound hydroxyl groups) are oxidized by Mn(VII). However, oxidation of the thioether group leads to LCM-sulfone [23, 60], which possess significantly lower antibacterial potency than the parent structure [60], possibly due to interruption of intermolecular hydrogen bonding patterns at adjacent hydroxyl and methyl groups.

TMP is a dihydrofolate reductase inhibitor, and the diaminopyrimidine moiety, which resembles part of the structure of 7,8-dihydrofolic acid, is critical to the compound's antibacterial activity [37]. Thus, elimination of antibacterial potency during Mn(VII) treatment is consistent with the observed cleavage of the pyrimidine ring during Mn(VII)-TMP reactions.

4.5 Supporting Information

4.5.1 Analytical and Bioassay Procedures

4.5.1.1 Analytical

Concentrations of the parent antibiotics were determined using a Shimadzu high performance liquid chromatograph (HPLC; VP series) equipped with photodiode array detection (PDA). The detailed HPLC methods are the same as those reported in [35]. Dissolved organic carbon (DOC) of Mn(VII)-reacted solutions was analyzed using a Shimadzu TOC analyzer (TOC-VCPN, Kyoto, Japan).

Organic reaction products were identified by liquid chromatography coupled with tandem mass spectrometry (LC-MS/MS). Analysis was performed on an Agilent 1200 LC/MSD Trap XCT Ultra instrument with a Zorbax Eclipse XDB-C18 column (2.1×50 mm, 3.5 μM particle size). Different gradient methods were used for separation of products for the three target antibiotics. The mobile phases and gradient methods (0.2 mL/min) are summarized in **Table 4.4**. For MS analyses, ionization was achieved through positive-mode electrospray (ESI$^+$) over a

mass-to-charge (m/z) range of 50–500. An ion trap was used to isolate and fragment target ions, and the auto-MS(2) mode was used with a fragmentation voltage of 1.0 V. A conversion dynode/electron multiplier system was used to detect and record the MS^1 and MS^2 spectra. For ciprofloxacin, product analysis was also performed on a Micromass Q-TOF ultima to obtain more fragments in MS^2 spectra and aid product identification. The same column and mobile phase gradient were used as described above. The collision induced dissociation (CID) energy applied was 35 V.

4.5.1.2 Antibacterial Activity Bioassays

Quantitative bioassays were used to determine the effects of Mn(VII) treatment on the bacterial growth inhibition potential of antibiotic solutions. For CPR and TMP, Mn(VII)-reacted solutions were prepared by dosing a series of 20-mL phosphate-buffered solutions (pH 7) with varying concentrations of Mn(VII) and allowing sufficient time for the reactions to reach completion. After reaction, excess hydroxylamine was added to reactors to reduce residual Mn(VII) and $MnO_{2(s)}$ to soluble Mn^{2+}. The quenched solutions were then subjected to solid phase extraction (SPE) to remove inorganic salts (e.g., Mn^{2+}, phosphate, hydroxylamine) before using in bioassays. For LCM, reaction samples were prepared using a different procedure because the antibacterial activity bioassay working concentration range was too high to permit use of SPE without overloading the resin cartridges. Instead, Mn(VII)-reacted LCM samples were prepared by dosing varying concentrations of Mn(VII) into LCM solutions and directly collecting filtered supernatant after allowing reactions to reach completion. To minimize potential artifacts from inorganic solution constituents on LCM bioassay results, reactions were conducted in unbuffered solutions and varying amounts of KCl were added to samples to obtain a constant K^+ concentration (to match the varying K^+ associated with different doses of $KMnO_4$). After reaction completion, suspensions were centrifuged and the supernatant was filtered and pH adjusted to 7 for use in bioassays (pH drifted from 7 to 9-10 during reactions).

For Mn(VII)-reacted CPR and TMP samples, SPE was performed using Oasis HLB cartridges (Waters, 500 mg, LP). First, SPE cartridges were sequentially conditioned with 5 mL methanol and 5 mL H_2O. Antibiotic solutions were then directly loaded to the preconditioned cartridges mounted on a Visiprep vacuum manifold (Sigma-Aldrich) and dropwise flow rates were maintained for the extraction process. After extraction, the cartridges were washed with 5 mL H_2O

85

to remove residual inorganic impurities. Five mL of acetone was then used to elute the sorbed antibiotics and organic products. The SPE eluates were then divided into two portions and dried under a gentle stream of air. One portion was reconstituted in phosphate buffer and analyzed for residual antibiotic concentration by HPLC-PDA. The other portion was reconstituted in deionized water and used to quantify antibacterial potency. SPE recoveries of the parent antibiotics were determined by comparing antibiotic concentrations in the eluates with the concentration in the corresponding SPE feed solutions (>76% recovery in all samples). The SPE recoveries of all individual oxidation products were not quantified, but HPLC data for several of the products show similar recoveries as the parent antibiotics. In addition, we expect similar SPE recoveries for many of products because the structures are similar to the parent antibiotics and the hydrophilic-lipophilic balance (HLB) SPE cartridges are optimized for extraction of both polar and non-polar compounds.

Antibacterial activity bioassays were adapted from methods described previously [39]. Growth of *Escherichia coli (E. coli)* reference strain DH5α was measured in triplicate in untreated and Mn(VII)-treated solutions of each target antibiotic and compared against antibiotic-free blanks to quantify the relative potency of solutions. *E. coli* were maintained on sterile Luria-Bertani (LB) solid medium. Tests show that the DH5α strain responds well to all three antibiotics. Cells were grown overnight on Iso-Sensitest broth (ISB), and media was autoclaved to sterilize. The working concentration range of each target antibiotic was first determined by measuring *E. coli* growth in solutions containing varying antibiotic concentrations. One mL antibiotic solutions of varying concentration were mixed with 100 μL of *E. coli* and 9 mL of ISB in a series of test tubes. Tubes were then incubated at 37°C and gently shaken. Bacterial growth after 6 hours was then quantified by measuring the change in optical density at $\lambda = 600$ nm ($\Delta OD_{600} = 6$ hour OD_{600} - initial OD_{600}) using a Varian Cary 300 Bio UV-Visible Spectrophotometer. Large ΔOD_{600} values correspond to strong growth and minimal growth inhibition from analytes in solution. The relative ability of Mn(VII) reaction products to inhibit bacterial growth was then tested by the same method, using 1 mL of SPE extracts (CPR and TMP) or solution filtrate (LCM) collected from reaction mixtures.

4.5.2   Identification of Antibiotic Oxidation Products

A large number of products are detected for Mn(VII) oxidation of the three antibiotics as summarized in **Table 4.1−Table 4.3**. **Figure 4.6−Figure 4.8** show the relative distribution of

LC-MS peak areas for different Mn(VII) reaction products of each parent antibiotic, providing a rough qualitative measure of the distribution of reaction products. However, it should be noted that the peak areas are from the mass spectrometry peaks and do not quantitatively correlate their absolute concentration since reference standards of the individual analytes are not available. Although a large number of reaction products were detected for each antibiotic using LC-MS/MS, it is likely that additional products were also formed but not detected, either because of their low concentration or the low sensitivity of the method for these analytes (e.g., due to poor electrospray ionization).

In general, structures of reaction products are proposed based on the mass of the pseudo-molecular ion (MH$^+$) observed in MS, the MS/MS fragmentation pattern (mass spectra of the parent compounds and reaction products are provided in **Table A.2−Table A.4** in Appendix A), and the chromatographic retention times (R.T.), along with previously reported information on common reactive sites in each antibiotic and general oxidation pathways for these reactive groups. The MS/MS fragmentation pathways of the parent antibiotics (**Table 4.5−Table 4.7**) are also proposed and serve as a basis for the elucidation of the structures of their products.

4.5.2.1   Ciprofloxacin (CPR)

Twelve products were detected by LC-MS/MS for CPR reactions with Mn(VII). The mass of MH$^+$, MS/MS fragment ions, R.T., and the proposed structures for the 12 products are summarized in **Table 4.1**.

The interpretation of the MS/MS spectra of CPR is shown in **Table 4.5**. The fragment ions showed loss of the carboxylic group, the cyclopropyl ring, the fluorine atom, and partial loss of the piperazine ring, with the core quinolone group remaining intact. The MS/MS fragmentation patterns of CPR and its products do not provide decisive information that can aid the elucidation of product structures. Therefore, proposed structures were primarily based on the observed molecular weights and expected reaction sites with Mn(VII). In addition, the "nitrogen rule" that a compound contains odd numbers of nitrogen atoms will have an odd molecular weight is also applied in determining the molecular formula of several compounds. As discussed in earlier work [35], there are three possible reactive sites in CPR: the aromatic tertiary amine group in the piperazine ring, the aliphatic secondary amine group in the piperazine ring and the cyclopropyl group. Therefore, proposed structures of products considered oxidative structural changes to these three sites.

Oxidation of amines by Mn(VII) was proposed to produce hydroxylated and acetylated products [48]. Proposed structures for products all conform with the observed MS/MS fragmentation patterns (**Table 4.5**). Several of the observed products (I, II, IV, V, VII, and X) were also detected with similar MS/MS fragmentation patterns in oxidation of CPR using other oxidation systems: O_3 [25], HOCl [22], ClO_2 [18], $MnO_{2(s)}$ [44], alkaline permanganate (pH>12) [45], photolysis [46], and photocatalysis [29], and same structures of these products were proposed.

The HPLC retention times of the products were used to supplement identification of products and exclude implausible structures. Because the core fluoroquinolone group remains intact in all products, the relative HPLC retention times of the oxidation products are heavily influenced by the basicity of the piperazine ring, especially considering that the mobile phases used for LC-MS/MS analysis contains 0.1% formic acid. Products with strong basicity will likely have shorter retention times because they will be present as charged species in the eluent matrix. The aliphatic secondary amine in CPR is responsible for the basicity of CPR since arylamines, amides, and nitrogen in aromatic heterocyclic rings have much weaker basicity [61]. Therefore, products that exhibit relatively short retention times are expected to retain the aliphatic amine group, whereas structural changes to the aliphatic secondary amine group is expected in products that exhibit much longer retention times than CPR. As shown in **Table 4.1,** products IV and VII have relatively short retention times and the aliphatic amine group in their structures is retained. Specifically, product VII and VIII have the same molecular weight and similar MS/MS fragmentation pattern, but their HPLC retention times differ dramatically. The longer retention time of VIII is proposed to result from the conversion the aliphatic tertiary amine to a less basic amide group that remains deprotonated and uncharged in the eluent matrix.

4.5.2.2   Lincomycin (LCM)

Seven products from Mn(VII) oxidation of LCM are detected by LC-MS/MS (**Table 4.2**). In comparison to CPR, the MS/MS fragmentation patterns observed for LCM oxidation products provide more valuable information for elucidating structural changes in oxidation products.

The MS/MS fragmentation pathway for LCM (m/z: 407) is proposed in Figure 4.7**Table 4.6**. The two characteristic fragmentation pathways used to identify structural changes in LCM oxidation products are: (a) the formation of an (MH-48) fragment ion (m/z: 359) from the loss of a methyl thioether [-SCH_4 (48)] group, and (b) the formation of the pyrrolidine fragment ion (m/z:

126) that is directly cleaved from the parent molecular ion. These two fragment ions are also the two most abundant fragment ions in the MS/MS spectra. The structures of the products are then proposed based on the two characteristic fragmentation pathways of LCM in combination with their molecular weights and chromatographic retention times as shown in **Table 4.2** and **Table 4.6**.

For product I, II, III and IV, the presence of a most abundant (MH-48) fragment ion and the absence of the pyrrolidine fragment ion suggest the intactness of the thioether group and structural modifications to the pyrrolidine ring. Products I, II, and IV were proposed to be demethylation, dehydrogenation, and carbonylation products of LCM, respectively, based on their molecular weight differences from LCM. In place of the pyrrolidine fragment ion, the fragment ions with m/z values of 112, 124, and 140 also support the proposed structural changes to the pyrrolidine ring of products I, II, and IV, respectively (note: the m/z 140 fragment ion of product IV was not directly observed but was seen in the MS/MS spectra of fragment ion 373 from product IV). For product III, the odd molecular weight of its neutral molecule suggests an odd number of nitrogen atoms in the molecule and thus the loss of one nitrogen atom from LCM. A lactone structure in place of the pyrrolidine ring was proposed for product III based on its molecular weight difference with LCM.

For product V, the most abundant fragment ion is an (MH-66) ion and the second most abundant ion is an (MH-48) ion. We propose product V to be a hydroxylated LCM with the hydroxyl group attached to either of the two alpha positions of the pyrroline amine. The (MH-66) fragment ion is thus from the loss of the thioether group and the hydroxyl group on the pyrrolidine ring. A minor pyrrolidine fragment ion is also seen, which is probably formed by the loss of hydroxyl group from the hydroxylated pyrrolidine ring.

For product VI, the most abundant ion is an (MH-80) fragment ion and the second most abundant ion is the pyrrolidine fragment ion. Thus oxidation of the thioether group to a sulfone group is proposed. The most abundant fragment ion (MH-80) is then from the loss of the sulfone group [-SO_2CH_4 (80)]. A minor (MH-48) fragment ion is also seen, which is proposed to forme by the loss of a SO group from the sulfone group.

For product VII, neither the (MH-48) fragment ion nor the pyrrolidine fragment ion is present and the most abundant fragment ion is an (MH-80) ion. Thus, structural changes are proposed to occur on both moieties. We propose product VII to be a LCM sulfone with the pyrrolidine amine group converted to an amide. Similar to product VI, the (MH-80) fragment ion is from the loss of the sulfone group [-SO_2CH_4 (80)]. Similar to product IV, the presence of a

fragment ion with an m/z of 140 is also supportive of the proposed structural change to the pyrrolidine ring.

The HPLC retention times of oxidation products can also be used to check whether a proposed structure also agree with its chromatographic behavior. Products I, II, and VI all have retention times either close to or shorter than that of LCM, indicating the presence of the pyrrolidine amine. The short retention time of product II might be due to its iminium ion form. In contrast, products III, IV, V and VII all have much longer retention times than LCM, resulting from the conversion of the pyrrolidine aliphatic amine to a less basic amide group, loss of the aliphatic amine group entirely, or addition of a hydroxyl group adjacent to the amine group.

4.5.2.3   Trimethoprim (TMP)

Seven products from Mn(VII)-oxidation of TMP are detected by LC-MS/MS (**Table 4.3**). After examining the MS/MS spectra of all products and the proposed fragmentation pathway of TMP, a common fragment ion is observed for TMP and several of the products (I, V, VI, and VII), which possesses m/z of 181 and corresponds to the trimethoxytoluene cation. For product II, a fragment ion with m/z of 183 is present instead of m/z of 181, and this fragment ion is proposed to be a pseudo-molecular ion of trimethoxytoluene. Therefore, the presence of a fragment ion with m/z of 181 or 183 indicates the intactness of the trimethoxytoluene moiety, and no structural changes were proposed to the trimethoxytoluene moiety for products I, II, V, VI, and VII. According to Freeman and co-workers [56], the Mn(VII) oxidation site of uracil (2,4-dihydroxylpyrimidine, structure similar to the 2,4-diaminopyrimidine moiety in TMP) is the C4=C5 double bond. Oxidation of TMP is also expected to occur at this site as well as the C5=C6 double bond (resonance structures exist for TMP, **Figure 4.4**). Thus, proposed structures for product I, II, V, VI, and VII include hydroxylated TMP and complicated amide, ketone, carboxylic acid-containing compounds resulting from cleavage of the pyrimidine ring upon oxidation of either the C4=C5 or C5=C6 double bonds.

For product III and IV, the absence of the fragment ion with m/z of 181 indicates a structural modification to the trimethoxytoluene moiety. Because the methoxy groups and the benzene ring are relatively inert towards Mn(VII) oxidation, the site of structural modification is proposed to be on the methylene group that bridges between the aromatic and pyrimidine rings. This group has also been proposed as the site of photolytic attack in TMP [55]. Therefore,

corresponding to their pseudo-molecular ion molecular weights, a hydroxylated TMP is proposed for product IV, and a ketone form of TMP is proposed for product III. In addition, the fragment ions of product III correspond well with those of TMP in that the parent compound and almost all fragment ions differ by a mass of 14, indicating relatively small structural changes occur in product III, as demonstrated by the proposed structure.

Finally, comparing the retention times between TMP and its products, we can see that only product III and VI have longer retention time than that of TMP, while the rest of the products have similar or shorter retention time. For product I, II, and V, the disruption of pyrimidine ring in TMP may increase hydrophilicity by destruction of the ring group, and addition of hydroxyl groups in IV and VII can also be expected to increase hydrophilicity. For product III and VI, the extended retention time may result from decreased basicity of N-1 in the pyrimidine ring upon formation of the electron-withdrawing carbonyl group adjacent to this site.

4.6 References Cited

[1]   Hirsch R., Ternes T., Haberer K. and Kratz K.-L. Occurrence of antibiotics in the aquatic environment *Science of the Total Environment*, **1999**, 225: 109-118.

[2]   Kolpin D. W., Furlong E. T., Meyer M. T., Thurman E. M., Zaugg S. D., Barber L. B. and Buxton H. T. Pharmaceuticals, hormones, and other organic wastewater contaminants in U.S. streams, 1999-2000: a national reconnaissance. *Environmental Science & Technology*, **2002**, 36: 1202-1211.

[3]   Ternes T. A. Occurrence of drugs in German sewage treatment plants and rivers. *Water Research*, **1998**, 32: 3245-3260.

[4]   Heberer T. Occurrence, fate, and removal of pharmaceutical residues in the aquatic environment: A review of recent research data. *Toxicology Letters*, **2002**, 131: 5-17.

[5]   Yang L. H., Ying G. G., Su H. C., Stauber J. L., Adams M. S. and Binet M. T. Growth-inhibiting effects of 12 antibacterial agents and their mixtures on the freshwater microalga *Pseudokirchneriella subcapitata*. *Environmental Toxicology and Chemistry*, **2008**, 27: 1201-1208.

[6]   Wilson B. A., Smith V. H., Denoyelles F. and Larive C. K. Effects of three pharmaceutical and personal care products on natural freshwater algal assemblages. *Environmental Science & Technology*, **2003**, 37: 1713-1719.

[7]   Pomati F., Castiglioni S., Zuccato E., Fanelli R., Vigett D., Rossetti C. and Calamari D. Effects of a complex mixture of therapeutic drugs at environmental levels on human embryonic cells. *Environmental Science & Technology*, **2006**, 40: 2442-2447.

[8]   Baquero F. Low-level antibacterial resistance: A gateway to clinical resistance. *Drug Resistance Updates*, **2001**, 4: 93-105.

[9]   Szczepanowski R., Linke B., Krahn I., Gartemann K. H., Gutzkow T., Eichler W., Puhler A. and Schluter A. Detection of 140 clinically relevant antibiotic-resistance genes in the plasmid metagenome of wastewater treatment plant bacteria showing reduced susceptibility to selected antibiotics. *Microbiology*, **2009**, 155: 2306-2319.

[10]   Watkinson A. J., Murby E. J. and Costanzo S. D. Removal of antibiotics in conventional and advanced wastewater treatment: Implications for environmental discharge and wastewater recycling. *Water Research*, **2007**, 41: 4164-4176.

[11]   Lindberg R. H., Olofsson U., Rendahl P., Johansson M. I., Tysklind M. and Andersson B. A. V. Behavior of fluoroquinolones and trimethoprim during mechanical, chemical, and active sludge treatment of sewage water and digestion of sludge. *Environmental Science & Technology*, **2006**, 40: 1042-1048.

[12]   Lindberg R. H., Wennberg P., Johansson M. I., Tysklind M. and Andersson B. A. V. Screening of human antibiotic substances and determination of weekly mass flows in five sewage treatment plants in Sweden. *Environmental Science & Technology*, **2005**, 39: 3421-3429.

[13]   Ikehata K., Naghashkar N. J. and Ei-Din M. G. Degradation of aqueous pharmaceuticals by ozonation and advanced oxidation processes: A review. *Ozone: Science and Engineering*, **2006**, 28: 353-414.

[14]   Ternes T. A., Meisenheimer M., McDowell D., Sacher F., Brauch H. J., Gulde B. H., Preuss G., Wilme U. and Seibert N. Z. Removal of pharmaceuticals during drinking water treatment. *Environmental Science & Technology*, **2002**, 36: 3855-3863.

[15]   Dodd M. C., Kohler H. P. E. and von Gunten U. Oxidation of antibacterial compounds by ozone and hydroxyl radical: Elimination of biological activity during aqueous ozonation processes. *Environmental Science & Technology*, **2009**, 43: 2498-2504.

[16]   Huber M. M., Korhonen S., Ternes T. A. and von Gunten U. Oxidation of pharmaceuticals during water treatment with chlorine dioxide. *Water Research*, **2005**, 39: 3607-3617.

[17] Chen W.-R., Ding Y., Johnston C. T., Teppen B. J., Boyd S. A. and Li H. Reaction of lincosamide antibiotics with manganese oxide in aqueous solution. *Environmental Science & Technology*, **2010**, 44: 4486-4492.

[18] Wang P., He Y. L. and Huang C. H. Oxidation of fluoroquinolone antibiotics and structurally related amines by chlorine dioxide: Reaction kinetics, product and pathway evaluation. *Water Research*, **2010**, 44: 5989-5998.

[19] Chamberlain E. and Adams C. Oxidation of sulfonamides, macrolides, and carbadox with free chlorine and monochloramine. *Water Research*, **2006**, 40: 2517-2526.

[20] Dodd M. C. and Huang C. H. Transformation of the antibacterial agent sulfamethoxazole in reactions with chlorine: Kinetics, mechanisms, and pathways. *Environmental Science & Technology*, **2004**, 38: 5607-5615.

[21] Dodd M. C. and Huang C. H. Aqueous chlorination of the antibacterial agent trimethoprim: Reaction kinetics and pathways. *Water Research*, **2007**, 41: 647-655.

[22] Dodd M. C., Shah A. D., von Gunten U. and Huang C.-H. Interactions of fluoroquinolone antibacterial agents with aqueous chlorine: Reaction kinetics, mechanisms, and transformation pathways. *Environmental Science & Technology*, **2005**, 39: 7065-7076.

[23] Dodd M. C., Buffle M. O. and von Gunten U. Oxidation of antibacterial molecules by aqueous ozone: Moiety-specific reaction kinetics and application to ozone-based wastewater treatment. *Environmental Science & Technology*, **2006**, 40: 1969-1977.

[24] Huber M. M., Canonica S., Park G. Y. and von Gunten U. Oxidation of pharmaceuticals during ozonation and advanced oxidation processes. *Environmental Science & Technology*, **2003**, 37: 1016-1024.

[25] De Witte B., Dewulf J., Demeestere K., Van De Vyvere V., De Wispelaere P. and Van Langenhove H. Ozonation of ciprofloxacin in water: HRMS identification of reaction products and pathways. *Environmental Science & Technology*, **2008**, 42: 4889-4895.

[26] Sharma V. K., Mishra S. K. and Nesnas N. Oxidation of sulfonamide antimicrobials by ferrate(VI) [$Fe^{VI}O_4^{2-}$]. *Environmental Science & Technology*, **2006**, 40: 7222-7227.

[27] Bhakta J. N. and Munekage Y. Degradation of antibiotics (trimethoprim and sulphamethoxazole) pollutants using UV and TiO_2 in aqueous medium. *Modern Applied Science*, **2009**, 3: 3-13.

[28] Hu L., Flanders P. M., Miller P. L. and Strathmann T. J. Oxidation of sulfamethoxazole and

related antimicrobial agents by TiO$_2$ photocatalysis. *Water Research*, **2007**, 41: 2612-2626.

[29]   Paul T., Dodd M. C. and Strathmann T. J. Photolytic and photocatalytic decomposition of aqueous ciprofloxacin: Transformation products and residual antibacterial activity. *Water Research*, **2010**, 44: 3121-3132.

[30]   Paul T., Miller P. L. and Strathmann T. J. Visible-light-mediated TiO$_2$ photocatalysis of fluoroquinolone antibacterial agents. *Environmental Science & Technology*, **2007**, 41: 4720-4727.

[31]   MWH. *Water Treatment: Principles and Design*, 2nd ed. Hoboken: Wiley, **2005**.

[32]   Waldemer R. H. and Tratnyek P. G. Kinetics of contaminant degradation by permanganate. *Environmental Science & Technology*, **2006**, 40: 1055-1061.

[33]   Hu L., Martin H. M., Arce-Bulted O., Sugihara M. N., Keating K. A. and Strathmann T. J. Oxidation of carbamazepine by Mn(VII) and Fe(VI): Reaction kinetics and mechanism. *Environmental Science & Technology*, **2009**, 43: 509-515.

[34]   Jiang J., Pang S.-Y. and Ma J. Oxidation of triclosan by permanganate (Mn(VII)): Importance of ligands and in situ formed manganese oxides. *Environmental Science & Technology*, **2009**, 43: 8326-8331.

[35]   Hu L., Martin H. A. and Strathmann T. J. Oxidation kinetics of antibiotics during water treatment with potassium permanganate. *Environmental Science & Technology*, **2010**, 44: 6416-6422.

[36]   Ladbury J. W. and Cullis C. F. Kinetics and mechanism of oxidation by permanganate. *Chemical Reviews*, **1958**, 58: 403-438.

[37]   Walsh C. *Antibiotics: Actions, Origins, Resistance*. Washington D. C.: ASM Press, **2003**.

[38]   Lee Y., Escher B. I. and von Gunten U. Efficient removal of estrogenic activity during oxidative treatment of waters containing steroid estrogens. *Environmental Science & Technology*, **2008**, 42: 6333-6339.

[39]   Wammer K. H., LaPara T. M., McNeill K., Arnold W. A. and Swackhamer D. L. Changes in antibacterial activity of triclosan and sulfa drugs due to photochemical transformations. *Environmental Toxicology and Chemistry*, **2006**, 25: 1480-1486.

[40]   Domagala J. M. Structure-activity and structure-side-effect relationships for the quinolone antibacterials. *Journal of Antimicrobial Chemotherapy*, **1994**, 33: 685-706.

[41]   Dodd M. C., Rentsch D., Singer H. P., Kohler H. P. E. and von Gunten U. Transformation of

β-lactam antibacterial agents during aqueous ozonation: Reaction pathways and quantitative bioassay of biologically-active oxidation products. *Environmental Science & Technology*, **2010**, 44: 5940-5948.

[42] Drlica K. and Zhao X. DNA gyrase, topoisomerase IV, and the 4-quinolones. *Microbiol Mol Biol Rev*, **1997**, 61: 377-392.

[43] Schlunzen F., Zarivach R., Harms J., Bashan A., Tocilj A., Albrecht R., Yonath A. and Franceschi F. Structural basis for the interaction of antibiotics with the peptidyl transferase centre in eubacteria. *Nature*, **2001**, 413: 814-821.

[44] Zhang H. C. and Huang C. H. Oxidative transformation of fluoroquinolone antibacterial agents and structurally related amines by manganese oxide. *Environmental Science & Technology*, **2005**, 39: 4474-4483.

[45] Thabaj K. A., Kulkarni S. D., Chimatadar S. A. and Nandibewoor S. T. Oxidative transformation of ciprofloxacin by alkaline permanganate - A kinetic and mechanistic study. *Polyhedron*, **2007**, 26: 4877-4885.

[46] Burhenne J., Ludwig M., Nikoloudis P. and Spiteller M. Photolytic degradation of fluoroquinolone carboxylic acids in aqueous solution . Part 1. Primary photoproducts and half-lives. *Environmental Science and Pollution Research*, **1997**, 4: 10-15.

[47] Paul T., Dodd M. C. and Strathmann T. J. Photolytic and photocatalytic decomposition of aqueous ciprofloxacin: Transformation products and residual antibacterial activity. *Water Research*, **2010**, 44: 3121-3132.

[48] Rawalay S. S. and Shechter H. Oxidation of primary, secondary, and tertiary amines with neutral permanganate. A simple method for degrading amines to aldehydes and ketones. *Journal of Organic Chemistry*, **1967**, 32: 3129-3131.

[49] Yan Y. E. and Schwartz F. W. Kinetics and mechanisms for TCE oxidation by permanganate. *Environmental Science & Technology*, **2000**, 34: 2535-2541.

[50] Walsh A. D. The structures of ethylene oxide, cyclopropane, and related molecules. *Trans Faraday Soc*, **1949**, 45: 179-190.

[51] Qiang Z., Adams C. and Surampalli R. Determination of ozonation rate constants for lincomycin and spectinomycin. *Ozone: Science and Engineering*, **2004**, 26: 525-537.

[52] Pospisil S., Sedmera P., Halada P. and Spizek J. Oxidation of lincomycin by hydrogen peroxide restricts its potential biotransformation with haloperoxidases. *Folia*

Microbiologica, **2001**, 46: 376-378.

[53] Walton J., Labine P. and Reidies A., eds. The chemistry of permanganate in degradative oxidations. Lancaster: CRC Press 1992.

[54] Dash S., Patel S. and Mishra B. K. Oxidation by permanganate: synthetic and mechanistic aspects. *Tetrahedron*, **2009**, 65: 707-739.

[55] Dedola G., Fasani E. and Albini A. The photoreactions of trimethoprim in solution. *Journal of Photochemistry and Photobiology A: Chemistry*, **1999**, 123: 47-51.

[56] Freeman F., Fuselier C. O., Armstead C. R., Dalton C. E., Davidson P. A., Karchesfski E. M., Krochman D. E., Johnson M. N. and Jones N. K. Permanganate ion oxidations. 13. Soluble manganese(IV) species in the oxidation of 2,4(1*H*,3*H*)-pyrimidinediones (uracils). *Journal of the American Chemical Society*, **2002**, 103: 1154-1159.

[57] Gardner K. A. and Mayer J. M. Understanding C-H bond oxidations: H· and H⁻ transfer in the oxidation of toluene by permanganate. *Science*, **1995**, 269: 1849-1851.

[58] Hanes J. W., Ealick S. E. and Begley T. P. Thiamin phosphate synthase: The rate of pyrimidine carbocation formation. *Journal of the American Chemical Society*, **2007**, 129: 4860-4861.

[59] Chu D. T. and Fernandes P. B. Structure-activity relationships of the fluoroquinolones. *Antimicrobial Agents and Chemotherapy*, **1989**, 33: 131-135.

[60] Sztaricskai F., Dinya Z., Batta G., Mocsári A., HollÓsi M., Majer Z., Masuma R. and Omura S. Chemical synthesis and structural study of lincomycin sulfoxides and a sulfone. *The Journal of Antibiotics*, **1997**, 50: 866-873.

[61] Solomons T. W. G. *Organic Chemistry*. New York: John Wiley & Sons, Inc., **1996**.

4.7 Figures and Tables
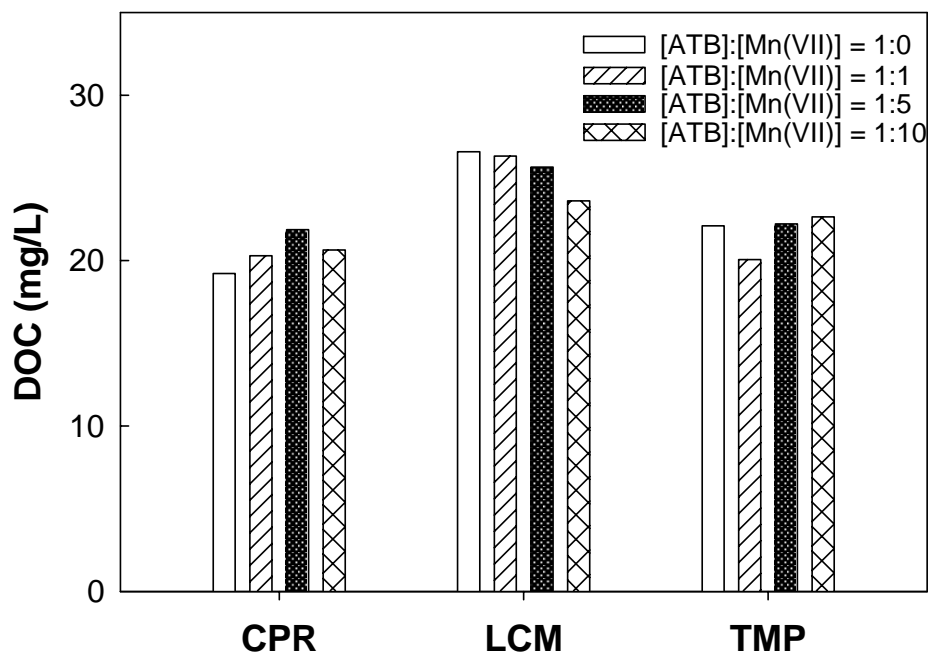
Figure 4.1. Measured dissolved organic carbon (DOC) concentration of the target antibiotics after treatment with different doses of Mn(VII). Reaction conditions: $[ATB]_0 =$ 100 μM, varying [Mn(VII)], 25 mM phosphate buffer, pH 7, room temperature.
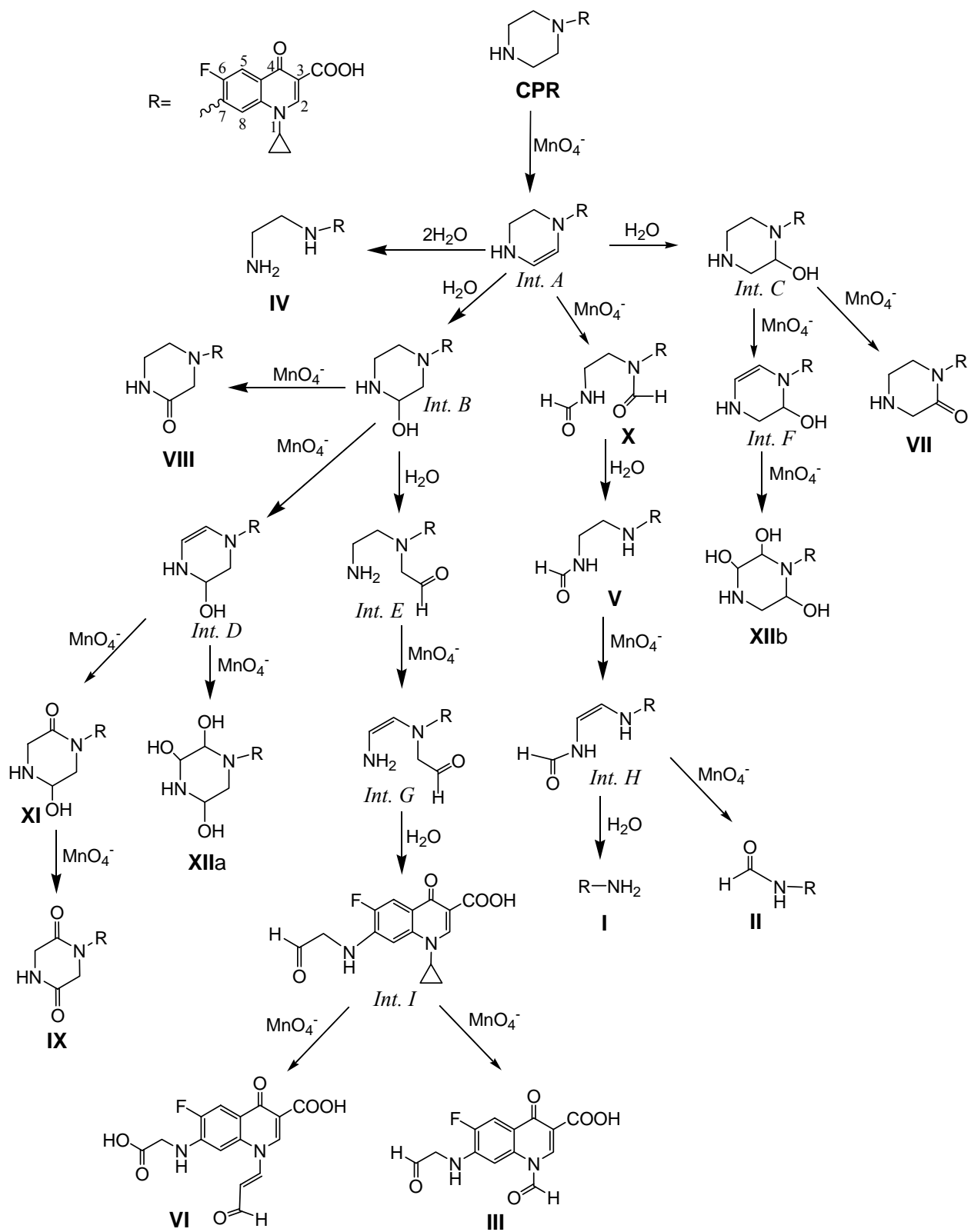
Figure 4.2. Proposed pathways for CPR reaction with Mn(VII).
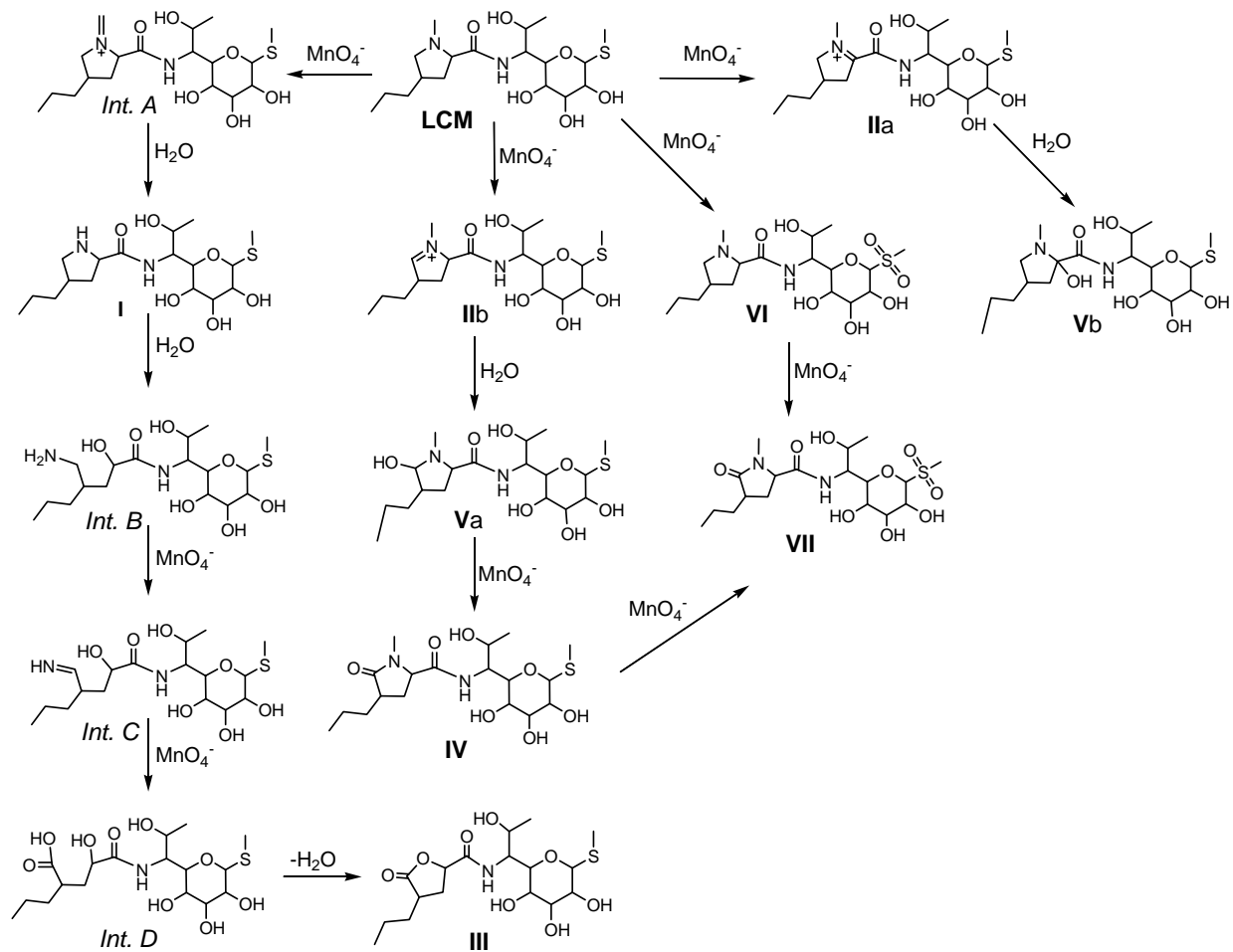
Figure 4.3. Proposed pathways for LCM reaction with Mn(VII).
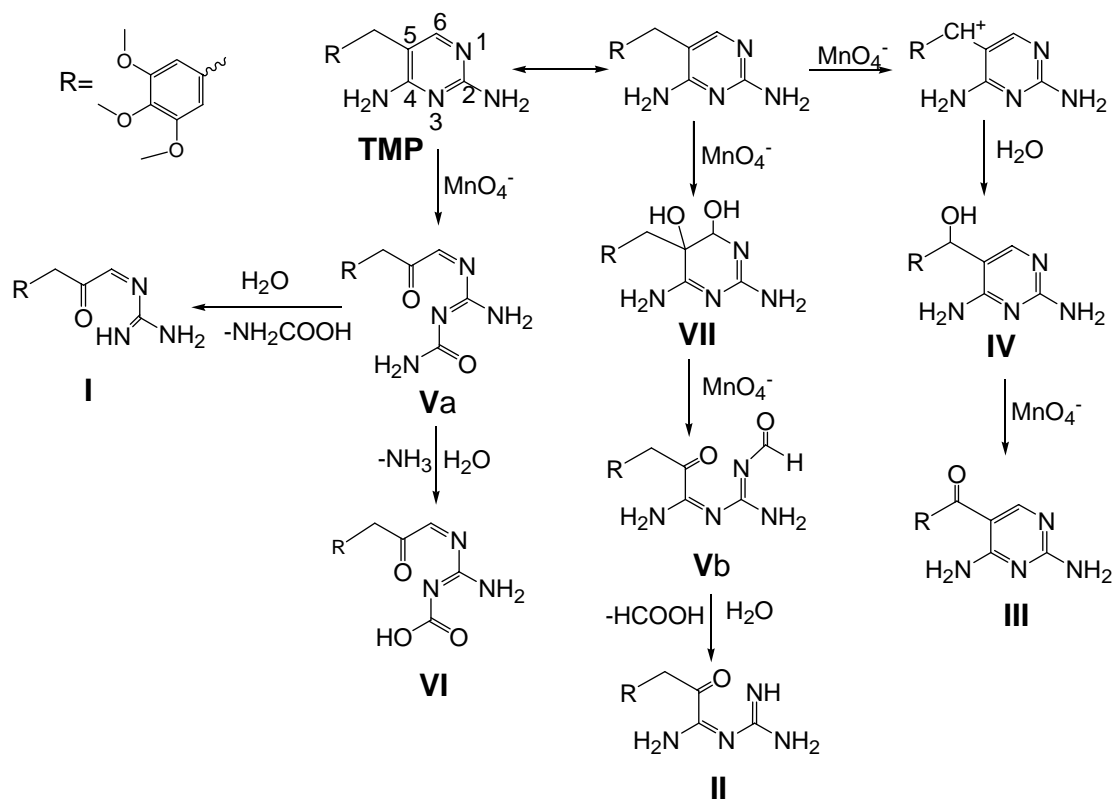
Figure 4.4. Proposed pathways for TMP reaction with Mn(VII).
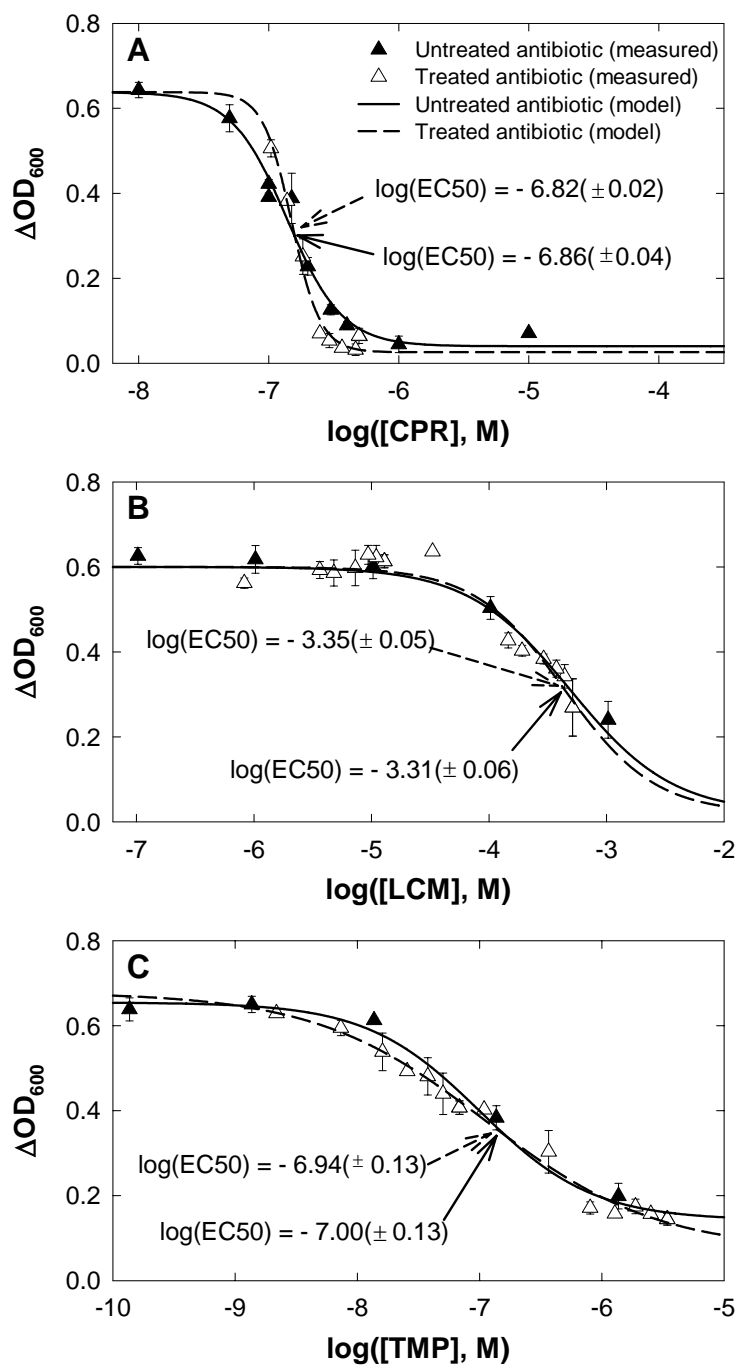
Figure 4.5. Antibacterial concentration-growth inhibition curves for untreated and Mn(VII)-treated antibiotics: (A) ciprofloxacin; (B) lincomycin; (C) trimethoprim. Uncertainties represent 95% confidence levels.
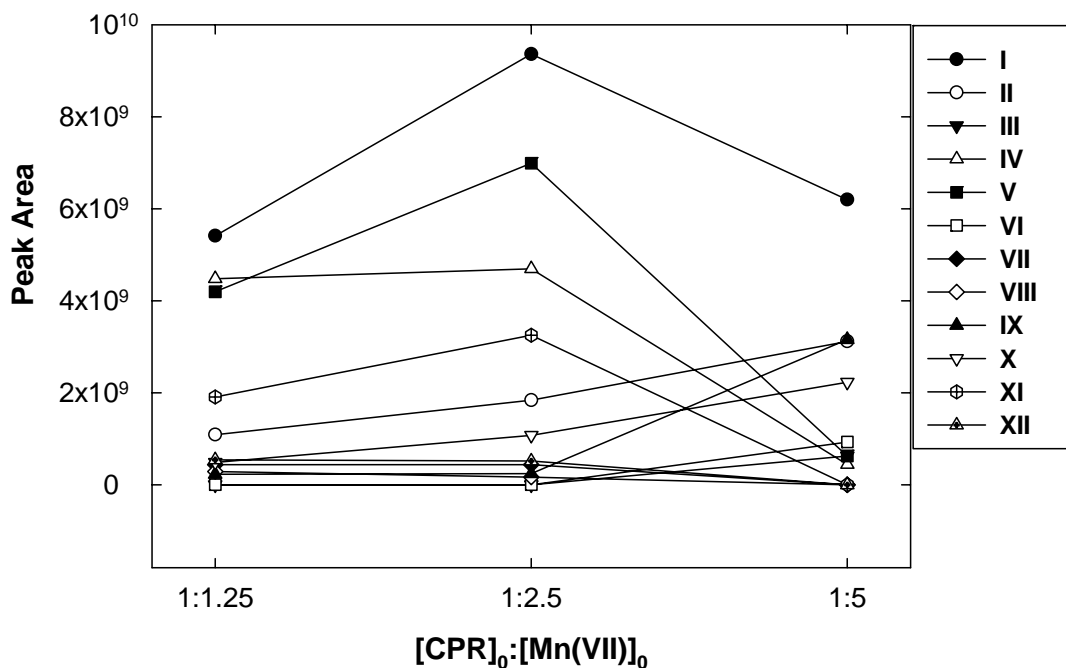
Figure 4.6. Integrated LC-MS peak areas of products from CPR reactions with Mn(VII):
$[CPR]_0 = 160$ μM, pH 7 (25 mM ammonium acetate), 25 ^{o}C.
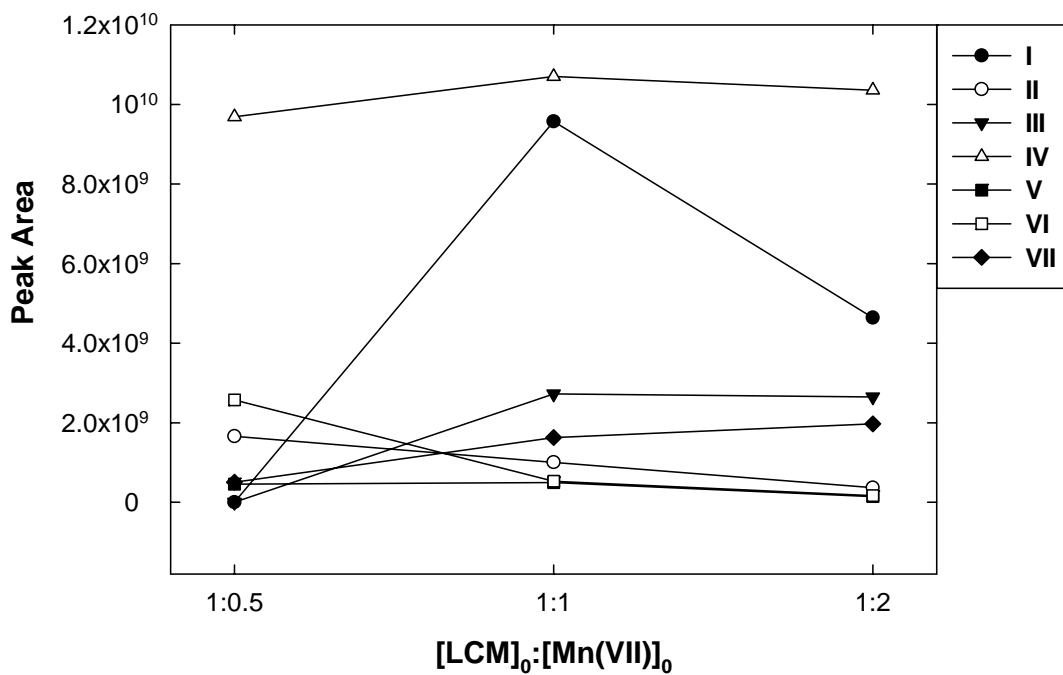
Figure 4.7. Integrated LC-MS peak areas of products from LCM reactions with Mn(VII):
$[LCM]_0 = 400$ μM, pH 7 (25 mM ammonium acetate), 25 ^{o}C.
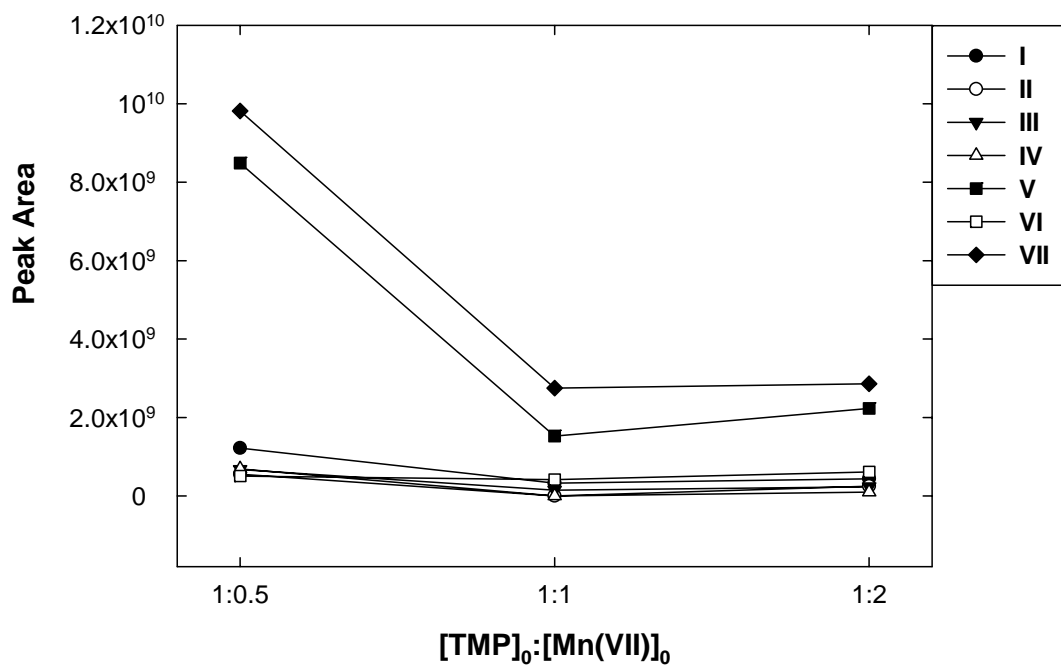
Figure 4.8. Integrated LC-MS peak areas of products from TMP reactions with Mn(VII): $[TMP]_0 = 200$ μM, pH 7 (25 mM ammonium acetate), 25 °C.
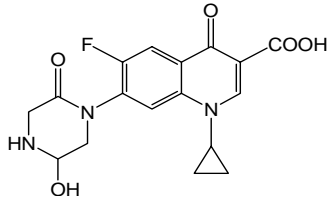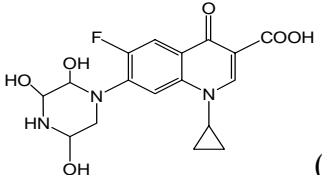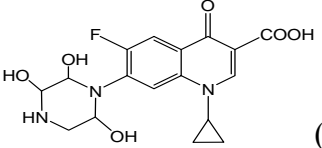
Table 4.1. Products of CPR-Mn(VII) reactions

Product ID	$[M+H]^+$ (m/z)[a]	R.T.[b] (min)	MS/MS (m/z)	Molecular formula[c]	Difference from CPR	Proposed structure
CPR[d]	332	3.2	314[e], 288, 268, 245[f], 231, 205	$C_{17}H_{18}FN_3O_3$	---	
I[d]	263	7.1	245[e], 217, 204[f], 189, 177	$C_{13}H_{11}FN_2O_3$	-(4C 7H N)	
II[d]	291	7.2	273[e], 245[f], 217, 205	$C_{14}H_{11}FN_2O_4$	-(3C 7H N) +O	
III	293	10.2	275[e]	$C_{13}H_9FN_2O_5$	-(4C 9H N) +2O	
IV[d]	306	2.1	288[e], 268[f], 245, 227, 203	$C_{15}H_{16}FN_3O_3$	-(2C 2H)	
V[d]	334	7.4	316[e], 245[f], 230, 217	$C_{16}H_{16}FN_3O_4$	-(C 2H) +O	

Table 4.1. (cont.)

Product ID	$[M+H]^+$ $(m/z)^a$	R.T.[b] (min)	MS/MS (m/z)	Molecular formula[c]	Difference from CPR	Proposed structure
VI	335	3.7	291^e	$C_{15}H_{11}FN_2O_6$	-(2C 7H N) +3O	
VII	346	1.6	328^f, 318^e	$C_{17}H_{16}FN_3O_4$	-2H +O	
VIII	346	9.7	328^e	$C_{17}H_{16}FN_3O_4$	-2H +O	
IX[d]	360	9.2	342^e, 332, 324, 314, 302^f	$C_{17}H_{14}FN_3O_5$	-4H +2O	
X	362	5.1	344^e, 318^f	$C_{17}H_{16}FN_3O_5$	-2H +2O	

Table 4.1. (cont.)

Product ID	$[M+H]^+$ (m/z)[a]	R.T.[b] (min)	MS/MS (m/z)	Molecular formula[c]	Difference from CPR	Proposed structure
XI[d]	362	5.7	344[e], 316, 273, 259[f], 245	$C_{17}H_{16}FN_3O_5$	-2H +2O	
XII	380	6.9	362[e], 334[f], 316	$C_{17}H_{18}FN_3O_6$	+3O	(a) or (b)

[a] The numbers indicate the mass of the protonated molecular ion, equal to the molecular weight of the analyte plus 1 (M.W. +1).
[b] R.T. represents retention time of each product peak in the LC-MS/MS chromatogram.
[c] Molecular formula of the neutral molecule.
[d] MS/MS spectra of these products are obtained in the Q-TOF instrument.
[e] Most abundant fragment ion.
[f] Second most abundant fragment ion.

Table 4.2. Products of LCM-Mn(VII) reactions
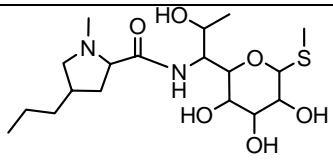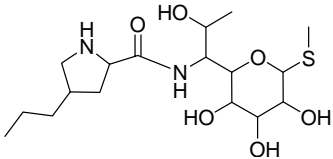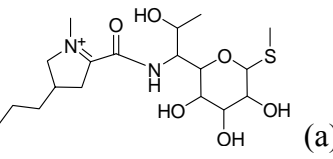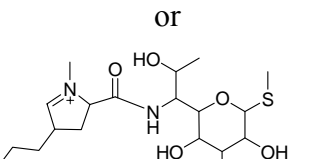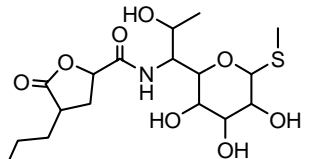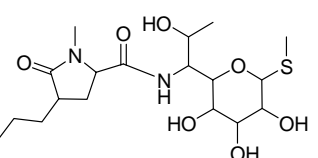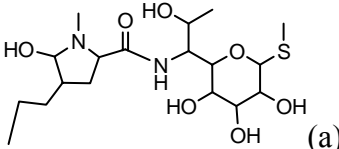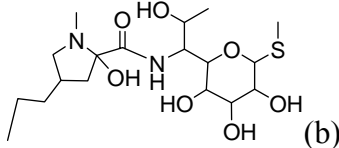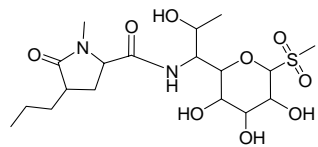
Product ID	$[M+H]^+$ (m/z)[a]	R.T.[b] (min)	MS/MS (m/z)	Molecular formula[c]	Difference from LCM	Proposed structure
LCM	407	2.7	389, 359[d], 341, 299, 172, 126[e]	$C_{18}H_{34}N_2O_6S$		
I	393	3.3	375[e], 345[d], 327, 285, 264, 216, 170, 112	$C_{17}H_{32}N_2O_6S$	-C 2H	
II[f]	405	1.9	387, 357[d], 297, 216, 198, 170, 124[e]	$C_{18}H_{33}N_2O_6S$	-H	(a) or (b)
III	408	6.8	390, 360[d], 342[e]	$C_{17}H_{29}NO_8S$	-(C N 5H) +2O	
IV	421	8.4	403, 373[d], 355[e], 323	$C_{18}H_{32}N_2O_7S$	-2H +O	

Table 4.2. (cont.)

Product ID	[M+H]$^+$ (m/z)^a	R.T.^{b} (min)	MS/MS (m/z)	Molecular formula^c	Difference from LCM	Proposed structure
V	423	6.0	405, 375^e, 357^d, 317, 299, 281, 126	C$_{18}$H$_{34}$N$_2$O$_7$S	+O	(a) (b)
VI	439	2.0	421, 391, 359^d, 341, 126^e	C$_{18}$H$_{34}$N$_2$O$_8$S	+2O	
VII	453	4.9	435, 373^d, 355^e, 140	C$_{18}$H$_{32}$N$_2$O$_9$S	-2H +3O	
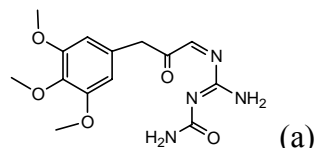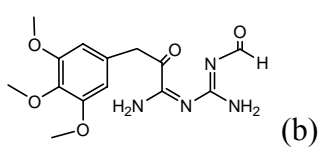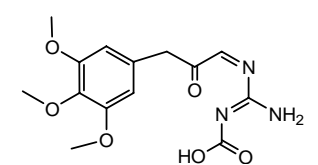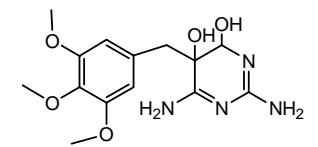
^{a} The numbers indicate the mass of the protonated molecular ion, equal to the molecular weight of the analyte plus 1 (M.W. +1).
^{b} R.T. represents retention time of each product peak in the LC-MS/MS chromatogram.
^{c} Molecular formula of the neutral molecule.
^{d} Most abundant fragment ion.
^{e} Second most abundant fragment ion.
^{f} This product exists as an iminium ion form, thus the molecular formula is for the ionic species instead of the neutral species.

Table 4.3. Products of TMP-Mn(VII) reactions

Product ID	[M+H]$^+$ (m/z)^a	R.T.^{b} (min)	MS/MS (m/z)	Molecular formula^c	Difference from TMP	Proposed structure
TMP	291	2.6	276, 261, 230^d, 181, 123^e, 110	C$_{14}$H$_{18}$N$_4$O$_3$		
I	280	1.8	237^e, 181^d	C$_{13}$H$_{17}$N$_3$O$_4$	-(C H N) +O	
II	295	1.7	278^d, 253, 236^e, 183, 113	C$_{13}$H$_{18}$N$_4$O$_4$	-C +O	
III	305	6.1	290, 275, 244^e, 195, 137^d	C$_{14}$H$_{16}$N$_4$O$_4$	-2H +O	
IV	307	1.7	289^d, 274^e, 243	C$_{14}$H$_{18}$N$_4$O$_4$	+O	

Table 4.3. (cont.)

Product ID	[M+H]$^+$ (m/z)[a]	R.T.[b] (min)	MS/MS (m/z)	Molecular formula[c]	Difference from TMP	Proposed structure
V	323	1.7	181	$C_{14}H_{18}N_4O_5$	+2O	(a) or (b)
VI	324	4.2	307[d], 281, 264, 236, 181[e]	$C_{14}H_{17}N_3O_6$	-(N H) +3O	
VII	325	2.0	280, 255, 221, 181[d], 143[e]	$C_{14}H_{20}N_4O_5$	+2H 2O	

[a] The numbers indicate the mass of the protonated molecular ion, equal to the molecular weight of the analyte plus 1 (M.W. +1).
[b] R.T. represents retention time of each product peak in the LC-MS/MS chromatogram.
[c] Molecular formula of the neutral molecule.
[d] Most abundant fragment ion.
[e] Second most abundant fragment ion.

Table 4.4. Gradient methods used for analysis of products

CPR		TMP		LCM	
Time (min)	B%[a]	Time (min)	B% [a]	Time (min)	B% [a]
0	0	0	0	0	0
3	15	12	40	10	15
6	30	16	60	15	20
15	70	17	90	16	50
17	0	18	0	17	0
19	0	20	0	19	0

[a] Mobile phase A = 95% H_2O + 5% acetonitrile + 0.1% formic acid. Mobile phase B = 95% acetonitrile + 5% H_2O + 0.1% formic acid

Table 4.5. Proposed fragmentation pathways for products from CPR oxidation

Product	Fragmentation Pathways

CPR

I

Table 4.5. (cont.)

Product	Fragmentation Pathways

II

III

IV

Table 4.5. (cont.)

Product	Fragmentation Pathways

V

Product V m/z: 334 →(-H$_2$O(18))→ m/z: 316 →(-C$_3$H$_5$NO(71))→ m/z: 245

m/z: 245 →(-NH(15))→ m/z: 230

m/z: 245 →(-CO(28))→ m/z: 217

VI

m/z: 291 ←(-CO$_2$(44))← Product VI m/z: 335 →(-CO$_2$(44))→ m/z: 291

VII

m/z: 318 ←(-CO(28))← Product VII m/z: 346 →(-H$_2$O(18))→ m/z: 328

VIII

Product VIII m/z: 346 →(-H$_2$O)→ m/z: 328

114

Table 4.5. (cont.)

Product	Fragmentation Pathways

Product IX m/z: 360 → -H₂O (18) → **m/z: 342** → **m/z: 324**

IX

Product IX → -CO(28) → **m/z: 332** → -H₂O (18) → **m/z: 314**

m/z: 342 → -CO(28) → **m/z: 314**

m/z: 342 → -C₂O(40) → **m/z: 302**

X

Product X m/z: 362 → -H₂O (18) → **m/z: 344**

Product X → -CO₂(44) → **m/z: 318**

XI

Product XI m/z: 362 → -H₂O(18) → **m/z: 344** → -CO(28) → **m/z: 316**

m/z: 344 → -C₄H₅NO₂(99) → **m/z: 245**

m/z: 316 → -CHNO(43) → **m/z: 273** → -CH₂(14) → **m/z: 259** → -CH₂(14) → **m/z: 245**

115

Table 4.5. (cont.)

Product	Fragmentation Pathways

Product XIIa m/z: 380 → -H₂O(18) → **m/z: 362** → -CO(28) → **m/z: 334** → -H₂O(18) → **m/z: 316**

XII

(Fragmentation of XIIa shown as an example, fragmentation of XIIb is analogous)

Table 4.6. Proposed fragmentation pathways for products from LCM oxidation

Product	Fragmentation Pathways
LCM	
I	

Table 4.6. (cont.)

Product	Fragmentation Pathways

(Fragmentation of IIa shown as an example, fragmentation of IIb is analogous)

II

III

IV

Table 4.6. (cont.)

Product	Fragmentation Pathways

V

Product Va m/z: 423 — -SCH$_4$(48) → m/z: 375

-H$_2$O(18)

m/z: 126 ← m/z: 405

m/z: 281 — -H$_2$O(18)

-SCH$_4$(48)

m/z: 357 — -C$_2$O(40) → m/z: 317 — -H$_2$O(18) → m/z: 299

(Fragmentation of Va shown as an example, fragmentation of Vb is analogous)

VI

m/z: 126

Product VI m/z: 439

-SO(48) / -H$_2$O(18) / -SO$_2$CH$_4$(80)

m/z: 391 / m/z: 421 / m/z: 359

-SO$_2$CH$_4$(80)

m/z: 341

VII

m/z: 140 ← m/z: 453 — -SO$_2$CH$_4$(80) → m/z: 373

-H$_2$O(18)

m/z: 355 ← -SO$_2$CH$_4$(80) ← m/z: 435

Table 4.7. Proposed fragmentation pathways for products from TMP oxidation

Product	Fragmentation Pathways

Table 4.7. (cont.)

Product	Fragmentation Pathways

III

Product IV m/z: 305

-OCH$_2$(30) → m/z: 275

→ m/z:195

-CH$_4$(16)   -NH(15) → m/z: 244

-NH(15) → m/z: 290

-OCH$_2$(30)   -CH$_4$(16) → m/z: 244

→ m/z: 137

IV

Product IV m/z: 307

-H$_2$O(18) → m/z: 289

-C$_2$H$_6$O(46) → m/z: 243

-NH(15) → m/z: 274

V

Product Va m/z: 323

Product Vb m/z: 323

→ m/z: 181

Table 4.7. (cont.)

Product	Fragmentation Pathways

VI

VII
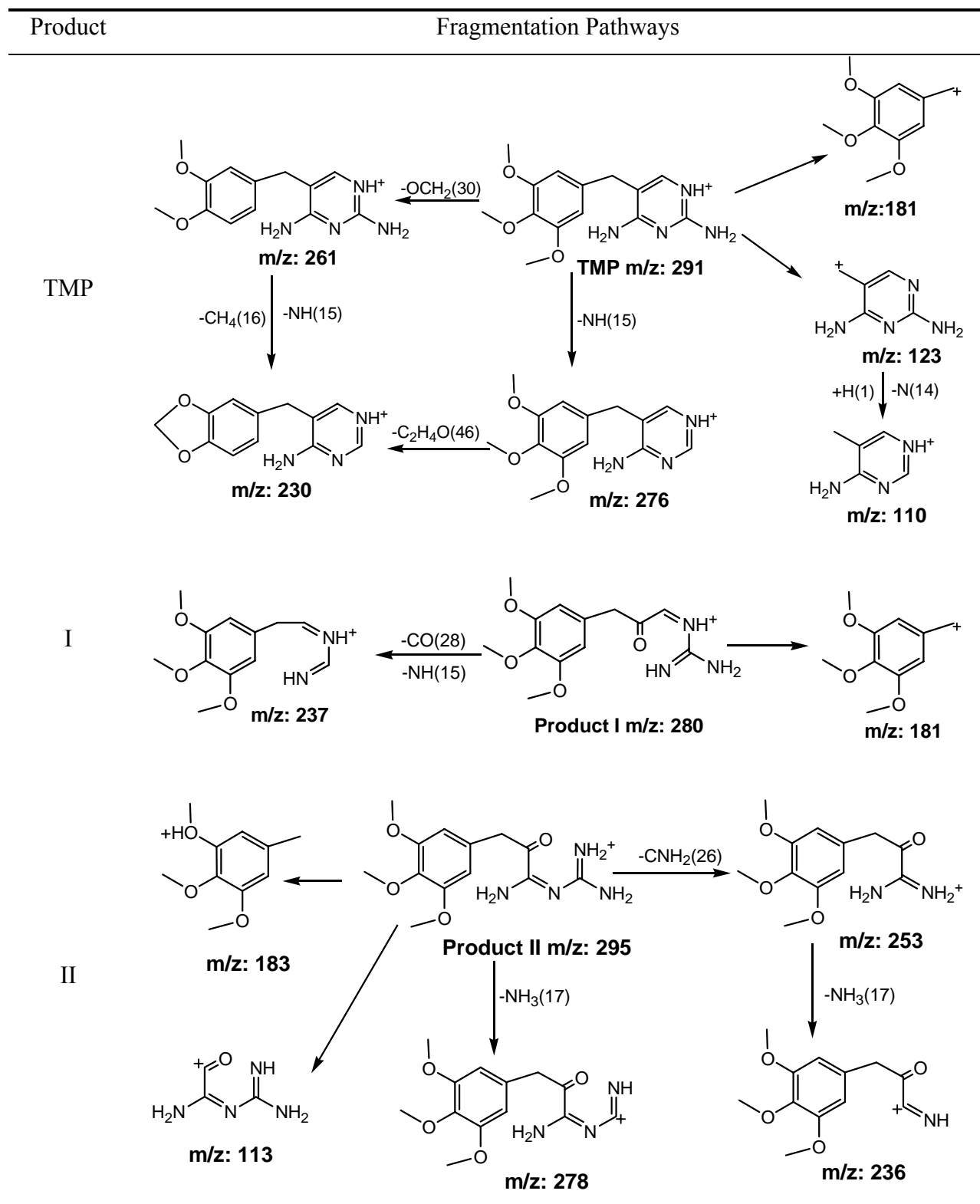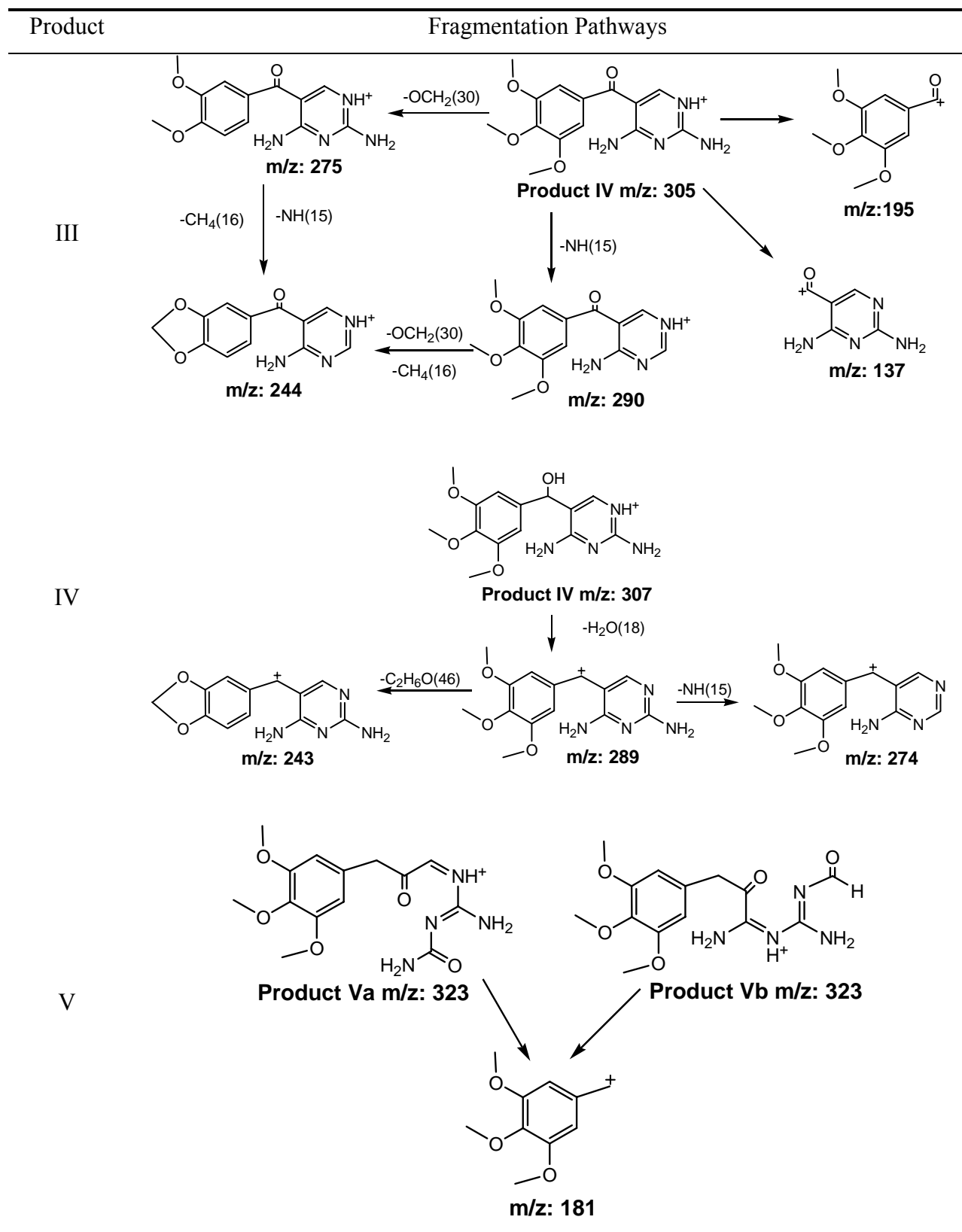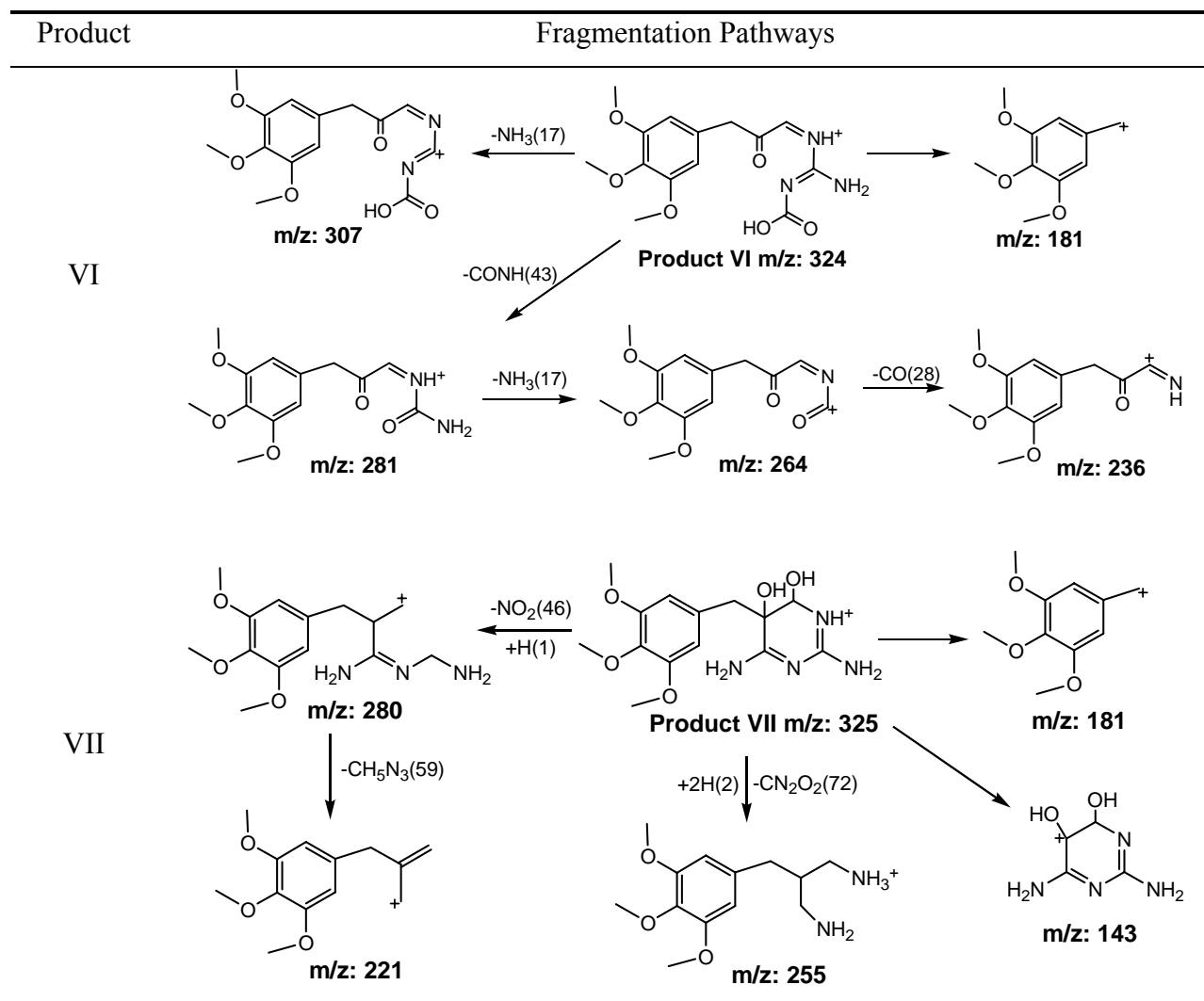
CHAPTER 5

OXIDATIVE REMOVAL OF 17α-ETHINYLESTRADIOL BY POTASSIUM PERMANGANATE: REACTION KINETICS AND PRODUCTS

5.1 Abstract

The presence of endocrine disrupting compounds (EDCs) in aquatic environments has been reported to cause fish feminization and affect fish reproduction. There are also serious concerns about EDCs' potential adverse effects on human health. This study examined the oxidative transformation of the synthetic steroid hormone 17α-ethinylestradiol (EE2), a potent EDC, by potassium permanganate [$KMnO_4$; Mn(VII)]. Reaction kinetics can be described by a second-order rate law with an apparent second-order rate constant (k_2) of $1.27(\pm0.02)\times10^2$ M^{-1} s^{-1} at pH 7 and 25 °C, and an activation energy (E_a) value of $37(\pm2)$ kJ mol^{-1}. Solution pH was found to significantly affect reaction kinetics, with k_2 increasing from 2.0×10^1 M^{-1} s^{-1} to 5.9×10^3 M^{-1} s^{-1} when pH increases from 4 to 9. The pH dependence can be quantitatively described by considering parallel reactions between MnO_4^- and two acid-base species of EE2. Predictions of EE2 oxidation from a kinetic model that included temperature, applied $KMnO_4$ dose, pH, and source water oxidant demand as input parameters agreed reasonably well with measurements conducted in four drinking water utility source waters. Nine reaction products, with structural changes indicating phenolic ring and ethynyl group oxidation, were identified by liquid chromatography-mass spectroscopy methods. Overall, results indicate that Mn(VII) treatment processes have good potential for treatment of EE2 and structurally related EDCs in contaminated source waters.

5.2 Introduction

Endocrine disrupting compounds (EDCs) are chemicals that interfere with functions of natural hormones and affect health, growth and reproduction of humans and animals [1]. EDCs have been widely detected in wastewater effluents and drinking water sources [2-5], raising serious concerns about potential adverse effects on human health and aquatic ecology, especially effects on aquatic organisms living in wastewater effluent-impacted habitats. Although there remains considerable debate about the potential risk of many classes of trace micropollutants, reports demonstrate that steroidal EDCs impact aquatic organisms at levels commonly detected in aquatic

environments receiving effluent from wastewater treatment facilities [4, 6-10]. Orn et al. [10] reported that zebrafish showed significant changes in sex ratios in favor of females after a partial life-cycle exposure to 1 ng/L of 17α-ethinylestradiol (EE2, **Table 5.1**), a synthetic steroid hormone that is a common active ingredient in oral contraceptive pills. Parrott et al. [6] reported egg fertilization success reduction and feminization of fathead minnows after a life-cycle exposure to <1 ng/L of EE2. Although EDCs are among the relatively susceptible group of compounds being effectively removed by conventional wastewater treatment processes [11], reported environmental levels of EDCs are often higher than the lowest concentration that can induce reproductive disturbance (sub μg/L). For example, a U.S. Geological Survey national reconnaissance detected EE2 in 15.7% of 139 surveyed U.S. streams with median and maximum concentrations of 73 ng/L and 831 ng/L, respectively [2].

A number of studies have explored the potential of drinking water oxidants for the treatment of steroid hormones like EE2 and elimination of estrogenic activity, including ozone [1, 12-14], free chlorine [15], combined chlorine [14], chlorine dioxide [16], ferrrate [17], manganese oxide [18], and UV/TiO$_2$ [19]. However, there is currently no comprehensive study addressing the potential use of potassium permanganate [KMnO$_4$; Mn(VII)], a widely used drinking water oxidant [20], for treatment of steroidal EDCs in water. Mn(VII) is used in water treatment plants to treat taste and odor problems, remove color, oxidize soluble iron(II) and manganese(II), control biological growth, and pre-oxidize disinfection byproduct precursor compounds [21]. Mn(VII) has also been reported to oxidize a wide range of organic contaminants [22] and is employed for in-situ remediation of contaminated groundwater [23, 24]. Recent studies have shown Mn(VII) is effective in oxidizing some pharmaceutically active micropollutants, including carbamazepine [25], three common antibiotics [26], triclosan [27], and bisphenol A [28]. Because of the shared highly reactive phenolic group among triclosan, bisphenol A, and EE2, Mn(VII) is also expected to be an effective oxidant for EE2 in water treatment.

The objective of this study was to characterize the reaction between Mn(VII) and EE2 under natural water conditions and evaluate the potential of applying Mn(VII) for oxidative treatment of steroidal EDCs in contaminated source waters. Results from detailed kinetics experiments are presented, including examination of the effects of Mn(VII) concentration, temperature, and pH on reaction kinetics. A kinetic model considering changing acid-base speciation of the phenolic/phenolate group in EE2 was used to quantitatively interpret the effects

124

of pH. A predictive kinetic model using results from experiments conducted in well-characterized laboratory solutions was also applied to predict Mn(VII) treatment in four drinking water utility source waters. Because tests showed no significant mineralization of EE2 during reactions with Mn(VII), liquid chromatography-mass spectrometry (LC-MS) methods were used to identify organic transformation products.

5.3 *Materials and Methods*

5.3.1 Reagents and Materials

All chemicals were of high purity and were used as received from Sigma-Aldrich-Fluka (USA). Solutions were prepared in reagent-grade deionized water (>17.3 MΩ·cm; Barnstead nanopure system). Glassware and plasticware was washed by soaking in a 1 M HCl or HNO_3 acid bath for over 24 h followed with repeatedly rinsing with deionized water. EE2 stock solutions (25 μM) were prepared in nanopure water with pH adjusted to ~10.6.

5.3.2 Batch Kinetics Experiments

Batch reaction experiments were conducted in 150-mL glass beakers immersed in a temperature-controlled circulating water bath. Reactions were initiated by spiking excess concentration of Mn(VII) into pre-equilibrated and pH-adjusted solutions containing 1 μM EE2 and 25 mM NaCl electrolyte. No pH buffers were used in kinetics experiments because previous reports [27, 28] and our preliminary tests for this study showed that phosphate buffer accelerates Mn(VII) oxidation of phenolic compounds under some pH condisions. Instead, pH was held constant during reactions by continuous monitoring and manual addition of HCl and NaOH as needed. After reaction initiation, aliquots were periodically collected for analysis and immediately quenched with excess hydroxylamine [25, 26], rapidly reducing residual Mn(VII) and $MnO_{2(s)}$ to dissolved Mn^{2+}. EE2 concentrations were then quantified by high perfomance liquid chromatography with photodiode array (HPLC-PDA) detection to monitor reaction progress.

5.3.3 Utility Source Water Experiments

Experiments were also conducted to measure Mn(VII) oxidation of EE2 in four drinking water utility source waters. For these experiments, a much lower initial EE2 concentration (500

ng/L) was used to better mimic environmental levels (ng/L - μg/L). Multiple reactors were prepared with 150-mL unfiltered source water amended with EE2 and reactions were initiated by spiking different doses of Mn(VII) and mixing rapidly. For each Mn(VII) dose, duplicate experiments were conducted. After the desired reaction time, excess hydroxylamine was added to quench any further reaction and then 500 ng/L E1 was added as an internal standard to account for varying solid phase extraction (SPE) efficiency. Water samples were then filtered (0.45 μm glass fiber) and concentrated using SPE cartridges (Waters, Oasis HLB, 500 mg, 60 μm) before analyzing with HPLC-PDA. Details of the SPE procedure are provided in the Section 5.5.1.2.

5.3.4   Reaction Intermediates and Products

To identify reaction products resulting from Mn(VII) oxidation of EE2, a series of 20 mL EE2 solutions (pH 7, 25 mM ammonium acetate) were treated with varying doses of Mn(VII) and analyzed by LC-MS methods. Ammonium acetate was used to both maintain pH and aid ionization in the mass spectrometer. Tests (data not shown) showed that the presence of ammonium acetate did not affect the reaction kinetics at pH 7. Elevated initial EE2 (100 μM in 5% (v/v) acetone) and Mn(VII) concentrations (40-500 μM) were used to facilitate detection of minor products. After allowing sufficient time for reactions to reach completion, samples were then filtered (PTFE, 0.45 μm) and analyzed by liquid chromatography-tandem mass spectrometry (LC-MS/MS) and liquid chromatography high resolution mass spectrometry (LC-HRMS). A similar series of Mn(VII)-reacted EE2 solutions (minus ammonium acetate) were also prepared and analyzed for changes in total dissolved organic carbon (DOC).

5.3.5   Analytical Methods

Details of analytical methods, including HPLC-PDA, DOC, LC-MS, are provided in Section 5.5.1.

5.4 Results and Discussion

5.4.1   Reaction Kinetics

Results from batch experiments (**Figure 5.1**) showed that EE2 was rapidly degraded by Mn(VII) under neutral pH conditions (e.g., $t_{1/2}$ = 9 min when $[Mn(VII)]_0$ = 10 μM, pH 7, 25 $^{\circ}$C).

The kinetics of EE2 decay could be described by a pseudo-first-order rate law when initial Mn(VII) concentration was in excess, and measured pseudo-first-order rate constants (k_{obs}, s^{-1}) for all batch kinetics experiments are listed in **Table 5.2**. Results in **Figure 5.2A** show that k_{obs} varied linearly with changing initial Mn(VII) concentration, indicating the reaction was also first-order with respect to Mn(VII) concentration, and confirming that overall reaction kinetics could be described by a generalized second-order rate law:

$$\frac{d[EE2]_{tot}}{dt} = -k_2[EE2]_{tot}[Mn(VII)]_{tot} \tag{5.1}$$

where $[EE2]_{tot}$ and $[Mn(VII)]_{tot}$ represent the total EE2 and Mn(VII) concentration, repectively, and k_2 is the apparent second-order rate constant (M^{-1} s^{-1}) valid at the solution conditions in question. At pH 7 and 25 ^{o}C, k_2 was determined to be $1.27(\pm0.02)\times10^2$ M^{-1} s^{-1}. Second-order rate constants for aqueous Mn(VII) reactions with a variety of organic compounds (e.g., chlorinated and aromatic hydrocarbons, ethers, amines, nitro explosives and substituted phenols) have been reported previously at similar solution conditions [22, 25-28], ranging from 7×10^{-6} M^{-1} s^{-1} to 3×10^2 M^{-1} s^{-1}, indicating that EE2 is among the more highly Mn(VII)-reactive compounds reported to date under natural water conditions. The EE2 structure contains phenolic and ethynyl functional groups, both of which have been reported to react with Mn(VII) [27-30]. Shao et al. [31] recently studied the oxidation of E1, a structurally related compound of EE2 but lacking the ethynyl group, with Mn(VII) and reported a k_2 of $\sim9.5\times10^1$ M^{-1} s^{-1} at pH 7 and 25 ^{o}C, only slightly slower than that of EE2 observe here.

Previous studies showed that EE2 is susceptible to oxidation by several other drinking water-related oxidants, including O_3, HOCl, NH_2Cl, ClO_2, UV/H_2O_2 ($\cdot OH$), and Fe(VI) [15-17, 32]. The k_2 values for EE2 reacting with different oxidants at pH 7 and ambient temperature are listed in **Table 5.1**. The reactivity of EE2 with Mn(VII) is lower than O_3 and ClO_2, but comparable with HOCl and Fe(VI) and significantly higher than NH_2Cl. With the exception of ClO_2 and NH_2Cl, the relative reactivity of EE2 with different oxidants follows the same general trend with the standard reduction potential of the oxidants at pH 7 ($E^o_{pH\,7}$, **Table 5.3**). Although $\cdot OH$ and O_3 exhibit the highest reactivity with EE2, EE2 treatment efficiency in organic-rich natural water matrices may be offset by lower stability and more rapid scavenging of these oxidants by non-target water constituents [33]. In addition, free chlorine will be rapidly converted to less reactive chloramine species in waters rich in ammonia and organic amines [20], whereas Mn(VII) is relatively unreactive with ammonia and will persist for longer times in such matrices [25].

127

Figure 5.2B shows that the dependence of k_2 on temperature (T) followed a trend consistent with the Arrhenius equation:

$$\ln(k_2) = -\frac{E_a}{R} \cdot \frac{1}{T} + \ln(A) \tag{5.2}$$

where E_a is the apparent activation energy, R is the universal gas constant, and A is the pre-exponential constant. At pH 7, E_a for Mn(VII)-EE2 reactions was determined to be 37($\pm$2) kJ mol^{-1}, corresponding to a doubling of reaction rates for every 14 $^{\circ}$C increase in temperature. The k_2 values for EE2 oxidation by Mn(VII) at other temperatures can thus be calculated using the determined E_a value and Equation (5.2). Shao et al. [31] reported an E_a of 43 kJ mol^{-1} for Mn(VII)-E1 reactions, similar to the value measured here.

Solution pH was also found to have significant effects on the rate constants of reaction between EE2 and Mn(VII) (**Figure 5.3**). For the pH range of 6 to 9, raising solution pH greatly enhanced the reaction rates, with k_2 increasing by ~300 fold when pH increased from 6 to 9, whereas little change was observed between pH 4 and 6. The pH dependent trend in the higher pH range is similar to that reported for EE2 oxidation by ClO_2 [16], and O_3 [13], both of which do not have acid-base speciation, and can be attributed to the deprotonated phenolate species (EE2$^-$, **Table 5.1**) having a higher electron density on the target reaction site and thus being more reactive with oxidants than the protonated conjugate acid species. The overall pH dependent trends for oxidation of EE2 by Fe(VI) [17] and HOCl [15] are different from the trend observed here due to the changing speciation of the oxidants themselves with changing pH. The slight increase of reaction rate constants at pH<5 was also reported with Mn(VII) oxidation of E1 and was attributed to the higher reduction potential of Mn(VII) at lower pH [31]. It could also be explained by the added Mn(VII) reactivity from the acid-catalyzed pathway at lower pH as reported in Mn(VII) oxidation of paracetamol [34].

The effects of pH on Mn(VII) reaction kinetics could be quantitatively described with a previously reported kinetic model [26] that considers parallel reactions between the anionic permanganate species (MnO_4^-, β_2), which predominates at natural water pH conditions, and individual species of target organic compounds with different protonation levels.

$$k_2 = k_{21}\beta_2\alpha_1 + k_{22}\beta_2\alpha_2 \tag{5.3}$$

For the pH range studied ($\beta_2 = 1$), Equation (5.3) is then simplified to:

$$k_2 = k_{21}\alpha_1 + k_{22}\alpha_2 \tag{5.4}$$

where k_{21} and k_{22} are the species-specific second-order rate constants for MnO_4^- (second protonation level of Mn(VII)) reacting with neutral and deprotonated EE2 species, respectively; α_1 and α_2 represent the equilibrium fraction of neutral and deprotonated EE2 species, respectively, both of which vary with changing pH condition. **Figure 5.3** shows the results of least-square fitting of the kinetic data with Equation (5.4) and the predicted contributions of individual EE2 species to the apparent second-order rate constants at different pH conditions. The model fits agreed closely with measured data and the fit-derived species-specific rate constants are listed in **Table 5.1** and **Figure 5.3**. The value of k_{22} is ~4 orders-of-magnitude larger than k_{21}, indicating that deprotonation of the phenolic group greatly enhances EE2 reactivity with Mn(VII). Comparison of the species-specific rate constants for EE2 with different common oxidants is provided in **Table 5.1**. Similar to Mn(VII), EE2 deprotonation significantly increased reactivity with HOCl, ClO_2, Fe(VI), and O_3, suggesting the deprotonated phenolate group is the major target functional group for all oxidants at circumneutral pH conditions.

5.4.2 EE2 Removal by Mn(VII) in Utility Source Waters

Oxidative removal of EE2 by Mn(VII) was measured in four drinking water utility source waters, the properties of which are summarized in Section 5.5.1.1 (TOC = 1.3-4.3 mg/L, alkalinity = 70 to 144 mg/L as $CaCO_3$, pH = 7.6-8.4). **Figure 5.5** shows the measured oxidation of EE2 in the four utility source waters with three different $KMnO_4$ doses (0.5, 1.0, and 2.0 mg/L). In general, EE2 is efficiently removed by low doses of $KMnO_4$ and short reaction times (2-12 min), and the percent of EE2 removal increases with the applied $KMnO_4$ dose. With 2 mg/L of $KMnO_4$ and 2-12 min of reaction time, there is >85% removal of EE2 in all source waters.

With the kinetic parameters determined in previous sections, the EE2 removal in natural water can be predicted using a kinetic model previously used to describe Mn(VII) oxidation of antibiotics [26]:

$$\text{EE2 Removal Fraction} = 1 - \exp\left\{-\underbrace{(k_{21}\alpha_1 + k_{22}\alpha_2)}_{A} \times \underbrace{\exp\left[-\frac{E_a}{R}\left(\frac{1}{T} - \frac{1}{298}\right)\right]}_{B} \times \underbrace{(Ct_{Mn})}_{C}\right\} \qquad (5.5)$$

where term A calculates the apparent second-order rate constant at 25 °C and the pH of interest by taking into account of the effects of EE2 speciation on the reactivity with Mn(VII) (**Table 5.1**). Term B corrects the rate constant to the temperature of interest using the Arrhenius equation and

129

the E_a values (**Figure 5.2B**). Term C, $Ct_{Mn(VII)}$, is the integrated Mn(VII) exposure during treatment ($\int_0^t [Mn(VII)] \cdot dt$), which is similar to the widely used Ct concept for modeling disinfection processes and accounts for the applied Mn(VII) dosage, treatment time, and oxidant demand of the source water matrix. The Mn(VII) demand of each source water was determined by measuring Mn(VII) decay in the absence of EE2 in separate experiments (**Table 5.4**) and integrating the Mn(VI) concentration over time using the trapezoidal method described in Chapter 3.

The accuracy of the predictive kinetic model shown in Equation (5.5) was tested by comparing the model prediction with the measured EE2 removal in utility source waters as shown in **Figure 5.5**. Overall, the model predictions agree closely with measurements, with a few exceptions where measured EE2 removals were higher than predicted. Previous studies observed similar higher-than-expected removal rates of estrone [31] and triclosan [27] during Mn(VII) treatment in natural water. This underestimation of model prediction might be attributed to the presence of various ligands in the utility source water matrix that could enhance the Mn(VII) oxidation of phenolics as demonstrated by Jiang et. al [28]. Specifically, He et al. [35] reported that high nominal molecular weight fraction of humic acid can greatly accelerate the phenol oxidation rate by Mn(VII). Nevertheless, the close agreement between measured and model predicted EE2 removal in utility source waters is notable given that the kinetic parameters used in Equation (5.5) were developed for batch reactors conducted at conditions very different from the source water reaction conditions used for experiments shown in **Figure 5.5**. (e.g., much different initial EE2 concentrations, well vs. poorly characterized source waters, absence vs. presence of suspended solid). Therefore, the predictive model developed here can be used to provide a conservative estimate of EE2 removal to drinking water utilities that currently apply Mn(VII) treatment.

5.4.3   Reaction Products and Pathways

Although EE2 was effectively oxidized by Mn(VII) in both artificial water and utility source water, tests showed that there was no change in DOC concentration of EE2 solutions after Mn(VII) treatment (**Figure 5.4**), indicating transformation to unknown organic products. Therefore, identification of reaction products is important to understand the fate of EE2 during Mn(VII) treatment. Nine products from Mn(VII) oxidation of EE2 were detected by LC-MS/MS analysis. **Table 5.5** lists the HRMS-determined molecular weight and molecular formula, the major observed MS/MS fragment ions (MS/MS spectra provided in **Table A.5** in Appendix A), the

chromotographic retention time, and the proposed structures for each product. Because the MS/MS fragmentation pattern did not provide decisive information in elucidating the product structures, the proposed structures of each product were mainly based on the determined molecular formula and the preknowledge that Mn(VII) oxidation occurs predominantly on the phenolic ring and the ethynyl group. Most products show a dominant loss of 18 followed by 28 from the pseudomolecular ion $[M+H]^+$, which is also seen in the MS/MS fragmentation pattern of the parent compound EE2 as illustrated in **Table 5.6**. The loss of 18 is proposed to be the loss of H_2O from the hydroxyl group at the C-17 position, and the subsequent sequential loss of 28 is proposed to come from the loss of ethenes (C_2H_4) from the steroid skeleton. For five products (III, VI, VII, VIII, and IX), a sequential loss of two H_2O molecules was observed in the MS/MS spectra, indicating the presence of an additional functional group that can give out a H_2O molecule during fragmentation, either a –OH or a –COOH group. The proposed structures for these products are consistent with this observation. Further confirmation of the proposed product structures by NMR analysis or comparison with reference standards is recommended for unequivocal identification.

A variety of oxidation products were proposed, including dehydrogenation (II), quinone (V), phenolic ring-hydroxylation (IV, VII, and IX), and phenolic ring-cleavage products (I, III, VI, and VIII), as well as products where the ethynyl group was oxidized to aldehydes and carboxylic acid (V and IX). In terms of LC-MS detection intensities, product IX and V are the two dominant products. **Table 5.5** lists the products detected following treatment with different Mn(VII) dosages. It should be noted that no coupling products are detected in all samples, even when EE2 is in much excess and unreacted EE2 could potentially react with the reduction product of Mn(VII), $MnO_{2(s)}$. This is somewhat surprising because oxidation of phenol by permanganate have been proposed to undergo a phenoxyl radical pathway [29] and coupling products are expected [36]. In addtion, a previous study [37] reported oxidation of phenol to diphenoquinone by $MnO_{2(s)}$ through a phenoxyl radical pathway. The absence of coupling products might be due to steric hindrance posed by the substituted steroid ring structure on the phenolic ring.

Hydroxylation products have been proposed and identified in several chemical oxidation [38, 39] and biotransformation [40-42] studies of EE2 and structurally related steroid hormones. The formation of hydroxylated EE2 might occur through a phenoxenium ion intermediate (shown in Equation (5.6)), which has been reported to be the intermediate of Mn(III) oxidation of phenol

[43]

phenoxenium ion (5.6)

monohydroxylated EE2   ortho-quinone (5.7)
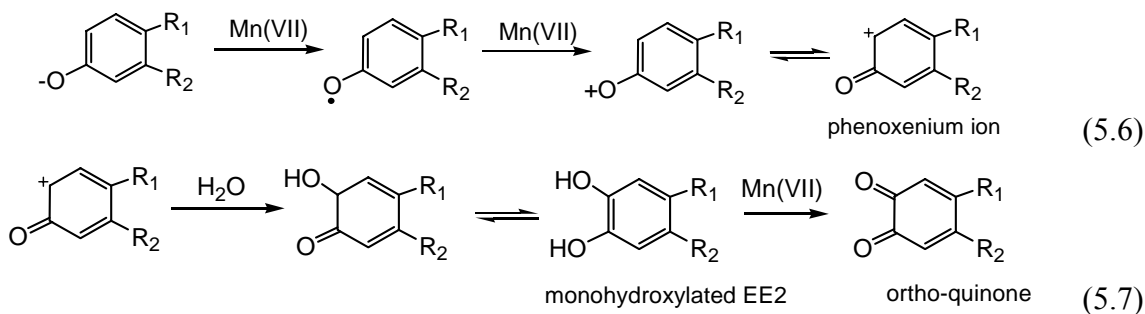
The phenoxenium ion is formed by two one-electron transfer steps from deprotonated EE2 to Mn(VII). Nucleophilic attack of H_2O molecule to the phenoxenium ion can then form a monohydroxylated EE2 (product IV), which can be further oxidized to its quinone form (product V). Different isomers of EE2 hydroxylation products are expected to form because of different resonance structures of the phenoxenium ion (not shown).

The monohydroxylated EE2 shown in Equation (5.7) can be further hydroxylated, forming product VII and IX, or oxidatively cleaved by Mn(VII) to form ring-cleavage products (I, II, VI, and VIII). The mechnism of oxidative cleavage of monohydroxylated EE2 by Mn(VII) might be similar to that of Mn(VII) oxidation of olefins, during which a diol compound is first formed and then further oxidized to aldehydes and carboxylic acids by Mn(VII) [44]. Cleavage of the phenolic ring to form carboxylic acids and aldehydes has been proposed previously for ozonation of EE2 and E2 [12, 39].

The dehydrogenation product (II) was previously reported as the major product of EE2 oxidation by Mn(III) [45], while Haaf et al. [46] also reported 9, 11-dehydrogenated estrone as one of the major metabolites of estrone in hamster liver. The dehydrogenation process is proposed to be initiated by a hydride abstraction at the C9 followed by a loss of proton at C11 to form a new C9=C11 double bond:

(5.8)
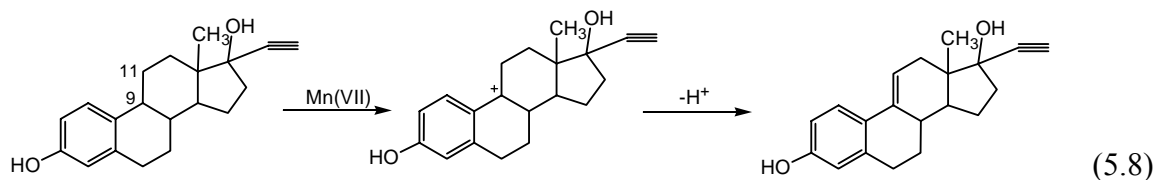
The abstraction of hydride from the α position of an aromatic ring by Mn(VII) has been previously established [47]. Hydride abstraction at the C9 position is prefered over the C6 position because of the tertiary carbocation intermediate formed is more stable than the otherwise secondary carbocation [48]. In addition, the stability of the tertiary carbocation intermediate is

increased by multiple possible resonance structures with the phenolic ring [48].

Product V and IX exhibit structural modifications to the ethynyl group. Oxidation of the ethynyl group by Mn(VII) to produce triple bond cleaved aldehydes as seen in product V has been previously reported [49]. The conversion of the ethynyl group to the carboxylic acid in product IX is proposed to occur through oxidative hydration (Equation (5.9)). Metal-catalyzed hydration of alkynes to form aldehydes or ketones has been well-established [50-52].

$$R-\!\!\!\equiv \xrightarrow{H_2O} \underset{R}{\overset{OH}{\diagup}} \rightleftharpoons R\overset{O}{\diagup}_H \xrightarrow{Mn(VII)} R\overset{O}{\diagup}_{OH} \tag{5.9}$$
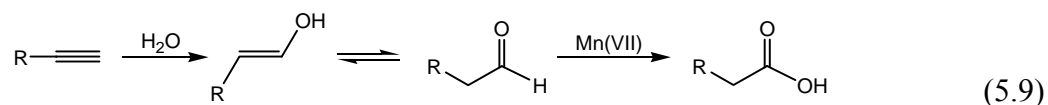
Overall, results in this study show that EE2 is efficiently oxidized by Mn(VII) in both artificial water and utility source water. The reaction follows second-order rate law and the apparent second-order rate constant was measured to be $1.27(\pm0.02)\times10^2$ M^{-1} s^{-1} at pH 7 and 25 ^oC, corresponding to a half-life of 14 min when treated with 1 mg/L of $KMnO_4$. The reaction rate constants were highly dependent on solution pH and temperature, with high pH resulting in greatly increased reaction rate constants. The effect of pH can be well-described with a kinetic model considering parallel reactions between the two different EE2 species and the MnO_4^- ion. A predictive kinetic model was found to estimate the EE2 removal resonably well in utility source water. The model takes into account of variation of pH, temperature, Mn(VII) dosage, contact time, and oxidant demand in different water matrix. The phenolic ring and ethynyl group are found to be the two target functional group in EE2. Dehydrogenation and hydroxylation products along with phenolic ring-cleavage products and products with structural modification on the ethynyl group are tentatively identified based on LC-MS data.

Among pharmaceutically active compounds commonly detected in drinking water sources, phenolic EDCs like 17α-ethinylestradiol are believed to possibly pose the greatest risk at environmental concentration levels (ng/L-µg/L) [6]. In agreement with other reports [27, 28], results in this study show that permanganate is a promising oxidant for treating phenolic EDCs in general. However, further research is needed to quantify the estrogenic activity of the reaction products and the extent of estrogenic activity removal during Mn(VII) treatment.

5.5 *Supporting Information*

5.5.1 Analytical Procedures

5.5.1.1 Measurement of EE2 concentration, DOC, and source water characteristics

EE2 concentration was determined using a Shimadzu model HPLC equipped with UV-Vis photodiode array detection. The stationary phase was a Novapak C-18 column (3.9×150 mm, 4 μm particle size) and the mobile phase (1 mL/min) was an isocratic mixture of 45% acetonitrile and 55% 10 mM phosphoric acid. The retention time was 5.6 min and the monitoring wavelength was 200 nm. **Figure 5.6** shows a representative HPLC calibration curve for EE2 at 200 nm with an injection volume of 400 µL. With this method, we were able to reliably quantify EE2 down to 50 nM. Dissolved organic carbon (DOC) was measured by a total organic carbon (TOC) analyzer (Shimadzu TOC-VCPH) and calibrated using potassium hydrogen phthalate standards.

Utility source water characteristics were determined using standard procedures described in Chapter 2. Source waters characteristics (except pH, which had drifted and was remeasured with new values shown in the caption of **Figure 5.5**) were summarized in **Table 5.8**. Briefly, ammonia concentration of source waters ranges from 0.2 to 0.6 mg/L as N; alkalinity ranges from 70 to 144 mg/L as $CaCO_3$; TOC ranges from 1.3 to 4.3 mg/L; total suspended solids (TSS) ranges from <1 to 5.3 mg/L; chloride ranges from 36 to 295 mg/L; nitrate ranges from 6.2 to 12 mg/L; sulfate ranges from 13 to 238 mg/L. To independently quantify the matrix oxidant demand during utility source water experiments, Mn(VII) decay of source waters was determined spectrophotometrically (λ = 525 nm) in 10 cm-optical-path cuvettes using a double-beam spectrophotometer (Shimadzu UV-2401PC). Water samples were filtered with 0.45 µM PTFE filters before analysis.

5.5.1.2 Solid phase extraction (SPE)

A SPE method described by Lagana et. al [53] was adapted for concentrating EE2 in utility source water experiments. SPE cartridges (Waters, Oasis HLB, 500 mg, 60 µm) were firstly preconditioned sequentially with 10 mL dichloromethane/methanol mixture (v:v, 50:50), 5 mL methanol, and 10 mL deionized water. A Visiprep vacuum manifold (Sigma-Aldrich) was used to introduce the 150 mL samples at 5 mL/min. After extraction, SPE cartridges were washed with 5 mL water and 0.4 mL methanol before eluting with 4 mL dichloromethane/methanol mixture (v:v,

50:50). The eluates were then evaporated to dryness and reconstituted in 1.5 mL acetonitrile/water mixture (v:v, 20:80) before analyzing with HPLC-UV. The average SPE recovery of the internal standard E1 was 82.7±6.4 %.

5.5.1.3　LC-MS

EE2 oxidation products were detected and identified by both LC-MS/MS and LC-HRMS methods. Low resolution LC-MS/MS analysis was performed on an Agilent 1200 LC/MSD Trap XCT Ultra instrument to obtain molecular weight and fragmentation patterns of EE2 oxidation products, while high resolution LC-MS (mass accuracy: 5 ppm) was performed on a Waters Q-TOF ultima to obtain the elemental composition of oxidation products. The same column (Zorbax Eclipse XDB-C18, 2.1×50 mm, 3.5 µm) and LC gradient were used for both methods. Separation of reaction products was achieved with a gradient method of two mobile phases (A: 95% H_2O + 5% acetonitrile + 0.1% formic acid; B: 95% acetonitrile + 5% H_2O + 0.1% formic acid) at 0.2 mL/min. The percentage of organic phase B was kept at 10% for the first minute and ramped up to 80% in the next 14 min. The percentage of B was then held at 80% for 1 minute before ramping down to 10% in the next 0.5 min. B% was kept at 10% for another 1.5 min to get the column ready for the analysis of the next sample. For MS analyses, both positive and negative electrospray ionization (ESI^+ and ESI^-) was applied over a mass-to-charge (m/z) range of 50-1000. Because ESI^- analysis only showed a subset of products detected in ESI^+, only results from ESI^+ are presented and used for structural elucidation. For low resolution LC-MS/MS analysis, isolation and fragmentation of ionized target compounds were completed with an ion trap under the auto-MS(2) mode with a fragmentation voltage of 1.0 V. The MS/MS spectra for EE2 and its oxidation products are shown in Appendix A.

5.5.2　Propagation of Uncertainty for EE2 Removal Prediction

The EE2 removal in natural waters can be predicted using the following equation:

$$\text{EE2 Removal Fraction} = 1 - \exp\left\{-\underbrace{(k_{21}\alpha_1 + k_{22}\alpha_2)}_{A} \times \underbrace{\exp\left[\frac{-E_a}{R}\left(\frac{1}{T} - \frac{1}{298}\right)\right]}_{B} \times \underbrace{(Ct_{Mn})}_{C}\right\} \qquad (5.10)$$

The uncertainty of EE2 removal prediction was determined according to Meyer [54]. First, term A is converted to the following form:

$$A = k_{21}\alpha_1 + k_{22}\alpha_2 = k_{21}(1 - \alpha_2) + k_{22}\alpha_2 = k_{21} + (k_{22} - k_{21})\alpha_2 \tag{5.11}$$

where α_1 and α_2 are the fractional concentrations of EE2 and can be calculated as:

$$\alpha_1 = \frac{[H^+]}{[H^+] + K_a} = \frac{10^{-pH}}{10^{-pH} + K_a}; \qquad \alpha_2 = \frac{K_a}{[H^+] + K_a} = \frac{K_a}{10^{-pH} + K_a} \tag{5.12}$$

Then, uncertainty of A (σ_A) can be expressed as:

$$\sigma_A = \sqrt{\sigma_{k_{21}}^2 + (\sigma_{k_{21}}^2 + \sigma_{k_{22}}^2) \cdot \alpha_2^2 + (k_{22} - k_{21})^2 \cdot \sigma_{\alpha_2}^2} \tag{5.13}$$

where $\sigma_{k21}, \sigma_{k22}$, and $\sigma_{\alpha2}$ are uncertainties of k_{21}, k_{22}, and α_2, respectively. σ_{k21} and σ_{k22} are obtained from model fitting of Equation (5.4), and $\sigma_{\alpha2}$ is derived from Equation (5.12) as following:

$$\sigma_{\alpha_2} = 2.3\alpha_1\alpha_2\sigma_{pH} \tag{5.14}$$

where σ_{pH} represents uncertainty of pH measurements and was assumed to be ±0.2 pH units.
Then, we let

$$D = -\frac{E_a}{R}\left(\frac{1}{T} - \frac{1}{298}\right) \tag{5.15}$$

and the uncertainty of D (σ_D) can be expressed as

$$\sigma_D = \frac{1}{R}\sqrt{\left(\frac{\sigma_{E_a}}{E_a}\right)^2 + \frac{\sigma_T^2}{\left(\frac{1}{T} - \frac{1}{298}\right)^2 T^4}} \tag{5.16}$$

where σ_{Ea} is the uncertainty of activation energy E_a and is obtained from model fitting of Arrhenius equation (5.2), σ_T is uncertainty of temperature and is assumed to be ±1 ^{o}C.
Then the uncertainty of term B (σ_B) an be expressed as

$$\sigma_B = B \cdot \sigma_D \tag{5.17}$$

Next, the uncertainty of term C (σ_C) can be expressed as

$$\sigma_C = C \cdot \sqrt{\left(\frac{\sigma_{C_{Mn(VII)}}}{C_{Mn(VII)}}\right)^2 + \left(\frac{\sigma_t}{t}\right)^2} \tag{5.18}$$

where $\sigma_{C_{Mn(VII)}}$ is the uncertainty of Mn(VII) concentration measurement and is assumed to be ±0.1 mg/L, σ_t is uncertainty of t and is assumed to be ±10 s.
The uncertainty of EE2 removal fraction can then be calculated as:

$$\sigma_{EE2\,Removal} = \exp(A \times B \times C) \times (A \times B \times C) \times \sqrt{\left(\frac{\sigma_A}{A}\right)^2 + \left(\frac{\sigma_B}{B}\right)^2 + \left(\frac{\sigma_C}{C}\right)^2} \tag{5.19}$$

5.6 References Cited

[1]   Bila D., Montalvao A. F., Azevedo D. D. and Dezotti M. Estrogenic activity removal of 17 β-estradiol by ozonation and identification of by-products. *Chemosphere*, **2007**, 69: 736-746.

[2]   Kolpin D. W., Furlong E. T., Meyer M. T., Thurman E. M., Zaugg S. D., Barber L. B. and Buxton H. T. Pharmaceuticals, hormones, and other organic wastewater contaminants in U.S. streams, 1999-2000: a national reconnaissance. *Environmental Science & Technology*, **2002**, 36: 1202-1211.

[3]   Esperanza M., Suidan M. T., Nishimura F., Wang Z. M. and Sorial G. A. Determination of sex hormones and nonylphenol ethoxylates in the aqueous matrixes of two pilot-scale municipal wastewater treatment plants. *Environmental Science & Technology*, **2004**, 38: 3028-3035.

[4]   Metcalfe C. D., Metcalfe T. L., Kiparissis Y., Koenig B. G., Khan C., Hughes R. J., Croley T. R., March R. E. and Potter T. Estrogenic potency of chemicals detected in sewage treatment plant effluents as determined by *in vivo* assays with Japanese medaka (Oryzias latipes). *Environmental Toxicology and Chemistry*, **2001**, 20: 297-308.

[5]   Ternes T. A., Stumpf M., Mueller J., Haberer K., Wilken R. D. and Servos M. Behavior and occurrence of estrogens in municipal sewage treatment plants - I. Investigations in Germany, Canada and Brazil. *Science of the Total Environment*, **1999**, 225: 81-90.

[6]   Parrott J. L. and Blunt B. R. Life-cycle exposure of fathead minnows (*Pimephales promelas*) to an ethinylestradiol concentration below 1 ng/L reduces egg fertilization success and demasculinizes males. *Environmental Toxicology*, **2005**, 20: 131-141.

[7]   Nash J. P., Kime D. E., Van der Ven L. T. M., Wester P. W., Brion F., Maack G., Stahlschmidt-Allner P. and Tyler C. R. Long-term exposure to environmental concentrations of the pharmaceutical ethynylestradiol causes reproductive failure in fish. *Environmental Health Perspectives*, **2004**, 112: 1725-1733.

[8]   Schafers C., Teigeler M., Wenzel A., Maack G., Fenske M. and Segner H. Concentration- and time-dependent effects of the synthetic estrogen, 17 alpha-ethinylestradiol, on reproductive capabilities of the zebrafish, Danio rerio. *Journal of Toxicology and Environmental Health-Part a-Current Issues*, **2007**, 70: 768-779.

[9]   Balch G. C., Mackenzie C. A. and Metcalfe C. D. Alterations to gonadal development and

reproductive success in Japanese medaka (Oryzias latipes) exposed to 17 alpha-ethinylestradiol. *Environmental Toxicology and Chemistry*, **2004**, 23: 782-791.

[10] Orn S., Holbech H., Madsen T. H., Norrgren L. and Petersen G. I. Gonad development and vitellogenin production in zebrafish (Danio rerio) exposed to ethinylestradiol and methyltestosterones. *Aquatic Toxicology*, **2003**, 65: 397-411.

[11] Oulton R. L., Kohn T. and Cwiertny D. M. Pharmaceuticals and personal care products in effluent matrices: A survey of transformation and removal during wastewater treatment and implications for wastewater management. *Journal of Environmental Monitoring*, **2010**, 12: 1956-1978.

[12] Huber M. M., Ternes T. A. and von Gunten U. Removal of estrogenic activity and formation of oxidation products during ozonation of 17α-ethinylestradiol. *Environmental Science & Technology*, **2004**, 38: 5177-5186.

[13] Deborde M., Rabouan S., Duguet J. P. and Legube B. Kinetics of aqueous ozone-induced oxidation of some endocrine disruptors. *Environmental Science & Technology*, **2005**, 39: 6086-6092.

[14] Lee Y., Escher B. I. and von Gunten U. Efficient removal of estrogenic activity during oxidative treatment of waters containing steroid estrogens. *Environmental Science & Technology*, **2008**, 42: 6333-6339.

[15] Deborde M., Rabouan S., Gallard H. and Legube B. Aqueous chlorination kinetics of some endocrine disruptors. *Environmental Science & Technology*, **2004**, 38: 5577-5583.

[16] Huber M. M., Korhonen S., Ternes T. A. and von Gunten U. Oxidation of pharmaceuticals during water treatment with chlorine dioxide. *Water Research*, **2005**, 39: 3607-3617.

[17] Lee Y., Yoon J. and von Gunten U. Kinetics of the oxidation of phenols and phenolic endocrine disruptors during water treatment with ferrate (Fe(VI)). *Environmental Science & Technology*, **2005**, 39: 8978-8984.

[18] Xu L., Xu C., Zhao M. R., Qiu Y. P. and Sheng G. D. Oxidative removal of aqueous steroid estrogens by manganese oxides. *Water Research*, **2008**, 42: 5038-5044.

[19] Ohko Y., Iuchi K. I., Niwa C., Tatsuma T., Nakashima T., Iguchi T., Kubota Y. and Fujishima A. 17 β-estrodial degradation by TiO_2 photocatalysis as means of reducing estrogenic activity. *Environmental Science & Technology*, **2002**, 36: 4175-4181.

[20] MWH. *Water Treatment: Principles and Design*, 2nd ed. Hoboken: Wiley, **2005**.

[21]   Singer P. C., Borchardt J. H. and Colthurst J. M. The effects of permanganate pretreatment on trihalomethane formation in drinking water. *Journal American Water Works Association*, **1980**, 72: 573-578.

[22]   Waldemer R. H. and Tratnyek P. G. Kinetics of contaminant degradation by permanganate. *Environmental Science & Technology*, **2006**, 40: 1055-1061.

[23]   MacKinnon L. K. and Thomson N. R. Laboratory-scale in situ chemical oxidation of a perchloroethylene pool using permanganate. *Journal of Contaminant Hydrology*, **2002**, 56: 49-74.

[24]   Kao C. M., Huang K. D., Wang J. Y., Chen T. Y. and Chien H. Y. Application of potassium permanganate as an oxidant for in situ oxidation of trichloroethylene-contaminated groundwater: A laboratory and kinetics study. *Journal of Hazardous Materials*, **2008**, 153: 919-927.

[25]   Hu L., Martin H. M., Arce-Bulted O., Sugihara M. N., Keating K. A. and Strathmann T. J. Oxidation of carbamazepine by Mn(VII) and Fe(VI): Reaction kinetics and mechanism. *Environmental Science & Technology*, **2009**, 43: 509-515.

[26]   Hu L., Martin H. A. and Strathmann T. J. Oxidation kinetics of antibiotics during water treatment with potassium permanganate. *Environmental Science & Technology*, **2010**, 44: 6416-6422.

[27]   Jiang J., Pang S.-Y. and Ma J. Oxidation of triclosan by permanganate (Mn(VII)): Importance of ligands and in situ formed manganese oxides. *Environmental Science & Technology*, **2009**, 43: 8326-8331.

[28]   Jiang J., Pang S.-Y. and Ma J. Role of ligands in permanganate oxidation of organics. *Environmental Science & Technology*, **2010**, 44: 4270-4275.

[29]   Lee D. G. and Sebastian C. F. The oxidation of phenol and chlorophenols by alkaline permanganate. *Canadian Journal of Chemistry-Revue Canadienne De Chimie*, **1981**, 59: 2776-2779.

[30]   Lee D. G. and Chang V. S. Oxidation of hydrocarbons. 9. The oxidation of alkynes by potassium permanganate. *Journal of Organic Chemistry*, **1979**, 44: 2726-2730.

[31]   Shao X., Ma J., Wen G. and Yang J. Oxidation of estrone by permanganate: Reaction kinetics and estrogenicity removal. *Chinese Science Bulletin*, **2010**, 55: 802-808.

[32]   Huber M. M., Canonica S., Park G. Y. and von Gunten U. Oxidation of pharmaceuticals

during ozonation and advanced oxidation processes. *Environmental Science & Technology*, **2003**, 37: 1016-1024.

[33]   Lee Y. and von Gunten U. Oxidative transformation of micropollutants during municipal wastewater treatment: Comparison of kinetic aspects of selective (chlorine, chlorine dioxide, ferrate(VI), and ozone) and non-selective oxidants (hydroxyl radical). *Water Research*, **2010**, 44: 555-566.

[34]   Kumar P. and Khan Z. Unusual stabilization of water-soluble colloidal MnO_2 during the oxidation of paracetamol by MnO_4^-. *Colloid & Polymer Science*, **2006**, 284: 1155-1162.

[35]   He D., Guan X. H., Ma J. and Yu M. Influence of different nominal molecular weight fractions of humic acids on phenol oxidation by permanganate. *Environmental Science & Technology*, **2009**, 43: 8332-8337.

[36]   Musso H. Phenol oxidation reactions. *Angewandte Chemie International Edition in English*, **1963**, 2: 723-735.

[37]   Ukrainczyk L. and Mcbride M. B. Oxidation of phenol in acidic aqueous suspensions of manganese oxides. *Clays and Clay Minerals*, **1992**, 40: 157-166.

[38]   Pereira R. O., Postigo C., de Alda M. L., Daniel L. A. and Barcel D. Removal of estrogens through water disinfection processes and formation of by-products. *Chemosphere*, **2011**, 82: 789-799.

[39]   Irmak S., Erbatur O. and Akgerman A. Degradation of 17β-estradiol and bisphenol A in aqueous medium by using ozone and ozone/UV techniques. *Journal of Hazardous Materials*, **2005**, 126: 54-62.

[40]   Yi T. and Harper W. F. The link between nitrification and biotransformation of 17α-ethinylestradiol. *Environmental Science & Technology*, **2007**, 41: 4311-4316.

[41]   Skotnicka-Pitak J., Garcia E. M., Pitak M. and Aga D. S. Identification of the transformation products of 17 a-ethinylestradiol and 17 β-estradiol by mass spectrometry and other instrumental techniques. *Trends in Analytical Chemistry*, **2008**, 27: 1036-1052.

[42]   Skotnicka-Pitak J., Khunjar W. O., Love N. G. and Aga D. S. Characterization of metabolites formed during the biotransformation of 17α-ethinylestradiol by nitrosomonas europaea in batch and continuous flow bioreactors. *Environmental Science & Technology*, **2009**, 43: 3549-3555.

[43]   Stone A. T. Reductive dissolution of manganese(III/IV) oxides by substituted phenols.

Environmental Science & Technology, **1987**, 21: 979-988.

[44]　Ladbury J. W. and Cullis C. F. Kinetics and mechanism of oxidation by permanganate. *Chemical Reviews*, **1958**, 58: 403-438.

[45]　Hwang S., Lee D. I., Lee C. H. and Ahn I. S. Oxidation of 17α-ethinylestradiol with Mn(III) and product identification. *Journal of Hazardous Materials*, **2008**, 155: 334-341.

[46]　Haaf H., Metzler M. and Li J. J. Metabolism of [4-^{14}C]estrone in hamster and rat hepatic and renal microsomes: Species-, sex- and age-specific differences. *The Journal of Steroid Biochemistry and Molecular Biology*, **1992**, 42: 389-397.

[47]　Gardner K. A. and Mayer J. M. Understanding C-H bond oxidations: H· and H⁻ transfer in the oxidation of toluene by permanganate. *Science*, **1995**, 269: 1849-1851.

[48]　Solomons T. W. G. *Organic Chemistry*. New York: John Wiley & Sons, Inc., **1996**.

[49]　Lee D. G., Lee E. J. and Chandler W. D. Oxidation of hydrocarbons. 16. Mechanism of the reaction between alkynes and permanganate ion. *Journal of Organic Chemistry*, **1985**, 50: 4306-4309.

[50]　Jennings P. W., Hartman J. W. and Hiscox W. C. Alkyne hydration using Pt(II) catalysts. *Inorganica Chimica Acta*, **1994**, 222: 317-322.

[51]　Mizushima E., Sato K., Hayashi T. and Tanaka M. Highly efficient AuI-catalyzed hydration of alkynes. *Angewandte Chemie*, **2002**, 114: 4745-4747.

[52]　Tokunaga M. and Wakatsuki Y. The first anti-Markovnikov hydration of terminal alkynes: Formation of aldehydes catalyzed by a rthenium(II)/phosphane mixture. *Angewandte Chemie International Edition*, **1998**, 37: 2867-2869.

[53]　Lagana A., Bacaloni A., De Leva I., Faberi A., Fago G. and Marino A. Analytical methodologies for determining the occurrence of endocrine disrupting chemicals in sewage treatment plants and natural waters. *Analytica Chimica Acta*, **2004**, 501: 79-88.

[54]　Meyer S. L. *Data analysis for scientists and engineers*: Wiley, **1975**.

[55]　Sharma V. K. Use of iron(VI) and iron(V) in water and wastewater treatment. *Water Science and Technology*, **2004**, 49: 69-74.

[56]　Djerassi C., Wilson J. M., Budzikiewicz H. and Chamberlin J. W. Mass spectrometry in structural and stereochemical problems. XIV.1 Steroids with one or two aromatic rings. *Journal of the American Chemical Society*, **1962**, 84: 4544-4552.

5.7 Figures and Tables
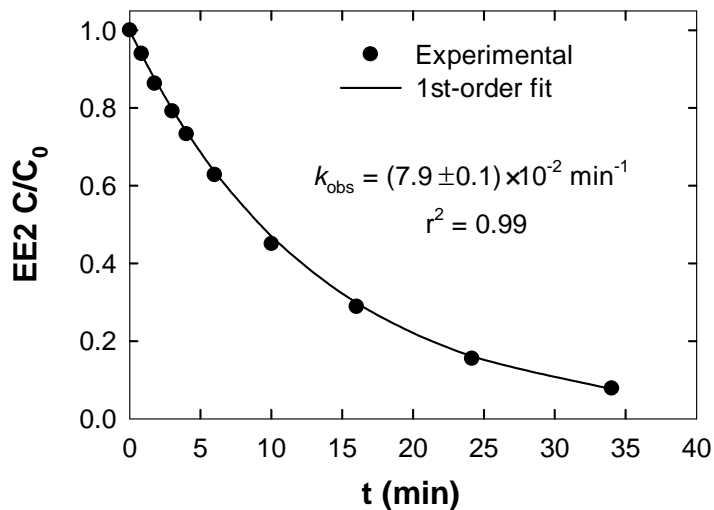
Figure 5.1. Representative batch reaction for oxidation of EE2 by excess concentrations of Mn(VII) and pseudo-first-order rate law model fit. Experimental conditions: $[EE2]_0 = 1$ μM, $[Mn(VII)]_0 = 10$ μM, 25 ^{o}C, pH 7, 25 mM NaCl. Uncertainty represents 1 σ.
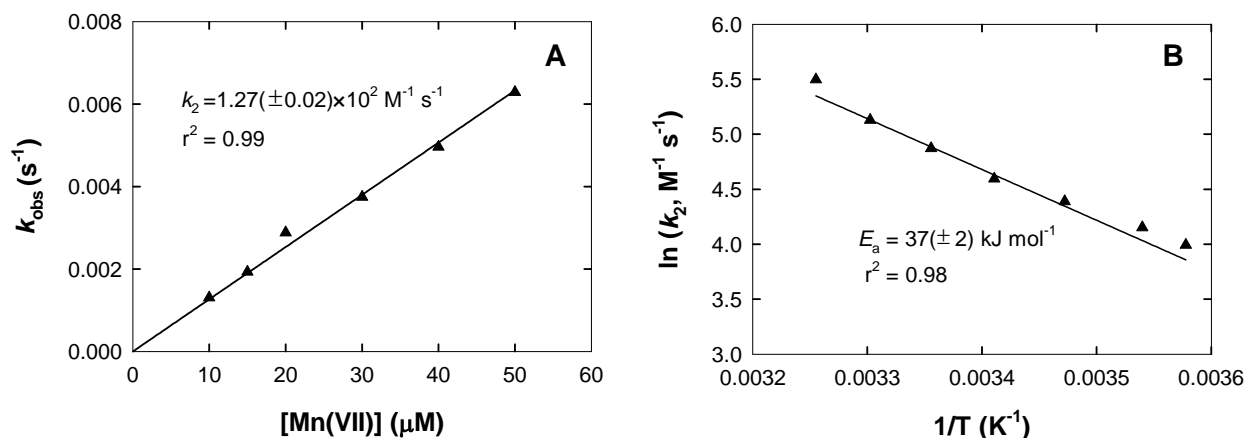
Figure 5.2. Effects of (A) Mn(VII) concentration and (B) temperature on rate constants of EE2 reaction with Mn(VII). Experimental conditions: $[EE2]_0 = 1$ μM, 25 mM NaCl, pH 7, 25 ^{o}C for (A); $[EE2]_0 = 1$ μM, $[Mn(VII)]_0 = 10$ μM, 25 mM NaCl, pH 7 for (B). Lines represent linear regressions of measured data. Uncertainties represent 1 σ.
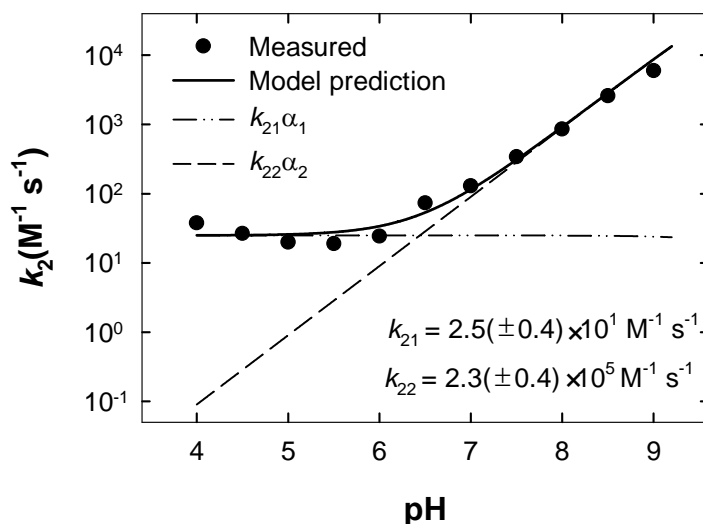
Figure 5.3. Effect of pH on measured and model-predicted rate constants for Mn(VII) reactions with EE2. $[EE2]_0 = 1$ µM, $[Mn(VII)]_0 = 10$ µM, 25 mM NaCl, 25 °C. Symbols represent measurements and lines indicate overall model predictions. Uncertainties represent 1 σ.
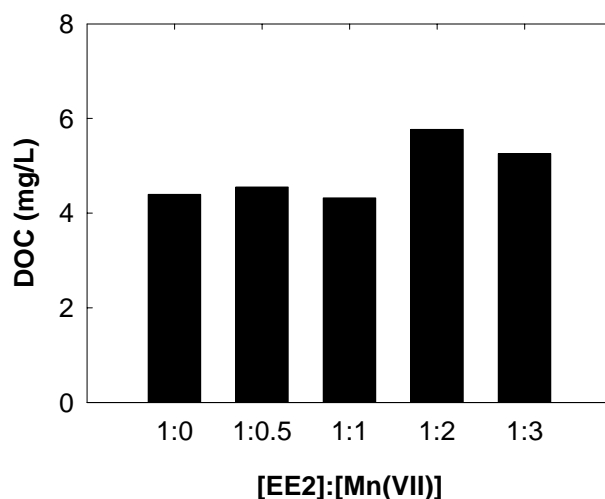
Figure 5.4. Measured dissolved organic carbon (DOC) concentration of EE2 solutions after treatment with different doses of Mn(VII). Reaction conditions: $[EE2]_0 = 18$ µM, varying $[Mn(VII)]$, pH 7, room temperature.
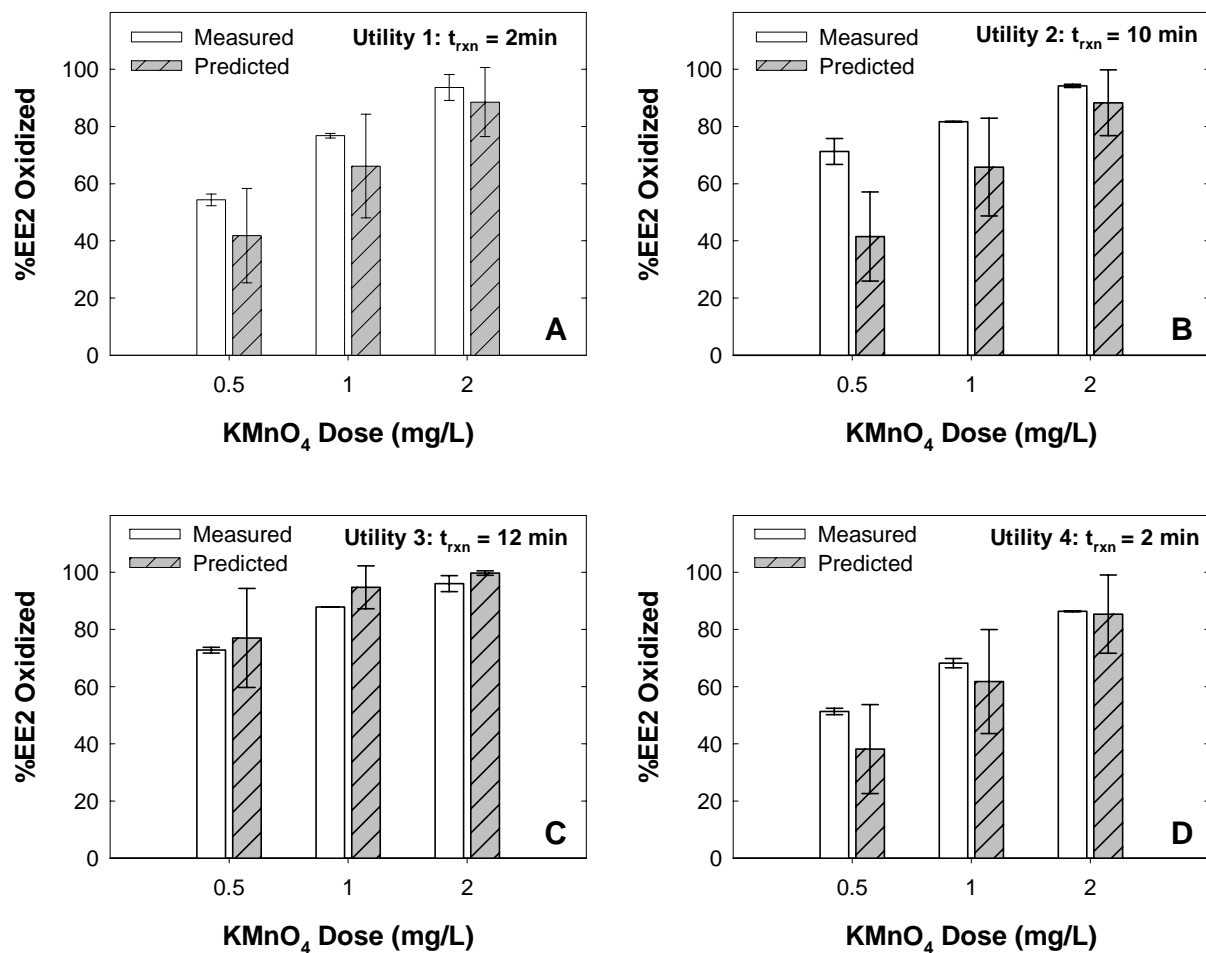
Figure 5.5. Comparison of measurements and model predictions for EE2 removal during treatment of utility source waters with Mn(VII). Experimental conditions: $[EE2]_0 = 500$ ng/L, pH = 8.4 (utility 1), 7.6 (utility 2), 8.0 (utility 3), 8.3 (utility 4), T = 16 °C (utility 1), 19 °C (utility 2), 18 °C (utility 3 and 4). Reaction times used in experiments varied among utilities due to different pH conditions of the individual source waters. Uncertainties for measured values are duplicate-averaged 1 σ, and uncertainties for predicted values represent 1 σ and are obtained by error propagation of Equation (5.3) considering ±1 σ uncertainty of fit-derived k_{21}, k_{22}, and E_a values, and assuming ±0.2 pH and ±1 °C uncertainty (see Section 5.5.2).
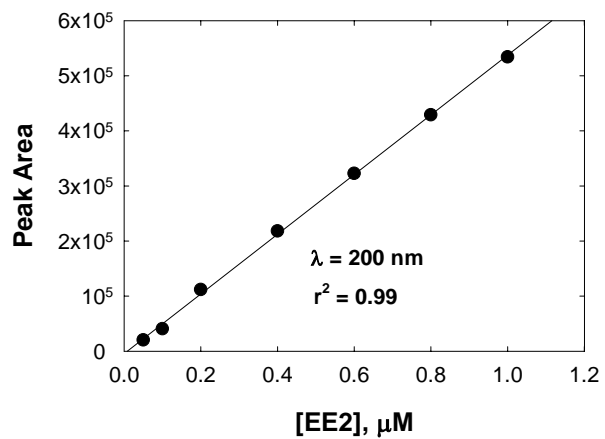
Figure 5.6. Representative HPLC calibration curve for EE2 at 200 nm with an injection volume of 400 μL.

Table 5.1. EE2 reactivity with Mn(VII) and other water treatment oxidants

17α-ethinylestradiol (EE2)
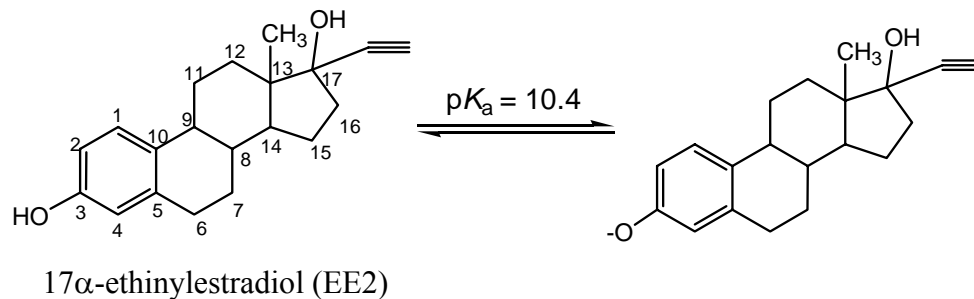
Oxidant	$k_2{}^a$ $(M^{-1} s^{-1})$	$k_{21}{}^b$ $(M^{-1} s^{-1})$	$k_{22}{}^c$ $(M^{-1} s^{-1})$	Reference
Mn(VII)	$1.27(\pm0.02)\times10^2$	$2.5(\pm0.4)\times10^1$	$2.3(\pm0.4)\times10^5$	This study
·OH^d	$9.8(\pm1.2)\times10^9$	---	---	Huber et al. [32]
O_3	3×10^6	$1.83(\pm0.38)\times10^5$	$3.65(\pm0.46)\times10^9$	Deborde et al. [13]
HOCl	1.15×10^2	$4.3(\pm0.5)$	$3.5(\pm0.1)\times10^5$	Deborde et al. [15]
NH_2Cl^e	2.5×10^{-1}	---	---	Lee et al. [14]
ClO_2	2×10^5	<200	$4.6(\pm0.8)\times10^8$	Huber et al. [16]
Fe(VI)	$7.3(\pm0.6)\times10^2$	$9.4(\pm0.2)\times10^2$	$5.4(\pm0.2)\times10^5$	Lee et al. [17]

[a] Apparent second-order rate constant. pH = 7, T = 25 °C for Mn(VII) and Fe(VI); 20 °C for ·OH, O_3, HOCl and ClO_2.
[b] Specific rate constant for neutral EE2 species.
[c] Specific rate constant for deprotonated anionic EE2 species.
[d] ·OH created in UV/H_2O_2 systems.
[e] Rate constant estimated from Figure 1 in Lee et al [14].

Table 5.2. Measured pseudo-first-order rate constants for EE2 oxidation by Mn(VII)[a]

pH	T (°C)	$[Mn(VII)]_0$ (μM)	k_{obs} (10^{-3} s^{-1})[b]
7	25	10	1.31(±0.01)
7	25	15	1.93(±0.02)
7	25	20	2.88(±0.05)
7	25	30	3.75(±0.06)
7	25	40	4.96(±0.07)
7	25	50	6.3(±0.2)
4	25	10	0.37(±0.03)
4.5	25	10	0.27(±0.01)
5	25	10	0.20(±0.01)
5.5	25	10	0.14(±0.01)
6	25	10	0.24(±0.01)
6.5	25	10	0.74(±0.01)
7.5	25	10	3.6(±0.1)
8	25	10	9.9(±0.2)
8.5	25	10	26.5(±0.4)
9	25	10	68(±2)
7	6.5	10	0.54(±0.02)
7	9.5	10	0.64(±0.02)
7	15	10	0.81(±0.01)
7	20	10	0.99(±0.02)
7	30	10	1.69(±0.03)
7	34	10	2.2(±0.1)

[a] Experimental conditions: $[EE2]_0$ = 1 μM, [NaCl] = 25 mM, no pH buffer.
[b] Uncertainties represent 1 σ from regression.

Table 5.3. Reduction potentials of common drinking water oxidants at pH 7

Oxidant	Reaction[a]	E^o	$E^o_{pH\,7}$ [b] (V)
Mn(VII)	$MnO_4^- + 4H^+ + 3e^- \rightleftharpoons MnO_{2(s)} + 2H_2O$	1.68 [20]	1.13
·OH	$\cdot OH + H^+ + e^- \rightleftharpoons H_2O$	2.59 [20]	2.18
O_3	$O_3 + 2H^+ + 2e^- \rightleftharpoons O_2 + H_2O$	2.08 [20]	1.67
HOCl	$HOCl + H^+ + 2e^- \rightleftharpoons Cl^- + H_2O$	1.48 [20]	1.27
NH_2Cl	$NH_2Cl + H_2O + 2e^- \rightleftharpoons NH_3 + Cl^- + OH^-$	1.61 [20]	1.41
ClO_2	$ClO_2 + e^- \rightleftharpoons ClO_2^-$	0.95 [20]	0.95
Fe(VI)[c]	$FeO_4^{2-} + 8H^+ + 3e^- \rightleftharpoons Fe^{3+} + 4H_2O$	2.20 [55]	1.10

[a] Half reactions under acidic conditions are shown.
[b] Reduction potentials at pH 7 were calculated using Nernst equation and E^o values at pH 0.
[c] Ferrate is an emerging oxidant and is included for comparison purposes.

Table 5.4. Permanganate decay in utility source waters[a]

Utility 1		Utility 2		Utility 3		Utility 4	
t (min)	[KMnO₄] (mg/L)	t (min)	[KMnO₄] (mg/L)	t (min)	[KMnO₄] (mg/L)	t (min)	[KMnO₄] (mg/L)
0.5	0.96	0.5	1.08	0.5	1.04	0.5	1.02
1	0.92	1	1.03	1	0.98	1	0.96
2	0.89	2	1.02	2	0.92	2	0.92
		5	0.95	8	0.88		
		10	0.83	12	0.79		

[a] Initial KMnO₄ concentration is 1 mg/L.

Table 5.5. Products of EE2-Mn(VII) reactions detected by LC-MS/MS
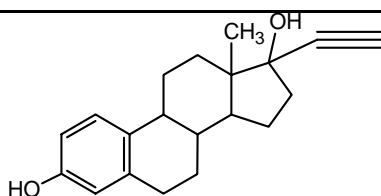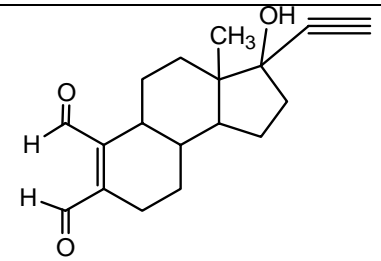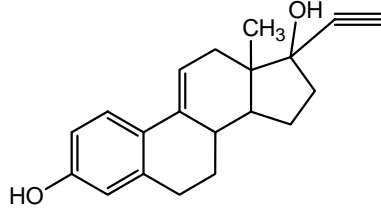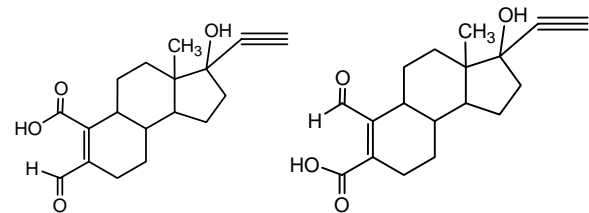
Product ID	$[M+H]^+$ $(m/z)^a$	R.T.[b] (min)	Major MS/MS Fragments[c] (m/z)	Molecular Formula	Theoractical mass for $[M+H]^+$	Difference from EE2[d]	Proposed Structure
EE2	297.1854	13.6	279, 251, 239, 223, 185, 159[e], 147	$C_{20}H_{24}O_2$	297.1849	---	
I	287.1648	10.7	269[e], 251, 241, 223, 209, 181	$C_{18}H_{22}O_3$	287.1647	-(2C 2H) +O	
II	295.1698	8.9	277[e], 249, 235, 221, 157, 133	$C_{20}H_{22}O_2$	294.1620	- 2H	
III	303.1613	7.5	285, 267[e], 239, 221, 177, 159	$C_{18}H_{22}O_4$	303.1596	-(2C 2H) +2O	

Table 5.5. (cont.)
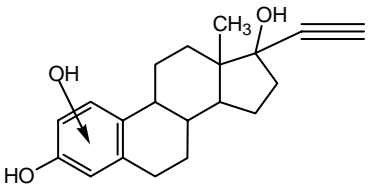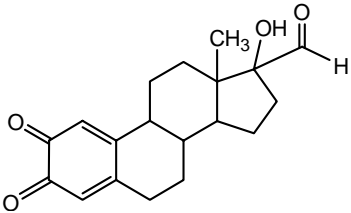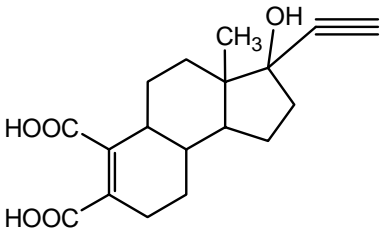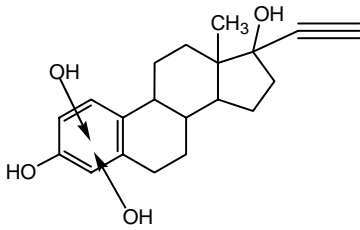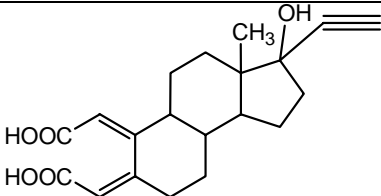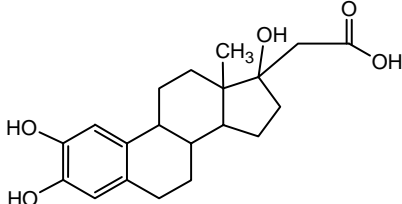
Product ID	[M+H]$^+$ (m/z)^a	R.T.^{b} (min)	Major MS/MS Fragments^c (m/z)	Molecular Formula	Theoractical mass for [M+H]$^+$	Difference from EE2^d	Proposed Structure
IV	313.1806	9.3	295^e, 267, 185, 173, 159,	$C_{20}H_{24}O_2$	313.1804	+O	
V	315.1599	12.5	297^e, 251, 223	$C_{19}H_{22}O_4$	315.1596	-(C 2H) +2O	
VI^f	319.1542	3.4	301, 283, 273^e, 255, 237	$C_{18}H_{22}O_5$	319.1546	-(2C 2H) +3O	

Table 5.5. (cont.)

Product ID	$[M+H]^+$ $(m/z)^a$	R.T.[b] (min)	Major MS/MS Fragments[c] (m/z)	Molecular Formula	Theoractical mass for $[M+H]^+$	Difference from EE2[d]	Proposed Structure
VII	329.1753	4.1	311[e], 293, 283, 265, 237	$C_{20}H_{24}O_4$	329.1753	+2O	
VIII	345.1696	8.5	327[e], 309, 285, 267, 239, 221, 159	$C_{20}H_{24}O_5$	345.1702	+3O	
IX	347.1874	4.2	329[e], 311, 293, 283, 265	$C_{20}H_{26}O_5$	347.1859	+(2H 3O)	

[a] The numbers are from high resolution LC-MS analysis on Waters Q-TOF ultima., equal to the molecular weight of the analyte plus 1 (M.W. +1).
[b] R.T. represents retention time of each product peak in the LC chromatogram obtained from from Agilent 1200 LC/MSD.
[c] MS/MS fragmentation pattern obtained from Agilent 1200 LC/MSD.
[d] Molecular formula difference from EE2.
[e] Most abundant fragment ion.
[f] Fragmentation pattern obtained from MS/MS of its ammonium adduct (m/z: 336).
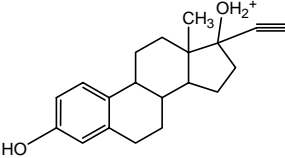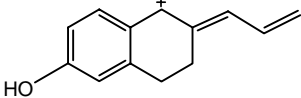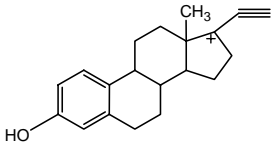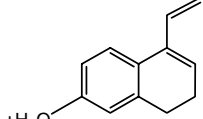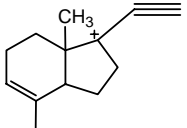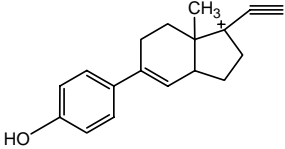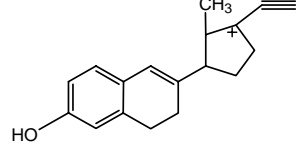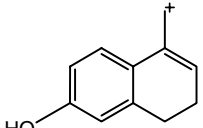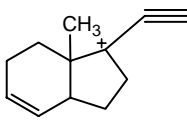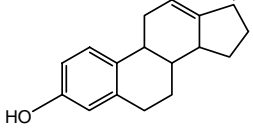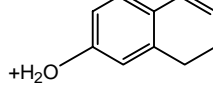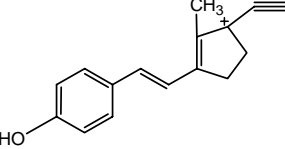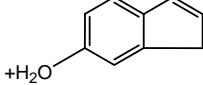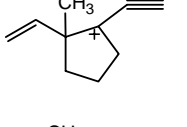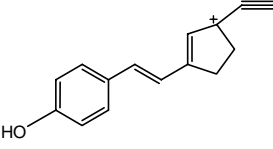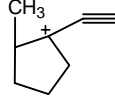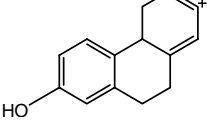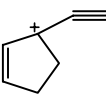
Table 5.6. Proposed structures for fragment ions of EE2[a]

m/z	Proposed Structure	m/z	Proposed Structure
297 (EE2)		185	
279		173[b]	
251[b]		159[b]	
239		147	
223		133[b]	
209		107	
197		91	

[a] For the fragmentation pathways leading to the formation of the proposed fragment ions, a previous report [56] on mass spectra interpretation of steroids is referred.

[b] Two plausible structures are proposed. The fragment ion could be either one of the two or could be a mixture of the two.

Table 5.7. Formation of EE2 reaction products under different Mn(VII) dosing

Product ID	$[EE2]_0/[Mn(VII)]_0$			
	1:0.4	1:1.2	1:2	1:5
I		√	√	√
II	√	√	√	√
III		√	√	√
IV	√	√	√	√
V	√	√	√	√
VI				√
VII	√	√	√	√
VIII	√	√	√	√
IX	√	√	√	√

Table 5.8. Utility source water characteristics

	Utility 1	Utility 2	Utility 3	Utility 4
Source Water Type	Reservoir	River	River	Reservoir
Ammonia (mg/L as N)	0.3	0.4	0.6	0.2
Alkalinity (mg/L as $CaCO_3$)	144	92	70	100
TOC (mg/L)	4.3	N/D[a]	1.3	N/D[a]
TSS (mg/L)	5.3	1.2	20	< 1
TDS (mg/L)	174	556	177	617
Chloride (mg/L)	36	295	17.2	88.1
Nitrate (mg/L)	12	14.2	6.2	8.0
Sulfate (mg/L)	13	24.6	46.3	238

[a] Below detection limit.

CHAPTER 6

INACTIVATION KINETICS OF BACTERIOPHAGE MS2 WITH POTASSIUM FERRATE(VI)

6.1 Abstract

Alternative disinfectants are needed to control viral pathogens while limiting the formation of toxic disinfection byproducts during water and wastewater treatment. This study investigates the potential of an emerging oxidant, ferrate [FeO_4^{2-}, Fe(VI)], as an alternative disinfectant. Batch kinetics experiments were conducted to quantify the inactivation kinetics of bacteriophage MS2, a surrogate for human enteric viruses, with potassium ferrate(VI) at 5-30 ^{o}C, pH 6-11 and Fe(VI) doses of 0.56 – 2.24 mg/L as Fe. The Chick-Watson model was able to describe the inactivation kinetics observed in individual batch experiments. The observed inactivation rate constant [k_{obs}; L/(mg Fe·min)] was found to be independent of initial MS2 concentration. Fe(VI) autodecomposes rapidly in circumneutral pH water, but k_{obs} was found to increase with increasing applied dosage of Fe(VI), possibly due to formation of a secondary disinfecting species during Fe(VI) decomposition. At pH 7 and 25 ^{o}C and with a Fe(VI) dose of 1.23 mg/L as Fe, the k_{obs} value was measured to be 2.27($\pm$0.05) L/(mg Fe·min), corresponding to a 4-log removal with a Ct of 4 (mg Fe·min)/L. The temperature dependence of k_{obs} could be described by the Arrhenius equation with an apparent activation energy of 39($\pm$6) kJ mol^{-1}. pH was found to significantly affect inactivation kinetics, with k_{obs} increasing from 0.043 L/(mg Fe·min) to 2.44 L/(mg Fe·min) when pH decreased from 11 to 6 (applied Fe(VI) dose of 1.12 mg/L as Fe). The effect of pH can be modeled by considering parallel MS2 inactivation processes involving different Fe(VI) species ($HFeO_4^-$ and FeO_4^{2-}), with the protonated Fe(VI) species being 54 times more reactive with MS2 than its conjugate base. Results from this study and previous reports on ferrate's high reactivity with many water contaminants suggest that ferrate has significant potential as a drinking water oxidant and disinfectanting agent.

6.2 Introduction

Disinfection processes using free chlorine as the primary disinfectant have been applied in drinking water facilities to control bacteria, viruses, and other pathogenic microorganisms for over

a century [1]. However, the Long Term 2 Enhanced Surface Water Treatment Rule and Stage 2 Disinfectants and Disinfection Byproducts Rule, released by the U.S. Environmental Protection Agency (USEPA) in 2006 in response to the need for better control of *Cryptosporidium parvum* oocysts and toxic disinfection byproducts (DBPs) [2, 3], has prompted many U.S. drinking water utilities to replace free chlorine as the primary disinfectant with alternative processes, most often UV disinfection or treatment with combined chlorine. This practice has raised serious concerns on the presence of viral pathogens in drinking water [4-6], especially enteric viruses, because viruses are much more resistant to UV light and combined chlorine than to free chlorine [1, 7]. In addition, a growing body of work shows that combined chlorine promotes formation of emerging classes of DBPs that are more toxic than regulated THM and TAA DBPs [8-10]. As a result, there remains strong interest in the development of alternative disinfection processes that are effective in both inactivating viral pathogens and producing fewer and less toxic DBPs than free chlorine [11, 12].

Potassium ferrate [K_2FeO_4, Fe(VI)] is a hypervalent form of iron that has attracted growing attention in recent years as an alternative oxidant and disinfectant for water and wastewater treatment [13-19]. Fe(VI) could be a promising alternative disinfectant for several reasons: (i) Fe(VI) is a strong oxidant reported to selectively oxidize amino acids and other biomolecules [20, 21]; (ii) past work has shown that Fe(VI) inactivates several pathogens, including coliphages f2 and Qβ, and *E. coli* [22-24]; (iii) the application of Fe(VI) is not believed to produce halogenated DBPs known to be mutagenic or carcinogenic [25, 26]; (iv) Fe(VI) does not oxidize bromide to bromate like ozone [27]; (v) the $Fe(OH)_{3(s)}$ byproduct of Fe(VI) reactions and autodecomposition can also act to promote physical removal of pathogens and secondary DBP precursors during sedimentation and filtration processes [15, 17], and (vi) Fe(VI) is more stable in organic-rich and ammonia-rich waters than O_3 and free chlorine [28].

This study examines for the first time Fe(VI) inactivation of bacteriophage MS2. MS2 is a commonly studied non-pathogenic surrogate for human enteric viruses found in drinking water [29, 30]. MS2 is a positive-sense single-stranded RNA phage that propagates in *E. coli*. The molecular structure of MS2 is well-characterized, with a small genome of 3,569 nucleotides, the full sequence of which has been established [31]. It possesses an icosahedral shape with a diameter of 27-34 nm and an isoelectric point of 3.9 [32, 33]. Previous studies have examined MS2 phage inactivation by common water disinfectants [34-38], including free chlorine, monochloramine, ozone, hydrogen peroxide, and chlorine dioxide, thereby enabling comparison with Fe(VI) studies

155

presented here. Objectives of this study were to quantify the process of MS2 inactivation by Fe(VI), including determining the inactivation rate law and obtaining kinetic parameters as a function of varying initial MS2 phage concentration, applied Fe(VI) dose, temperature and solution pH. The resulting kinetics trends were also used to infer mechanistic insights into the controlling inactivation mechanisms.

6.3 Materials and Methods

6.3.1 Virus Propagation and Viability Assessment

Bacteriophage MS2 (ATCC 15597-B1) and its bacterial host *E. coli* (ATCC 15997) were obtained from the American type culture collection (Manassas, VA). *E. coli* cells were grown and maintained using slants and tryptic soy broth (TSB) suspensions, and stored at 4 ^{o}C prior to use. MS2 stocks were grown in *E. coli* suspensions and purified by sequential centrifugation, microfiltration and ultrafiltration as reported previously [39]. The final concentrate from the ultrafiltration membrane was then diluted in 1 mM phosphate buffer solution (PBS) to a final MS2 concentration of 10^{11} plaque forming units per mililiter (pfu/mL) and stored at 4 ^{o}C until use.

MS2 phage concentration was determined by MS2 viability assessment with the soft agar overlay method [40]. In general, quenched MS2 samples from inactivation experiments underwent serial dilutions with TSB solutions. Each dilution was then mixed with the host bacteria *E. coli* solution in TSB and soft agar, and the mixture was spread onto pre-prepared hard agar plates. After solidification, the plates were inverted and incubated at 37 ^{o}C overnight. The plaques formed were then visually enumerated to quantify the MS2 phage concentration.

6.3.2 Ferrate(VI) Preparation and Measurement

K_2FeO_4 was prepared according to a method reported by Delaude and Laszlo [41], yielding a material with an iron content that is 98% Fe(VI). Fe(VI) stock solutions were prepared in 5 mM phosphate/1 mM borate buffer mixture (pH ~9.1), where aqueous Fe(VI) is reported to be most stable [20, 42]. Stock solutions were used within 30 min of preparation to minimize artifacts from Fe(VI) decomposition.

A colorimetric method described by Lee et. al. [43] was used to determine Fe(VI) concentrations. In this method, 2,2'-azino-bis(3-ethylbenzothiazoline-6-sulfonate) (ABTS) is

rapidly oxidized by Fe(VI) to produce a stable radical cation, ABTS$^{\bullet+}$, with high molecular absorptivity ($\varepsilon_{415\,nm}$ = 34,000 M^{-1} cm^{-1}), which permits sensitive detection by UV-visible spectrophotometry.

6.3.3   MS2 Inactivation Experiments

Inactivation experiments were conducted in a 200 mL continuously stirred batch reactor immersed in a circulating constant temperature water bath. To minimize Fe(VI) autodecomposition, Fe(VI) stock solution was added to buffered (10 mM phosphate for pH<9, and 10 mM phosphate/2 mM borate for pH 9-11) and pH-adjusted solutions shortly before initiating reactions. Reactions were initiated by spiking MS2 phage stock solution into the reactor, while simultaneously withdrawing an aliquot of reactor solution to quantify the initial Fe(VI) concentration. Due to Fe(VI) autodecomposition, the initial Fe(VI) concentration differed from the applied Fe(VI) dose. Aliquots were then periodically collected to monitor reaction progress. Two aliquots were collected at each time point, one for MS2 phage viability assessment and one for analysis of Fe(VI) concentration. The aliquot collected for MS2 viability assessment was quenched with excess sodium thiosulfate, which quickly reduces Fe(VI) to Fe(III) [44]. The remaining viable MS2 phage concentration was then determined by the soft agar overlay method. The other aliquot was mixed with excess ABTS and a buffer mixture of acetate and phosphate (pH 4.1), which prevents the precipitation of Fe(III) and avoids interference of the optical monitoring from Fe(III) precipitates [45]. The remaining Fe(VI) concentration in each sample was then analyzed as ABTS^{+} by spectrophotometry within 1 hour.

6.4   Results and Discussion

6.4.1   Inactivation Kinetics Model

Experimental results show that MS2 phage can be effectively inactivated by Fe(VI). **Figure 6.1A** shows a representative inactivation data for MS2 phage in Fe(VI)-treated solution at pH 7.0. The individual batch inactivation kinetics is well described by the Chick-Watson model:

$$\ln\left(\frac{N}{N_0}\right) = -k_{obs}Ct \tag{6.1}$$

where N_0 and N are MS2 phage concentrations initially present and following a treatment time t,

respectively; k_{obs} [L/(mg Fe·min)] is the observed MS2 phage inactivation rate constant at the experimental conditions in question; and Ct ($\int_0^t [Fe(VI)]_{tot} dt$, (mg Fe·min)/L) is the integrated exposure to Fe(VI) as the reaction proceeds, which accounts for Fe(VI) decay during batch experiments. Previous studies established that Fe(VI) decay follows second-order kinetics with respect of Fe(VI) concentration [46], which is also observed in our studies (**Figure 6.1B**). As a result, Ct values corresponding to different reaction times can be calculated as:

$$Ct = \int_0^t [Fe(VI)]dt = \int_0^t (\frac{[Fe(VI)]_0}{k_d [Fe(VI)]_0 t + 1})dt = \frac{1}{k_d} \ln(k_d [Fe(VI)]_0 t + 1) \qquad (6.2)$$

where k_d (L/(mg Fe·min)) is the second-order rate constant of Fe(VI) autodecomposition observed in each batch reaction. As shown in **Figure 6.1B**, second-order fit-derived k_d at pH 7 and 25 ^{o}C is 0.102 L/(mg Fe·min), which is slower than two previously reported values. Cho et al. [24] measured a k_d of 0.135 L/(mg Fe·min) at pH 7.1 and 25 ^{o}C, while the model fitting from Rush et al. [46] indicated a k_d of 0.214 L/(mg Fe·min). The different k_d values might be due to different experimental conditions used (e.g., buffer concentration, temperature, and presence/absence of pathogens) [24]. Nevertheless, the relatively slower k_d value observed here indicates the Fe(VI) decay is predominantly from autodecomposition instead of reactions with MS2 phage or the broth as suggested by Schink et al [22]. The experimental conditions for each batch inactivation experiment and measured k_{obs} and k_d values are summarized in **Table 6.1**.

As shown in **Figure 6.1A**, the Chick-Watson model described in Equation (1.1) fits well with the measured data and the fitted inactivation rate constant is 2.27(±0.05) L/(mg Fe·min) at pH 7 and 25 ^{o}C, corresponding to a 4-log inactivation with a Ct of ~4 (mg Fe·min)/L. Comparing with Fe(VI), ozone, free chlorine, and chlorine dioxide are more effective towards MS2 phage inactivation, whereas monochloramine is much less effective and hydrogen peroxide does not inactivate MS2 phage [34-38]. Shin et al. reported that an applied ozone dose of 0.37 mg/L can inactivate >3-log of MS2 phage within 10 s at pH 7 and 5 ^{o}C [38]. Barbeau et al. [34, 35] reported a free chlorine Ct of 0.45 mg·min/L and a chlorine dioxide Ct of 1.47 mg·min/L were required to achieve a 4-log removal of MS2 at pH 6.5 and 7 ^{o}C, respectively. In comparison, 2 mg/L monochloramine yielded only 1-log inactivation after 3 hrs of contact time at pH 8 and 5 ^{o}C [37]. Although Fe(VI) is a weaker disinfectant for MS2 phage when compared to ozone and free chlorine, Fe(VI) is also less reactive with many solution matrix components [28], which may lead to

comparable efficient disinfection (i.e., ΔN per applied disinfectant dose) in natural waters with high disinfectant demand.

The susceptibility of MS2 phage to Fe(VI) oxidation is comparable to two other phages, f2 and Qβ, both of which are single stranded RNA coliphages and have been used as model pathogens for enteric viruses [22, 23]. Schink et al. [22] reported that a contact time of 5.7 min is required to obtain a 2-log inactivation of f2 phage with 0.28 mg/L Fe(VI) at pH 6.9 and 24 °C, while Kazama et al. [23] reported a contact time of 5 min is required to achieve 2-log inactivation of Qβ phage with 0.4 mg/L Fe(VI) at pH 7 and 25 °C. However, inactivation of *E. coli* by Fe(VI) was reported with a k_{obs} value of 0.625 L/(mg Fe·min) [24], 72% slower than the k_{obs} measured for MS2 phage, suggesting much different Fe(VI) inactivating mechanisms between bacteria and viruses.

6.4.2 Effect of Initial MS2 Concentration and Fe(VI) Concentration

Figure 6.2 shows the effect of initial MS2 concentration on the inactivation kinetics. From **Figure 6.2**, we can see that there is no significant difference in the kinetic profiles observed for MS2 inactivation using different N_0 values (ranging from 4.3×10^5 to 1.3×10^7) and the measured data from five sets of inactivation experiments can be described reasonably well by the Chick-Watson model with a single k_{obs} value, suggesting that the kinetics of MS2 phage inactivation is not sensitive to initial phage concentration, as is commonly reported for disinfection processes [7, 47].

The effect of dosed Fe(VI) concentration on the inactivation kinetics was also investigated. As expected and predicted by the Chick-Watson rate law, higher inactivation rates (dN/dt) were observed with increased Fe(VI) doses. However, according to Equation (1.1), the observed inactivation rate constant (k_{obs}) should be independent of the initial Fe(VI) concentration because the term *Ct* already incorporates the variation of Fe(VI) concentration. However, **Figure 6.3** shows the MS2 inactivation profiles for batch inactivation experiments with different dosed Fe(VI) concentration, and it can be seen that the inactivation rate constant increased with the increases in the applied Fe(VI) dose. When target dosed Fe(VI) concentration increases by a factor of 4 (from 0.56 to 2.24 mg/L), k_{obs} increases roughly the same amount from 1.44(±0.03) L/(mg Fe·min) to 4.5(±0.02) L/(mg Fe·min). This result is surprising because a previous study on the inactivation of *E. coli* by Fe(VI) reported that the Chick-Watson inactivation rate constant was independent of Fe(VI) dose [24]. In addition, it should be noted that the dosed [Fe(VI)] is different from the actual

measured $[Fe(VI)]_0$ due to the Fe(VI) autodecomposition occurring during two time lapses: (1) between Fe(VI) stock preparation and use, and (2) between Fe(VI) stock addition to the batch reactions and the time when MS2 phage is added to initiate the reaction (**Table 6.1** listed the measured $[Fe(VI)]_0$ for each experiment). The actual measured $[Fe(VI)]_0$ for Exp. 7 and Exp. 8 is only ~1.4 mg/L (applied dose ~2.2 mg/L), close to the measured $[Fe(VI)]_0$ of Exp. 1, but k_{obs} values obtained in Exp. 7 and Exp. 8 are roughly twice the value measured in Exp.1. Therefore, the improved inactivation efficiency at higher dosed $[Fe(VI)]_0$ would not seem to be directly resulting from a higher concentration of Fe(VI) in solution, but rather some byproducts of the Fe(VI) decomposition process. Kazama [48] reported a similar phenomenon where solutions containing completely decomposed Fe(VI) still possessed inactivating capacity for coliphage Qβ, and the involvement of long-lived oxidative intermediate species from Fe(VI) decomposition was proposed. Further research is needed to identify the active species. Although kinetics experiments were conducted for the same target Fe(VI) dose, exact replication of Fe(VI) dose and initial Fe(VI) concentration was difficult due to Fe(VI)'s instability in aqueous solution (**Table 6.1**).

6.4.3   Effect of Temperature

Figure 6.4 shows effects of temperature on MS2 phage inactivation by Fe(VI). As expected, rates of inactivation increase with increasing temperature. When temperature increases from 5 ^{o}C to 30 ^{o}C, k_{obs} increases by nearly a factor of 4 from 7.7($\pm$0.2)$\times10^{-1}$ L/(mg Fe·min) to 3.0($\pm$0.2) L/(mg Fe·min). The Fe(VI) autodecomposition was found to be less temperature dependent compared to the inactivation of MS2 phage. From 5 ^{o}C to 30 ^{o}C, measured k_d only increased by 70% from 5.8($\pm$0.4)$\times10^{-2}$ L/(mg Fe·min) to 9.9($\pm$0.9)$\times10^{-2}$ L/(mg Fe·min) (**Table 6.1**). The temperature dependence of MS2 phage inactivation can be described by the Arrhenius equation:

$$\ln(k_{obs}) = -\frac{E_a}{R} \cdot \frac{1}{T} + \ln(A) \tag{6.3}$$

where E_a is the apparent activation energy, R is the universal gas constant, and A is the pre-exponential constant. At pH 7, E_a for MS2 phage inactivation by Fe(VI) was determined to be 39($\pm$6) kJ/mol, corresponding to a doubling of inactivation rates every 13 ^{o}C increase in temperature. Fe(VI) autodecomposition was found to have a much weaker temperature dependence compared to MS2 inactivation process, with a fit-derived activation energy of 14($\pm$2)

kJ/mol, corresponding to a doubling of rates every 42 °C increase in temperature. For practical treatment applications, it will be important to know how the temperature dependence of inactivation process compares to the Fe(VI) reactions with non-target water constituents that consume Fe(VI).

6.4.4   Effect of pH

Figure 6.5A shows the effect of pH on the kinetics profiles of MS2 phage inactivation. It can be seen that inactivation kinetics is highly dependent on pH, with higher inactivation rates occurring at lower pH conditions. When pH decreases from 11 to 6, a 50-fold increase in k_{obs} was observed (Figure 6.5B). In general, Fe(VI) exhibits higher oxidation and disinfection activity at lower pH [22, 23, 49], a trend attributed to the changing acid-base speciation of Fe(VI). Under the pH range studied, Fe(VI) is characterized by three acid-base species related by two pK_as [20]:

$$H_2FeO_4 = H^+ + HFeO_4^-, \ pK_{a1} = 3.5 \tag{6.4}$$

$$HFeO_4^- = H^+ + FeO_4^{2-}, \ pK_{a2} = 7.3 \tag{6.5}$$
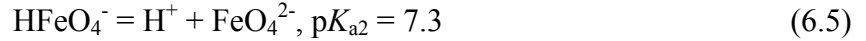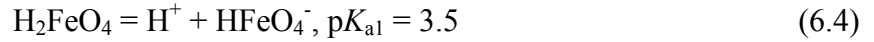
A number of studies have shown that protonated Fe(VI) species (H_2FeO_4 and $HFeO_4^-$) are much stronger oxidants than deprotonated FeO_4^{2-} [20, 49, 50]. Protonation of FeO_4^{2-} reduces the electron-donating capacity of the coordinated oxygen ligands, thereby making the metal center a stronger oxidant [51]. In addition, it is possible that protonation reduces electrostatic repulsion between the negatively charged MS2 particulate and Fe(VI) species and thus enhances its reactivity.

To quantitatively model the observed pH effect, an inactivation model considering parallel MS2 phage inactivation by different Fe(VI) species can be considered:

$$H_2FeO_4 + MS2 \rightarrow Fe(III) + MS2_{inactivated} \quad k_{\alpha 1} \tag{6.6}$$

$$HFeO_4^- + MS2 \rightarrow Fe(III) + MS2_{inactivated} \quad k_{\alpha 2} \tag{6.7}$$

$$FeO_4^{2-} + MS2 \rightarrow Fe(III) + MS2_{inactivated} \quad k_{\alpha 3} \tag{6.8}$$
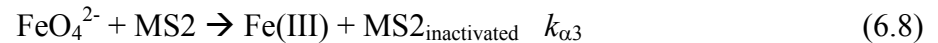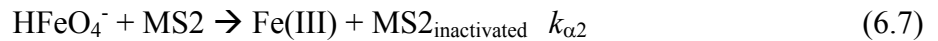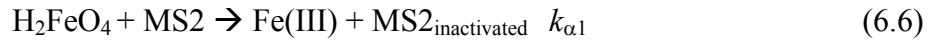
where $k_{\alpha i}$ (i = 1, 2, 3) is the Fe(VI) species-specific inactivation rate constant. Assuming each inactivation process with Fe(VI) species also follows Chick-Watson law and assuming that equilibrium between Fe(VI) species is maintained during reaction with MS2 phage, the total inactivation of MS2 phage can be expressed as:

$$\ln\left(\frac{N}{N_0}\right) = -\left(k_{\alpha 1}\alpha_1 + k_{\alpha 2}\alpha_2 + k_{\alpha 3}\alpha_3\right)\int_0^t [Fe(VI)]_{tot}\,t \tag{6.9}$$

where α_i (i =1, 2, 3) is the pH-dependent fractional concentration of each Fe(VI) species, which can be calculated using pK_a values listed in Equations (6.4) and (6.5). Combining Equations (1.1) and (6.9), we can get

$$k_{obs} = k_{\alpha 1}\alpha_1 + k_{\alpha 2}\alpha_2 + k_{\alpha 3}\alpha_3 \tag{6.10}$$

Thus, $k_{\alpha i}$ (i = 1, 2, 3) can be determined by fitting the trend in k_{obs} measured at different pH conditions. Scientist® for Windows® was used for the fitting process and results are shown in **Figure 6.5B**. Fitting results show that the kinetics model depicted by Equation (6.10) fits well with experimental data. Contribution from the fully protonated species (H_2FeO_4) was found to be negligible due to its extremely low concentration in the pH range studied. The fit-derived species-specific inactivation rate constants and the inactivation contribution from individual Fe(VI) species are shown in **Figure 6.5B**. As expected, the mono-protonated species ($HFeO_4^-$) was found to exhibit ~50 times higher reactivity with MS2 phage compared to the fully deprotonated species (FeO_4^{2-}), with $k_{\alpha 2}$ = 3.8(±0.5) L/(mg Fe·min) and $k_{\alpha 3}$ = 0.07(±0.1) L/(mg Fe·min). This result is in line with our previous study [49] on Fe(VI) oxidation of a neutral drug carbamazepine, which showed the reactivity of $HFeO_4^-$ being much higher than that of FeO_4^{2-}. Cho et al. [24] also reported that the reactivity of $HFeO_4^-$ on *E. coli* inactivation is 3 times higher than that of FeO_4^{2-} while the fully protonated Fe(VI) species (H_2FeO_4) exhibits reactivity two orders of magnitude higher than the two deprotonated Fe(VI) species.

6.4.5   Mechanistic Considerations

The MS2 virus particle is composed of three parts: the genome RNA, the maturation protein (A-protein), and the coat protein [31, 32]. Because the viral RNA and the A-protein are protected in an icosahedral shell of the coat protein [32] and the active Fe(VI) oxidizing species is ionic, the loss of MS2 phage infectivity by Fe(VI) oxidation is likely due to oxidative structural alteration to the coat protein. Valegard et al. [32] established the 3-dimentional structure of MS2 phage and revealed that the building block of the icosahedral shell has a hydrophobic surface containing eight amino acids, including cysteine (101), methionine (108), proline (117), two leucines (111 and 112), and three isoleucines (104, 118, and 119). Among them, only cysteine and methionine have side chains that are expected to have high reactivity with Fe(VI). Johnston and Read [44] reported a pH-independent second-order rate constant for $HFeO_4^-$ reaction with methionine (analogous to $k_{\alpha 2}$ in this study) to be 6.5×10^3 M^{-1} s^{-1}, which is comparable to the

observed $k_{\alpha2}$ here (3.8 L/(mg Fe·min), equivalent to a bimolecular rate constant of 3.5×10^3 M^{-1} s^{-1}). Reaction of Fe(VI) with cysteine was reported to be much faster than methionine with an observed apparent second-order rate constant of 1×10^5 M^{-1} s^{-1} at pH 10.17 [52], whereas the apparent MS2 phage inactivation rate constant with Fe(VI) at pH 10 is only 7.8×10^1 M^{-1} s^{-1}. Therefore, it seems methionine 108 is the more likely site of inactivation by Fe(VI). However, the reactivity of amino acid in its free form might be quite different from its reactivity in peptides, where there is a more complex environment. Thus, we can not exclude the possibility of cysteine 101 or other amino acids being the site of inactivation by Fe(VI). In fact, Wigginton et al. [53] identified cysteine 101 as the active site in MS2 phage inactivation by $^1O_2$. To confirm the site of oxidation, further analysis of the virus coat protein using mass spectrometry methods as demonstrated by Wigginton et al. [53] could be applied. Further research is also required to probe the inactivation mechanism at a molecular microbiological level, to identify the MS2 phage life cycle event (e.g., attachment, cell entry, genome ejection, A-protein assembly) responsible for the loss of its infectivity after reacting with Fe(VI) [54, 55].

Results in this study show that Fe(VI) is a promising alternative disinfectant for water treatment. Fe(VI) effectively inactivates MS2 phage: a 2-log removal of MS2 phage can be achieved with 1 mg/L Fe(VI) dose and a contact time of 2 min at pH 7 and 25 ^{o}C. Individual batch inactivation experiments can be fitted with the Chick-Watson model, and the inactivation rate constant was found to be dependent on Fe(VI) dose, temperature and pH. The effect of pH was successfully modeled by considering parallel reactions of different Fe(VI) species with MS2 phage. The methionine 101 residue on the MS2 coat protein surface was suspected to be the reactive site of inactivation by Fe(VI) due to comparable kinetics of the two processes. However, research is needed to further identify the site(s) of attack and investigate the inactivation mechanism in greater detail.

6.5 References Cited

[1]   MWH. *Water Treatment: Principles and Design*, 2nd ed. Hoboken: Wiley, **2005**.

[2]   USEPA. National primary drinking water regulations: Long Term 2 Enhanced Surface Water Treatment Rule. *Federal Register*, **2006**, 71: 653-702.

[3]   USEPA. National primary drinking water regulations: Stage 2 Disinfectants and Disinfection Byproducts Rule. *Federal Register*, **2006**, 71: 388-493.

[4]   Chang S. L. Waterborne viral infections and their prevention. *Bulletin of the World Health Organization*, **1968**, 38: 401-414.

[5]   Dowd S. E., Gerba C. P. and Pepper I. L. Confirmation of the human-pathogenic microsporidia *enterocytozoon bieneusi*, *encephalitozoon intestinalis*, and *vittaforma corneae* in Water. *Applied and Environmental Microbiology*, **1998**, 64: 3332-3335.

[6]   Grabow W. O. K. and Albert B. Chapter 1 Overview of health-related water virology. *Perspectives in Medical Virology*: Elsevier **2007**:1-25.

[7]   Page M. A., Shisler J. L. and Marinas B. J. Kinetics of adenovirus type 2 inactivation with free chlorine. *Water Research*, **2009**, 43: 2916-2926.

[8]   Richardson S. D., Thruston A. D., Caughran T. V., Chen P. H., Collette T. W., Schenck K. M., Lykins B. W., Rav-Acha C. and Glezer V. Identification of new drinking water disinfection by-products from ozone, chlorine dioxide, chloramine, and chlorine. *Water, Air, & Soil Pollution*, **2000**, 123: 95-102.

[9]   Choi J. and Valentine R. L. Formation of N-nitrosodimethylamine (NDMA) from reaction of monochloramine: a new disinfection by-product. *Water Research*, **2002**, 36: 817-824.

[10]   Sedlak D. L. and von Gunten U. The chlorine dilemma. *Science*, **2011**, 331: 42-43.

[11]   Mitch W. A., Sharp J. O., Trussell R. R., Valentine R. L., Alvarez-Cohen L. and Sedlak D. L. N-Nitrosodimethylamine (NDMA) as a drinking water contaminant: A review. *Environmental Engineering Science*, **2003**, 20: 389-404.

[12]   Boorman G. A., Dellarco V., Dunnick J. K., Chapin R. E., Hunter S., Hauchman F., Gardner H., Cox M. and Sills R. C. Drinking water disinfection byproducts: Review and approach to toxicity evaluation. *Environmental Health Perspectives*, **1999**, 107: 207-217.

[13]   Sharma V. K. Potassium ferrate(VI): an environmentally friendly oxidant. *Advances in Environmental Research*, **2002**, 6: 143-156.

[14]   Jiang J. Q. Research progress in the use of ferrate(VI) for the environmental remediation. *Journal of Hazardous Materials*, **2007**, 146: 617-623.

[15]   Jiang J. Q. The exploration of potassium ferrate(VI) as a disinfectant/coagulant in water and wastewater treatment. *Chemosphere*, **2006**, 63: 212-219.

[16]   Jiang J. Q. The application of potassium ferrate for sewage treatment. *Journal of Environmental Management*, **2006**, 79: 215-220.

[17]   Jiang J. Q. and Lloyd B. Progress in the development and use of ferrate(VI) salt as an

oxidant and coagulant for water and wastewater treatment. *Water Research*, **2002**, 36: 1397-1408.

[18]   Sharma V. K. Use of iron(VI) and iron(V) in water and wastewater treatment. *Water Science and Technology*, **2004**, 49: 69-74.

[19]   Sharma V. K. Disinfection performance of Fe(VI) in water and wastewater: a review. *Water Science and Technology*, **2007**, 55: 225-232.

[20]   Sharma V. K. Potassium ferrate(VI): an environmentally friendly oxidant. *Advances in Environmental Research*, **2002**, 6: 143-156.

[21]   Sharma V. K. and Bielski B. H. Reactivity of ferrate(VI) and ferrate(V) with amino acids. *Inorganic Chemistry*, **1991**, 30: 4306-4310.

[22]   Schink T. and Waite T. D. Inactivation of f2 virus with ferrate(VI). *Water Research*, **1980**, 14: 1705-1717.

[23]   Kazama F. Viral inactivation by potassium ferrate. *Water Science and Technology*, **1995**, 31: 165-168.

[24]   Cho M., Lee Y., Choi W., Chung H. and Yoon J. Study on Fe(VI) species as a disinfectant: quantitative evaluation and modeling for inactivating *Escherichia coli*. *Water Research*, **2006**, 40: 3580-3586.

[25]   DeLuca S. J., Chao A. C., Asce M. and Smalwood C. J. Ames test of ferrate treated water. *Journal of Environmental Engineering*, **1983**, 109: 1159-1167.

[26]   Schuck C. A., De Luca S. J., Peralba M. D. R. and De Luca M. A. Sodium ferrate (IV) and sodium hypochlorite in disinfection of biologically treated effluents. Ammonium nitrogen protection against THMs and HAAs. *Journal of Environmental Science and Health Part a-Toxic/Hazardous Substances & Environmental Engineering*, **2006**, 41: 2329-2343.

[27]   Sharma V. K. Disinfection performance of Fe(VI) in water and wastewater: a review. *Water Science and Technology*, **2007**, 55: 225-232.

[28]   Lee Y. and von Gunten U. Oxidative transformation of micropollutants during municipal wastewater treatment: Comparison of kinetic aspects of selective (chlorine, chlorine dioxide, ferrate(VI), and ozone) and non-selective oxidants (hydroxyl radical). *Water Research*, **2010**, 44: 555-566.

[29]   Oh B. S., Jang H. Y., Jung Y. J. and Kang J.-W. Microfiltration of MS2 bacteriophage: Effect of ozone on membrane fouling. *Journal of Membrane Science*, **2007**, 306: 244-252.

[30] Havelaar A. H., Vanolphen M. and Drost Y. C. F-specific RNA bacteriophages are adequate model organisms for enteric viruses in fresh-water. *Applied and Environmental Microbiology*, **1993**, 59: 2956-2962.

[31] Fiers W., Contreras R., Duerinck F., Haegeman G., Iserentant D., Merregaert J., Min Jou W., Molemans F., Raeymaekers A., Van den Berghe A., Volckaert G. and Ysebaert M. Complete nucleotide sequence of bacteriophage MS2 RNA: Primary and secondary structure of the replicase gene. *Nature*, **1976**, 260: 500-507.

[32] Valegard K., Liljas L., Fridborg K. and Unge T. The 3-dimensional structure of the bacterial-virus MS2. *Nature*, **1990**, 345: 36-41.

[33] Dowd S. E., Pillai S. D., Wang S. Y. and Corapcioglu M. Y. Delineating the specific influence of virus isoelectric point and size on virus adsorption and transport through sandy soils. *Applied and Environmental Microbiology*, **1998**, 64: 405-410.

[34] Barbeau B., Huffman D., Mysore C., Desjardins R., Clement B. and Prevost M. Examination of discrete and confounding effects of water quality parameters during the inactivation of MS2 phages and *Bacillus subtilis* spores with chlorine dioxide. *Journal of Environmental Engineering and Science*, **2005**, 4: 139-151.

[35] Barbeau B., Huffman D., Mysore C., Desjardins R. and Prevost M. Examination of discrete and confounding effects of water quality parameters during the inactivation of MS2 phages and *Bacillus subtilis* spores with free chlorine. *Journal of Environmental Engineering and Science*, **2004**, 3: 255-268.

[36] Hall R. M. and Sobsey M. D. Inactivation of hepatitis-A virus and MS2 by ozone and ozone-hydrogen peroxide in buffered water. *Water Science and Technology*, **1993**, 27: 371-378.

[37] Shin G. A. and Sobsey M. D. Reduction of norwalk virus, poliovirus 1 and coliphage MS2 by monochloramine disinfection of water. *Water Science and Technology*, **1998**, 38: 151-154.

[38] Shin G. A. and Sobsey M. D. Reduction of Norwalk virus, poliovirus 1, and bacteriophage MS2 by ozone disinfection of water. *Applied and Environmental Microbiology*, **2003**, 69: 3975-3978.

[39] Li Q., Page M. A., Marinas B. J. and Shang N. K. Treatment of coliphage MS2 with palladium-modified nitrogen-doped titanium oxide photocatalyst illuminated by visible

light. *Environmental Science & Technology*, **2008**, 42: 6148-6153.

[40]   Adams M. H. *Bacteriophages*. New York: Interscience, **1959**.

[41]   Delaude L. and Laszlo P. A novel oxidizing reagent based on potassium ferrate(VI). *Journal of Organic Chemistry*, **1996**, 61: 6360-6370.

[42]   Lee Y., Cho M., Kim J. Y. and Yoon J. Chemistry of ferrate (Fe(VI)) in aqueous solution and its applications as a green chemical. *Journal of Industrial and Engineering Chemistry*, **2004**, 10: 161-171.

[43]   Lee Y., Yoon J. and von Gunten U. Spectrophotometric determination of ferrate (Fe(VI)) in water by ABTS. *Water Research*, **2005**, 39: 1946-1953.

[44]   Johnson M. D. and Read J. F. Kinetics and mechanism of the ferrate oxidation of thiosulfate and other sulfur-containing species. *Inorganic Chemistry*, **1996**, 35: 6795-6799.

[45]   Lee Y., Yoon J. and von Gunten U. Spectrophotometric determination of ferrate (Fe(VI)) in water by ABTS. *Water Research*, **2005**, 39: 1946-1953.

[46]   Rush J. D., Zhao Z. W. and Bielski B. H. J. Reaction of ferrate(VI)/ferrate(V) with hydrogen peroxide and superoxide anion - A stopped-flow and premix pulse radiolysis study. *Free Radical Research*, **1996**, 24: 187-198.

[47]   Luh J. and Marinas B. J. Inactivation of *Mycobacterium avium* with free chlorine. *Environmental Science & Technology*, **2007**, 41: 5096-5102.

[48]   Kazama F. Inactivation of coliphage Qβ by potassium ferrate. *FEMS Microbiology Letters*, **1994**, 118: 345-349.

[49]   Hu L., Martin H. M., Arce-Bulted O., Sugihara M. N., Keating K. A. and Strathmann T. J. Oxidation of carbamazepine by Mn(VII) and Fe(VI): Reaction kinetics and mechanism. *Environmental Science & Technology*, **2009**, 43: 509-515.

[50]   Li C., Li X. Z. and Graham N. A study of the preparation and reactivity of potassium ferrate. *Chemosphere*, **2005**, 61: 537-543.

[51]   Sharma V. K., Smith J. O. and Millero F. J. Ferrate(VI) oxidation of hydrogen sulfide. *Environmental Science & Technology*, **1997**, 31: 2486-2491.

[52]   Read J. F., Bewick S. A., Graves C. R., MacPherson J. M., Salah J. C., Theriault A. and Wyand A. E. H. The kinetics and mechanism of the oxidation of s-methyl-L-cysteine, L-cystine and L-cysteine by potassium ferrate. *Inorganica Chimica Acta*, **2000**, 303: 244-255.

[53]   Wigginton K. R., Menin L., Montoya J. P. and Kohn T. Oxidation of virus proteins during UV$_{254}$ and singlet oxygen mediated inactivation. *Environmental Science & Technology*, **2010**, 44: 5437-5443.

[54]   Page M. A., Shisler J. L. and Marinas B. J. Mechanistic aspects of adenovirusserotype 2 inactivation with free chlorine. *Applied and Environmental Microbiology*, **2010**, 76: 2946-2954.

[55]   Sirikanchana K., Shisler J. L. and Marinas B. J. Effect of exposure to UV-C irradiation and monochloramine on adenovirus serotype 2 early protein expression and DNA replication. *Applied and Environmental Microbiology*, **2008**, 74: 3774-3782.

6.6 Figures and Tables
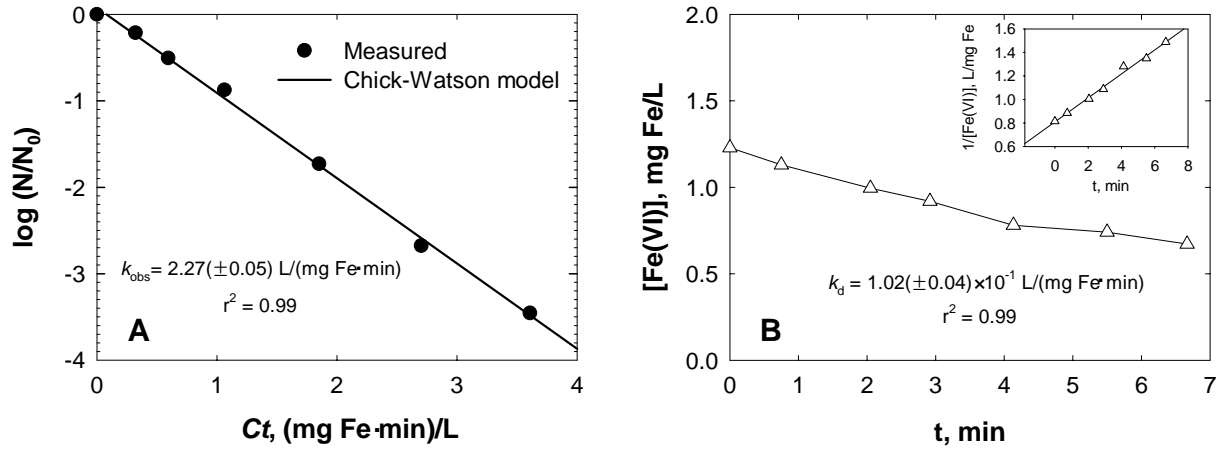
Figure 6.1. (A) Inactivation kinetics of MS2 phage by Fe(VI), and (B) Fe(VI) decay during the batch experiments (inset shows second-order rate law fit for Fe(VI) autodecomposition). Experimental conditions: $N_0 = 4.3 \times 10^5$ pfu/mL, $[Fe(VI)]_0 = 1.23$ mg Fe/L, pH = 7 (10 mM phosphate), 25 °C. Uncertainties represent 1 σ.
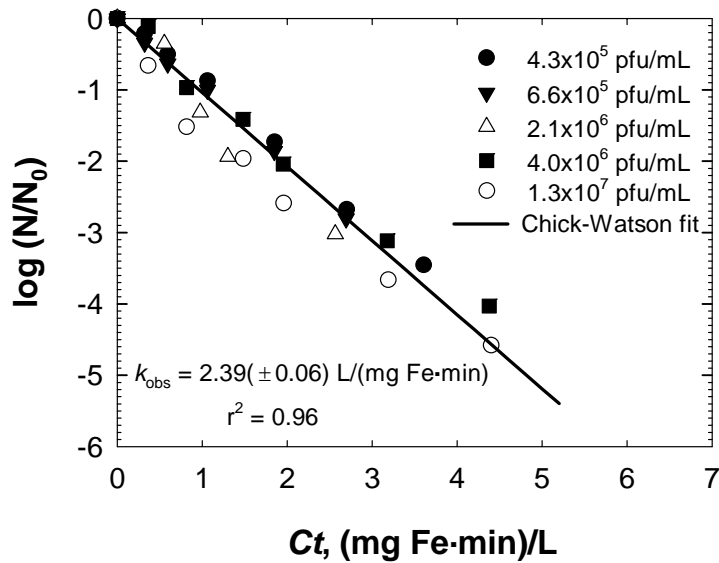
Figure 6.2. Effect of initial MS2 phage concentration on the inactivation kinetics at pH 7 and 25 °C. Experimental conditions are listed in Table 6.1. The line and k_{obs} shown are from a single regression with the five data sets combined. Uncertainty represents 1 σ.
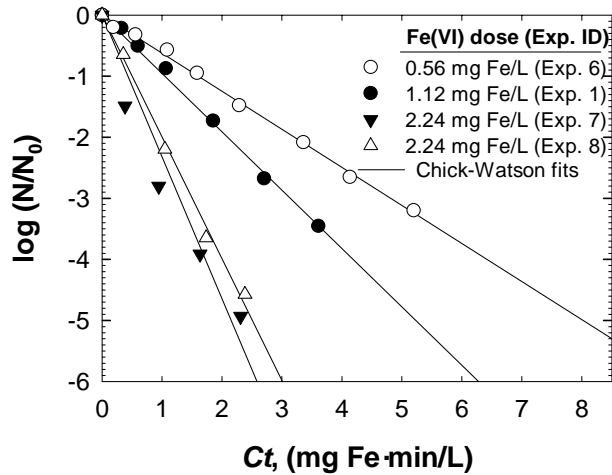
Figure 6.3. Effect of Fe(VI) dose on MS2 phage inactivation kinetics at pH 7 and 25 °C. Experimental conditions are listed in Table 6.1.
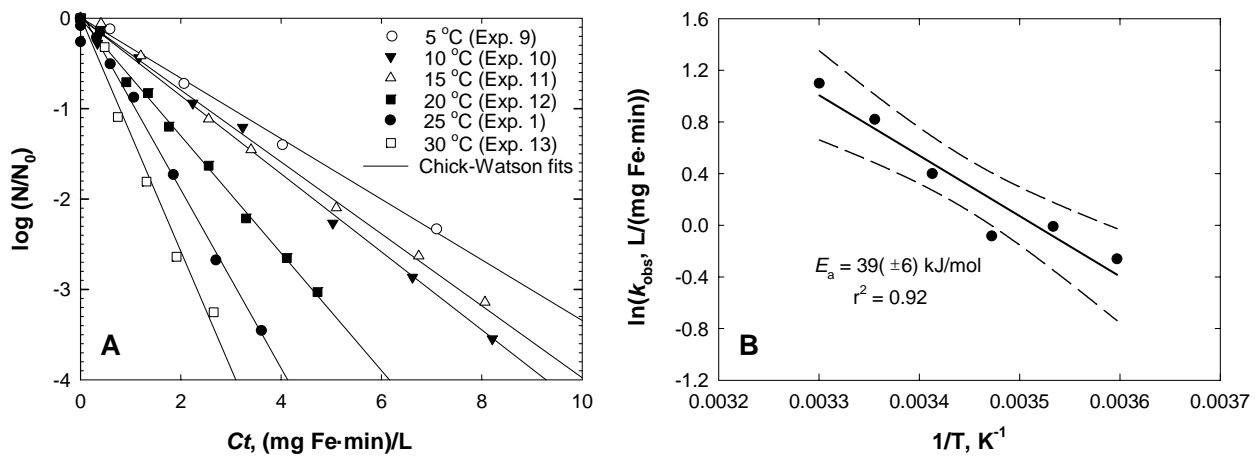
Figure 6.4. Effect of temperature on the MS2 inactivation kinetics at pH 7. (A) kinetics profiles; (B) Arrhenius fitting, dashed lines show 95% confidence intervals. Experimental conditions are listed in Table 6.1. Uncertainty in E_a represents 1 σ.
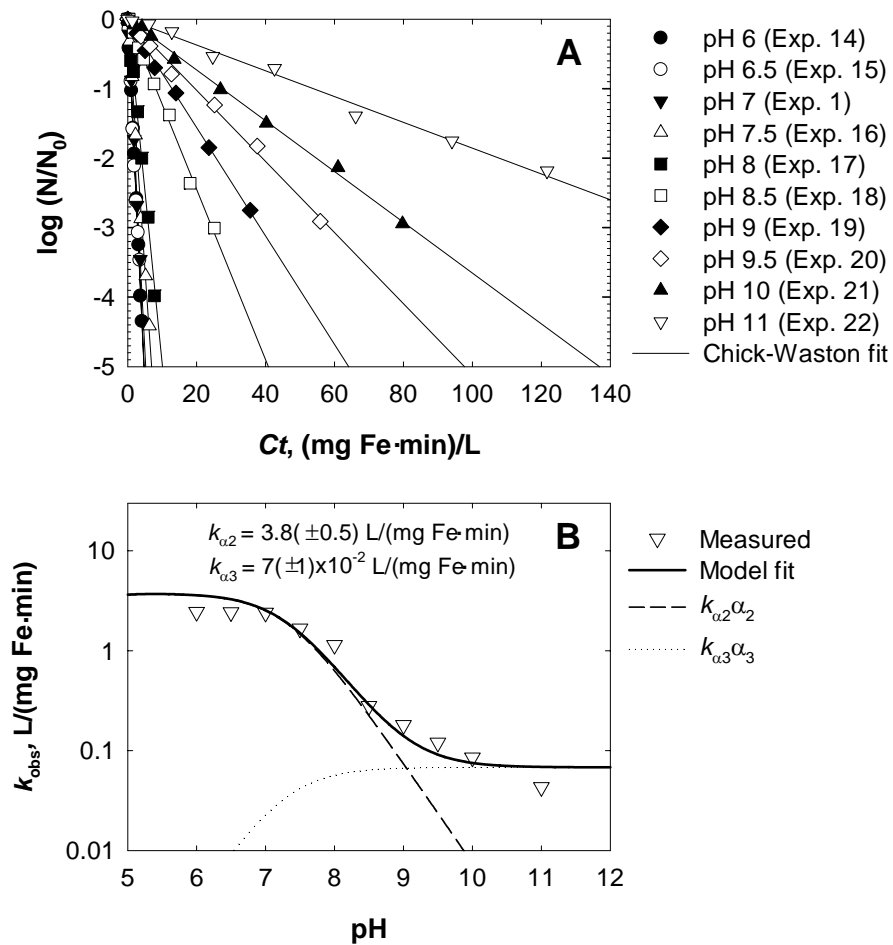
Figure 6.5. Effect of pH on the MS2 phage inactivation kinetics at 25 °C. (A) Inactivation kinetics profiles; (B) Model fitting results with Equation (6.10) (solid line) and contribution from individual Fe(VI) species: $HFeO_4^-$ (dashed line), FeO_4^{2-} (dotted line). Experimental conditions are listed in Table 6.1. Uncertainties represent 1 σ.

Table 6.1. Experimental conditions, measured inactivation rate constants, and second-order constants of Fe(VI) decay for each inactivation experiment

Exp. ID	pH	T ($^\circ$C)	Buffer[a]	Measured N_0 (pfu/mL)	Measured $[Fe(VI)]_0$[b] (mg Fe/L)	k_{obs}[c] (L/(mg Fe·min))	k_d[d] (L/(mg Fe·min))
1	7	25	10 mM PBS	4.3×10^5	1.23	2.27($\pm$0.05)	1.02($\pm$0.04)$\times10^{-1}$
2	7	25	10 mM PBS	1.3×10^7	1.35	2.3 ($\pm$0.2)	9.3($\pm$0.7)$\times10^{-2}$
3	7	25	10 mM PBS	6.6×10^5	1.23	2.37($\pm$0.05)	1.09($\pm$0.08)$\times10^{-1}$
4	7	25	10 mM PBS	2.1×10^6	1.36	2.9($\pm$0.4)	9.3($\pm$0.1)$\times10^{-2}$
5	7	25	10 mM PBS	4.0×10^6	1.37	2.2($\pm$0.1)	9.6($\pm$0.9)$\times10^{-2}$
6	7	25	10 mM PBS	7.3×10^6	0.57[e]	1.44($\pm$0.03)	1.03($\pm$0.03)$\times10^{-1}$
7	7	25	10 mM PBS	7.3×10^6	1.43[f]	4.7($\pm$0.5)	3($\pm$1)$\times10^{-2}$
8	7	25	10 mM PBS	1.1×10^7	1.42[f]	4.5($\pm$0.2)	3.7($\pm$0.3)$\times10^{-2}$
9	7	5	10 mM PBS	4.4×10^4	1.46	7.7($\pm$0.2)$\times10^{-1}$	5.8($\pm$0.4)$\times10^{-2}$
10	7	10	10 mM PBS	1.3×10^5	1.22	9.9($\pm$0.3)$\times10^{-1}$	7.3($\pm$0.2)$\times10^{-2}$
11	7	15	10 mM PBS	1.6×10^5	1.26	9.2($\pm$0.3)$\times10^{-1}$	8.1($\pm$0.1)$\times10^{-2}$
12	7	20	10 mM PBS	3.2×10^5	0.95	1.49($\pm$0.04)	8.3($\pm$0.2)$\times10^{-2}$
13	7	30	10 mM PBS	1.7×10^5	1.44	3.0($\pm$0.2)	9.9($\pm$0.9)$\times10^{-2}$
14	6	25	10 mM PBS	8.8×10^5	1.14	2.44($\pm$0.04)	2.3($\pm$0.1)$\times10^{-1}$
15	6.5	25	10 mM PBS	2.6×10^5	1.24	2.42($\pm$0.09)	1.5($\pm$0.1)$\times10^{-1}$
16	7.5	25	10 mM PBS	1.1×10^6	1.52	1.66($\pm$0.04)	8.5($\pm$0.9)$\times10^{-3}$
17	8	25	10 mM PBS	7.4×10^5	1.63	1.14($\pm$0.04)	$<1\times10^{-3}$

Table 6.1. (cont.)

Exp. ID	pH	T (^{o}C)	Buffer[a]	Measured N_0 (pfu/mL)	Measured $[Fe(VI)]_0$[b] (mg Fe/L)	k_{obs}[c] (L/(mg Fe·min))	k_d[d] (L/(mg Fe·min))
18	8.5	25	10 mM PBS	1.7×10^6	1.54	$2.8(\pm 0.1) \times 10^{-1}$	$<1 \times 10^{-3}$
19	9	25	10 mM PBS/2 mM BBS	1.7×10^6	1.56	$1.8(\pm 0.1) \times 10^{-1}$	$<1 \times 10^{-3}$
20	9.5	25	10 mM PBS/2 mM BBS	5.9×10^6	1.33	$1.2(\pm 0.1) \times 10^{-1}$	$<1 \times 10^{-3}$
21	10	25	10 mM PBS/2 mM BBS	7.3×10^6	1.36	$8.4(\pm 0.1) \times 10^{-2}$	$<1 \times 10^{-3}$
22	11	25	10 mM PBS/2 mM BBS	2.7×10^6	1.24	$4.3(\pm 0.1) \times 10^{-2}$	$<1 \times 10^{-3}$

[a] PBS: phosphate buffer solutions; BBS: borate buffer solutions.
[b] Unless otherwise noted, the applied target initial Fe(VI) dose is 1.12 mg/L (20 μM). The actual measured initial Fe(VI) concentration varies because of the lapse between Fe(VI) stock addition and the reaction initiation (MS2 phage stock spiking).
[c] Apparent inactivation rate constant from Chick-Watson model fitting.
[d] Second-order rate constant of Fe(VI) autodecomposition.
[e] Target initial Fe(VI) concentration was 0.56 mg/L (10 μM).
[f] Target initial Fe(VI) concentration was 2.24 mg/L (40 μM). The actual measured $[Fe(VI)]_0$ is much smaller due to faster Fe(VI) autodecomposition at higher initial concentration [46].

CHAPTER 7
SUMMARY AND CONCLUSIONS

7.1 General Summary

This study provides the first systematic assessment of the reactivity of Mn(VII) and Fe(VI) with widely detected classes of organic micropollutants and Fe(VI) reactions with the commonly studied viral surrogate, MS2 bacteriophage. Results from this study demonstrate the effectiveness of using Mn(VII) and Fe(VI) salts to selectively treat a number of important PhACs and a representative viral pathogen. Both Mn(VII) and Fe(VI) are selective oxidants that target compounds with specific electron-rich moieties, including olefinic, phenolic, amino, cyclopropyl, thioether, and alkyne groups. **Table 7.1** summarizes the reactivity of surveyed PhACs with Mn(VII) and Fe(VI). The proposed reactive groups in each PhAC are also listed. It is likely that other organic contaminants with above listed functional groups will also be susceptible to Mn(VII) and Fe(VI) oxidation. Fe(VI) was also found to be effective towards inactivation of a viral pathogen, MS2 bacteriophage.

The reaction kinetics of Mn(VII) oxidation of several representative PhACs and Fe(VI) oxidation of carbamazepine were carefully characterized for the first time. The effects of Mn(VII)/Fe(VI) concentration, PhAC concentration, temperature, and pH on reaction rates were investigated and corresponding kinetic parameters were determined. Oxidation of PhACs by Mn(VII) and Fe(VI) can be described by second-order kinetics models and temperature dependence of the reactions can be described using the Arrhenius equation. Solution pH was found to be an important factor that affects the reaction rate constants with most PhACs. The pH dependent trends can often be explained by the change of electron density on the target reactive group upon protonation/deprotonation. The pH dependences of PhAC reaction rates can also be quantitatively described using models that account for changing acid-base speciation of the target PhACs and oxidant. These models assume parallel reactions between individual PhAC species and individual oxidant species with characteristic rate constants. **Table 7.2** summarizes the kinetic parameters for the representative PhACs studied in Chapters 2-5. In general, O_3 exhibits higher reactivity than Mn(VII) with all PhACs, while NH_2Cl is a weaker oxidant than Mn(VII) and an overall superior reactivity of HOCl and ClO_2 to Mn(VII) is not seen. Notably, carbamazepine, a

PhAC with prevalent occurrence in U.S. stream water/source water [1], is resistant to HOCl and ClO$_2$, but shows high reactivity with Mn(VII).

The effect of non-target water constituents on the Mn(VII) oxidation kinetics was extensively studied with one representative PhAC, carbamazepine. Most common non-target water constituents were found to have negligible effects on reaction kinetics, while the effect of reduced species, e.g., Fe(II), Mn(II), S(-II), can be accounted for by assuming a stoichiometric permanganate demand of the constituents that lowers the effective concentration of permanganate available for reactions with the PhACs of interest. A practical kinetics model that takes into account the applied Mn(VII) dose, temperature, pH, and Mn(VII) demand of non-target water constituents was then developed to predict the extent of PhAC oxidation by Mn(VII) at relevant water treatment conditions. Tests in utility source waters with more environmentally-relevant concentrations of PhACs validated the applicability of the predictive kinetic model.

Products from Mn(VII) and Fe(VI) oxidation reactions with representative PhACs were identified and corresponding reaction pathways were proposed. Product analysis results show that the target micropollutants are incompletely oxidized by Mn(VII) and Fe(VI) and a variety of products with partial structural modification to the parent compounds are produced. Oxidation products were identified for carbamazepine, ciprofloxacin, lincomysin, trimethoprim, and 17α-ethinylestradiol using liquid chromatography-tandem mass spectrometry methods. Oxidation of olefinic, phenolic, amino, cyclopropyl, thioether, and alkyne groups lead to a variety of oxygen insertion products (e.g., alcohol, ketone, amide, and sulfone), dehydrogenation and dealkylation products, oxidative ring-cleavage products (aldehyde, amide, and carboxylic acid), as well as some rearrangement products from reaction intermediates.

Since little mineralization was achieved during Mn(VII) and Fe(VI) oxidation, bioassay studies were also conducted to quantify the pharmaceutical potency of PhAC solutions after Mn(VII) treatment. For three representative antibiotics, ciprofloxacin, lincomysin, and trimethoprim, bioassays quantifying the antibacterial activity of ciprofloxacin and trimethoprim solutions before and after treatment with Mn(VII) indicate that oxidation products exhibit negligible antibacterial activity in comparison with the parent antibiotic compounds. The reduction of antibacterial activity was also related to the proposed oxidation products and pathways. Mn(VII) oxidation produces products that either disrupt the intactness of an essential molecular moiety or possess structural modifications that were reported to significantly reduce

the parent compound's potency.

Inactivation experiments with MS2 phage show that Fe(VI) is a promising alternative disinfectant for viral pathogens. The inactivation kinetics of individual batch experiments can be described by the Chick-Watson model and the reaction rates were found to be highly dependent on pH. Similar to PhAC reactions with Mn(VII) and Fe(VI), the pH effect can be modeled by considering the changing speciation of Fe(VI) and assuming parallel inactivation pathways for each Fe(VI) species. The kinetic parameters obtained for the MS2 phage inactivation by Fe(VI) are also listed in **Table 7.2**. In general, Fe(VI) is more effective towards MS2 phage inactivation than monochloramine and hydrogen peroxide, while less effective than ozone, free chlorine, and chlorine dioxide. The susceptibility of MS2 phage to Fe(VI) is comparable to two other phages, f2 and Qβ, but higher than *E. coli*, a bacterial pathogen.

7.2 *Applicability of Results to Water and Wastewater Treatment*

Results from this study advanced our understanding on the fate of many PhACs in treatment plants that currently apply Mn(VII) for the control of manganese and iron, taste and odor, biofouling, etc. Results suggest that PhACs containing phenolic, olefinic, amine, thioether, and alkyne groups will be oxidized to some degree during existing Mn(VII) treatment processes. Bioassay tests with several representative PhACs confirm that partial oxidation of PhACs can greatly reduce their pharmaceutical potency. For the representative PhACs studied, the predictive kinetic model developed in this work can help utilities predict the level of removal in existing Mn(VII) treatment processes or determine Mn(VII) dosing and reactor residence time requirements for achieving a desired level of removal.

Although permanganate is not often used at wastewater treatment facilities, it may be an effective approach for selectively oxidizing Mn(VII)-reactive PhACs (e.g., carbamazepine, phenolic EDCs) in these facilities. Less selective oxidants, such as $\cdot OH$, O_3, and HOCl, although highly reactive with many of the same PhACs, might be inefficient within such matrices because their lower stability and the rapid scavenging of these oxidants by the high levels of organic matter and/or ammonia in the water. In contrast, the more selective Mn(VII) persists for longer times within such matrices, possibly enabling a higher degree of PhAC oxidation for the same applied oxidant doses.

Ferrate salts are not currently used in field scale drinking water or wastewater treatment

operations, although their use for a variety of treatment purposes is gaining increasing attention among water quality researchers [2-5]. Results presented in this study as well as other recent reports by several other groups [6-9] support the use of ferrate for oxidizing PhACs and inactivating pathogens during water and wastewater treatment. The primary limitations on the use of ferrate by the water industry are the lack of low cost bulk commercial sources for the reagent and its instability in water, which prevents long-term storage of stock solutions. Aqueous feedstock solutions of ferrate need to be prepared just prior to use. Recent reports suggest that it may be possible to generate ferrate on-site electrochemically [10, 11] or chemically [12] immediately prior to being introduced to treatment reactors. If these technologies can be made economical, practical applications of ferrate for water/wastewater treatment may become widely used.

7.3 Future Research

This study investigated the efficiency and effectiveness of using Mn(VII) and Fe(VI) to treat a variety of PhACs and the potential of using Fe(VI) as an alternative disinfectant. Some related future research topics are outlined below:

- *Flow-through reactors and pilot scale tests*. The oxidation and inactivation experiments were conducted in batch reactors in this study. Tests in flow-through reactors and pilot scale tests can be done to confirm whether similar reactivity can be achieved and whether the obtained kinetic parameters are applicable.

- *Validation of the predictive kinetic model in wastewater-related matrices*. A predictive kinetic model was developed in this study to estimate the extent of PhAC removal and was validated by tests in natural waters. It will be a good practice to test PhAC removal by Mn(VII) in wastewater-related matrices and compare test results with estimates from the predictive kinetic model. Comparsion of the efficiency between Mn(VII) and other drinking water oxidants (e.g., ozone, free chlorine) in oxidative removal of PhAC in wastewater matrix is also desired to see whether the greater stability of Mn(VII) in organic-rich matrices can compensate for its lower reactivity with PhACs.

- *Establishment of a quantitative structure-activity relationship (QSAR) for phenolic compounds*. Many organic contaminants in water contain a phenolic moiety, which is shown to exhibit high reactivity with Mn(VII), and thus it will be helpful to establish a QSAR for Mn(VII) oxidation of phenolic compounds using simple substituted phenols.

The established QSAR can be used to predict the reactivity of different target phenolic contaminants with Mn(VII) during water treatment processes. Development of QSARs for oxidation of phenolic compounds by Fe(VI) have been reported [13].

- *Identification of reaction products at non-neutral pH conditions*. Products from Mn(VII)/Fe(VI) and PhAC reactions reported in this study were identified at neutral conditions. It is possible that different sets of products will be formed under more acidic or basic conditions and further research can be done to identify reaction products under these conditions.

- *Confirmation of proposed structures for reaction products with multiple analytical techniques*. Although ^{1}H-NMR analysis was applied in one instance here, LC-MS/MS analysis was the primary tool used to identify reaction products in this study. Therefore, structures postulated in this study are only the best plausible representatives with the information available. For the large number of products obtained in this study, it is difficult and time consuming to isolate each product and apply multiple analytical techniques to identify the structures of each product. However, interested researchers can take efforts to isolate major products formed during PhAC-Mn(VII) reactions and confirm structures proposed in this study using other analytical tools, including ^{1}H-NMR, ^{13}C-NMR, FTIR, UV-Vis spectroscopy, etc. Individual isolated products can also be assessed for pharmaceutical potency in comparison to their parent PhACs.

- *Testing of biodegradability of reaction products*. Because little mineralization was achieved and various organic reaction products were produced during Mn(VII)/Fe(VI) oxidation of PhACs, it is important to test the biodegradability of the reaction products compared to the parent compounds.

- *Estrogenic activity of EE2 reaction products*. Among PhACs commonly detected in drinking water sources, phenolic EDCs like 17α-ethinylestradiol are believed to possibly pose the greatest risk at environmental concentration levels (ng/L-μg/L) [14]. This study shows that phenolic compounds in general have high reactivity with Mn(VII). However, further research is needed to demonstrate the estrogenic activity removal of EDC solutions along with the parent compound degradation during the Mn(VII) oxidation processes. In addition, bioassays for many types of PhACs, e.g., anticonvulsant drugs, are not available, and require further development.

- *Further investigation of the effect of Fe(VI) dose on MS2 phage inactivation kinetics*. This study shows that Fe(VI) dose rather than the initial measured Fe(VI) concentration affects the Chick-Watson inactivation rate constants, possibly due to a long-lived active species produced during Fe(VI) autodecomposition. Further research is needed to investigate the detailed mechanism behind this phenomenon. It will also be interesting to see how the non-target water constituents would affect the inactivation efficiency of MS2 phage by Fe(VI).

- *Inactivation mechanism of MS2 phage by Fe(VI)*. The inactivation mechanism of MS2 phage by Fe(VI) is worth investigating. Mass spectrometry might be an applicable technique as Wigginton et al. [15] have applied the technology to correlate the MS2 virus inactivation by UV_{254} and $^1O_2$ to chemical modifications of certain parts of the MS2 coat protein during the inactivation process. Molecular microbiological tools, as reported by Page et al. [16], can also be applied to evaluate whether genome damage occurs and identify the MS2 phage life cycle event (e.g., attachment, cell entry, genome ejection, A-protein assembly) responsible for the loss of its infectivity after reacting with Fe(VI).

- *Fe(VI) inactivation with other pathogens of concern*. To further evaluate the potential of Fe(VI) as an alternative disinfectant, its reactivity with other pathogens of concern (e.g., adenovirus, coxsackie virus) should be characterized. Although Fe(VI) application in water does not produce chlorinated DBPs and Fe(VI) does not oxidize bromide to bromate, tests need to be done to evaluate whether Fe(VI) oxidation of iodide in the presence of many other non-target water constituents form toxic iodinated DBPs. It is also of interest to see whether there is any synergistic effect of sequentially applying Fe(VI) and other disinfectants (e.g., free chlorine, monochloramine).

- *Development of economical on-site ferrate generation technologies*. As mentioned earlier, the high cost of ferrate and its instability in water limits its large scale application. Therefore, further research focusing on the development of economical on-site ferrate generation technologies is recommended.

7.4 References Cited
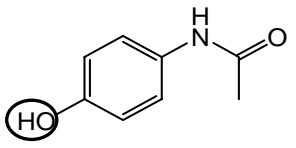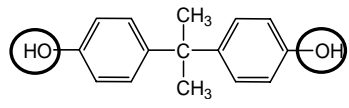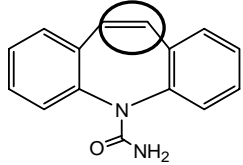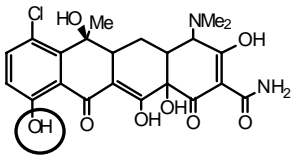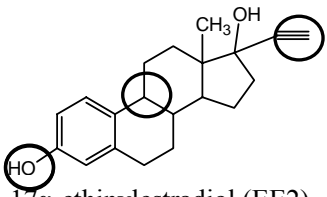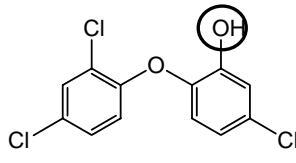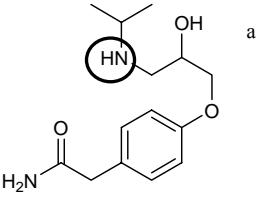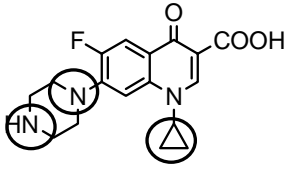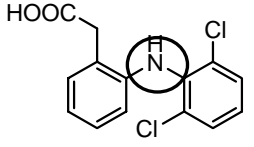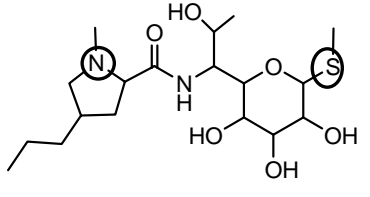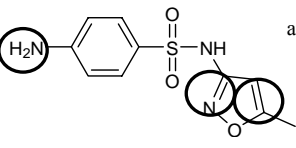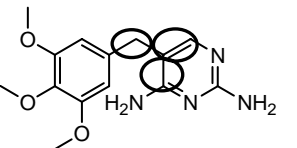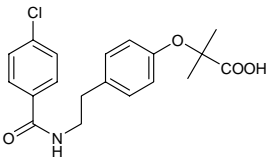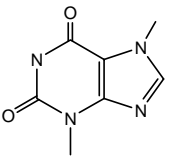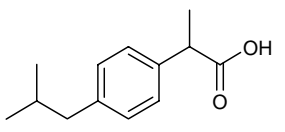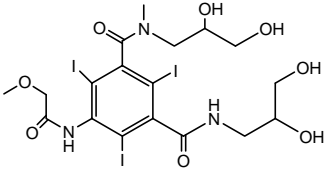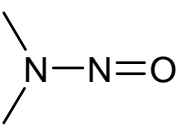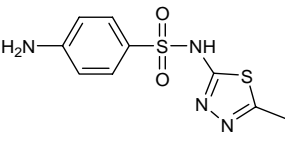
[1]   Kumar A. and Xagoraraki I. Pharmaceuticals, personal care products and endocrine-disrupting chemicals in U.S. surface and finished drinking waters: A proposed

ranking system. *Science of the Total Environment*, **2010**, 408: 5972-5989.

[2]   Sharma V. K. Potassium ferrate(VI): An environmentally friendly oxidant. *Advances in Environmental Research*, **2002**, 6: 143-156.

[3]   Jiang J. Q. Research progress in the use of ferrate(VI) for the environmental remediation. *Journal of Hazardous Materials*, **2007**, 146: 617-623.

[4]   Lee Y., Zimmermann S. G., Kieu A. T. and von Gunten U. Ferrate (Fe(VI)) application for municipal wastewater treatment: A novel process for simultaneous micropollutant oxidation and phosphate removal. *Environmental Science & Technology*, **2009**, 43: 3831-3838.

[5]   Jiang J. Q., Wang S. and Panagoulopoulos A. The role of potassium ferrate(VI) in the inactivation of *Escherichia coli* and in the reduction of COD for water remediation. *Desalination*, **2007**, 210: 266-273.

[6]   Sharma V. K., Mishra S. K. and Nesnas N. Oxidation of sulfonamide antimicrobials by ferrate(VI) [$Fe^{VI}O_4^{2-}$]. *Environmental Science & Technology*, **2006**, 40: 7222-7227.

[7]   Sharma V. K., Li X. Z., Graham N. and Doong R. A. Ferrate(VI) oxidation of endocrine disruptors and antimicrobials in water. *J Water Supply: Res Technol - AQUA*, **2008**, 57: 419-426.

[8]   Sharma V. K. Oxidative transformations of environmental pharmaceuticals by Cl_2, ClO_2, O_3, and Fe(VI): Kinetics assessment. *Chemosphere*, **2008**, 73: 1379-1386.

[9]   Cho M., Lee Y., Choi W., Chung H. and Yoon J. Study on Fe(VI) species as a disinfectant: quantitative evaluation and modeling for inactivating *Escherichia coli*. *Water Research*, **2006**, 40: 3580-3586.

[10]   Canizares P., Arcis M., Saez C. and Rodrigo M. A. Electrochemical synthesis of ferrate using boron doped diamond anodes. *Electrochemistry Communications*, **2007**, 9: 2286-2290.

[11]   Licht S. and Yu X. W. Electrochemical alkaline Fe(VI) water purification and remediation. *Environmental Science & Technology*, **2005**, 39: 8071-8076.

[12]   Perfiliev Y. D., Benko E. M., Pankratov D. A., Sharma V. K. and Dedushenko S. K. Formation of iron(VI) in ozonalysis of iron(III) in alkaline solution. *Inorganica Chimica Acta*, **2007**, 360: 2789-2791.

[13]   Lee Y., Yoon J. and von Gunten U. Kinetics of the oxidation of phenols and phenolic

endocrine disruptors during water treatment with ferrate (Fe(VI)). *Environmental Science & Technology*, **2005**, 39: 8978-8984.

[14]　Parrott J. L. and Blunt B. R. Life-cycle exposure of fathead minnows (*Pimephales promelas*) to an ethinylestradiol concentration below 1 ng/L reduces egg fertilization success and demasculinizes males. *Environmental Toxicology*, **2005**, 20: 131-141.

[15]　Wigginton K. R., Menin L., Montoya J. P. and Kohn T. Oxidation of virus proteins during UV_{254} and singlet oxygen mediated inactivation. *Environmental Science & Technology*, **2010**, 44: 5437-5443.

[16]　Page M. A., Shisler J. L. and Marinas B. J. Mechanistic aspects of adenovirusserotype 2 inactivation with free chlorine. *Applied and Environmental Microbiology*, **2010**, 76: 2946-2954.

7.5 Figures and Tables

Table 7.1 Summary of PhACs reactivity with Mn(VII) and Fe(VI) (proposed reactive sites shown in circles)

High reactivity

acetaminophen (ACT) bisphenol A (BPA) carbamazepine (CBZ) chlortetracycline (CTC) 17α-ethinylestradiol (EE2)

triclosan (TRC)

Moderate reactivity

atenolol (ATN) [a] ciprofloxacin (CPR) diclofenac (DCL) lincomycin (LCM)

sulfamethoxazole (SMX) [a] trimethoprim (TMP)

No/Low reactivity

bezafibrate (BZF) caffeine (CFF) ibuprofen (IBP)

Iopromide (IPR) NDMA sulfamethizole (SMZ)

[a] ATN and SMX showed moderate reactivity with Fe(VI), but no significant reactivity with Mn(VII).

Table 7.2. List of kinetic parameters for PhAC-Mn(VII) and PhAC-Fe(VI) reactions, and Fe(VI) inactivation of MS2 phage

Contaminant	Oxidant/ Disinfectant	k_2[a] (M⁻¹ s⁻¹)	k_{21}[b] (M⁻¹ s⁻¹)	k_{22}[b] (M⁻¹ s⁻¹)	k_{23}[b] (M⁻¹ s⁻¹)	$k_{\alpha2}$[c] (M⁻¹ s⁻¹)	$k_{\alpha3}$[c] (M⁻¹ s⁻¹)	E_a (kJ mol⁻¹)
carbamazepine (CBZ)	Mn(VII)	3.0(±0.3)×10²	---	---	---	---	---	22(±2)
carbamazepine (CBZ)	Fe(VI)	7.0(±0.3)×10¹	---	---	---	1.4(±0.5)×10²	3.8(±1.9)×10⁻¹	---
ciprofloxacin (CPR)	Mn(VII)	6.1(±0.2)×10⁻¹	0.52(±0.05)	0.34(±0.08)	1.2(±0.1)	---	---	54(±3)
lincomycin (LCM)	Mn(VII)	3.6(±0.1)	0.5(±0.1)	43(±6)	---	---	---	68(±4)
trimethoprim (TMP)	Mn(VII)	1.6(±0.1)	---	2.6(±0.3)	0.17(±0.05)	---	---	49(±5)
17α-ethinylestradiol (EE2)	Mn(VII)	1.27(±0.02)×10²	2.5(±0.4)×10¹	2.3(±0.4)×10⁵	---	---	---	37(±2)
MS2 phage	Fe(VI)	2.27(±0.05)	---	---	---	3.8(±0.5)	0.07(±0.02)	39(±6)

[a] All k_2 values are for pH 7 and 25 °C. Uncertainties represent 1 σ.
[b] Species-specific rate constants for Mn(VII) reactions.
[c] Species-specific rate constants for Fe(VI) reactions.

APPENDIX A

MS/MS SPECTRA OF PHACS AND THEIR REACTION PRODUCTS

Table A. 1. MS/MS spectra of carbamazepine (CBZ) and its reaction products with Mn(VII) and Fe(VI)

CBZ (m/z: 237)
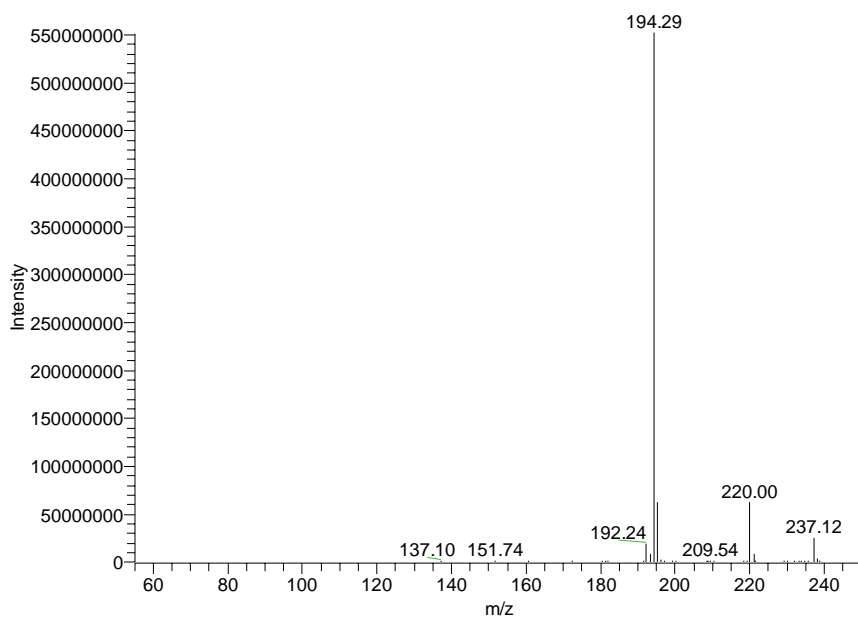
Product II (m/z: 224)
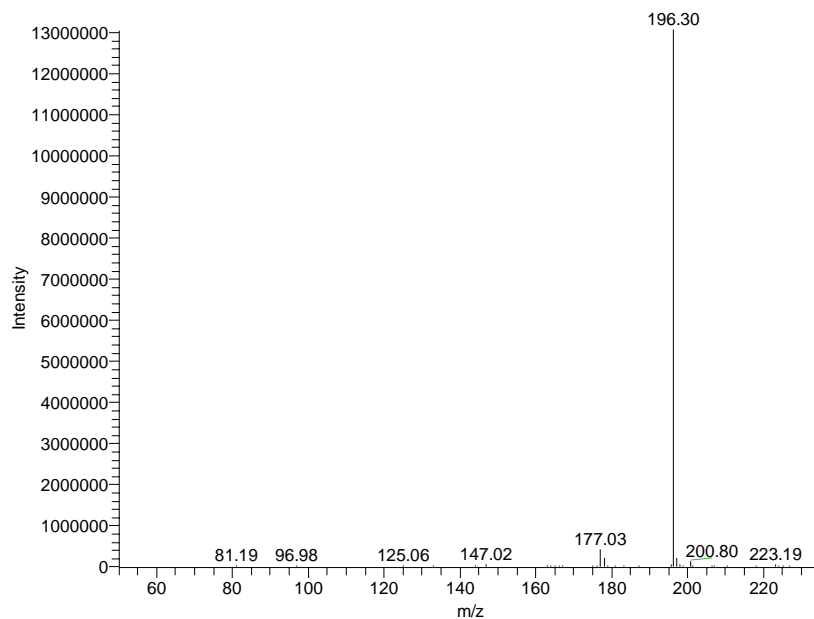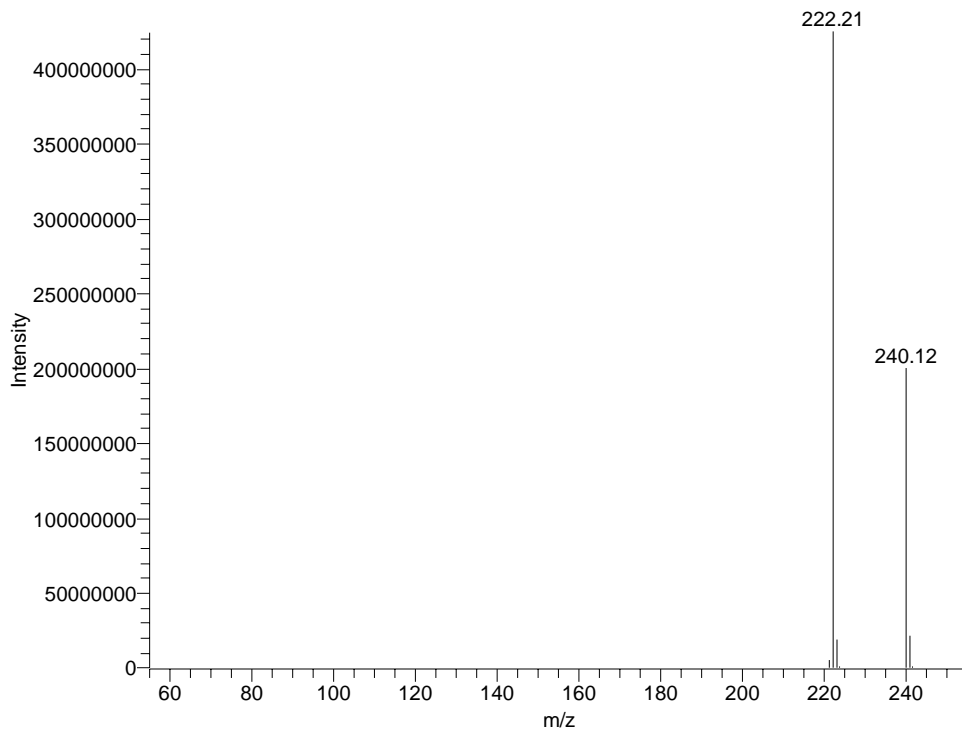
Product III (m/z: 240)

Product IV (m/z: 251)
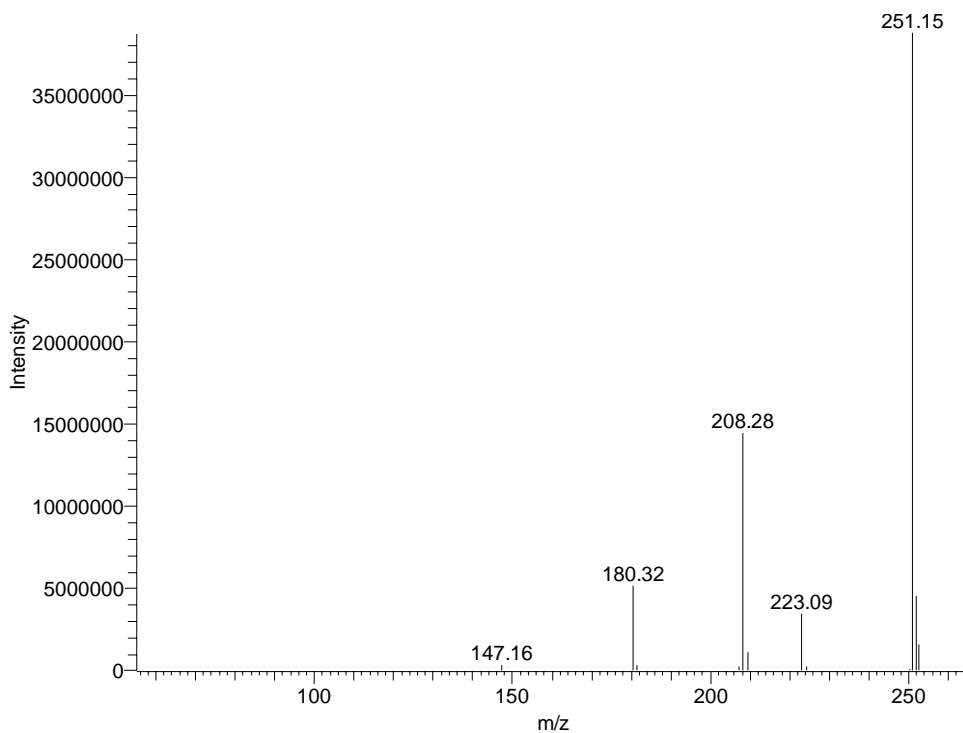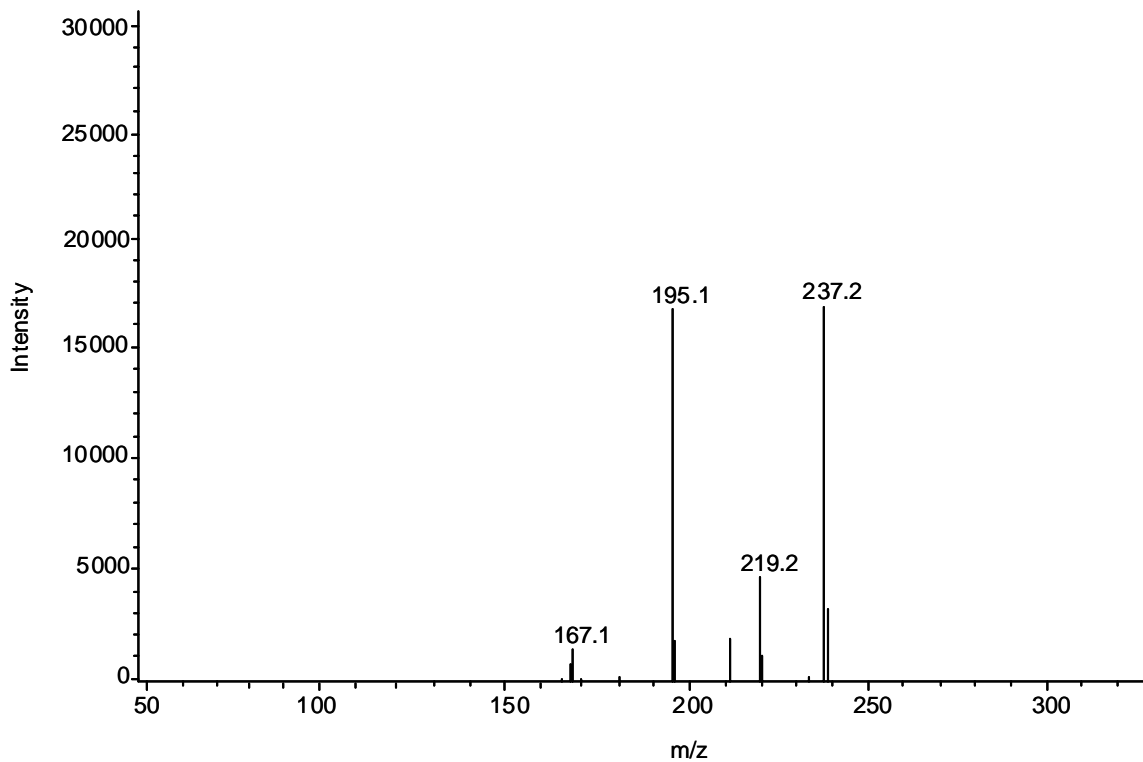
Product V (m/z: 255)

Product VI (m/z: 258)
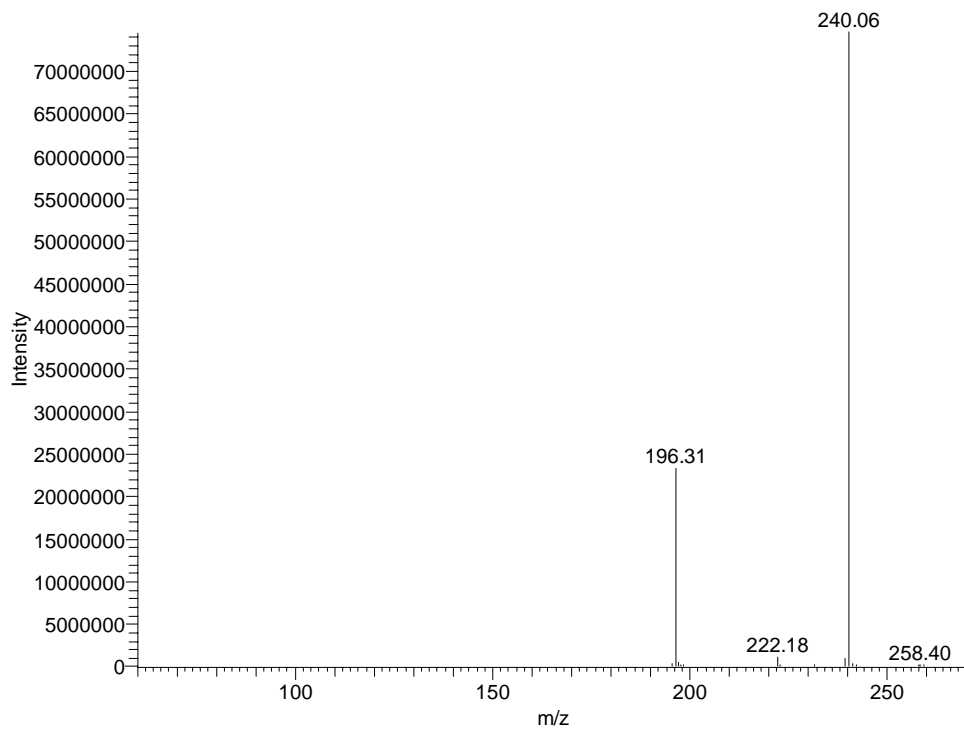
Product VII (m/z: 267)

Product VIII (m/z: 271)
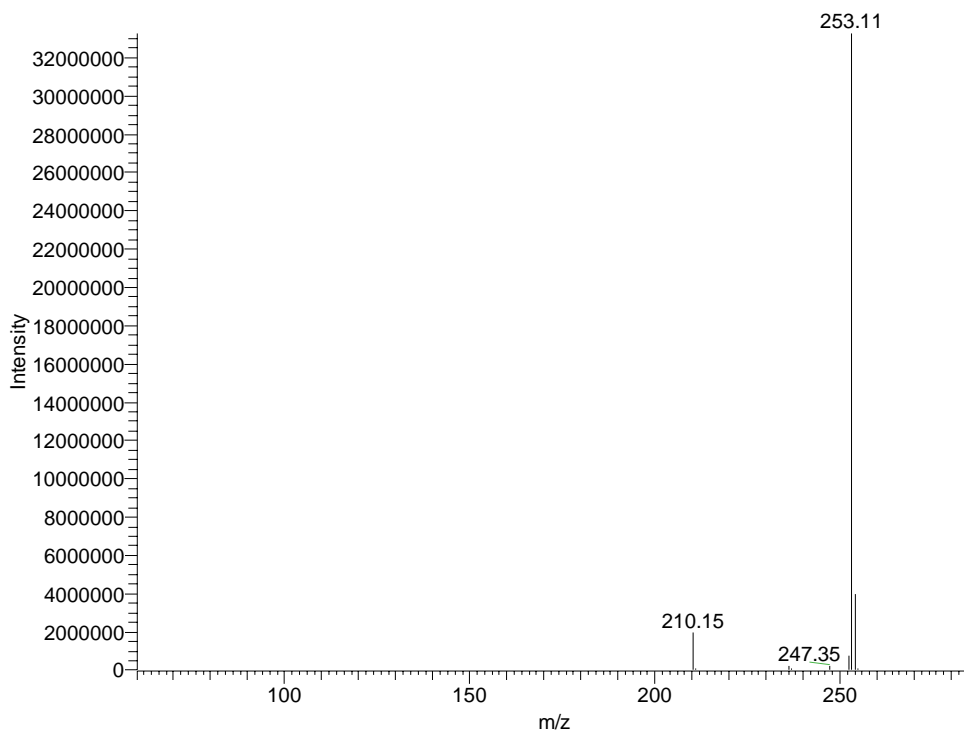
Table A. 1. (cont.)

Product IX (m/z: 283)

Product X (m/z: 285)
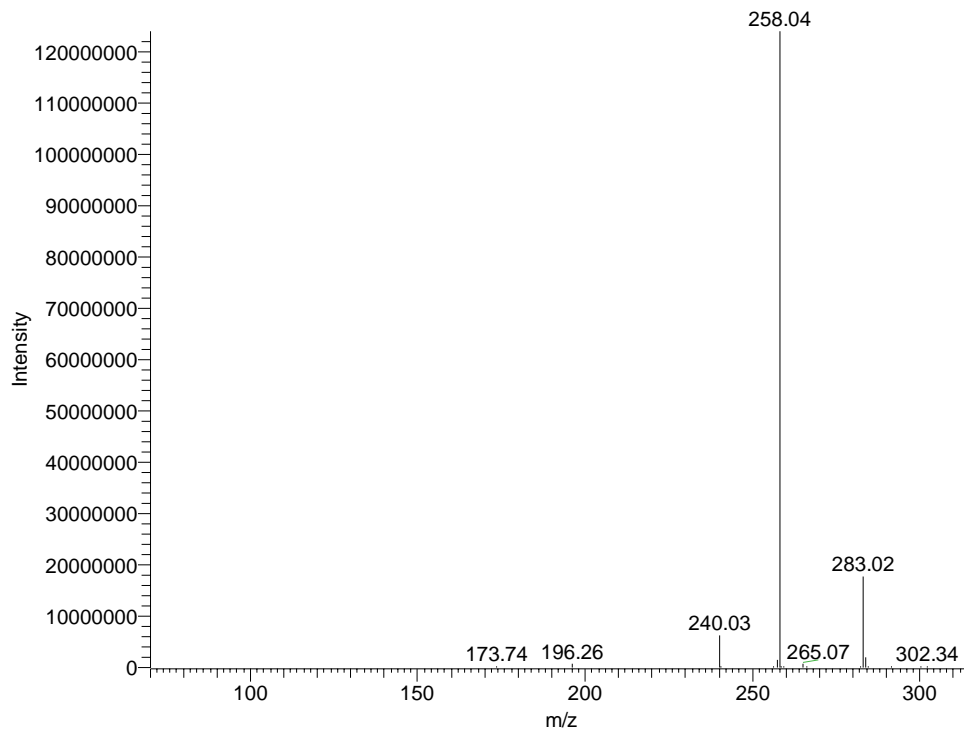
Product XI (m/z: 301)

Product XII (m/z: 303)
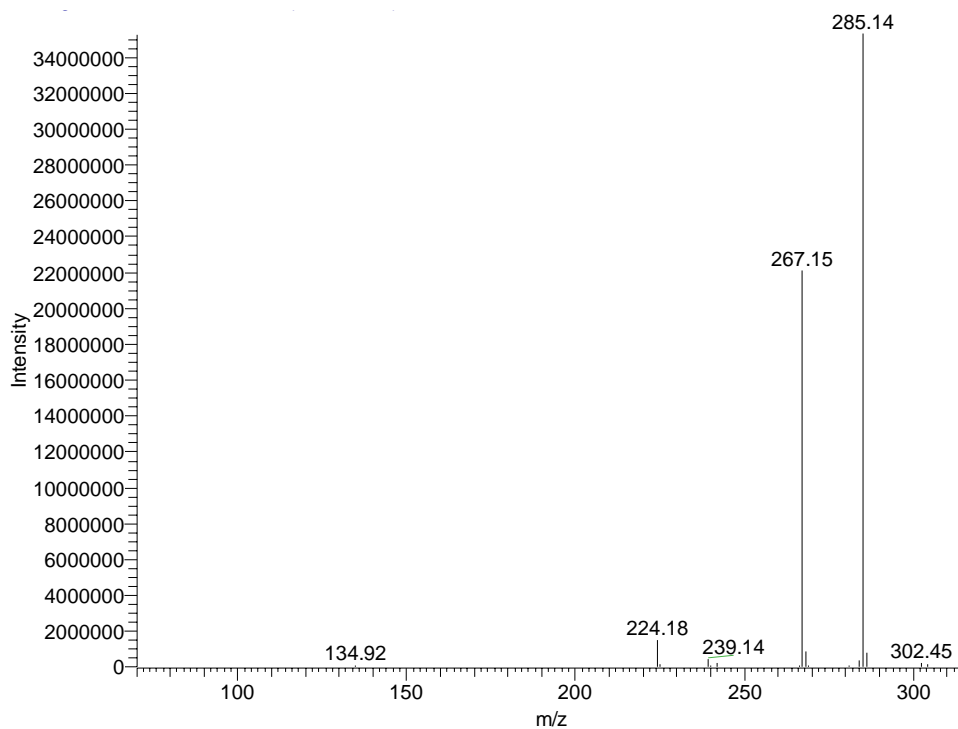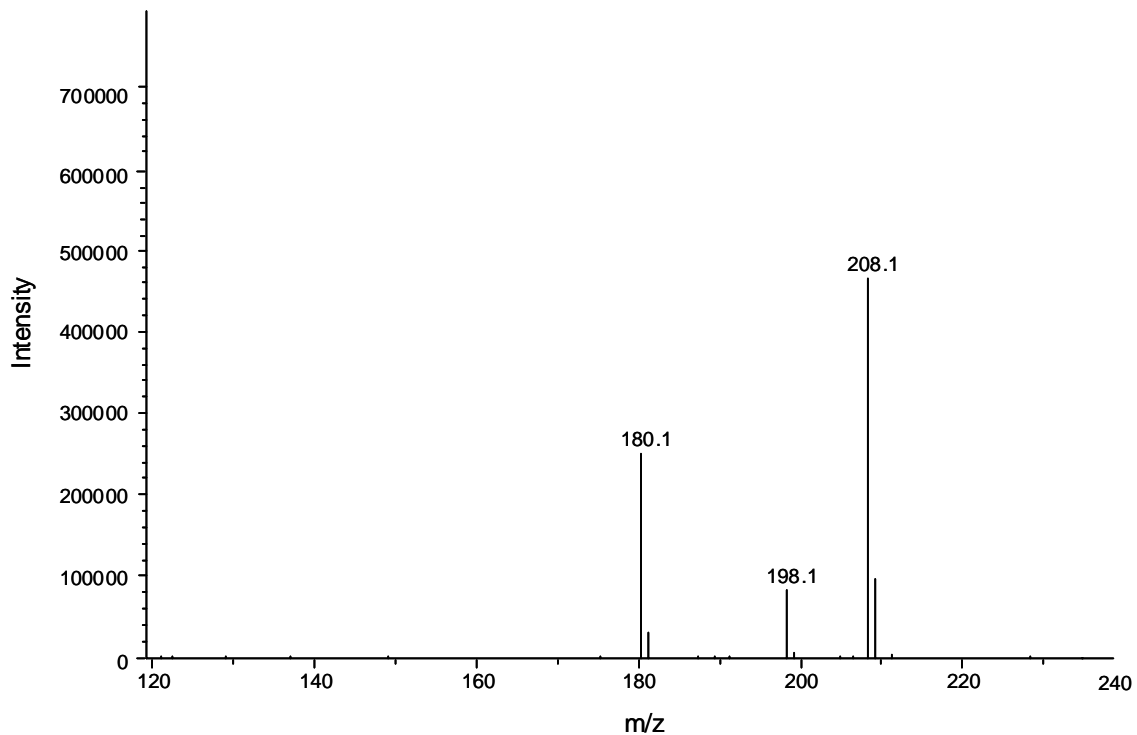
Product XIII (m/z: 226)

Product XIV (m/z: 267)
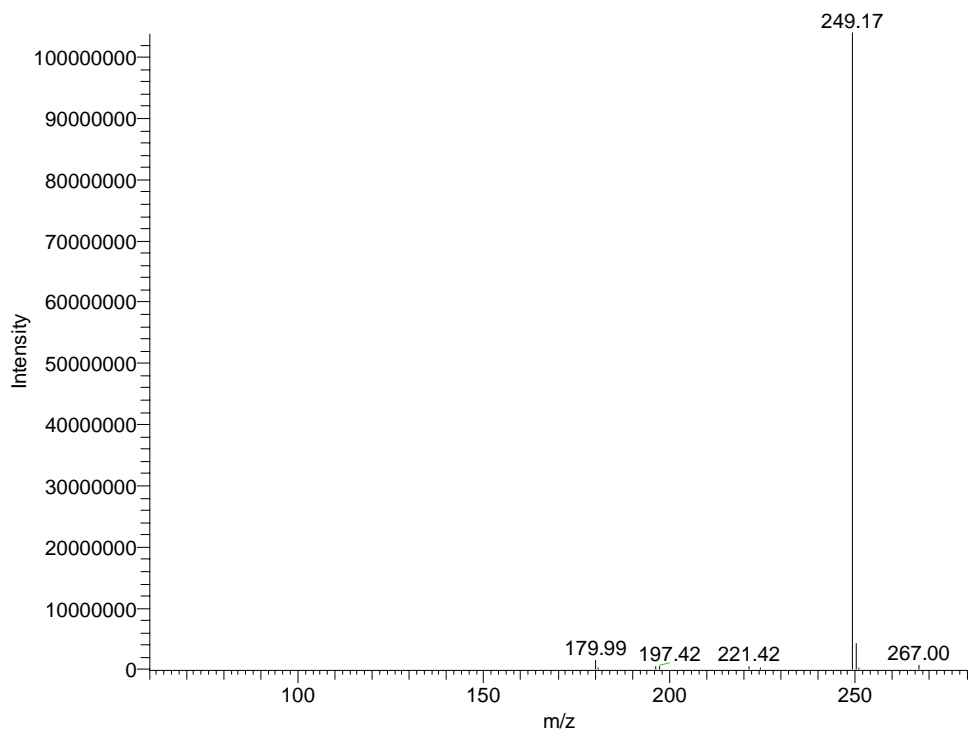
Table A. 2. MS/MS spectra of ciprofloxacin (CPR) and its reaction products with Mn(VII)

CPR (m/z: 332)*
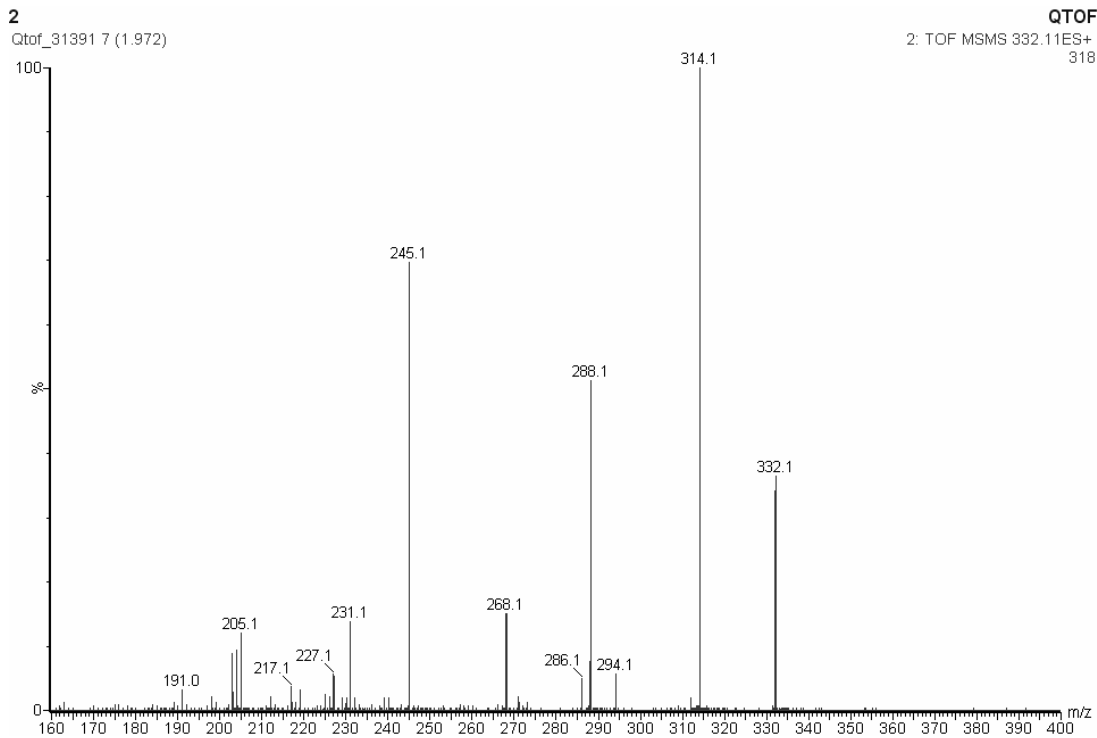
Product I (m/z: 263)*
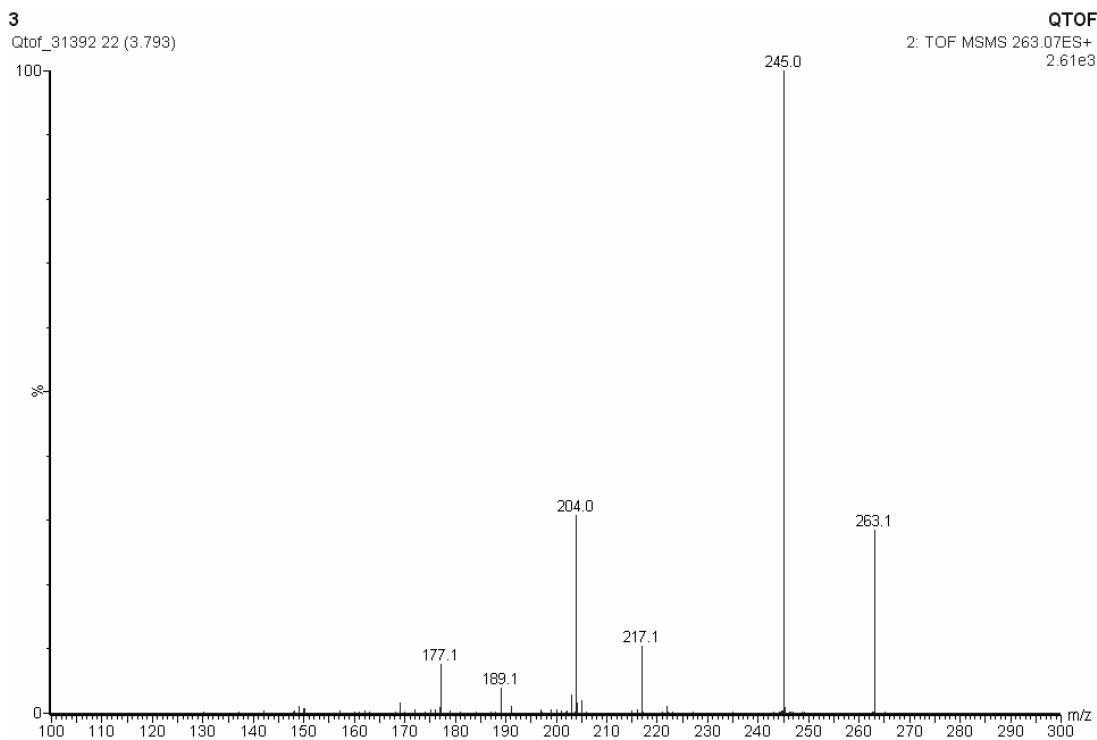
Table A. 2. (cont.)

Product II (m/z: 291)*
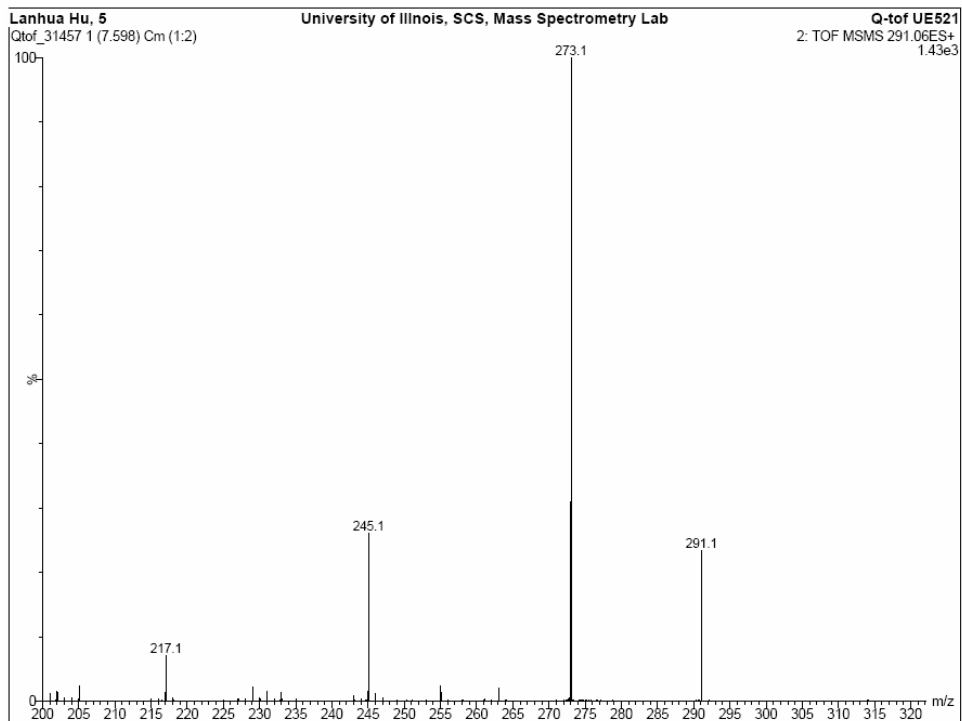
Product III (m/z: 293)
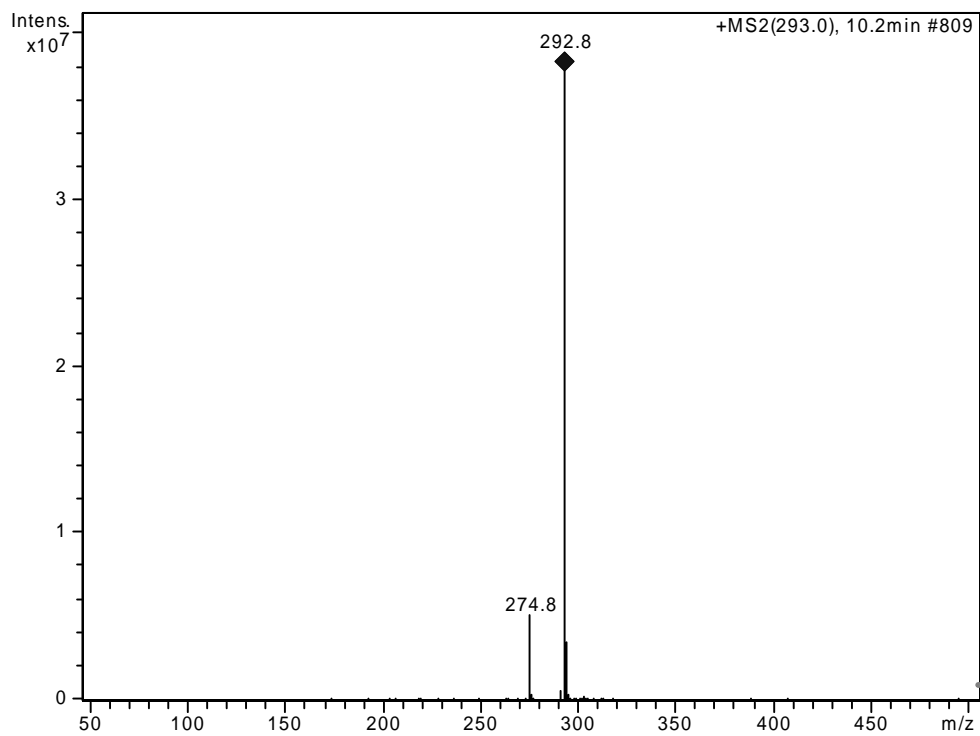
Table A. 2. (cont.)

Product IV (m/z: 306)*

Product V (m/z: 334)*
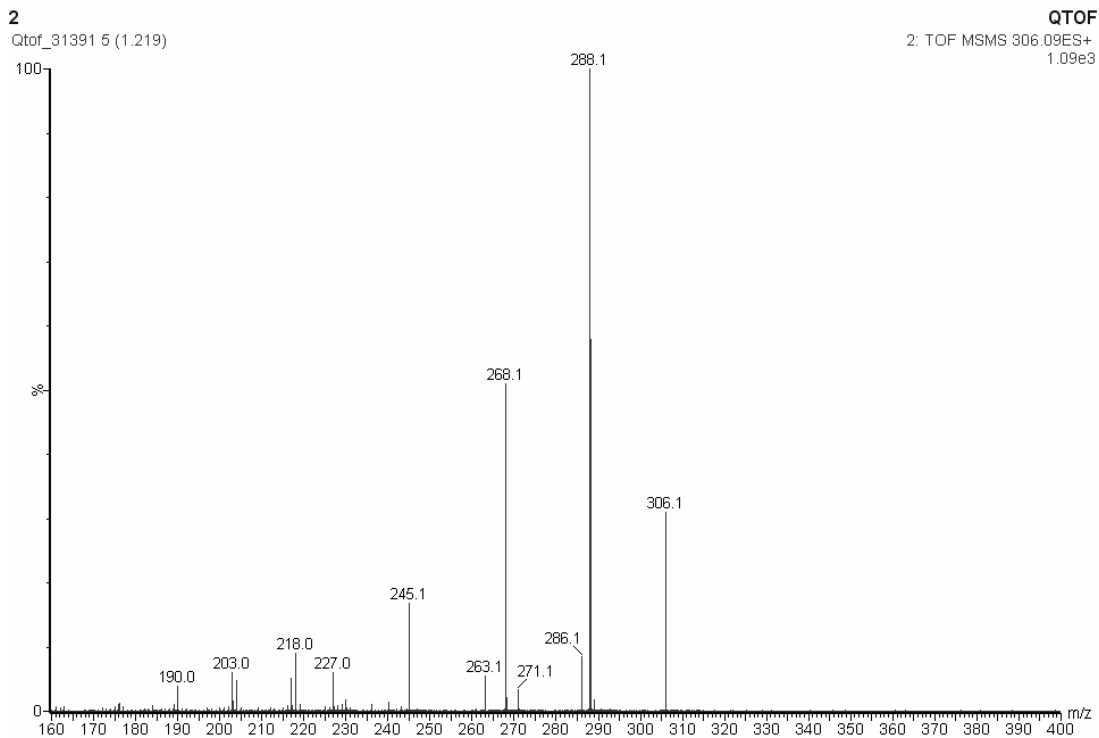
Product VI (m/z: 335)
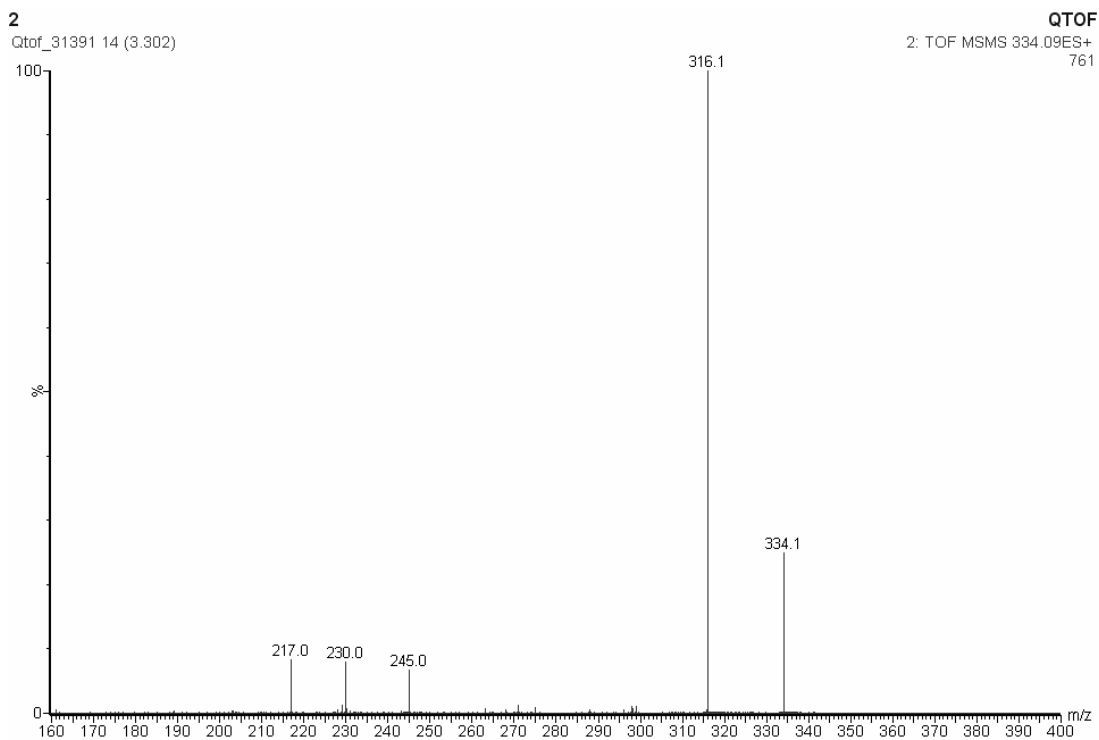
Product VII (m/z: 346)
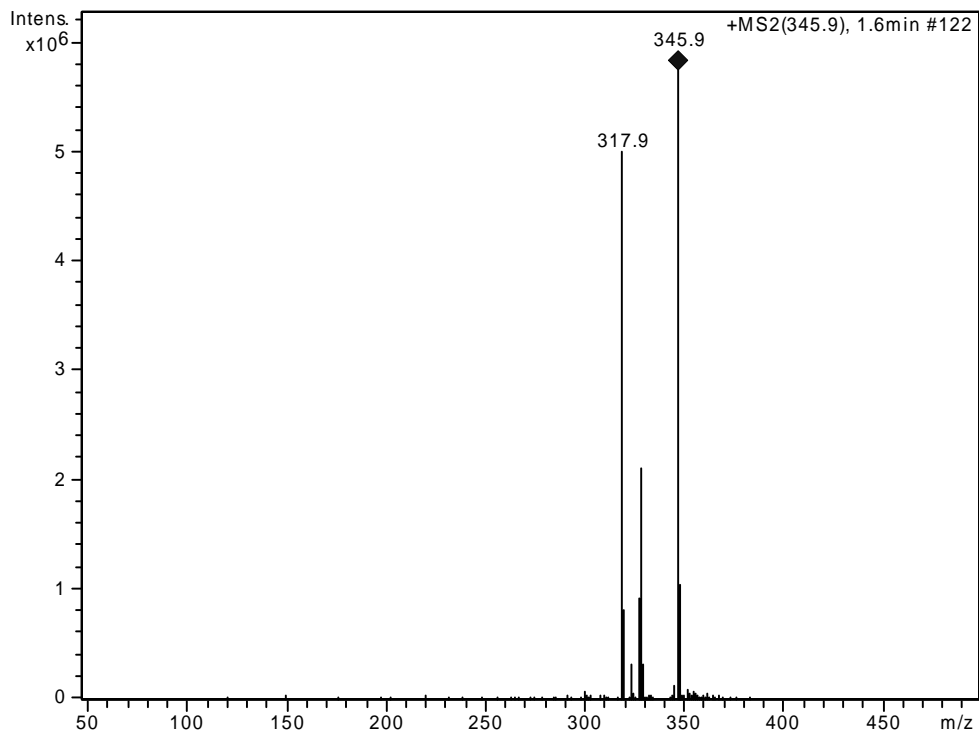
Table A. 2. (cont.)

Product VIII (m/z: 346)

+MS2(345.9), 9.7min #808

Product IX (m/z: 360)*

4

Qtof_31393 11 (1.834)
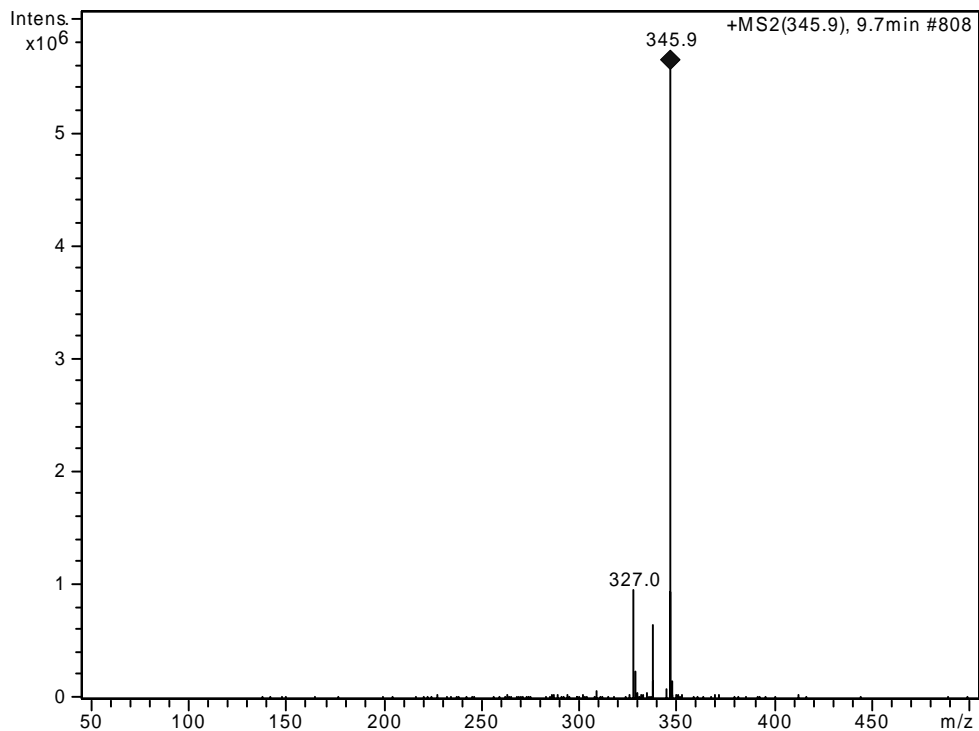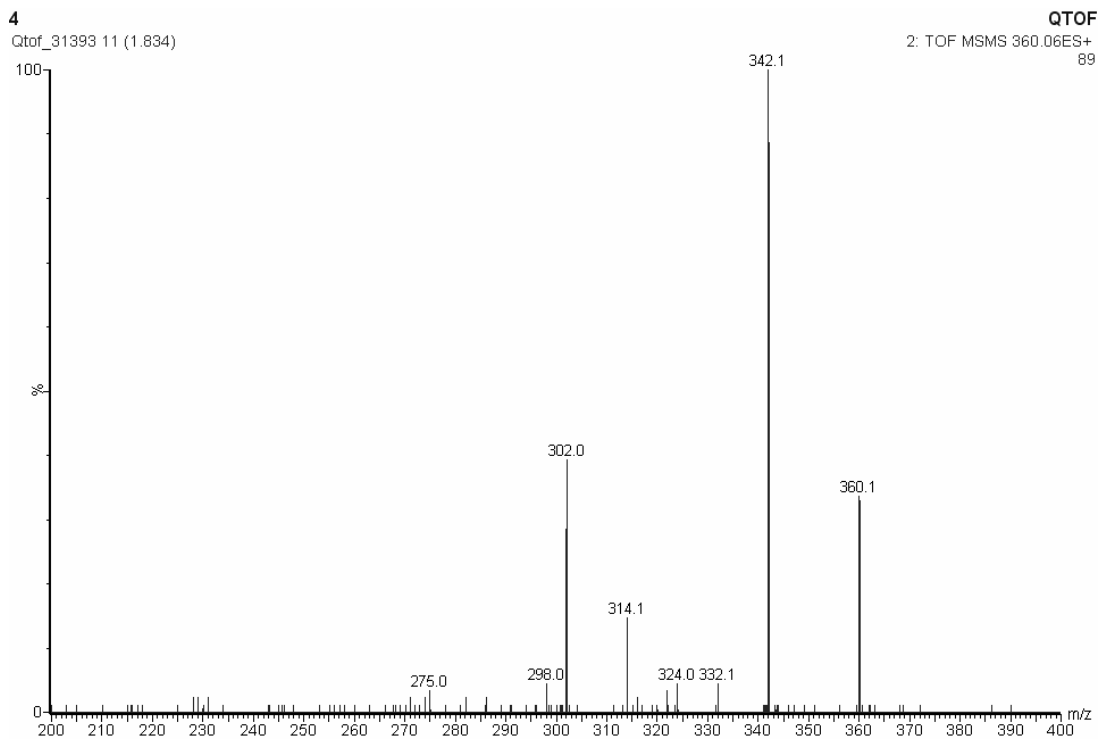
QTOF
2: TOF MSMS 360.06ES+
89
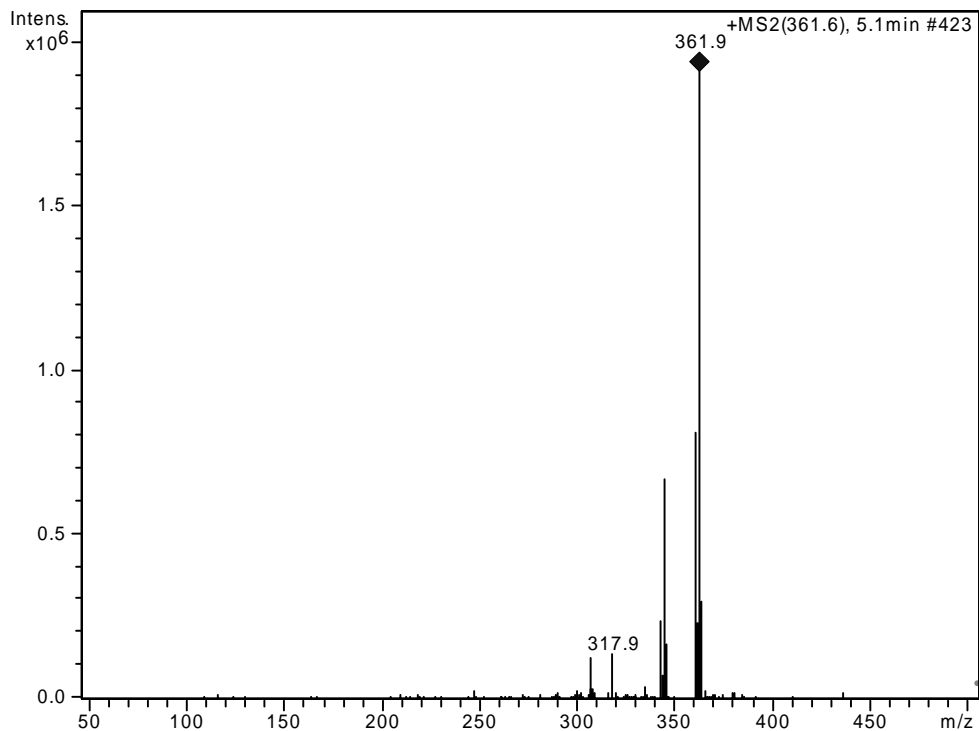
Product X (m/z: 362)

Product XI (m/z: 362)*
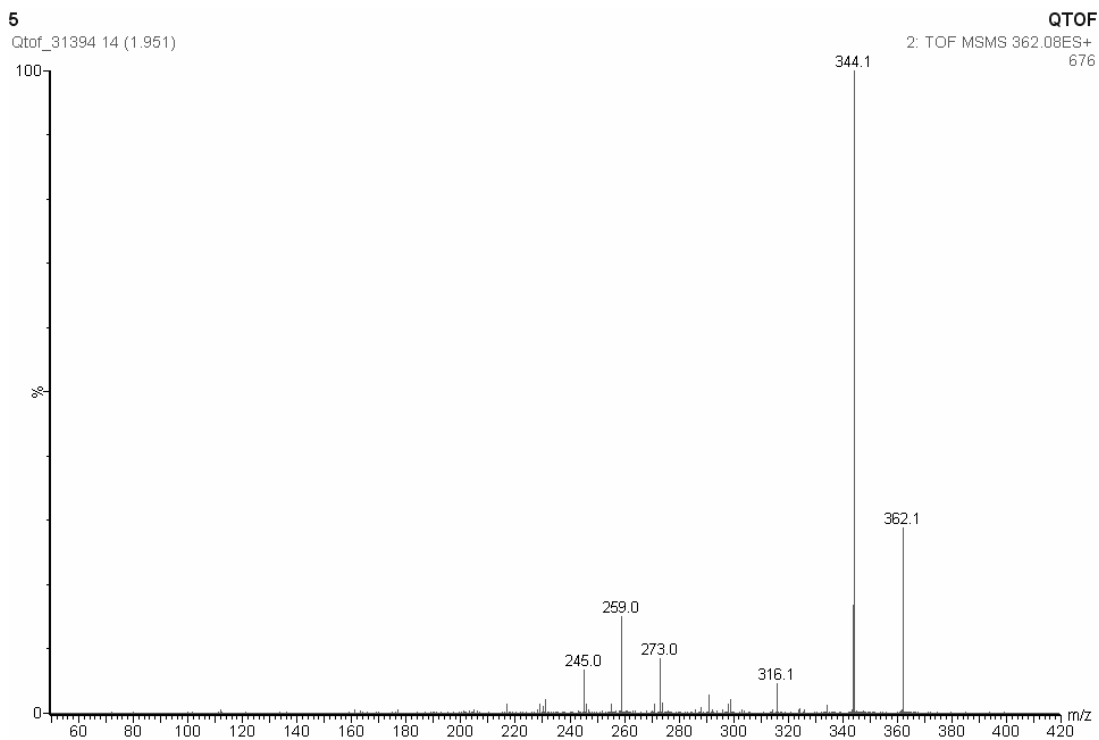
Product XII (m/z: 380)
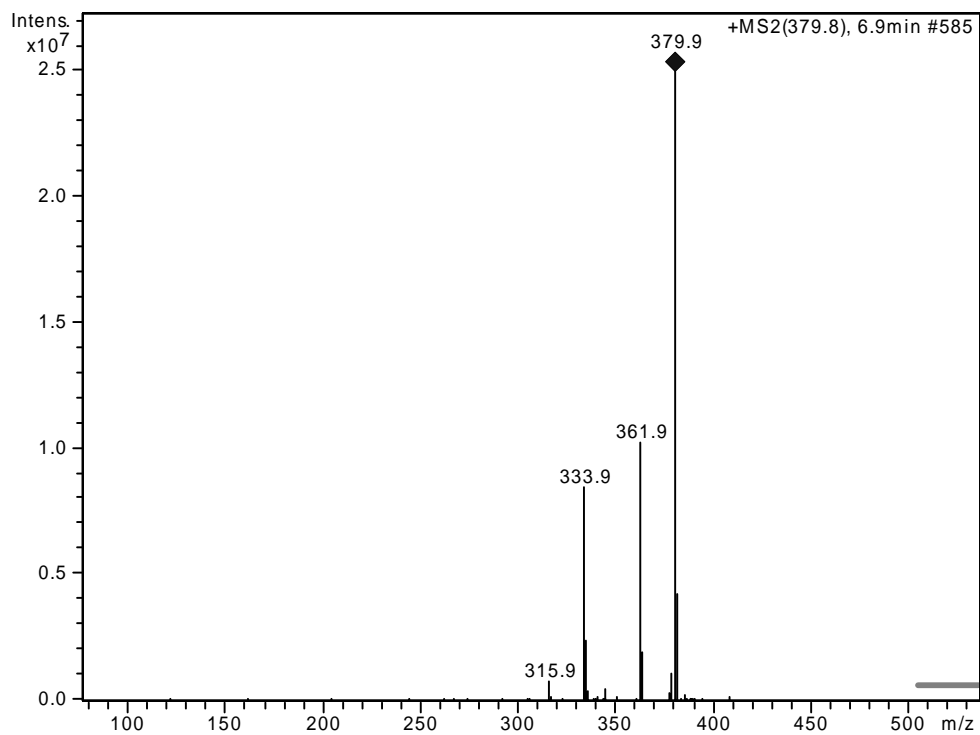
* Spectra obtained in the Q-TOF instrument

Table A. 3. MS/MS spectra of lincomycin (LCM) and its reaction products with Mn(VII)

LCM (m/z: 407)
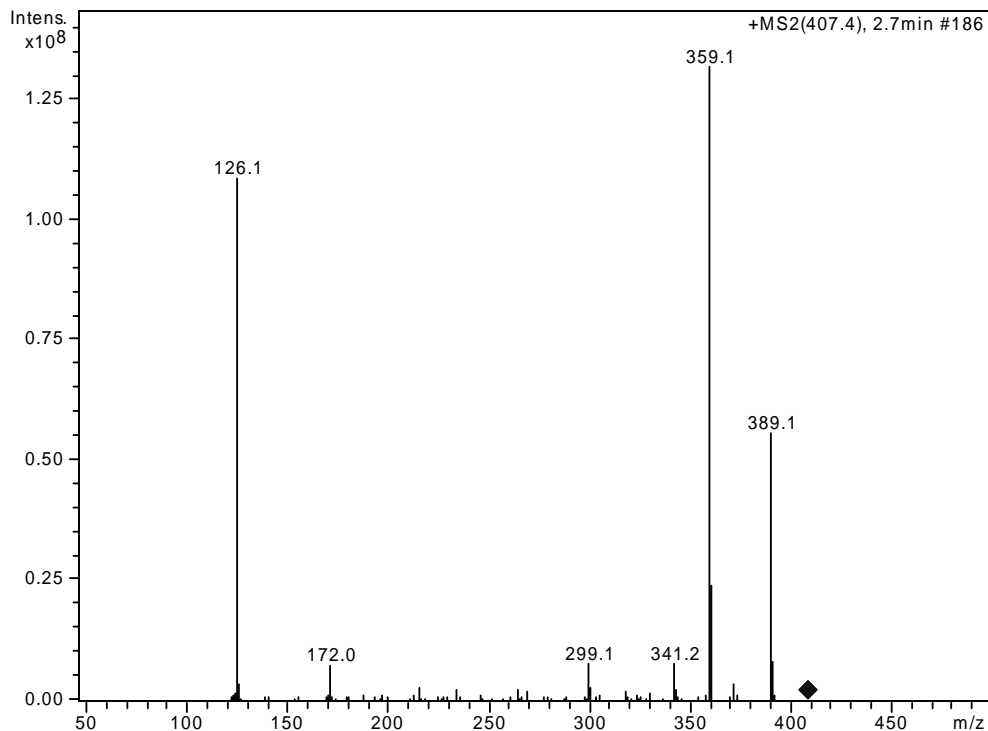
Product I (m/z: 393)
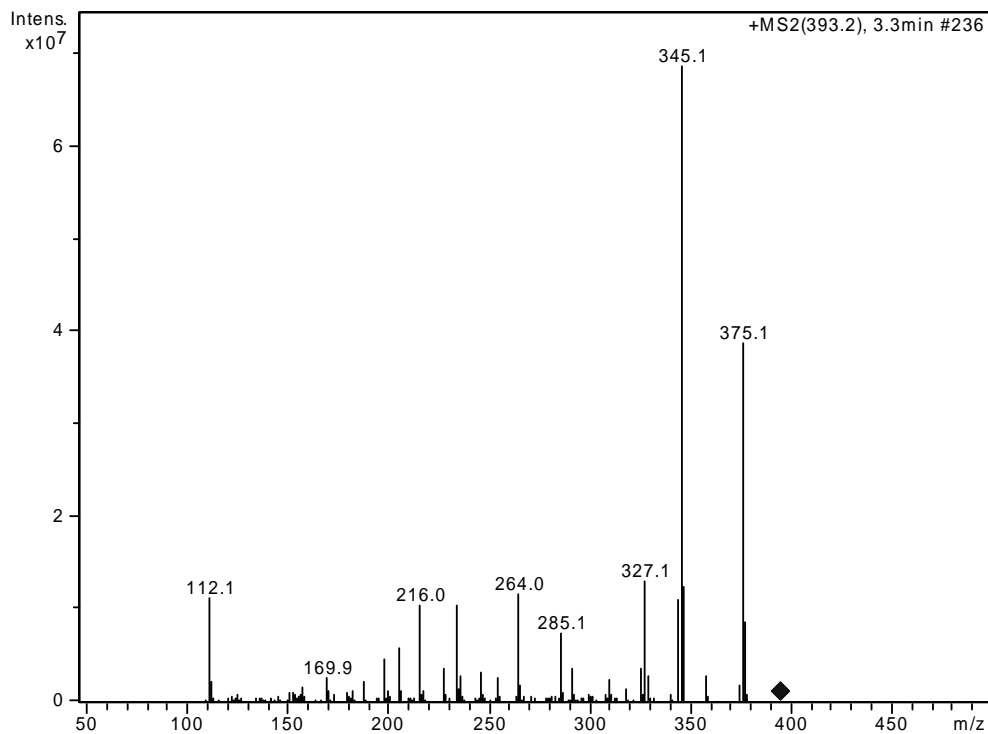
Table A. 3. (cont.)

Product II (m/z: 405)
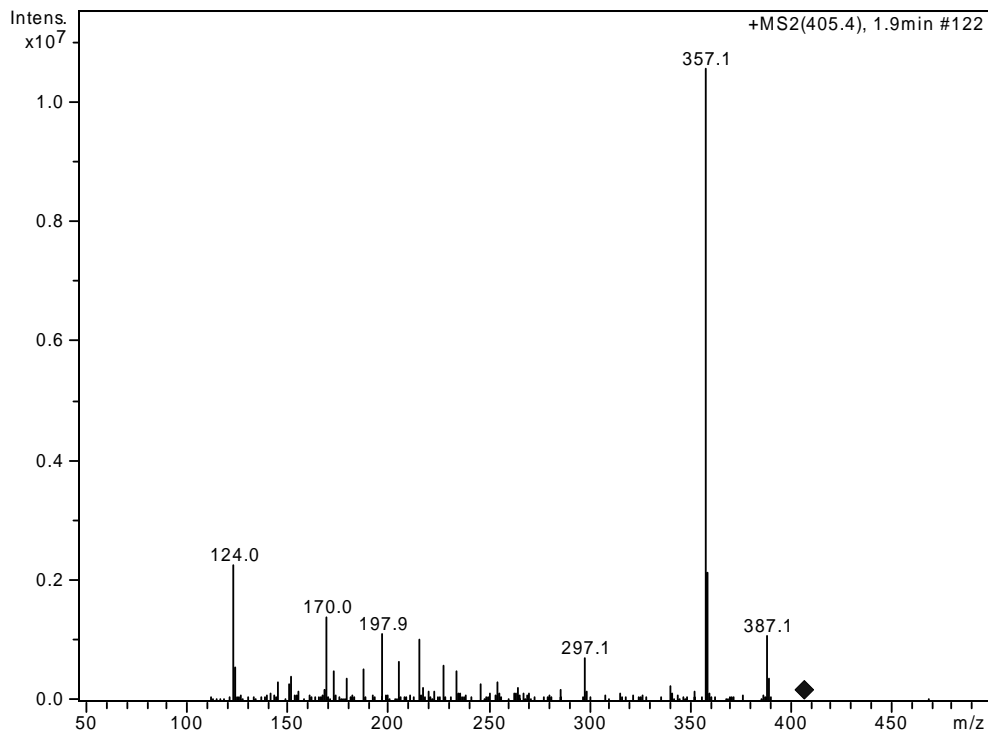
Product III (m/z: 408)
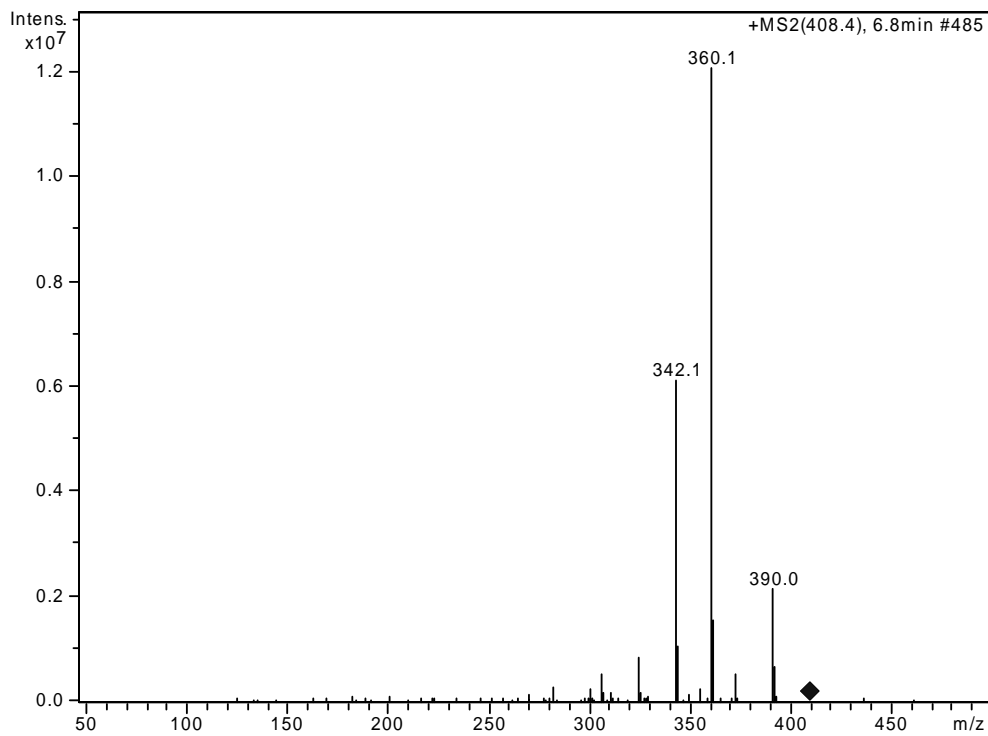
Table A. 3. (cont.)

Product IV (m/z: 421)

Spectrum labels: +MS2(421.4), 8.4min #605; peaks at 323.1, 355.1, 373.1, 403.0
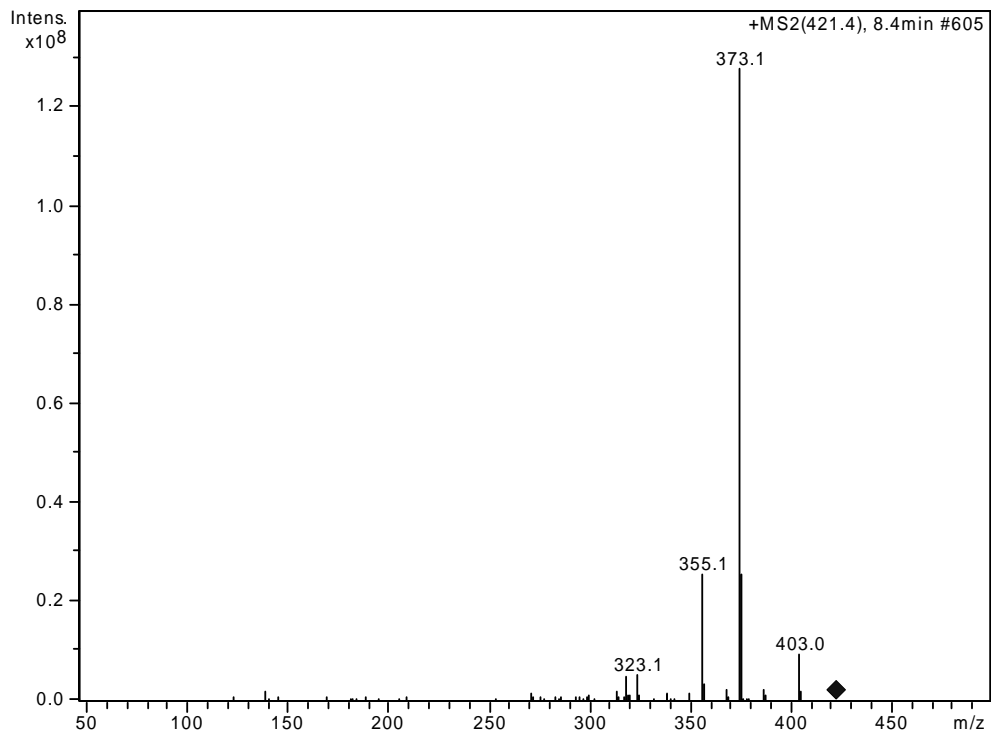
Fragment ion of product IV (m/z 373)

Spectrum labels: +MS2(373.2), 8.7min #715; peaks at 140.0, 283.1, 313.1, 337.1, 355.1
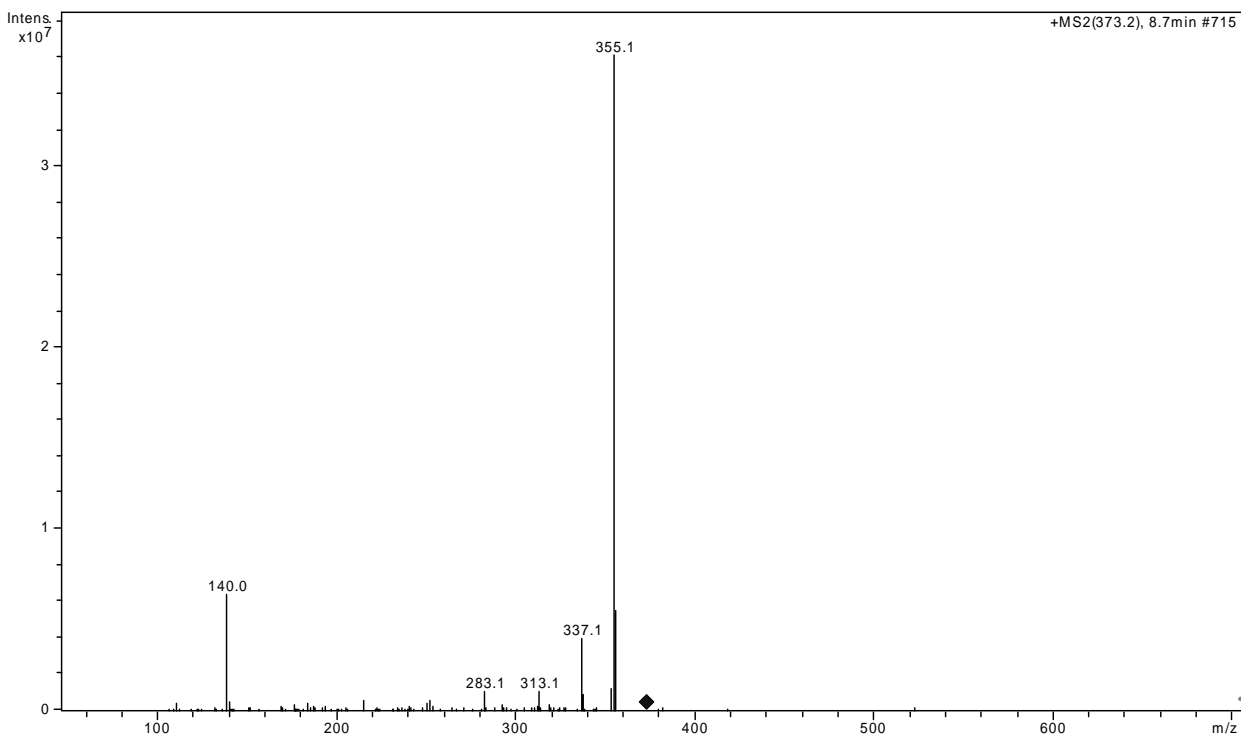
Product V (m/z: 423)
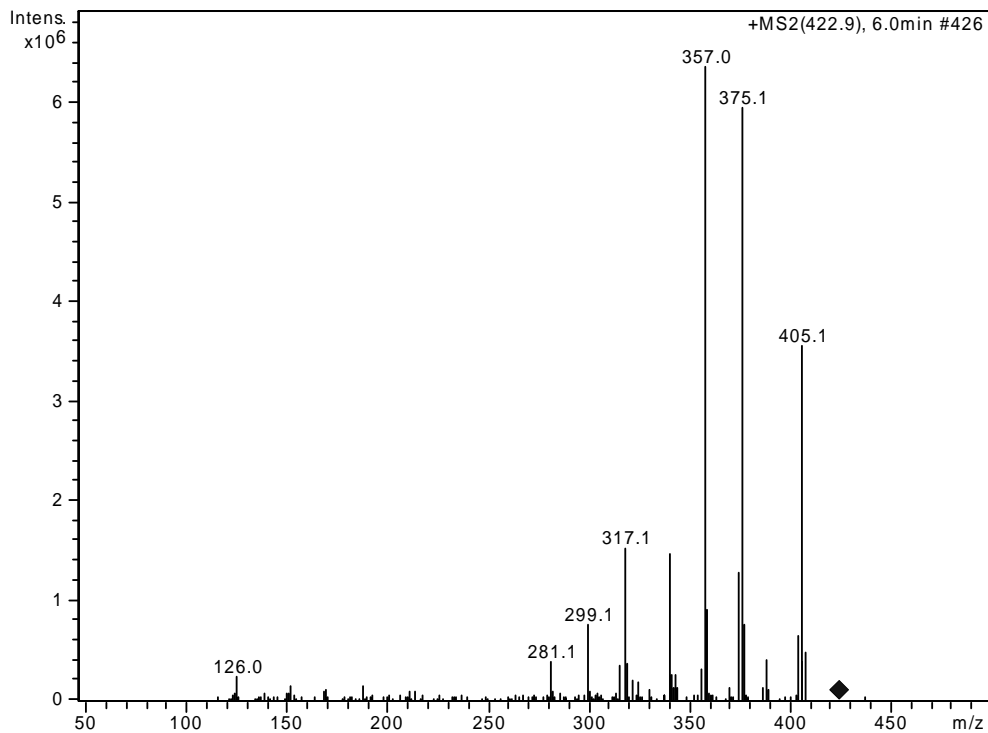
Product VI (m/z: 439)
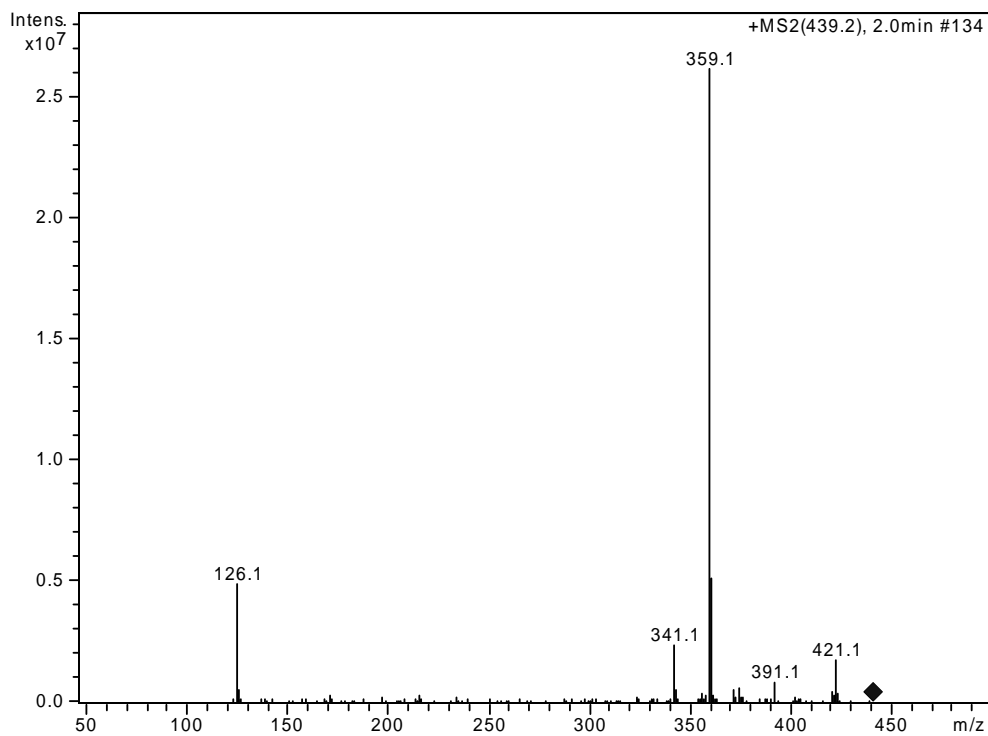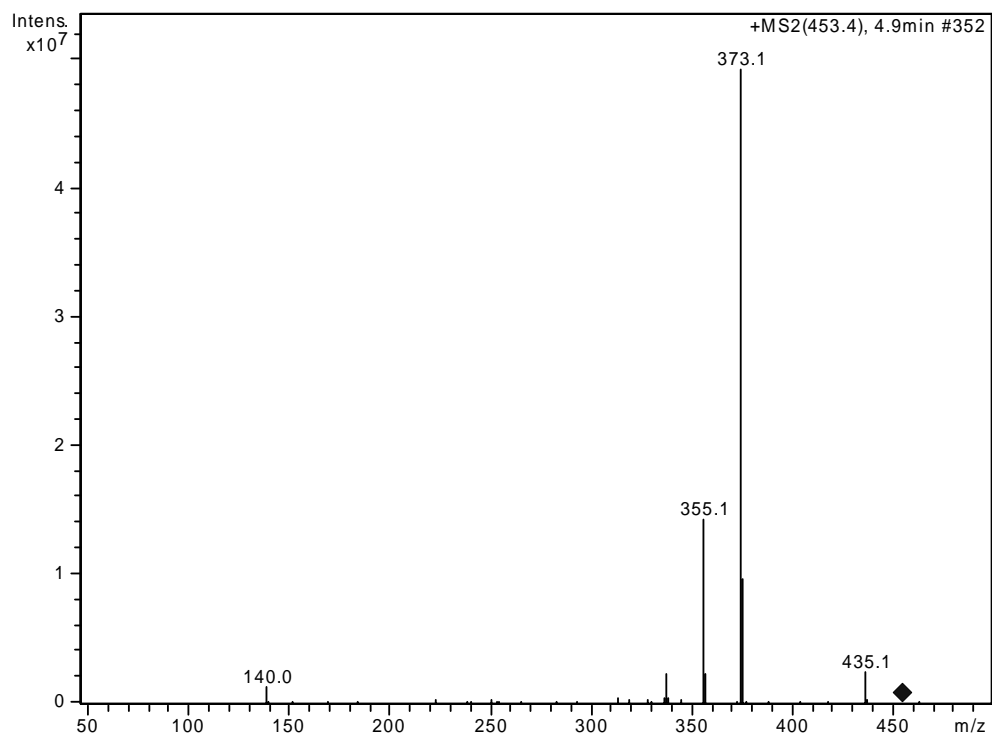
Product VII (m/z: 453)

Table A. 4. MS/MS spectra of trimethoprim (TMP) and its reaction products with Mn(VII)

TMP (m/z: 291)
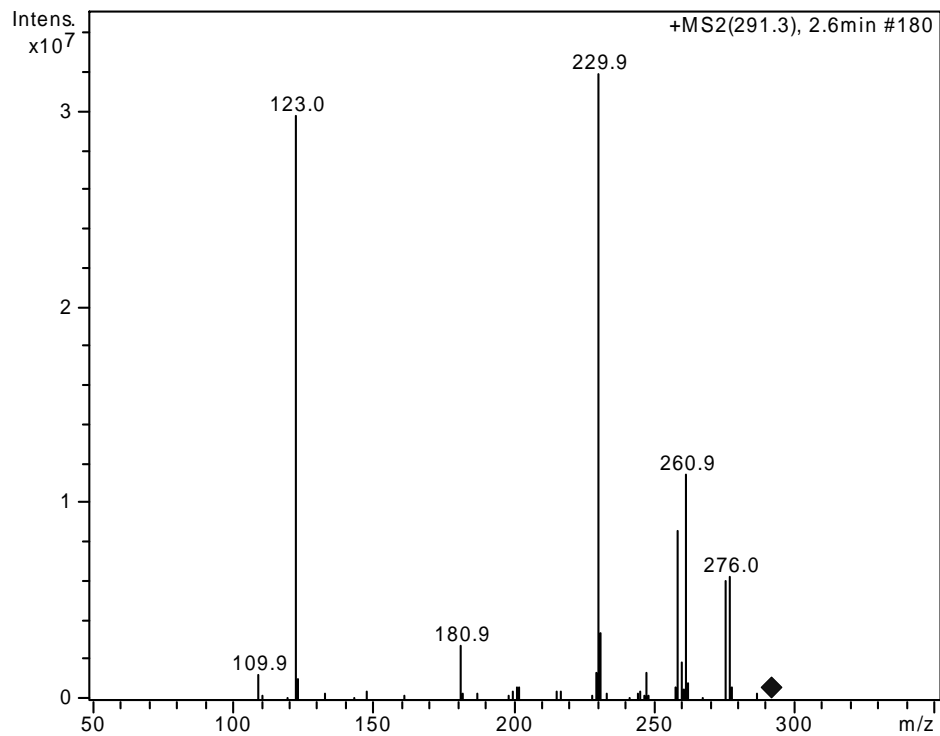
Product I (m/z: 280)
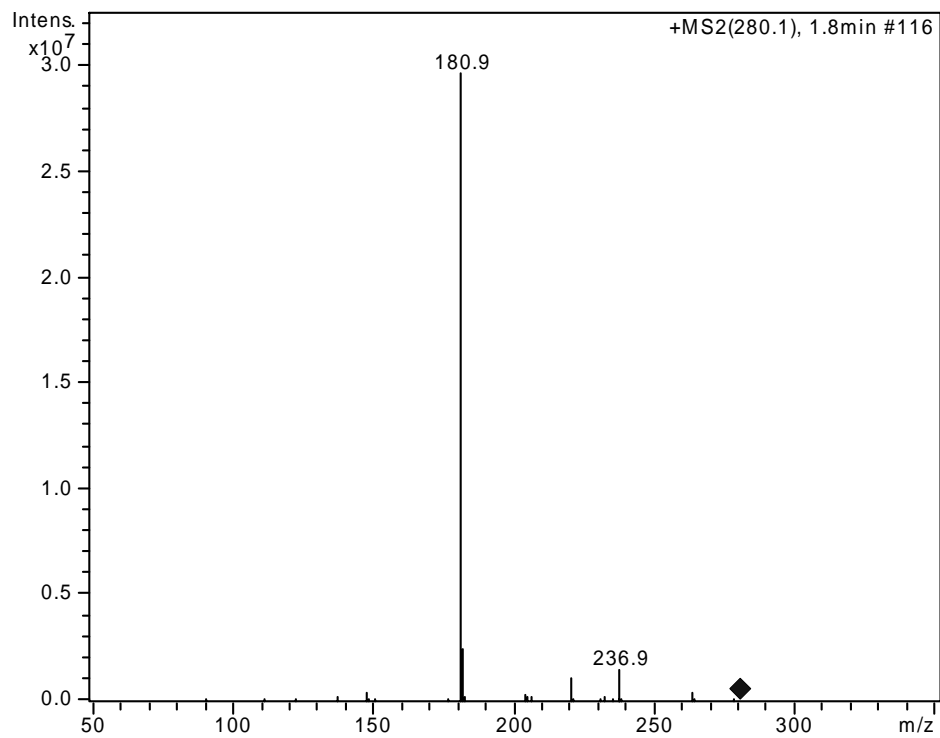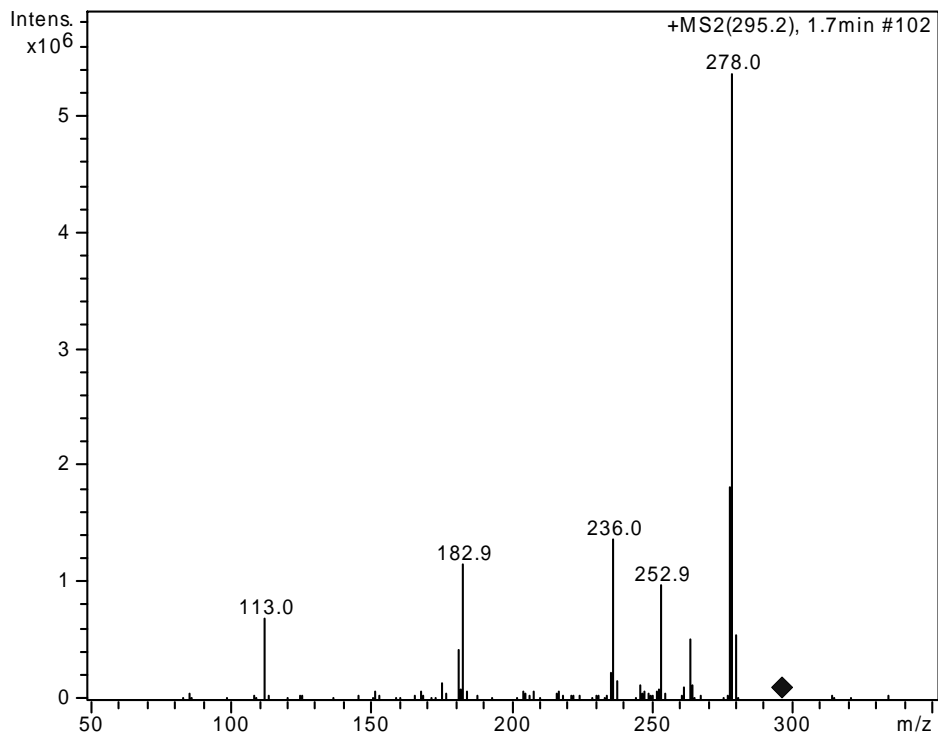
Product II (m/z: 295)

Product III (m/z: 305)
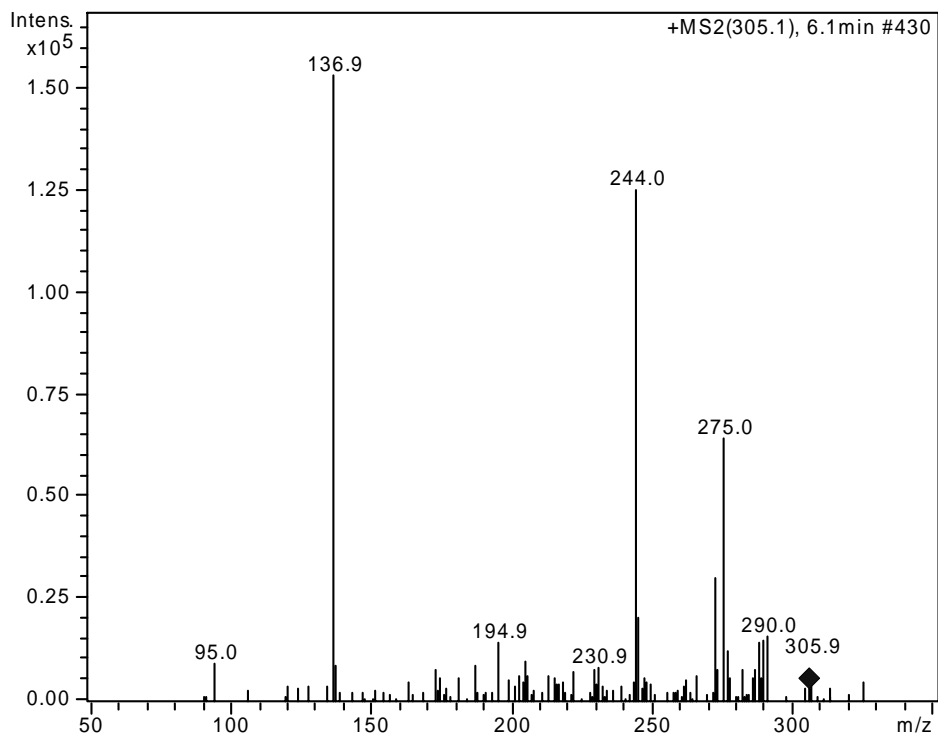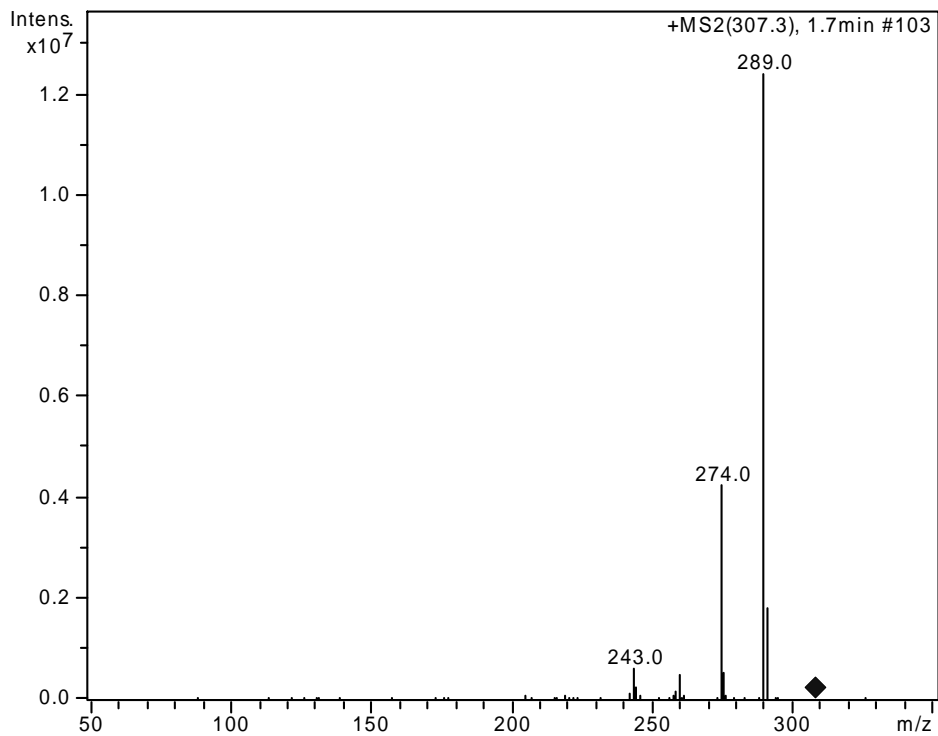
Product IV (m/z: 307)

Product V (m/z: 323)
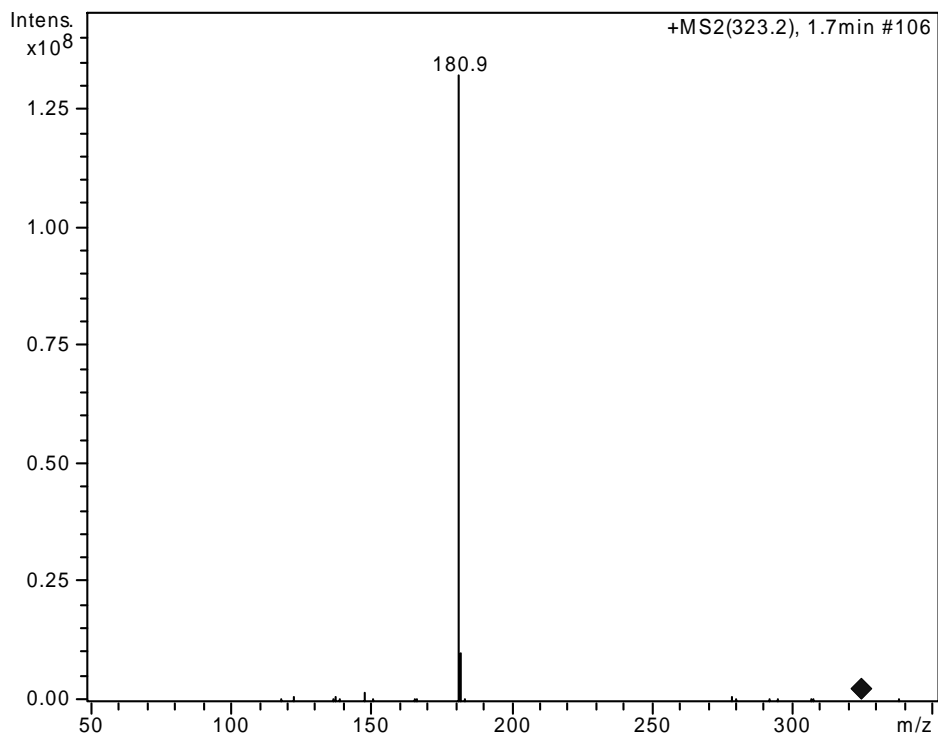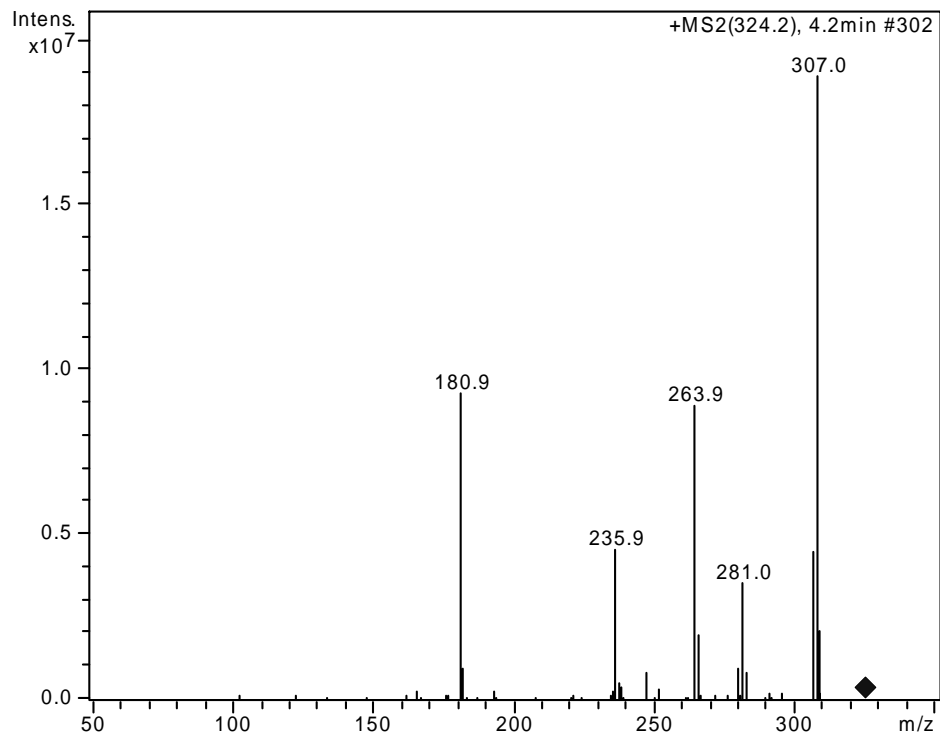
Product VI (m/z: 324)

Product VII (m/z: 325)
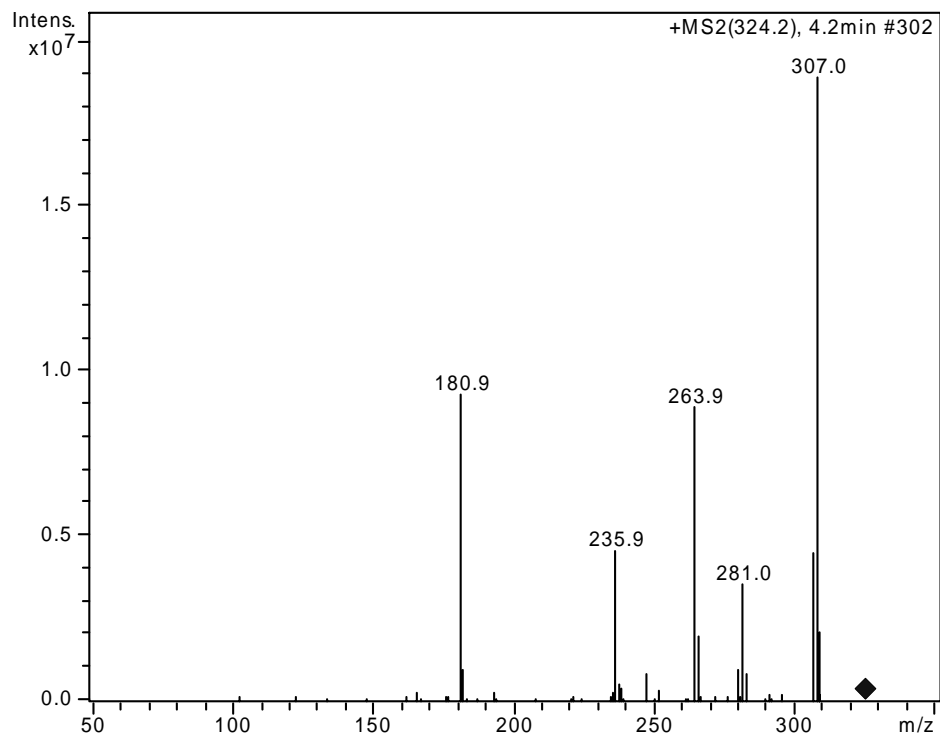
Table A. 5. MS/MS spectra of 17α-ethinylestradiol (EE2) and its reaction products with Mn(VII)

EE2 (m/z: 297)
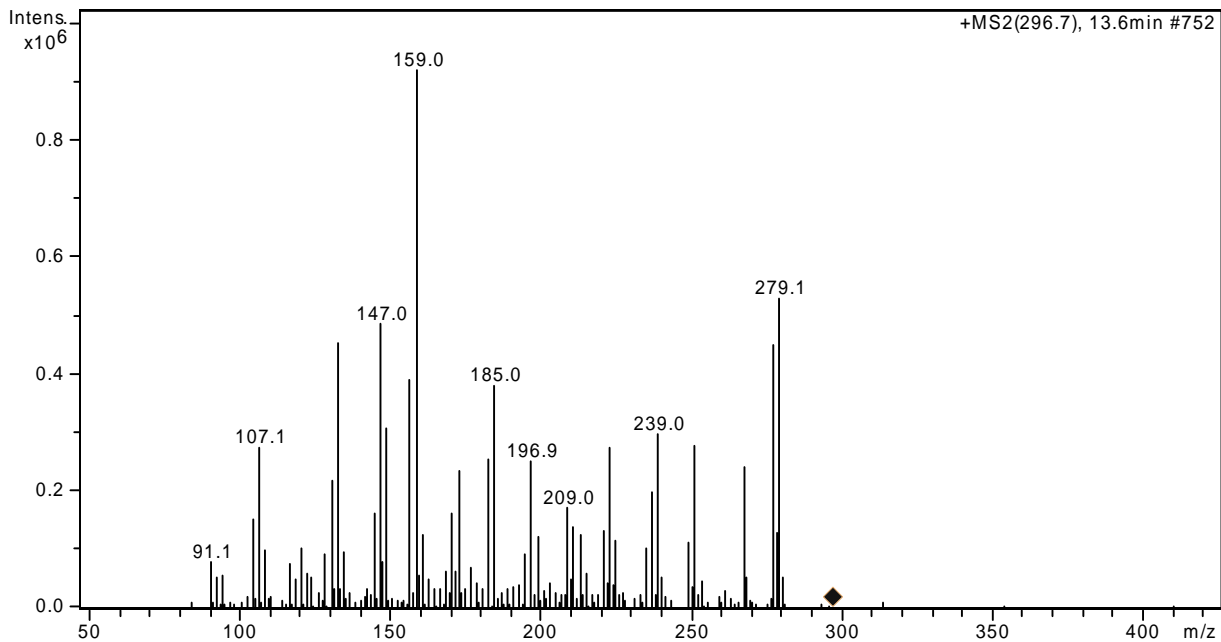
Product I (m/z: 287)
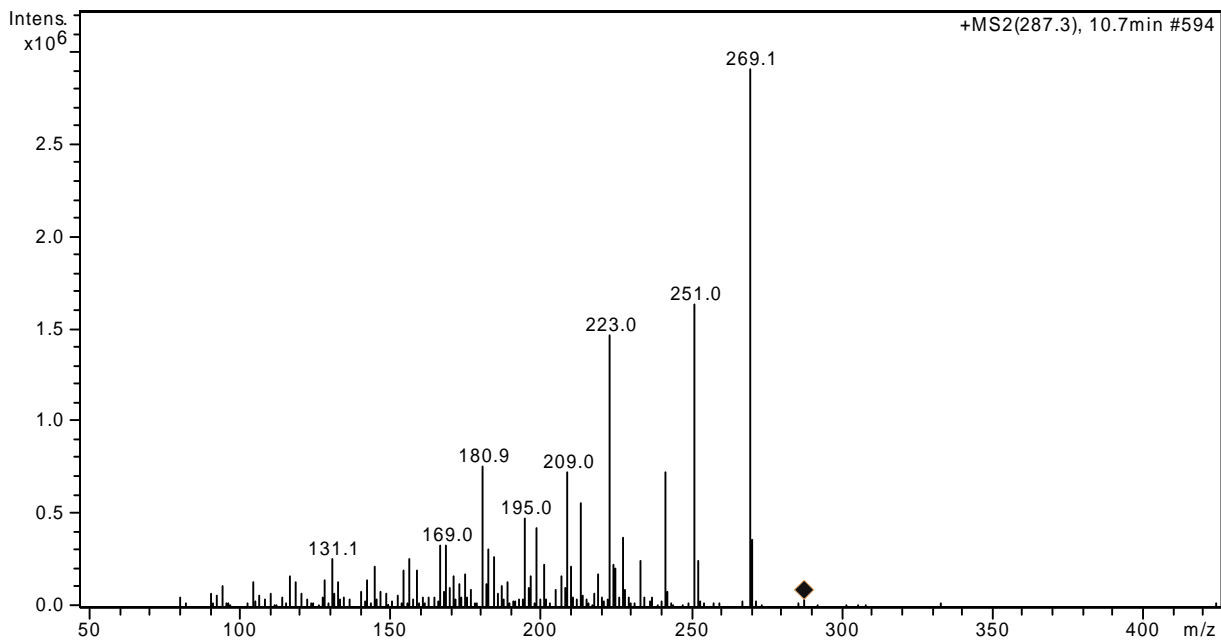
Table A. 5. (cont.)

Product II (m/z: 295)
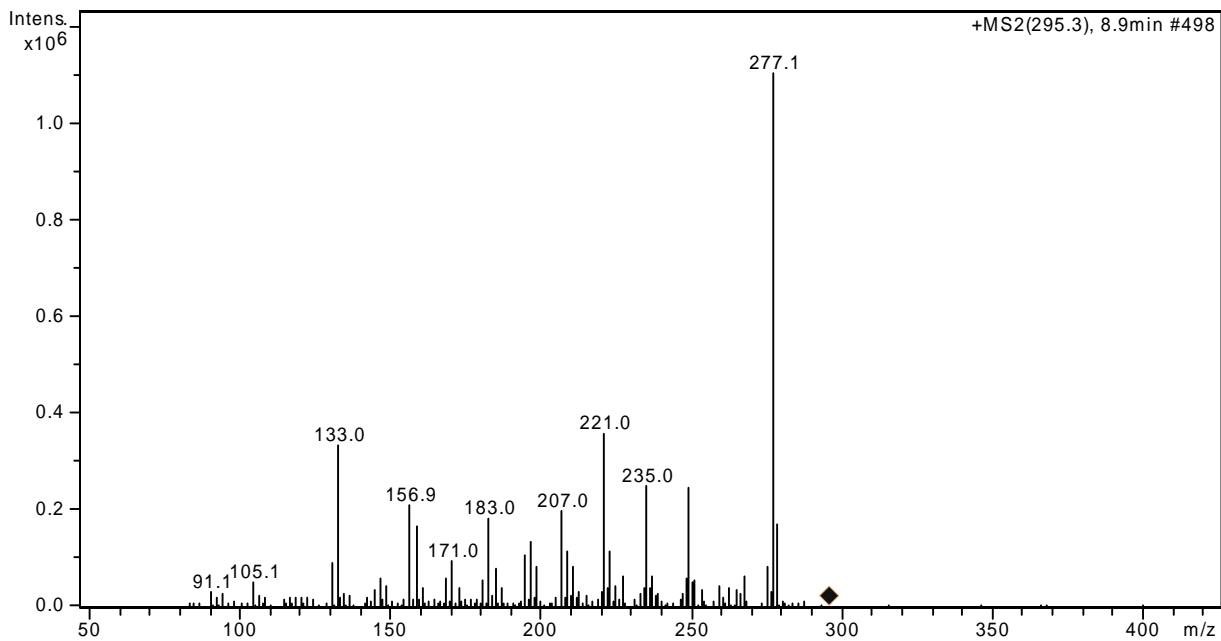
Product III (m/z: 303)
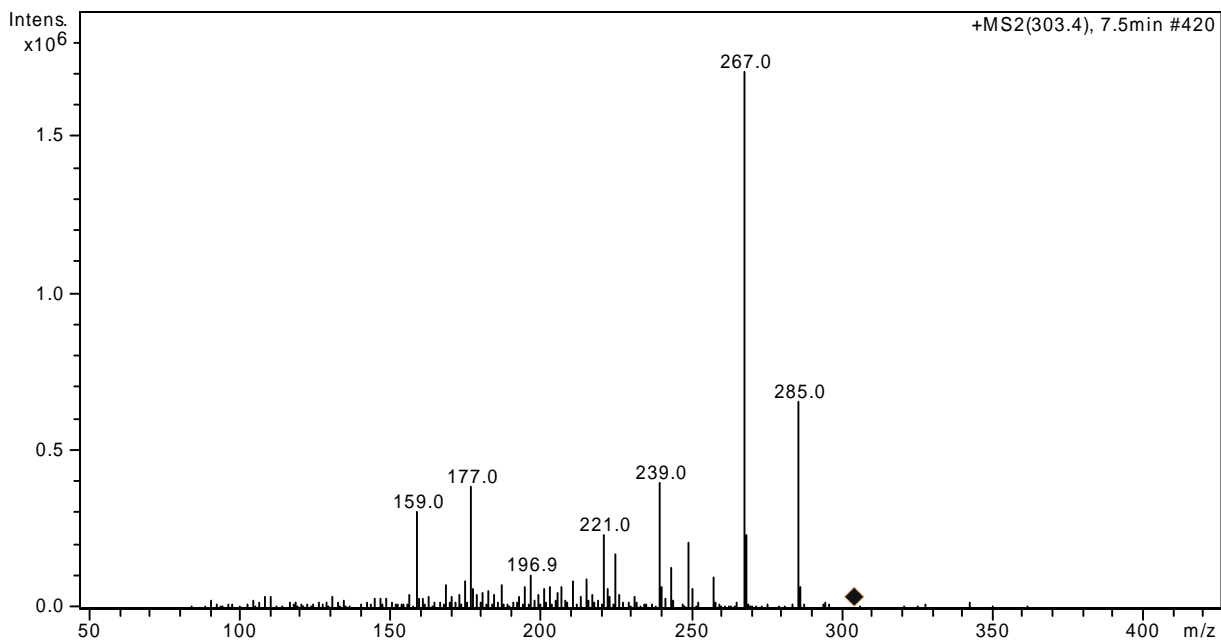
Table A. 5. (cont.)

Product IV (m/z: 313)
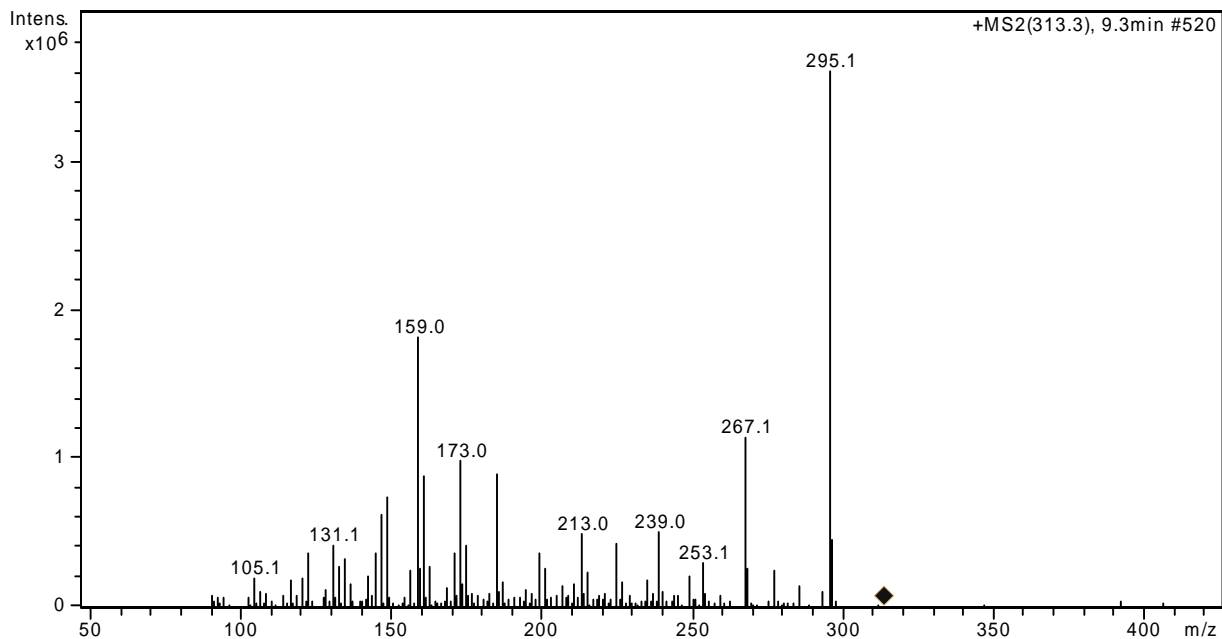
Product V (m/z: 315)
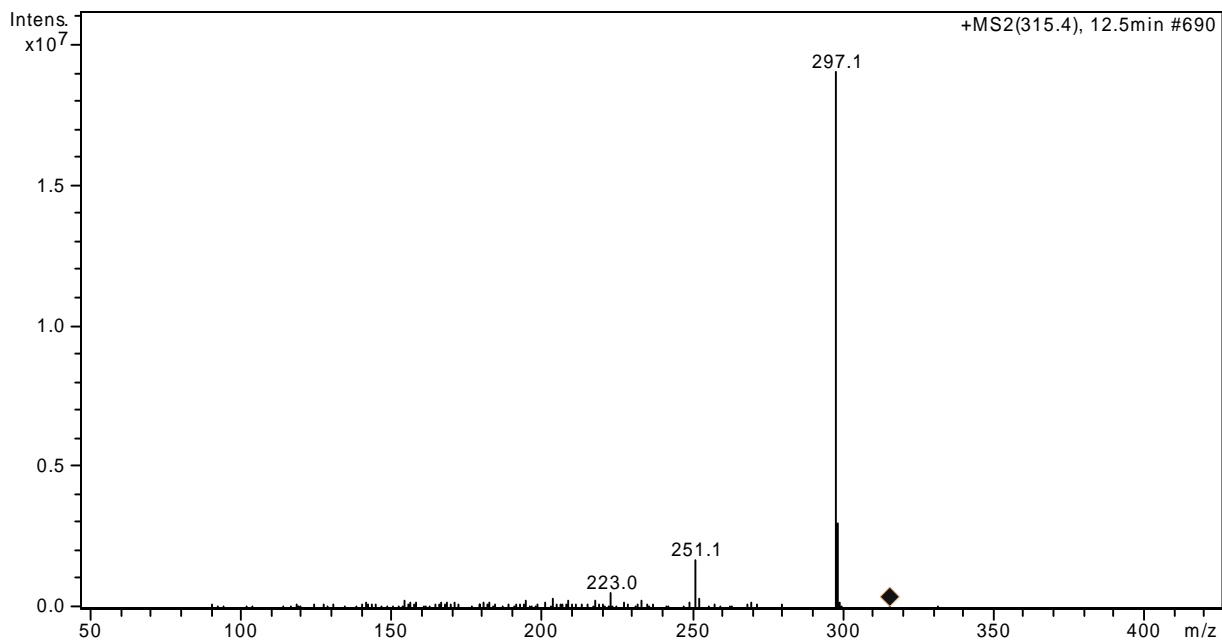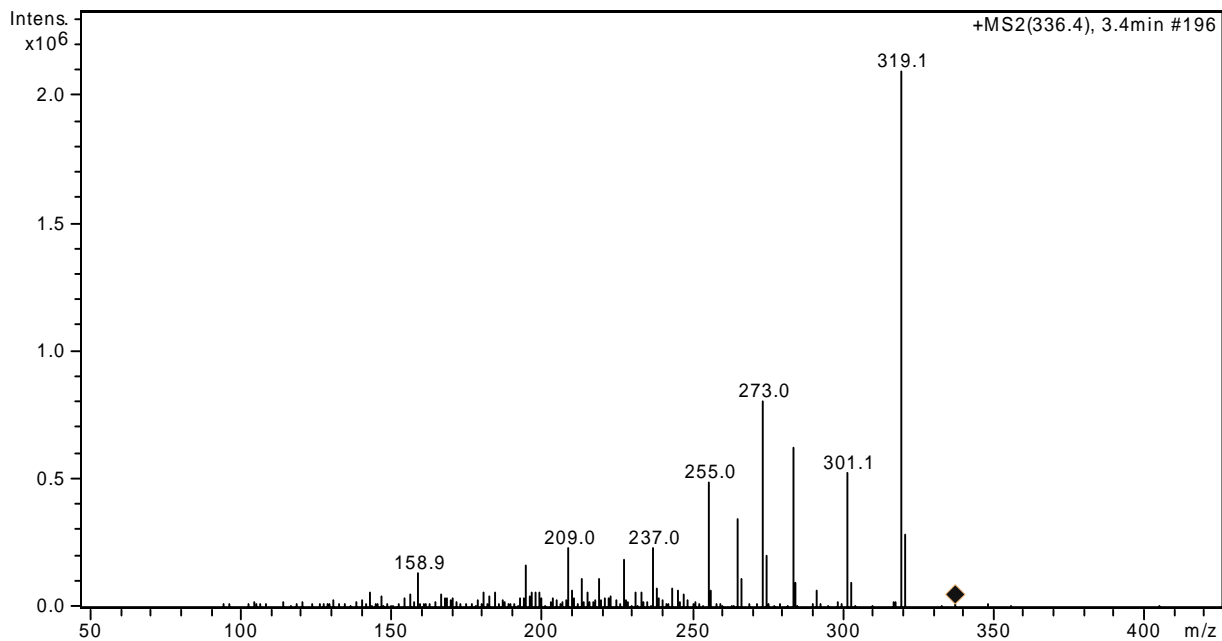
Product VI (m/z: 319)

Product VII (m/z: 329)
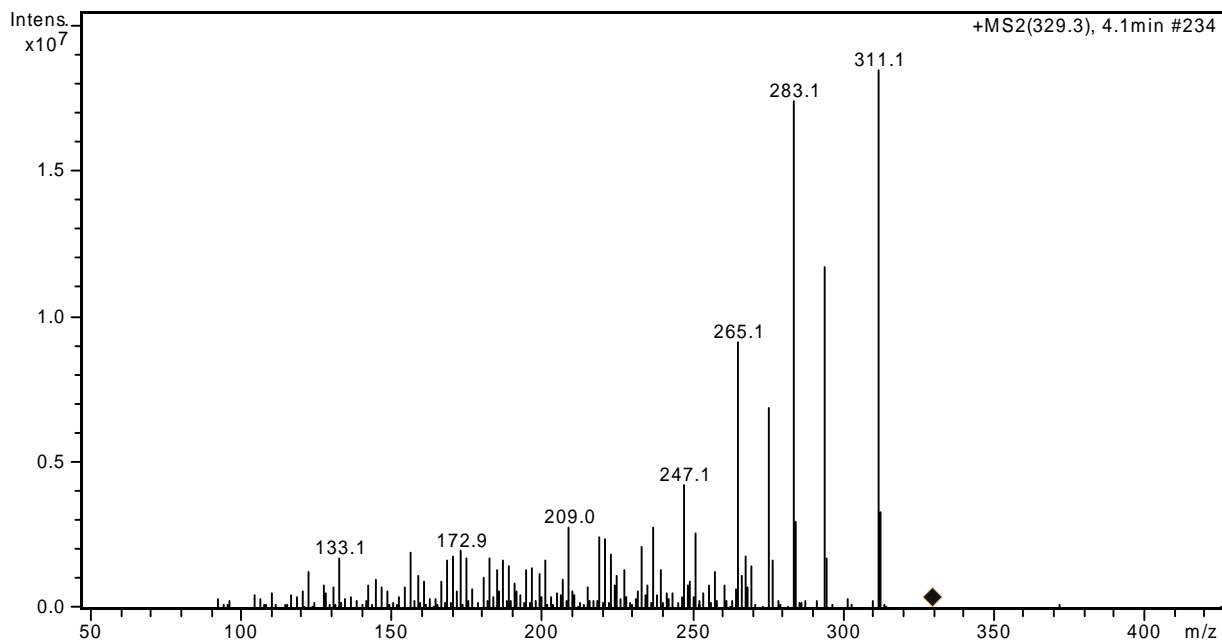
Product VIII (m/z: 345)

Product IX (m/z: 347)